Ph. D. Thesis

Thermo-Optic and Nonlinear-Optical studies on CdSe Quantum Dots for Photonic Applications

Anju K. Augustine

International School of Photonics
Cochin University of Science and Technology

Thermo-Optic and Nonlinear-Optical Studies on CdSe Quantum Dots for Photonic Applications

Ph. D. Thesis submitted to

Cochin University of Science and Technology

in partial fulfilment of the requirements for the award of the Degree of

Doctor of Philosophy

Anju K. Augustine
Reg No: 4376

International School of Photonics
Cochin University of Science and Technology
Cochin- 682022, Kerala,India

June 2015

Thermo-Optic and Nonlinear-Optical studies on CdSe Quantum Dots for Photonic Applications

Ph.D Thesis in the field of photonics

Author:
Anju K. Augustine
Research Fellow, International School of Photonics
Cochin University of Science and Technology
Kochi-22,India
Email: srrosmin2009@gmail.com

Research Advisors:
Dr.M. Kailasnath
Director and Assistant Professor, International School of Photonics
Cochin University of Science and Technology
Kochi-22,India
Email: kailas@cusat.ac.in

Dr. V P N Nampoori
Emeritus Professor, International School of Photonics
Cochin University of Science and Technology
Kochi-22,India
Email: vpnnampoori@cusat.ac.in

International School of Photonics
Cochin University of Science and Technology
Kochi-22,India
URL:www.photonics.cusat.edu

June 2015

Front cover: TEM image of Au NPs
Back cover : Photo induced studies on CdSe nanofluid

INTERNATIONAL SCHOOL OF PHOTONICS
COCHIN UNIVERSITY OF SCIENCE AND TECHNOLOGY
COCHIN- 682022, KERALA,INDIA

Certificate

Certified that the work presented in this thesis entitled "**Thermo-Optic and Nonlinear-Optical studies on CdSe Quantum Dots for Photonic Applications**" is based on the original work done by Ms.Anju K. Augustine under our guidance and supervision at the International School of Photonics, Cochin University of Science and Technology, Kochi-22, India and has not been included in any other thesis submitted previously for the award of any degree.

Certified that relevant corrections and modifications suggested by the audience during the pre-synopsis seminar have been incorporated in this thesis.

Kochi 682022	Prof. V P N Nampoori	Dr.M. Kailasnath
23.06.2015	(Co-guide)	(Supervising Guide)

Declaration

Certified that the work presented in this thesis entitled "**Thermo-Optic and Nonlinear-Optical studies on CdSe Quantum Dots for Photonic Applications**" is based on the original work done by me under the guidance of Dr. M. Kailasnath, Director and Associate Professor, International School of Photonics, Cochin University of Science and Technology, Kochi-22, India and the co-guidance of Dr. V. P. N Nampoori, Emeritus Professor, International School of Photonics, Cochin University of Science and Technology, Kochi-22, India and it has not been included in any other thesis submitted previously for the award of any degree.

Kochi 682022 Anju K. Augustine
23.06.2015

"സകലതും അറിയുന്ന ജ്ഞാനം,എന്റെ പ്രവർത്തികളിൽ എന്നെ
ബുദ്ധി പൂർവ്വം നയിക്കും" (ജ്ഞാനം9:11)

Contents

Dedicated to the Almighty God

Acknowledgement

"He arms me with strength and makes my way perfect"(Ps18:32)

First and foremost, praises and thanks to **God Almighty** for His showers of blessings throughout my research work to complete it successfully. I have experienced your guidance day by day. I will keep on trusting you for my future.

At the end of my thesis, it is a pleasant task to express my thanks to all those who contributed in many ways to the success of this study and made it an unforgettable experience for me. I express my deep and sincere gratitude to my guide and supervisor Dr. M. Kailasnath,the present Director of ISP, for being my guiding light through this educational process with constant support, able guidance, valuable suggestions, approachability and freedom of work extended to me throughout the period. I am extremely indebted to my co-guide Prof. V.P.N Nampoori for tirelessly guiding me with scholarly inputs and consistent encouragement through every step of this work. Much gratitude is also extended to Prof. P. Radhakrishnan for unselfishly providing time and energy by giving valuable suggestions to the work. I would like to express the heartfelt gratitude to Prof. C. P. Girijavallabhan for providing invaluable guidance throughout this research.Thanking Mrs Sheenu Thomas for her loving concern extended throughout my work.

I take this opportunity, to express special thanks to my friends and research colleagues Mathew,Divya,Aparna,Anand,Pradeep,Indu,Jaison,Suneetha,Ratheesh, Adrin,Linslal,Roopa,Bejoy,Linesh, Boby sir, Musfir, Manju,Bini,Aleena,Nideep, Sreeja,Ajeena,Rajeena,Sony,Sabitha,Jessy,Priyamvada miss,Ajmal,Bony,Mintu, Jayaprakash,Arun, and Hradya for their liberal help whenever I was in need. Special thanks to all teaching and non-teaching staff, MSc and MTech students for giving me the support in a very special way.

I am very much indebted to Catholic Church and Sacred Heart congregation, I belong. I remember all the general and provincial superiors, councillors, mother in charges and all my sisters in our congregation for their loving concern and prayerful support. I specially thank the sisters and inmates of DSS convent,where I spent during my research. Thanks to Jesus youth group.

I owe a lot to my loving parents, sister, brother and their families, who encouraged and wished me at every stage of my personal, religious and academic life with their loving concern, prayer and sincere support. Finally, my thanks go to all the people who have supported me directly or indirectly to complete the research work .

Sr.Anju.K.Augustine

Preface

Photonics can be defined as the science and technology of light and other forms of radiant energy. It mainly deals with the generation, manipulation, transport, detection and the applications in a variety of fields including communication, sensing, display, imaging, medical, defence and industrial. Due to the structural and optical properties, nanomaterials are the most suitable one for the detailed study in the field of photonics. Since materials are directly related to the photonic technology, some specific features will not be sufficient for its effective use. Rather, a complete characterization of materials is necessary for a comparative study of different materials to identify the most appropriate one. Even though optical techniques like simple absorption studies and luminescence studies are the most suitable method for their detailed optical characterization, they have some kind of limitations in many situations. Thermo-optic methods which is essentially an optical method, can be employed for any sample since at least a part of the excitation energy will be liberated through nonradiative channels. Moreover, nonlinear-optical characterization methods give information about the different nonlinear parameters and properties of the sample.

The tunability of optical properties of quantum dots, by controlling their physical dimension in nanometer length scale, allows the fabrication of display devices, cascade lasers and light sources of different colors from materials possessing same chemical composition. Recent studies have shown that quantum dot based hybrid systems are useful in the design of photovoltaic devices and random lasers. Even though CdSe QDs based photonic materials have been much studied, a detailed analysis of this material using thermo-optic and nonlinear-optical methods has not been carried out. In our thesis, we have included the study of optical and thermo-optic properties of CdSe QDs in the context of applications such as solar cells, random lasers and optical limiters.

Main objectives of the present investigation are (i) to synthesis water soluble CdSe quantum dots for the photonic applications, (ii) to study the thermal and nonlinear properties of CdSe quantum dots based materials and (iii) to develop CdSe quantum dots based solar cells and random lasers. The thesis is divided into seven chapters:

Chapter1: Introduction to studies on CdSe quantumdots based photonic materials using thermo-optic and nonlinear-optical methods

The first part of the present chapter gives a general introduction to the subject matter contained in the thesis. It includes a short description of the importance of photonics, photonic materials and it's applications in this new era. Nanophotonics and nanomaterials are specially discussed in this section. Importance of quantum confinement effect in the properties of quantum dots is also presented. In the second part of this chapter demonstrates characteristics and applications of CdSe quantum dots in the field of photonics and the role of thermo-optic and nonlinear-optical methods in the investigations of photonic materials. Finally,the overall aim and organization of the thesis is addressed.

Chapter2: Material preparation and characterization techniques

This chapter is devided into three parts. The first section describes the experimental techniques used for the synthesis and characterization of the photonic material in the present work. Specifications and experimental methods used for analysis of the samples are discussed along with the basic theory. Preparation methods, structural and optical characterization methods are briefly included. Second part of the chapter mainly discuss about the main charecterization methods included in our study. Thermal lens and photo acoustic methods are the two thermo-optic methods, where Z-scan technique is the better nonlinear optical method which are specially described. Finally, applications of the photonic materials in devices such as solar cell and random laser are explained along with the experimental section.

Chapter3: Linear optical studies on CdSe based quantum dots.

In this chapter, the method of preparation and the linear optical studies of the CdSe quantum dot based photonic materials and its dependence on various parameters like preparation methods, particle size, bandgap, solution pH etc. are included. Influence of metal nanoparticles on the optical properties of CdSe quantum dots are also studied. Photo induced studies on the samples are discussed in the final section.

Chapter 4: Thermo-optic studies in CdSe based quantum dots

This chapter demonstrates the thermo optic studies on CdSe based nanomaterials. First part of the chapter includes thermal lens study on the samples where the second part is mainly focussed on the photo acoustic charecterization on CdSe quantum dots based materials. Thermal lens study give information about thermal diffusivity of the material while photo acoustics characterization method shows the photo acoustic signal variation of the sample at different input conditions. Both, continuous and pulsed lasers are used for the photo acoustic study. Both of the thermo-optic studies give details about the nonradiative emission property of the samples.

Chapter5: Nonlinear-optical studies on CdSe quantum dots based photonic materials

In the present chapter, we focus on the evaluation of nonlinear optical changes of CdSe based nanocolloids employing the technique of single beam z-scan, at a wavelength of 532 nm. Open-aperture curve exhibits reverse saturable absorption property and it varies at different conditions. Nonlinear absorption coefficient and third order susceptibility are calculated. The Enhanced absorption property can be attributed to free carrier absorption following two photon absorption. Influence of the particle size, presence of metal nanoparticles and the solution pH of CdSe quantum dots on the nonlinear properties are presented. These studies show that colloidal CdSe quantum dots based photonic materials can be used as a potential nonlinear optical material.

Chapter6: Applications of CdSe quantum dots based photonic materials in the fabrication of solar cells and random lasers.

This chapter includes the study of the applications of CdSe quantum dots as the promising photonic material. It is devided in to two parts : Quantum dot sensitized solar cells prepared with CdSe quantum dots are discussed in the first section where these material acts as the sensitizeres. Thermal characterizations and the metal incorporated studies of the solar cells exhibit variations on efficiency at different conditions. Finally, CdSe quantum dots based random lasers are discussed with varying particle size of the material.

Chapter7: General Conclusion and Future Work

Significant conclusions of the present work and the few observations regarding future prospects are discussed in this final section.

List of Publications

A. Journal Publications:

- Anju K. Augustine, S.Mathew, P. Radhakrishnan, V. P. N. Nampoori, and M. Kailasnath,"Size Dependent Optical Nonlinearity and Optical Limiting Properties of Water Soluble CdSe Quantum Dots", Journal of Nanoscience,Volume 2014, 623742(7 pages), 2014.
- Anju. K.Augustine, S. Mathew, C. P. Girijavallabhan, P. Radhakrishnan,V. P. N Nampoori & M. Kailasnath,"Size dependent variation of thermal diffusivity of CdSe nanoparticles based nanofluid using laser induced mode-matched thermal lens technique",J Opt. vol.44, 85-91, 2015.
- Anju K Augustine, P Radhakrishnan, V P N Nampoori and M Kailasnath,"Enhanced random lasing from a colloidal CdSe quantum dot-Rh6G system", Laser Phys. Lett., vol.12, 025006 (4pp), 2015.
- Anju K Augustine, C P Girijavallabhan, V P N Nampoori and M Kailasnath,"Influence of pH on the thermo-optic properties of CdSe QDs prepared by a microwave irradiation method",Laser Phys. Lett., vol.11, 115901 (6pp), 2014.
- Anju K. Augustine, V.P.N. Nampoori, M. Kailasnath,"Rapid synthesize of gold nanoparticles by microwave irradiationmethod and its application as an optical limiting material", Optik, vol.125, pp.6696-6699, 2014.
- Anju K Augustine, V P N Nampoori and M Kailasnath,"Tuning of particle size and bandgap of CdSe nanoparticles prepared by reflux method", Asian Journal of physics, vol.23, pp.683-686, 2014.
- Anju. K. Augustine, C. P. Girijavallabhan, V. P. N Nampoori & M. Kailasnath,"Charge and Heat Transfer Mechanism in Directly Coupled CdSe-Metal Nano hybrids", (Published online) Journal of electronic materials, DOI: 10.1007/s11664-015-3766-9, 2015
- Aparna Thankappan, S. Divya, Augustine K Anju, C. P. Girijavallaban, P. Radhakrishnan, Thomas Sheenu and V. P. N. Nampoori, " Highly efficient betanin dye based ZnO and ZnO/Au Schottky barrier solar cell",Thin Solid Films, vol.583, 102-107, 2015.
- Anju.K.Augustine, K. P. Sandhya, V.P.N Nampoori and M. Kailasnath, "Thermo- optic studies on Quantum Dot Sensitized Solar cell (communicated)
- Anju.K.Augustine, V.P.N Nampoori and M. Kailasnath,"Enhanced conversion efficiency of metal doped - CdSe QuantumDot sensitized solar cells"(communicated)

B. Conference Publications:

- Anju.K.Augustine, Alina C. Kuriakose VPN Nampoori and M Kailasnath,"Optical nonlinear studies of gold nanoparticles synthesized by microwave irradiation method", ICAPM, M.G University Kottayam, Kerala, October,2013.
- Anju.K.Augustine, VPN Nampoori and M Kailasnath,"Influence of PH on thermo -optic properties of CdSe QDs prepared by microwave irradiation method",ICAMA, Alphonsa college PALA, March, 2014.
- Anju K. Augustine, Higgins W., Mayank S., K. P. Sandhya,P. Radhakrishnan,V. P. N. Nampoori and M. Kailasnath,"Annealing Effect on CdSe Based Quantum Dot Sensitized Solar Cells", PSWS-2015, St.Thereas college EKM, March, 2015.
- Anju.K.Augustine,Anand V.R, C.P. Girijavallabhan, P. Radhakrishnan, V.P.N Nampoori and M. Kailasnath,"Photoaccoustic Investigations on CdSe based nano fluids", PSWS-2015, St.Thereas college EKM, March, 2015.
- Anju.K.Augustine, VPN Nampoori and M Kailasnath,"Tuning of particle size and band gap of CdSe nanoparticles prepared by reflux method", Swadeshi science congress, M.G university Kottayam, Kerala, November, 2013.
- Anju.K.Augustine, VPN Nampoori and M Kailasnath ,"Synthesis and characterization of Gold nanoparticles by rapid microwave irradiation method, NLS-22, Manipal, India, January, 2014.
- Anju.K.Augustine, VPN Nampoori and M Kailasnath,"Strong fluorescence emission from CdSe nanoparticles prepared by aqueous route", National seminar on Recent trends in experimental physics, Devamatha college, Kuravilangadu, Kottayam, March, 2013.
- Anju.K.Augustine, VPN Nampoori and M Kailasnath,"Strong fluorescence emission from CdSe nanoparticles prepared by microwave assisted reduction method", National seminar on recent trends in conducting polymers and polymer nano structures, Aquinas college Edacochin, August, 2013.
- Anju.KAugustine,Arun S., Basil A.M, Nikhil P, VPN Nampoori and M Kailasnath"Charecterization of Photoaccoustic cell", Annual photonics work shop, ISP, CUSAT, Cochin, February, 2013.
- Alina C. Kuriakose , Anju K. Augustine, V.P.N. Nampoori, M. Kailasnath, "Energy transfer from CdS nanoparticles to sodium fluorescein dye",NLS-22, Manipal, India, January, 2014.

List of Figures

List of Tables

List of Abbreviations

AO	Accousto optic
BG	Band Gap
CW	Continuous Wave
CB	Conduction Band
CQDs	Colloidal Quantum Dots
DSSCS	Dye-ensitized solar cells
DFWM	Degenerate Four Wave Mixing
DSO	Digital Storage Oscilloscope
DLS	Dynamic Light Scattering
DPSS	Diode pumped solid state
ESA	Exited state absorption
FCA	Free carrier absorption
FTIR	Fourier Transform Infrared spectroscopy
FWHM	Fullwidth half maximum
FF	Fill factor
IPCE	Internal photoconversion efficiency
LSPR	Localized surface Plasmon resonance
LEDs	Light emitting diodes
MEG	Multiple exciton generation
MSA	Mercapto succinic acid
MPA	Mercapto propanoic acid
NLO	Nonlinear optics
NPs	Nanoparticles
NCs	Nanocrystals
NH	Nanohybrids
OLT	Optical limiting threshold
PA	Photo acoustic
PAS	Photo acoustic spectroscopy
PTD	photothermal deflection
PT	photothermal
PZT	Piezoelectric transducer/Lead Zirconate-Titanate
QDs	Quantum dots
QLEDs	QDs based light emitting diodes
QDSSCs	QD sensitized solar cells
QYs	Quantum yields
RSA	Reverse Saturable Absorption
RL	Random Laser
RG	Rosencwaig and Gersho
SEM	Scanning Electron Microscopy
SA	Saturable Absorption
SP	Surface plasmons
SPR	Surface Plasmon resonance
SAED	Selected area electron diffraction
TL	Thermal lens
TLS	Thermal lens spectroscopy
THG	Third Harmonic Generation
TPA	Two photon absorption
TEM	Transmission electron microscop
UV	Ultraviolet
VB	Valence band
XRD	X-ray Diffraction

Chapter 1

Introduction to studies on CdSe quantum dots based photonic materials using thermo-optic and nonlinear-optical methods

---

The present chapter gives a general introduction to the subject matter contained in this thesis. It includes a short description of the importance of photonics and photonic materials and the photo-induced changes that occur during photon matter interaction, with special emphasis to the nonradiative processes taking place in condensed matter and the associated detection schemes. Nanophotonics and nanomaterials are specially discussed in this chapter. The role of thermo-optic and nonlinear-optical methods for the investigations on nanophotonic materials is also addressed. The chapter concludes by pointing out the significance of the material properties and the applications that are selected for the present investigations.

1.1 Photonics and photonic materials

During the beginning of the 20^{th} centuary, Albert Einstein and other scientists showed that light consists of a different kind of tiny fundamental particles, called " photon". Presently the word "photonics" has been coined to describe the science and technology which deals with the generation, manipulation, transport, detection, and use of light and other forms of radiant energy. All those materials which are directly related to the photonic technology are generally termed as photonic materials, analogues to the electronic materials in electronics.They interact strongly with light and it includes all light absorbing or emitting materials eg. semiconductors, organic materials such as dyes and liquid crystals.

1.2 Motivation of the thesis

Applications of photonics are ubiquitous. But,for the effective use of this modern technology in any of these potential applications, suitable materials are necessary for the generation, manipulation, detection and display of light. Since the advent of the laser in the1960s the study of nonlinear optical properties of material has become readily accessible. Some of the potential applications of nonlinear optics include quantum computing, quantum imaging, optical switching, optical power limiting, and nonlinear optical image processing[1-4]. Consequently, variety of new photonic materials are suitable for different applications have been developed. But, mere development of a new material with some specific features will not be sufficient for its effective use in any of the applications. Rather, a complete characterization of materials is necessary for a comparative study of different materials to identify the most appropriate one. Materials with the required properties of large optical non-linearity combined with high optical transparency and high resistance to laser damage are necessary for nonlinear-optical applications. Thermo-optic/photo-thermal methods can be employed for any sample since at least a part of the excitation energy will be liberated through nonradiative channels. Moreover, among the different photo thermal configurations, appropriate method can be chosen depending on the specifications and properties of the sample[5,6].

1.3 Nanophotonics

Nanomaterials are especially well suited for photonics applications because they can be constructed in such a manner as to produce enhanced linear, nonlinear and thermo-optic response. Areas of research in photonic applications with nanomaterials are referred as nanophotonics. In the last decade, significant breakthroughs have been witnessed in the area of nanophotonic materials and devices [7-10]. Nanophotonic materials have become increasingly popular in a variety of tasks, including biosensing, imaging, optoelectronics and photovoltaics. The main interest in such nanoscale systems is due to their novel optical properties. Confining one or more dimensions to the nanometer scale, the photonic interactions of such materials exhibit dramatic changes. This quantum confinement of electrical carriers within nanoparticles and efficient energy and charge transfer over nanoscale distances are the key contributory factors for their novel optical properties. Nanostructured photonic materials, including plasmonic and optical materials have provided access to optical functionalities that are not easily attainable using conventional materials [5, 9]. In particular, semiconductor quantum dots (QDs) can provide efficient band-tunable luminescence in the visible - infrared range, suggesting their use as light emitters and contrast agents in bioimaging. Noble metal nanostructures are capable of supporting free electron oscillations (surface plasmons), yielding to a series of effects, including resonant absorption/scattering in visible-infrared range, drastic electric field enhancement for surface enhanced Raman scattering or improved photovoltaic response, imaging beyond the diffraction limit and ultra-sensitive response in biosensing etc.

1.3.1 Quantum dots

Materials with size reduced to the nanoscale dimension show different properties compared to that of the bulk. As the size of the system decreases the 'quantum size effect' becomes prominent where the electronic properties of solids are changed. In a semiconductor crystallite material for which diameter is smaller than the size of it's exciton Bohr radius, the excitons are squeezed, leading to quantum confinement. In this state of confinement, the energy levels can then be modeled using the particle in a box model with discrete energy levels, in which the energy of different

states are dependent on the length of the box [11-13]. QDs are said to be in the 'weak confinement regime' if their radii are of the order of the exciton Bohr radius; and in the'strong confinement regime' if their radii are smaller than the exciton Bohr radius. If the size of the quantum dot is small enough that, the quantum confinement effects dominate (typically less than 10 nm), the electronic and optical properties are highly tunable [8, 14, 15]. An important effect of such confinement is the increase of surface area to volume ratio. It causes to change the optical, mechanical, thermal and catalytic properties of materials significantly. All these distinct properties enable unique applications of nanomaterials.

QDs are sometimes referred to as artificial atoms because of their discrete energy levels similar to atoms. The engineering of band gap of QDs with size to tune the desired optical properties make research on semiconductor QDs attractive in the field of nanotechnology. Semiconductor QDs are usually composed of atoms from groups II-VI, III-V, or IV-VI of the periodic table. The basic experimental relationship between size and optical spectra was first established and confirmed for ZnS and CdS colloidal semiconductor nanocrystals (NCs) [5]. Numerous research have been carried out since then to synthesize colloidal semiconductor and study their optical properties [16-18]. Wide band gap materials are suitable for high power, high temperature electronic devices and short wavelength optoelectronics because of their inherent properties such as larger band gap, higher electron mobility and higher breakdown field strength.Wide band gap II-VI compounds are characterized by the direct band gap with either zinc blend or wurtzite structures or large exciton binding energy. Band gap energy and exciton binding energy of typical II-VI compounds are shown in Table 1.1 [5, 19, 20].

1.3.2 Important features of quantum dots

(a) Quantum confinement effects

Quantum confinement describes the confinement of the exciton within the physical boundaries of the semiconductor. This arises as soon as the dimension of a nanocrystal (R) becomes comparable to the Bohr radius (a_B) of the exciton wave function, leading to significant changes in the electronic and optical properties. Confinement of energy is an important

effect of this. The exciton entity can be modeled using the particle in the box. The electron and the hole can be seen as hydrogen in the Bohr model with the hydrogen nucleus replaced by the hole of positive charge and negative electron mass. Then the energy levels of the exciton can be represented as the solution to the particle in a box at the ground level (n = 1) with the mass replaced by the reduced mass. Thus by varying the size of the quantum dot, the confinement energy of the exciton can be controlled. There is Coulomb attraction between the negatively charged electron and the positively charged hole. The negative energy involved in the attraction is proportional to Rydberg's energy and is inversely proportional to square of the size-dependent dielectric constant of the semiconductor. When the size of the semiconductor crystal is smaller than the exciton Bohr radius, the Coulomb interaction must be modified to fit the situation. Therefore, the sum of these energies can be represented as [8, 21, 22]

$$E_{confinement} = \frac{h^2\pi^2}{8\pi^2 a^2}(\frac{1}{m_e} + \frac{1}{m_h}) = \frac{h^2\pi^2}{8\pi^2\mu a^2} \tag{1.1}$$

$$E_{exciton} = \frac{1}{\epsilon_r^2}\frac{\mu}{m_e}R_e = -R_y^* \tag{1.2}$$

$$E = E_{bandgap} + E_{confinement} + E_{exciton} \tag{1.3}$$

$$E_{bandgap} + \frac{h^2\pi^2}{8\pi^2\mu a^2} + -R_y^* \tag{1.4}$$

where R_y^* is the Rydberg's energy, μ is the reduced mass, a is the radius, m_e is the free electron mass, m_h is the hole mass and ϵ_r is the dielectric

Material	BG energy (eV)	Exciton binding energy (meV)
CdSe	1.74	16
CdS	2.42	29
CdTe	1.49	11
ZnS	3.60	39
ZnSe	2.70	20
ZnTe	2.50	13

Table 1.1: Band gap energy at room temperature and exciton binding energy of II-VI compounds

constant of the material. Although the above equations were derived using simplifying assumptions, the implications are clear; the energy of the QDs are dependent on their size due to the quantum confinement effects, which dominate below the critical size leading to changes in the optical properties. This effect of quantum confinement on the QDs have been experimentally verified and is a key feature of many emerging electronic structures. Besides confinement in all three dimensions (i.e.quantum dot), other quantum confined semiconductors include:

* Quantum wires, which confine electrons or holes in two spatial dimensions and allow free propagation in the third.

* Quantum wells, which confine electrons or holes in one dimension and allow free propagation in two dimensions [19, 23, 24].

From figure 1.1 it is observed that, quantum confinement is responsible for the colors of cadmium selenide (CdSe) nanofluids [19, 25]. Electrons

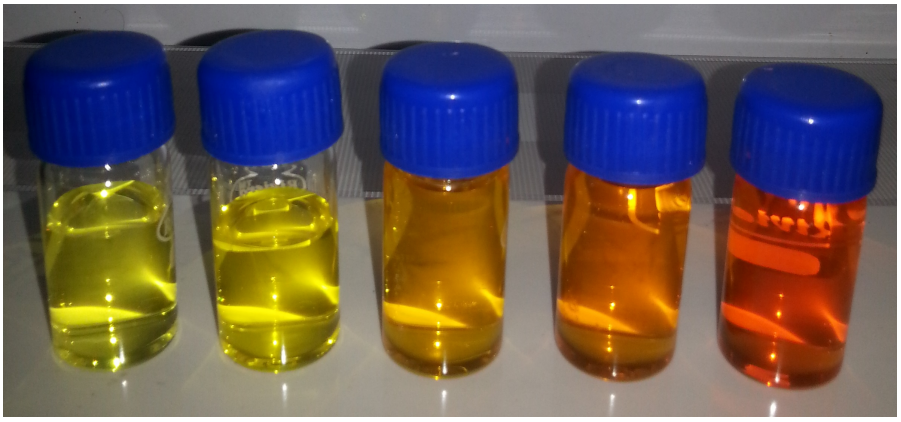

Figure 1.1: Quantum confinement is responsible for the colors of CdSe nanofluids.

within the tiny specks of semiconductor scatter photons for which energy is less than a minimum determined by the size of the crystallite and absorb those photons for which energy is higher. The largest particles can absorb lower- energy photons and appears as red, whereas the smallest absorb only higher- energy quanta and appear as yellow.

(b) Exciton and exciton oscillator strength

We define exciton as a bound state of an electron in a conduction band and a hole in a valence band which can play central roles in optical responses of semiconductors or insulators. The relation between number of excitons and the optical responses is a long standing problem in exciton physics. In low-dimensional structures, the Coulomb correlative effects or the excitonic effects become more prominent than in bulk structures, leading to peculiar optical characteristics combined with the geometrical confinement effects. Under a weak excitation condition, only an electron and a hole are created, which form a bound state due to the Coulomb attraction and can be solved by a two-body problem, with the use of effective mass approximation. But, the inter-particle Coulomb interaction plays an essential role in the case of stronger excitation where many electrons and holes are excited in semiconductors. The dimensionality of exciton systems depends on the ratio of the particle size R to the exciton effective Bohr radius, a_B.Th e oscillator strength is one of the main excitonic characteristics, providing unique information about the geometry of the exciton wave function in a structure. This enhanced coupling strength is due to the quantum confinement and the piezoelectricity in QDs. Nonlinear optical effects are enhanced, especially in nanomaterials when the associated optical transition has a large optical oscillator strength. The oscillator strength is increased due to an increase in density of states at around the band gap energy. This would contribute to realization of low threshold nonlinear optical devices at room temperature or even at higher temperatures [5,26].

(c) Size dependence and band gap engineering

Semiconductor nanoparticles (NPs) exhibit a change in their electronic properties relative to that of the bulk material; as the size of the solid becomes smaller, the band gap becomes larger. This size-dependence of the optical properties leading to band gap engineering of QDs has been one of the core subjects of research work during the last decade. There are three types of nanometer-size semiconductors having zero, one and two dimensional structures with respect to the confinement of electrons, holes and/or excitons. This results in size quantization of their momenta and energies. In a weak confinement regime, a translational motion of

an exciton is size quantized and in a strong confinement regime, motions of electrons and holes are individually quantized. Example of weak confinement regime is CuCl dot where the nano crystal size is larger than the exciton Bohr radius [21] and strong confinement regime are seen in CdSe dots and GaAs wells, where the spatial size is smaller than the exciton Bohr radius. Figure 1.2 shows the band gap variation of the II-VI semiconductors with respect to their size variation. From equation(1.4)

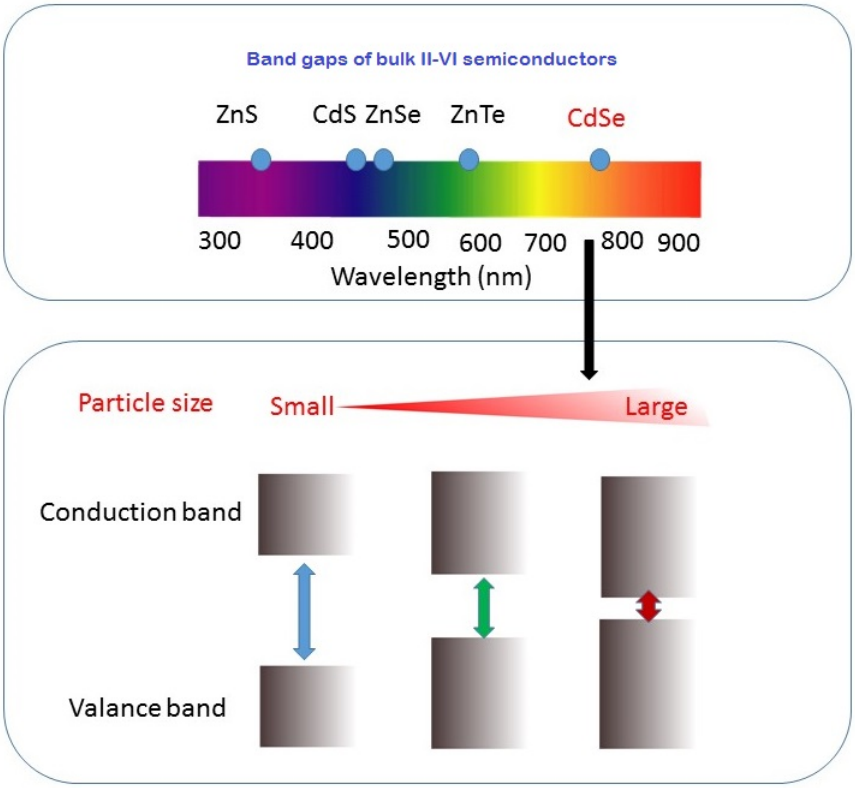

Figure 1.2: Band gap variation of the II-VI semiconductors with respect to their size variation.

it is clear that, the quantum confinement terms follow a^{-2} and shift E to higher energy as the radius decreases. In this equation, the correlation between electron and hole positions induced by the Coulomb interaction

is not strong, and the major effect is the electron and hole confinement energy. Therefore, the QD energy band gap increases as the particle size is reduced.

(d) Optical properties

NPs are a bridge between bulk materials and atomic or molecular structures. The properties of materials change as their size approaches the nanoscale and the percentage of atoms at the surface of a material becomes significant. The size of the NPs is finite, so the continuous energy band of the bulk crystal transforms into a series of discrete states. The NPs frequently display photoluminescence and sometimes display electro luminescence. It is well known that quantum confinement effect modifies the electronic structure of nanocrystals when their diameter is comparable to or smaller than the diameter of the bulk exciton [27]. The optical properties of a semiconductor have their genesis in both intrinsic and extrinsic effects. Intrinsic optical transitions take place between the electrons in the conduction band and holes in the valence band, including excitonic effects due to the Coulomb interaction. Extrinsic properties are related to dopants/impurities or point defects and complexes, which usually create electronic states in the band gap, and therefore influence both optical absorption and emission processes.

1.Absorption

To investigate the optical properties of QDs, the first approach is the understanding of the behavior of their particular absorption spectra. The spectrum is characterized by the sharp band-edge and close to that, by the series of exciton states. The spectral positions of the absorption peaks shift to higher energies and the lines become broader with decreasing sizes of the NPs. This size-dependent effect can be attributed to the three-dimensional quantum confinement effect of the semiconductor materials. As a result of the quantum confinement effect, the absorption coefficient of QD is strongly dependent on the radius of the QD. The widespread QD systems based on II-VI materials show absorption structures in the visible and near ultra violet part of the spectrum and therefore compatible with a large number of laser sources used in experiments [5].

2.Fluorescence

The fluorescence of the QDs are generated when valence electron after excitation with a certain energy returns to the ground state to combine with the hole and release the energy in the form of photons. The energy of the emitted photon is determined by the size of the quantum dot due to quantum confinement effects [28]. The energy of the emitted photon is the sum of the band gap energy between occupied level and unoccupied energy level, the confinement energies of the hole and that of the excited electron, and the bound energy of the exciton as shown in figure 1.3. The QDs of the same material, but with different

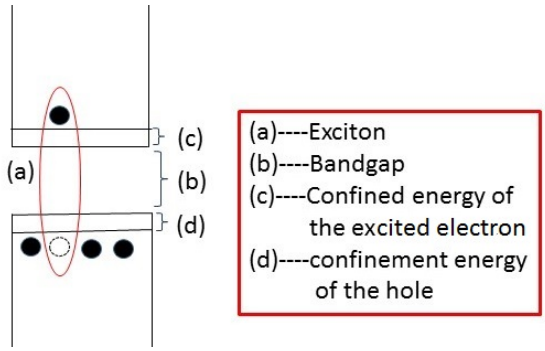

Figure 1.3: Illustration of the energy levels associated with an excited electron in a QD.

sizes, can emit light of different colors. The physical reason is the quantum confinement effect. The larger dot gives low energy fluorescence spectrum. Conversely, smaller dots emit bluer light. The coloration is directly related to the energy levels of the QD. The band gap energy that determines the energy of the fluorescent light is inversely proportional to the size of the QD. Larger QDs have more energy levels which are also more closely spaced. This allows the QD to absorb photons containing less energy, i.e, those closer to the red end of the spectrum. The lifetime of fluorescence is determined by the size of the QD. Larger dots have more closely spaced energy levels in which the electron-hole pair can be trapped. Therefore, electron-hole pairs in larger dots live longer, causing larger dots to show a longer life time [29].

3.Multiple exciton generation

Another unique and valuable property of QDs is the multiple exciton generation (MEG). Upon exciting with a photon, an electron from the valence band (VB) jumps to a high level in the conduction band (CB) and generates one exciton (electron-hole pair). If the energy of the photon is at least twice as large as the band gap of the given QD, the exciton will have a very high kinetic energy, which can be released to excite another electron jumping from the VB to the CB by impact ionization[30]. As a result, one photon now generates two excitons as the process shown in figure 1.4, allowing enhanced internal quantum efficiency. This property of QDs is helpful to increase the efficiency of QD based photovoltaic devices and light emitting devices.

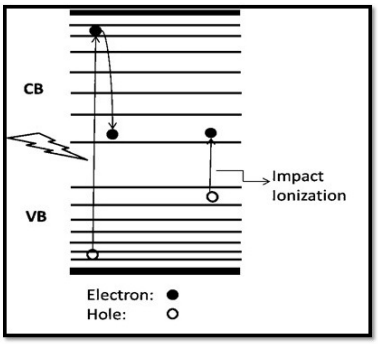

Figure 1.4: Schematics of the process of multiple exciton generation in QDs.

1.3.3 Applications of Quantum Dots

QDs are of great interest for their applications in solar cells, nanolasers, sensors and light emitting diodes (LEDs) due to size dependent absorption and emission properties, narrow size distribution and high luminescent efficiency. The ability to tune band gap in accordance with the size of QDs makes them very desirable in solar cell applications. QD can be used in solar cell in different configurations such as QD sensitized solar cells (QDSSCs) and solar cells with a QD multilayer. Various advantages over dyes such as of photo stability, high molar extinction coefficients, size dependent optical properties and low costs makes QDs to replace the

dyes in the solar cell applications.Due to the narrow bandgap emission and thermal stability of QDs, QDs based light emitting diodes (QLEDs) have attracted demanding research and commercialization as compared to organic LEDs. QDs are also being used in fluorescence tagging to replace molecular dyes for bioimaging, diagnostics, drug delivery and therapeutic applications due to their superior properties over conventional dyes such as higher extinction coefficients, higher quantum yields(QYs), less photo bleaching, tunable absorbance and emissions with size, broad excitation and narrow emission spectrum. Another feature of QDs is that, the broad absorption spectra of the QDs allow single wavelength excitation of emission from different-sized QDs. Different sizes of QDs can also be used for multicolor optical coding for biological analysis. Doped QDs are being considered as the new group of materials with better luminescence to be used as bio-probes [19].

1.4 CdSe QDs as the selected photonic material

Classification of CdSe belongs to a II-VI semiconductor of the n-type material. The structure of CdSe can be either hexagonal-wurtzite or cubic-zinc blende type. The cubic CdSe structure is unstable and may converts to the wurtzite form upon moderate heating. Bare CdSe QDs possess surface defects due to the unsaturated Cd^{2+} and Se^{-} sites, which act as traps for excitons, enhancing phonon assisted recombination thereby lowering luminescence quantum yield. CdSe QDs find a wide range of applications in optoelectronic devices, photo catalysis, solar energy conversion and biological imaging and labeling. Human tissue is permeable to far infra-red light. By injecting appropriately prepared CdSe QDs into injured tissue, it may be possible to image the tissue in those injured areas. Various methods are developed to prepare CdSe QDs including organic synthetic methods and methods using aqueous media. Compared with the organic phase routes, the synthesis methods using aqueous media are simple, green and highly reproducible, and the products exhibit good water solubility and stability. The main property of CdSe QDs is it's optical property [31-34].

1.5 Photon-material interactions and characterizations

Absorption of photons by atoms or molecules will result in a series of processes or effects in a material [3, 35, 36]. The relaxation of energy of the excited level may be of radiative processes, such as spontaneous or stimulated emission, or by nonradiative processes which mainly results in heat generation. If the absorbed energy of the photon is high, direct photochemical changes such as photo decomposition, photo-ionization etc.of the excited molecule may take place. Vaporization of the material and plasma generation are the destructive changes which may occurs as a result of photon-matter interaction at very high power densities of the incident light. If the changes are chemical, it may be either reversible or irreversible. Figure 1.5 shows the main channels of photo induced changes that occur in a sample.

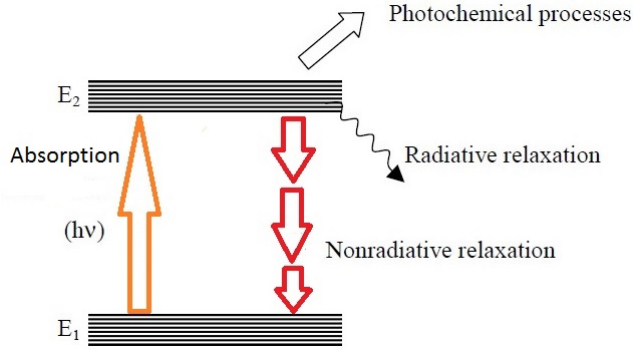

Figure 1.5: Main channels of photo induced changes that occur in a sample.

$$h\nu = E_2 - E_1 \tag{1.5}$$

Where $h\nu$ is the energy of the absorbed photon and E_1, E_2 represents the energies of the lower and upper levels respectively. The absorbed energy will be liberated through radiative, nonradiative or photo chemical processes and each of these processes has specific quantum yield [37-39]. The total quantum yield of all the channels of de-excitation is given by

$$n_r + n_{nr} + n_{pc} = 1 \tag{1.6}$$

here n_r , n_{nr} and n_{pc} are the quantum yields of radiative, nonradiative and photochemical processes respectively. Accordingly, the intensity I_{abs} of the laser radiation absorbed will be distributed over all these channels,

$$I_{abs} = I_r + I_{nr} + I_{pc} \tag{1.7}$$

where I_r, I_{nr} and I_{pc} are the amount of energy liberated through the radiative, nonradiative and photochemical processes respectively.

1.5.1 Photothermal methods an overview

Measurement of the energy absorbed or that released through any of these relaxation channels assists the study of various properties and parameters of the sample. Samples which absorb energy and liberate at least a part of the excitation energy through nonradiative relaxation, not only carries the information regarding the absorbed energy but also the details regarding thermal properties of the sample. Such spectroscopic methods based on the measurement of photo-induced changes in the thermal state of a sample are called the photothermal (PT) methods. Along with the change in temperature of the sample,this nonradiative relaxation brings about changes in many other parameters such as density, pressure, refractive index etc.

Depending on the mode of detection there exist a number of PT techniques. It is to be noted that PT spectroscopy measures optical absorption more accurately in highly scattering solutions, in solids and at interfaces because the scattered or reflected light will not contribute to PT signals. The detected PT signal depends on the optical absorption coefficient at the incident wavelength as well as on how heat diffuses through the sample. Dependence of PT signal on how heat diffuses through the specimen allows the investigation of transport and structural properties such as thermal diffusivity, thermal effusivity, thermal conductivity, voids, etc. A brief account of the different PT methods and the techniques which are applied in our samples are depicted in figure 1.6. Even though all these techniques are based on the same principle, the detecting parameter changes from one technique to other [40-44].

Photothermal calorimetry deals with the temperature change occurring in the sample due to nonradiative de-excitation and it can be di-

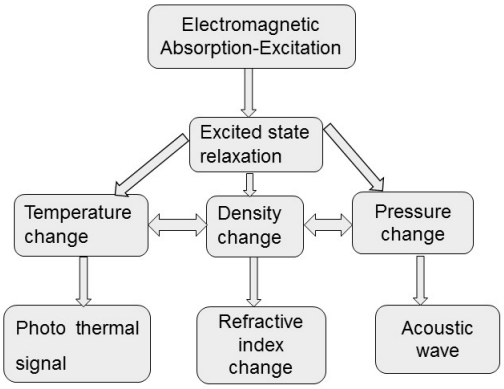

Figure 1.6: Brief account of the different PT methods discussed in this thesis.

rectly measured using thermocouples, thermistors or pyroelectric devices. Photo pyroelectric technique,used to study the information about the structural, thermal and optical properties of the sample while PT radiometry measures the temperature change indirectly by monitoring the infrared emission. Two PT techniques namely, PT interferometry and PT surface deflection method are employed for the evaluation of material parameters. PT interferometric technique can be effectively applied for samples having homogenous deformation occurring due to temperature changes. The optical path length change that occurs due to photothermally induced refractive index variation can be effectively measured using this technique. PT surface deflection spectroscopy can be used to study the change in surface angle due to spatially heterogeneous expansion or contraction.

In thermal lens(TL) spectroscopy the spatially varying refractive index profile arising due to PT effect as a result of irradiation with pump beam is studied. Focusing or de-focusing of the probe beam causes the refractive index profile to be curved and can act either as a converging or diverging lens depending on the sign of $\frac{dn}{dt}$. Light transmitted through an aperture placed beyond the PT lens will vary with the strength of the lens formed. A detailed overview of this technique is given in the second chapter. This technique allows the determination of thermal diffusivity,

thermal conductivity, temperature coefficient of the optical path length, optical absorption coefficient and fluorescence quantum efficiency. In the case of opaque solid samples, refractive index gradient due to temperature dependent index of refraction is studied making use of bending of materials which is commonly called PT deflection spectroscopy. In PT refraction spectroscopy, the detected signal is due to the combined effects of both deflection and lensing. PT diffraction technique is based on the probe-beam diffraction due to a periodic index of refraction (grating) generated when two pump-beams cross each other, inside or at the surface of a sample [3].

Pressure change associated with the transient temperature change in the specimen is detected using pressure transducers such as microphones or piezoelectric crystals in opto acoustic or photo acoustic (PA) technique. It is different from that of the acousto-optic (AO) effect. The two types of pumping mechanism commonly employed in PT experiments are pulsed optical excitation or modulated continuous wave optical radiation. Excitation through intensity modulated optical radiation results in periodic thermal waves and the amplitude and phase of the generated PT signal is a function of the frequency of modulation of incident radiation. These thermal waves carry information about the thermal, transport and optical properties of the specimen under investigation.

The present thesis deals with the use of two thermo-optic methods, namely, mode matched thermal lens technique to investigate the thermal and transport properties of CdSe QDs based photonic materials and photo acoustic technique to measure the acoustic signals generated due to the pressure variations generated in these samples [44-46].

1.6 Nonlinear optics

Field induced modifications in the optical properties of materials is studied in nonlinear optics (NLO). Measurements using conventional light sources give a polarization P which is linearly dependent on electric field strength E

$$P = \epsilon \chi E \tag{1.8}$$

where χ is the susceptibility of vacuum.The interaction of electric field with matter obeying this relation comes under linear optics. With high power lasers, which has high degree of spectral purity, coherence, intensity and directionality, it became possible to irradiate atoms and molecules with radiation of intensity comparable to the inter atomic field. Thus induced polarization becomes a function of higher powers of electric field showing nonlinear (NL) dependence on electric field. In such cases, polarization is expressed as

$$P = \epsilon(\chi^{(1)}E^1 + \chi^{(2)}E^2 + \chi^{(3)}E^3 + \cdots) \tag{1.9}$$

Here $\chi^{(2)}$ and $\chi^{(3)}$ are called second order and third order susceptibilities respectively. Many of these effects appeared in the NL optical regime, like second harmonic generation, third harmonic generation, optical limiting etc. are absent in linear regime. The magnitude and response of third order nonlinear susceptibility is one of the important parameters of NLO materials and several techniques exist for measuring these parameters. Z-scan, Degenerate Four Wave Mixing (DFWM), Third Harmonic Generation (THG), Time resolved optical Kerr effect, three wave mixing, ellipse rotation, beam distortion measurements etc. are different techniques used for this purpose. Using z-scan, the sign and magnitude of the third order susceptibility tensor can be calculated. DFWM can give both the magnitude and response of the third order nonlinearity. Similarly, THG is another technique used for the measurement of the magnitude of the third order susceptibility tensor. Electro absorption is used for the dispersion studies of third order nonlinearity and the time resolved optical Kerr effect is used for the photo physical processes determining the nonlinearity [5, 47].

1.6.1 Nonlinear absorption

The amount of light absorbed in most of the absorbing, materials increases linearly with input irradiance, giving rise to a constant transmittance. This is referred to as linear absorption and is independent of intensity of light. In such cases, absorption in the sample can be fully explained by Beer-Lambert law. If α is the linear absorption coefficient, transmitted intensity I_t is related to input intensity I_0 by

$$I_t = I_0 e^{-\alpha l} \tag{1.10}$$

where l is the sample length. Any deviation from the behaviour in the above equation is called nonlinear absorption. Here α can increase or decrease with respect to incident intensity so that α becomes a function of wavelength as well as the irradiance (I). The intensity dependent absorption arises due to third order optical nonlinearity in which the complete refractive index can be written as

$$n_I = n_0 + n_2 I \tag{1.11}$$

Both n_0 and n_2 are complex quantities where n_0 is the linear index of refraction, n_2 the intensity dependent refractive index and I denotes the irradiance of the laser beam within the sample. For a given wavelength, if α increases with intensity, the effect is called Reverse saturable absorption (RSA). On the other hand, if there is a decreases of α with intensity, the process is called saturable absorption(SA). In RSA, sample becomes more and more opaque as intensity is increased due to enhanced absorption at higher intensities. This phenomenon is exploited in passive optical power limiting to protect optical sensors, including human eye, from intense laser pulses. Optical limiting is achieved primarily by materials, which absorb strongly at high intensities i.e. RSA. A number of compounds have been found to possess such a property [48-51].

1.6.2 Excited state absorption and two photon absorption

At sufficiently high intensities, enhanced absorption of radiation in the transparent region of the spectrum is observed due to multi photon absorption process. When ground state absorption is bleached at high optical intensities, absorption of photo carriers in the excited state to higher state occurs which is called as the exited state absorption(ESA). In the process of two photon absorption (TPA), an atom makes a transition from its ground state to the excited state by the simultaneous absorption of 2 photons of identical or different frequences. One of the reason for reverse saturable absorption to occur is the absorption cross section σ_{12} being greater than σ_{01} where σ_{12} is the absorption cross section from the first excited molecular state to the higher state and σ_{01} is the absorption cross section from ground state to first excited state. As the optical excitation intensity increases, more molecules are promoted to the excited state, thus giving rise to higher absorption. General classification of TPA process is the resonant TPA and the non resonant TPA.

In resonant TPA which is also called as sequential TPA, a transition happens through two separate one photon transitions. In non resonant TPA, there need not be an Intermediate state for the atom before reaching at the final excited state. The nonlinear absorption in this case is proportional to the square of the instantaneous intensity as follows

$$\frac{\partial I}{\partial z} = -\alpha I + \beta I^2 \tag{1.12}$$

where α is the linear absorption coefficient and β is the TPA coefficient. Energy level diagram showing ESA and TPA are shown in figure 1.7. The nonlinear dependence on intensity implies that such a process can

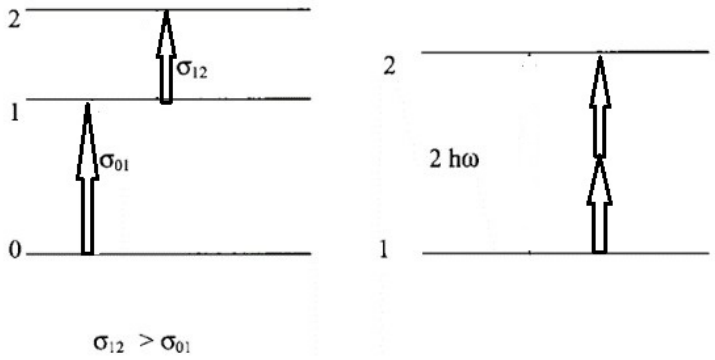

Figure 1.7: Energy level diagram showing (a) Excited State absorption and (b) two Photon Absorption.

be localized to a chosen region of the absorbing material by focusing the radiation. This has served as the basis of a host of new technologies like 2 and 3 photon microscopy, fluorescence correlation spectroscopy in live cells, optical data storage, lithography, optical limiting etc.

1.6.3 Free carrier absorption

In addition to TPA, large refractive nonlinearities can occur due to free carriers generated in the material. In semiconductors, the absorption of a photon with energy greater than the band gap will promote an electron to the conduction band, where it is a free carrier and can contribute current flow when a field is applied. These free carrier will relax to the

lower conduction band where it will recombine with an excited hole in the valence band after a characteristic recombination time and at high intensities they are again excited to the higher conduction band levels. This process is called free carrier absorption (FCA) [52-55].

1.6.4 Nonlinear optical properties of quantum dots

Due to quantum confinement effects and interfacial effects nanometer sized semiconductor materials exhibit large third order NLO effect. Quantum confined stark effect and large relatively fast NLO response in colour glass filters containing CdS:Se nanoparticles by Jain and Lind are the two important discoveries in the early eighties. Another important factor determining the NLO effects of quantum dots is the large number of atomic vacancies or defects on its surfaces that can become trapped states for electric charge. These trapped states would cause nonradiative transfer for photo excited carriers and can contribute to NLO effects when excited by external radiation. Optical nonlinearities in the transparent spectral region of semiconductors can be classified into two main categories, viz; (1) third order nonlinearity arising from bound-electronic effects and TPA and (2) FCA due to the photo excitation of free carriers.

1.7 Selected applications on CdSe QDs

In the recent decades, QDs also referred to as semiconductor nanocrystals, have come at the research focus in many areas of technical applications, like biomarkers, light-emitting diodes, photovoltaic devices, random lasers etc. due to their unique electronic and optical properties. The two important applications which we have studied on CdSe QDs are discussed below.

1.7.1 Quantum dots-sensitized solar cells

In particular, quantum dots-sensitized solar cells (QDSSCs) are of great interest because of their excellent performance of low-cost, photo stability, high molar extinction coefficients and size-dependent optical properties. Inspite of the progress in research and development of QDSSCs, their efficiency level is still lower than that of the dye-sensitized solar cells (DSSCs). This is mainly due to the high electron loss between

electrolyte and electrodes (photo electrode and counter electrode) and the relatively narrow absorption spectra of most of the efficient QDs. Thus, to increase the conversion efficiency, much effort has been concentrated to develop properties of QDs referring to electron transport rate, light harvesting ability, the catalytic ability of counter electrode and decrease of charge recombination. At present the performance of various nanosized materials like CdS, CdSe, CdTe, PbS, PbSe has been studied by various groups for photo catalyst and solar cell applications. QDSSCs have also shown potential in further improving the performance of the most efficient multi junction solar cell devices due to the flexibility in band gap tuning. Inorganic semiconductors have several advantages over conventional dyes. (i) The band gap of semiconductor QDs can be tuned by size to match the solar spectrum. (ii) Their large intrinsic dipole moments can lead to rapid charge separation and a large extinction coefficient, which is known to reduce the dark current and increase the overall efficiency. (iii) In addition, semiconductor QD sensitizers provide new chances to utilize hot electrons or generate multiple charge carriers with a single photon[56-59]. Hence, nanosized narrow band gap semiconductors are ideal candidates for the optimization of a solar cell for improved performance.

Recently, various nanosized semiconductors have been studied for photo catalyst and solar cell applications. Among these sensitizers, CdSe has shown much promise as an impressive sensitizer due to its reasonable band gap of about 1.70eV, which has a strong absorption of the solar spectrum. The use of CdSe quantum dots, which may produce more than one electron-hole pair per single absorbed photon (also known as multiple exciton generation (MEG)), is a promising solution to enhance power conversion efficiency. Furthermore, the creation of a type-II heterojunction by growing CdSe QDs on the TiO_2 surface greatly enhances charge separation. All these effects are known to increase the exciton concentration, quantum yield, and lifetime of hot electrons and therefore, the performance of QDSSCs. This enables better current-matching and hence the improved output current of the entire device, leading to higher efficiencies [60-63]. Novel works have been done in the area of plasmonic solarcell devices which showed an enhancement in the photo current. This could be achieved by using silver nanoparticles on the

surface of the material device.

A new type of nanostructure that combines the strong resonant light-harvesting properties of plasmonic NPs with the exclusive absorption capabilities of QDs have been developed. Such structures are the basis for a new class of intermediate band solar cells that may attain high efficiency. The interaction between excitons and plasmons, in hybrid structures of semiconductor and metal NPs, has attracted major attention in the last years due to the interesting effects that have been observed such as energy transfer, enhanced luminescence etc.[64-69]. In particular, several works showed enhanced photoluminescence, due to plasmon-enhanced absorption at or above the QDs ground-state, when the exciting light matches the plasmonic resonance of appropriately designed metal NPs, located in a near-field vicinity of the dots. As reported earlier, it is possible to enhance the long wavelength photon absorption of the QDSSCs by employing light trapping. This can be achieved by depositing metal nanoparticles on the solar cell surface. The light incident on the nanoparticles is scattered strongly due to excitation of localized surface plasmons(SP)[70]. A fraction of scattered light is coupled into the solar cell. The nanoparticles scatter light at random angles and the light coupled into the cell at angles greater than the critical angle for total internal reflection at the cell/air interface is trapped inside the cell, and results in enhanced absorption in the cell. Plasmonic light trapping can be incorporated into the solar cells after the general device fabrication sequence. Important steps for the fabrication of QDSSCs are shown in figure 1.8 (adapted from refrence 63).

Efficiency of QDSSCs depends on:

- Photo induced charge transfer processes- charge injection from an excited QD into wide band gap material like TiO_2
- Transport of electrons to the collecting electrode surface
- Hole transfer to the redox couple
- Regeneration of the redox couple
- Recombination of electrons from the QD and the oxidized form of the redox couple

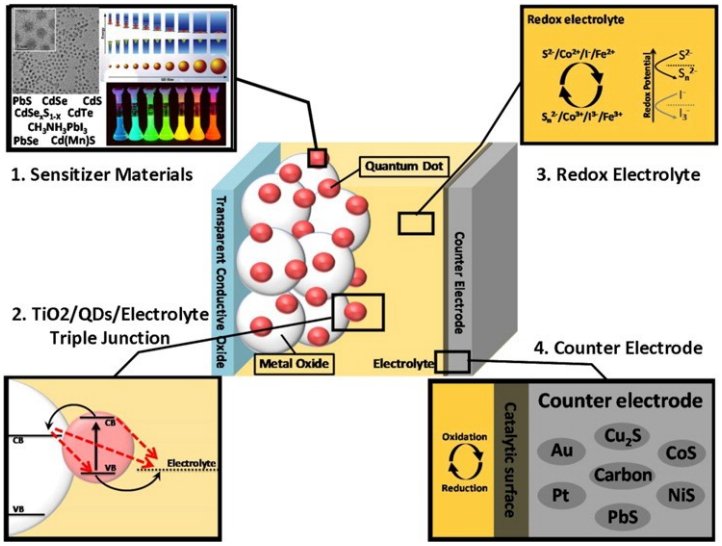

Figure 1.8: Important steps for the fabrication of QDSSCs.

- Interfacial recombination of electrons from TiO_2 and the oxidized form of the redox couple [71-74].

1.7.2 Random Lasers

Random laser(RL) differs from conventional laser in that its cavity is formed not by mirrors but by multiple scattering in a disordered gain medium as shown in figure 1.9, in which a random collection of QDs containing laser dye is excited (for example, by an external light source) to obtain population inversion. The QDs then scatter light and amplify it in the process. The propagation of the light waves becomes that of an amplified random walk. Random lasers have been demonstrated in a variety of materials, including liquid dyes, polymers, semiconductors and dielectric crystals, and their potential applications range from medicine to laser fusion. The two major elements of conventional lasers are the gain medium, which provides light amplification, and the optical resonator (cavity), which provides feedback and, in its simplest form, can consist of just two parallel mirrors. In contrast, random lasers do not require any cavity or optics besides possibly the optics used in the pumping channel. This makes them inexpensive, simple and robust in

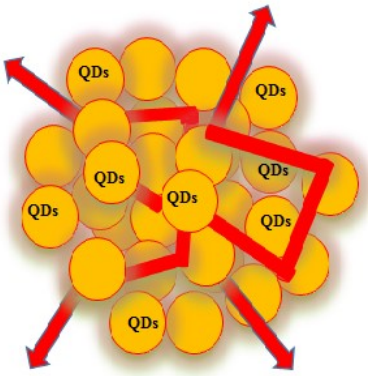

Figure 1.9: Multiple light scattering with gain.

operation[75-78]. Random lasers have been classified as incoherent feedback RL and coherent feedback RL as shown in figure 1.10.

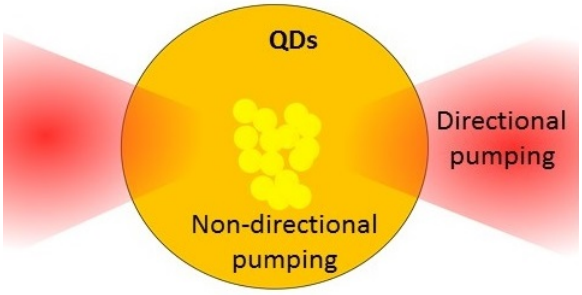

Figure 1.10: Different classes of random laser emission.

In the first random laser proposed by Letokhov in 1967, the incoherent feedback was governed by photon diffusion in an ensemble of scatterers. The wavelength of the random laser emission is determined by the maximum of the gain spectrum rather than the feedback. In random lasers with coherent feedback, the mode density is much lower, and the emission peaks corresponding to different lasing modes are well resolved. However, these spectral lines are randomly positioned, and statistically the spectrum of stimulated emission is again determined by the gain band [79-80].

1.8 Overall aim and organization of the thesis

The overall aim of the study was to optimize and characterize photonic material for photonic device applications using thermo optic and nonlinear- optical methods. Within this broad theme, the research had a number of specific objectives:

- To select a potential photonic material for the study
- Characterize the material by thermo-optic and nonlinear optical methods.
- To explore the ideas for the development of photonic device applications.

The relationship between the chapters and the general organization of the thesis are presented in figure 1.11. In this thesis, investigations

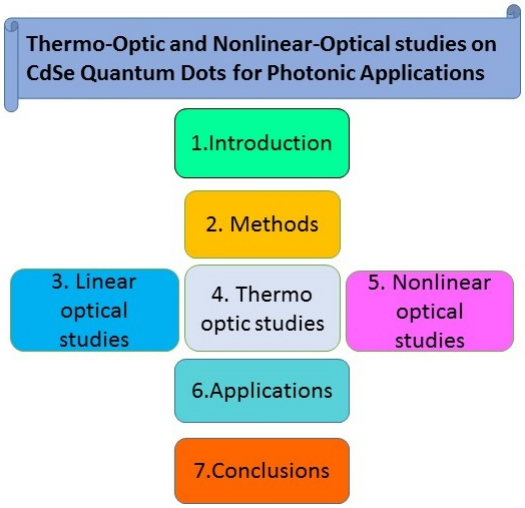

Figure 1.11: The general organization of the thesis and the connections between individual chapters.

on CdSe QD based materials which have tunable optical properties is synthesized and characterized for photonic applications.The preparation of Quantum dot sensitized solar cells using prepared CdSe QDs is one of the important applications we studied. Performance of Random lasers

using these material as scatters is also observed. Calculations on thermal diffusivity, optical limiting and nonlinear susceptibility of the samples are also valuable parameters for various applications in photonics.

1.9 References

[1] S. Kasap and P. Capper, Springer Handbook of Electronic and Photonic Materials. Springer Science & Business Media, 2007.

[2] A. Serpengzel, G. Badenes and G. C. Righini,"Photonic materials, devices, and applications II," in Proceeding of SPIE, 2007, pp. 659310.

[3] N. A. George, Photoacoustic and PT Deflection Studies on Certain Selected Photonic Materials, Ph. D. Thesis. CUSAT,Kochi,2001.

[4] P. Knight, "Fundamentals of Photonics," Journal of Modern Optics, vol. 39, pp. 1400-1400, 1992.

[5] L. M. Irimpan, Spectral and Nonlinear Optical Characterization of ZnO Nanocomposites,Ph. D. Thesis. CUSAT,Kochi,2008.

[6] A. Kurian, Characterization of Photonic Materials using Thermal Lens Technique,Ph. D. Thesis. CUSAT,Kochi, 2002.

[7] Y. Shen, C. S. Friend, Y. Jiang, D. Jakubczyk, J. Swiatkiewicz and P. N. Prasad,"Nanophotonics: interactions, materials, and applications," The Journal of Physical Chemistry B, vol. 104, pp. 7577-7587, 2000.

[8] P. N. Prasad, Nanophotonics. John Wiley & Sons, 2004.

[9] R. Kirchain and L. Kimerling, "A roadmap for nanophotonics," Nature Photonics, vol. 1, pp. 303-305, 2007.

[10] V. M. Shalaev and S. Kawata, Nanophotonics with Surface Plasmons. Elsevier, 2006.

[11] T. Yao and J. Woo, Physics and Applications of Semiconductor Quantum Structures. CRC Press, 2001.

[12] X. Peng, L. Manna, W. Yang, J. Wickham, E. Scher, A. Kadavanich and A. P. Alivisatos,"Shape control of CdSe nanocrystals," Nature, vol. 404, pp. 59-61, 2000.

[13] Z. A. Peng and X. Peng,"Nearly monodisperse and shape-controlled CdSe nanocrystals via alternative routes: nucleation and growth," J. Am. Chem. Soc., vol. 124, pp. 3343-3353, 2002.

[14] V. Jungnickel and F. Henneberger,"Luminescence related processes in semiconductor nanocrystals-the strong confinement regime," J Lumin, vol. 70, pp. 238-252, 1996.

[15] Norris, D. J., and M. G. Bawendi."Measurement and assignment of the size-dependent optical spectrum in CdSe quantum dots." Physical Review B vol.53,pp.16338,1996.

[16] A. M. Smith and S. Nie,"Semiconductor nanocrystals: structure, properties, and band gap engineering," Acc. Chem. Res., vol. 43, pp. 190-200, 2009.

[17] C. B. Murray, S. Sun, W. Gaschler, H. Doyle, T. A. Betley and C. R. Kagan,"Colloidal synthesis of nanocrystals and nanocrystal superlattices," IBM Journal of Research and Development, vol. 45, pp. 47-56, 2001.

[18] I. Moreels, K. Lambert, D. Smeets, D. De Muynck, T. Nollet, J. C. Martins, F. Vanhaecke, A. Vantomme, C. Delerue and G. Allan,"Size-dependent optical properties of colloidal PbS quantum dots," ACS Nano, vol. 3, pp. 3023-3030, 2009.

[19] R. Vinayakan and K. George Thomas, Cadmium Selenide Based Core-Shell Quantum Dots for Biosensing and Imaging Applications, PhD diss., National Institute for Interdisciplinary Science and Technology, CSIR, 2009.

[20] C. N. R. Rao, A. Mller and A. K. Cheetham, Nanomaterials Chemistry: Recent Developments and New Directions. John Wiley & Sons, 2007.

[21] L. Brus,"Zero-dimensional excitons in semiconductor clusters," Quantum Electronics, IEEE Journal Of, vol. 22, pp. 1909-1914, 1986.

[22] L. Brus,"Electronic wave functions in semiconductor clusters: experiment and theory," J. Phys. Chem., vol. 90, pp. 2555-2560, 1986.

[23] M. Jarosz, The Physics and Chemistry of Transport in CdSe Quantum Dot Solids, PhD diss., Massachusetts Institute of Technology, 2004.

[24] C. E. Finlayson, D. S. Ginger and N. C. Greenham, "Enhanced Frster energy transfer in organic/inorganic bilayer optical microcavities," Chemical Physics Letters, vol. 338, pp. 83-87, 2001.

[25] D. V. Talapin, A. L. Rogach, A. Kornowski, M. Haase and H. Weller, "Highly luminescent monodisperse CdSe and CdSe/ZnS nanocrystals synthesized in a hexadecylamine-trioctylphosphine oxide-trioctylphospine mixture," Nano Letters, vol. 1, pp. 207-211, 2001.

[26] J. Piprek, Semiconductor Optoelectronic Devices: Introduction to Physics and Simulation. Academic Press, 2003.

[27] F. W. Wise, "Lead salt quantum dots: the limit of strong quantum confinement," Acc. Chem. Res., vol. 33, pp. 773-780, 2000.

[28] R. Shahid,"Green Chemical Synthesis of II-VI Semiconductor Quantum Dots," KTH Royal Institute of Technology, 2012.

[29] S. Mahajan, M. Rani, R. Dubey and J. Mahajan,"Synthesis of cdse crystal using hot injection method,"International Journal of Latest Research in Science and Technology ,Vol.2,Pp.518-521 , 2013 .

[30] V. Mlinar, "Engineered nanomaterials for solar energy conversion," Nanotechnology, vol. 24, pp. 042001, 2013.

[31] J. Xu and M. Xiao,"Lasing action in colloidal CdS/CdSe/CdS quantum wells," Appl. Phys. Lett., vol. 87, pp. 173117, 2005.

[32] W. Xu, Y. Wang, S. Liang, R. Xu, G. Zhang, F. Xu and D. Yin,"Optimized synthesis and fluorescence spectrum analysis of CdSe quantum dots," J. Dispersion Sci. Technol., vol. 29, pp. 953-957, 2008.

[33] X. Xu, Y. Wang, L. Zhou, L. Wu, J. Guo, Q. Niu, L. Zhang and Q. Liu, "Synthesis and characterisation of CdSe nanocrystals using NaHSeO3 as selenium source," Micro & Nano Letters, vol. 7, pp. 589-591, 2012.

[34] M. L. Landry, T. E. Morrell, T. K. Karagounis, C. Hsia and C. Wang, "Simple Syntheses of CdSe Quantum Dots," J. Chem. Educ., vol. 91, pp. 274-279, 2013.

[35] J. Winefordner and I. Kolthoff," A Series of Monographs on Analytical Chemistry and Its Applications", Chemical analysis-new york-interscience then john wiley,1993.

[36] Lyjo, Joseph K., and P. Radhakrishnan. "Optical and thermal characterization of dye intercalated montmorillonites and rare earth doped materials." PhD diss., Cochin University of Science And Technology, 2009.

[37] R. Philip,"Nonlinear optical properties of selected laser dyes investigated using photoacoustics, fluorescence and stimulated scattering hot injection method", Ph. D. Thesis. CUSAT,Kochi,1993.

[38] E. D. Olsen, Modern Optical Methods of Analysis. McGraw-Hill Companies, 1975.

[39] Vladimir P.. Zharov and V. S. Letokhov, Laser Optoacoustic Spectroscopy. Springer Berlin, 1986.

[40] J. RAVI, Photothermal and Photoacoustic Investigations on Certain Polymers and Semiconducting Materials, Ph. D. Thesis. CUSAT. . Kochi,2003

[41] C. Bindhu and C. Girijavallabhan, Studies on Laser Induced Phatothermal Phenomena in Selected Organic Compounds and Fullerenes, Ph. D. Thesis. CUSAT,Kochi,1998.

[42] A. R. Kumar, applications of laser induced photoacoustic effect for the study of gases and solids, Ph. D. Thesis. CUSAT,Kochi,1992.

[43] H. H. Jaff and M. Orchin, "Theory and applications of ultraviolet spectroscopy," 1962.

[44] E. L. Wehry, Modern Fluorescence Spectroscopy. Plenum Press, 1976.

[45] D. Fournier,"AC Boccara in Photothermal Investigations of Solids and Fluids, ed. JA Sell," 1989.

[46] T. Nandini, photohermal investigations on certain organic molecules and their plasma polymerised thin films.,Ph. D. Thesis. CUSAT,Kochi, 2005.

[47] R. L. Thomas, Synthesis and Characterization of Tellurium Oxide Glasses for Photonic Applications, Ph. D. Thesis. CUSAT,Kochi,2013.

[48] H. Fan, X. Wang, Q. Ren, X. Zhao, G. Zhang, J. Chen, D. Xu, G. Yu and Z. Sun,"Investigation of the nonlinear absorption and optical limiting properties of two [Q] 2 [Cu (C 3 S 5) 2] compounds," Optics &Laser Technology, vol. 42, pp. 732-736, 2010.

[49] I. Gerdova and A. Hach, "Third-order non-linear spectroscopy of CdSe and CdSe/ZnS core shell quantum dots," Opt. Commun., vol. 246, pp. 205-212, 2005.

[50] L. De Boni, E. L. Wood, C. Toro and F. E. Hernandez,"Optical saturable absorption in gold nanoparticles," Plasmonics, vol. 3, pp. 171-176, 2008.

[51] M. A. K. Abdelhalim, M. M. Mady, M. M. Ghannam, M. S. Al-Ayed and A. Alhomida, "The effects of gold nanoparticles size and concentration on viscosity, flow activation energy, dielectric and optical properties," African Journal of Biotechnology, vol. 10, pp. 13121-13127, 2013.

[52] D. Maikhuri, S. Purohit and K. Mathur,"Linear and nonlinear intraband optical properties of ZnO quantum dots embedded in SiO_2 matrix," AIP Advances, vol. 2, pp. 012160, 2012.

[53] N. Venkatram, R. S. S. Kumar and D. N. Rao, "Nonlinear absorption and scattering properties of cadmium sulphide nanocrystals with its application as a potential optical limiter," J. Appl. Phys., vol. 100, pp. 074309, 2006.

[54] H. Fan, X. Wang, Q. Ren, X. Zhao, G. Zhang, J. Chen, D. Xu, G. Yu and Z. Sun, "Investigation of the nonlinear absorption and optical limiting properties of two [Q] 2 [Cu (C 3 S 5) 2] compounds," Optics &Laser Technology, vol. 42, pp. 732-736, 2010.

[55] I. Gerdova and A. Hach, "Third-order non-linear spectroscopy of CdSe and CdSe/ZnS core shell quantum dots," Opt. Commun., vol. 246, pp. 205-212, 2005.

[56] H. Chen, C. Su, J. Chen, T. Yang, N. Hsu and W. Li, "Preparation and characterization of pure rutile TiO_2 nanoparticles for photocatalytic study and thin films for dye-sensitized solar cells," Journal of Nanomaterials, vol. 2011, pp. 47, 2011.

[57] F. A. de Castro, F. Nesch, C. Walder and R. Hany,"Challenges found when patterning semiconducting polymers with electric fields for organic solar cell applications," Journal of Nanomaterials, vol. 2012, pp. 10, 2012.

[58] T. Zdanowicz, T. Rodziewicz and M. Zabkowska-Waclawek, "Theoretical analysis of the optimum energy band gap of semiconductors for fabrication of solar cells for applications in higher latitudes locations," Solar Energy Mater. Solar Cells, vol. 87, pp. 757-769, 2005.

[59] J. Tian, R. Gao, Q. Zhang, S. Zhang, Y. Li, J. Lan, X. Qu and G. Cao,"Enhanced performance of CdS/CdSe quantum dot cosensitized solar cells via homogeneous distribution of quantum dots in TiO2 film," The Journal of Physical Chemistry C, vol. 116, pp.18655-18662, 2012.

[60] G. K. Mor, K. Shankar, M. Paulose, O. K. Varghese and C. A. Grimes, "Use of highly-ordered TiO_2 nanotube arrays in dye-sensitized solar cells," Nano Letters, vol. 6, pp. 215-218, 2006.

[61] Y. Li, L. Wei, R. Zhang, Y. Chen and J. Jiao,"Annealing effect on photovoltaic performance of CdSe quantum-dots-sensitized TiO_2 nanorod solar cells," Journal of Nanomaterials, vol. 2012, pp. 1, 2012.

[62] I. Hod, V. Gonzlez-Pedro, Z. Tachan, F. Fabregat-Santiago, I. Mora-Ser, J. Bisquert and A. Zaban,"Dye versus quantum dots in sensitized solar cells: participation of quantum dot absorber in the recombination process," The Journal of Physical Chemistry Letters, vol. 2, pp. 3032-3035, 2011.

[63] I. Hod and A. Zaban,"Materials and interfaces in quantum dot sensitized solar cells: Challenges, advances and prospects," Langmuir, vol. 30, pp. 7264-7273, 2013.

[64] B. O'regan and M. Grtzel,"A low-cost, high-efficiency solar cell based on dye-sensitized colloidal TiO_2 films," 1991.

[65] Y. Li, L. Wei, R. Zhang, Y. Chen and J. Jiao,"Annealing effect on photovoltaic performance of CdSe quantum-dots-sensitized TiO_2 nanorod solar cells," Journal of Nanomaterials, vol. 2012, pp. 1, 2012.

[66] C. Hgglund, M. Zch and B. Kasemo,"Enhanced charge carrier generation in dye sensitized solar cells by nanoparticle plasmons," Appl. Phys. Lett., vol. 92, pp. 013113, 2008.

[67] Mrunal Deshpande, R.Seyezhai, "Review of hybrid solar cells based on cdse and tio_2 materials" ,international journal of innovative research in computer and communication engineering,Vol. 2, pp.3387-3392,2014.

[68] M. Yamaguchi,"Multi-junction solar cells and novel structures for solar cell applications," Physica E: Low-Dimensional Systems and Nanostructures, vol. 14, pp. 84-90, 2002.

[69] J. Tian, R. Gao, Q. Zhang, S. Zhang, Y. Li, J. Lan, X. Qu and G. Cao, "Enhanced performance of CdS/CdSe quantum dot cosensitized solar cells via homogeneous distribution of quantum dots in TiO2 film," The Journal of Physical Chemistry C, vol. 116, pp. 18655-18662, 2012.

[70] H. A. Atwater and A. Polman,"Plasmonics for improved photovoltaic devices," Nature Materials, vol. 9, pp. 205-213, 2010.

[71] K. Catchpole and A. Polman,"Plasmonic solar cells," Optics Express, vol. 16, pp. 21793-21800, 2008.

[72] S. Fahr, C. Rockstuhl and F. Lederer,"Metallic nanoparticles as intermediate reflectors in tandem solar cells," Appl. Phys. Lett., vol. 95, pp. 121105, 2009.

[73] S. Divya, A. Thankappan, C. Vallabhan, V. Nampoori, P. Radhakrishnan and A. Mujeeb, "Electrolyte/photoanode engineered performance of TiO2 based dye sensitised solar cells," J. Appl. Phys., vol. 115, pp. 064501, 2014.

[74] K. Catchpole and A. Polman, "Plasmonic solar cells," Optics Express, vol. 16, pp. 21793-21800, 2008.

[75] Y. Wang, V. D. Ta, Y. Gao, T. C. He, R. Chen, E. Mutlugun,H. V. Demir and H. D. Sun,"Stimulated Emission and Lasing from CdSe/CdS/ZnS CoreMultiShell Quantum Dots by Simultaneous ThreePhoton Absorption," Adv Mater, vol. 26, pp. 2954-2961, 2014.

[76] L. Cerdn, E. Enciso, V. Martn, J. Bauelos, I. Lpez-Arbeloa, A. Costela and I. Garca-Moreno,"FRET-assisted laser emission in colloidal suspensions of dye-doped latex nanoparticles," Nature Photonics, vol. 6, pp. 621-626, 2012.

[77] H. Cao, Y. Zhao, S. Ho, E. Seelig, Q. Wang and R. Chang, "Random laser action in semiconductor powder," Phys. Rev. Lett., vol. 82, pp. 2278, 1999.

[78] D. S. Wiersma,"The physics and applications of random lasers," Nature Physics, vol. 4, pp. 359-367, 2008.

[79] R. C. Polson, M. E. Raikh and Z. V. Vardeny, "Universal properties of random lasers," Selected Topics in Quantum Electronics, IEEE Journal Of, vol. 9, pp. 120-123, 2003.

[80] Y. Boucher and P. Feron,"Generalized transfer function: A simple model applied to active single-mode microring resonators," Opt. Commun., vol. 282, pp. 3940-3947, 2009.

Chapter 2

Material preparation and characterization techniques

This chapter gives an overview on the synthesis of the photonic materials and their characterization techniques used in the present work. Reflux and microwave irradiation methods are used for the synthesis of CdSe QDs. Structural and linear optical characterization methods used for the study are explained. Thermal lens and photo acoustic methods are the selected thermo-optic techniques applied on the material while Z-scan method is used for the nonlinear-optical characterization. Experimental methods along with the theory of these techniques are discussed. Basic ideas of solar cell and random lasers are given as the applications of CdSe QDs.

2.1 Introduction

Nanotechnology represents the design, production and application of materials at atomic, molecular and macromolecular scales, in order to produce new nanosized materials. Advances in nanophotonics devices have proceeded rapidly for the last 10 years. It causes an enormous increase in number and diversity of photonic applications which have resulted from significant advances in the computational design tools and their accessibility, the emergence of new nanofabrication technique and realization of new optical and structural characterization methods. The selection of appropriate method for the preparation of nanoparticles (NPs) depends on the physical, chemical character of the material to be loaded. Synthesis of NPs using microwave heating has been on the increase in recent years. Fabrication of high quality NPs can be achieved by simple operations compared with the more conventional NP synthesis methods. Applications of NPs in various fields require an inexpensive and simple process of synthesizing high quality shaped NPs. In this regard, recent years have witnessed significant research being done in the use of microwave radiation in NP synthesis. Although various techniques have been applied for the synthesis of NPs, there are some features to consider that are common to all the methods. That is, the synthesis of NPs requires the use of a device or process [1, 2] that fulfills the following conditions:

- Control of particle size, shape, size distribution, crystal structure and composition distribution .
- Improvement of the purity of NPs.
- Control of aggregation.
- Stabilization of physical properties, structures and reactants.
- Higher reproducibility .
- Higher mass production, scale-up and lower costs.

2.2 Preparation methods of nanoparticles

Methods of preparation of NPs can be divided into physical and chemical methods based on whether or not there exist resonant chemical reactions. On the other hand, these methods can be classified in to solid phase synthesis, liquid phase synthesis, gas phase synthesis and vapour phase synthesis. Solid phase method includes thermal decomposition, solid state reaction, spark discharge and stripping and milling methods. Liquid phase method for synthesizing NPs includes mainly precipitation, hydrolysis, spray, solvent thermal, solvent evaporation pyrolysis, oxidation reduction, emulsion, radiation, chemical synthesis and sol-gel processing. The gas phase method includes gas-phase evaporation method, chemical vapor reaction, chemical vapor condensation and sputtering method. In our work we emphasize synthesis of NPs in the liquid phase. A brief description of the other methods like gas phase synthesis and vapour phase synthesis [3] are also given.

2.2.1 Liquid phase synthesis

- Co-precipitate method: It is a method of carrying down of substances by a precipitate, normally soluble under the conditions employed. It involves simultaneous occurrence of nucleation, growth, coarsening or agglomeration process.

- Sol-gel processing: In materials science, the sol-gel process is a method for producing solid materials from small molecules. The method is used for the fabrication of metal oxides.

- Microemulsion: Microemulsion method is one of the recent and ideal techniques for the preparation of inorganic NPs. Oil and water are immersible and they separate into two phases when mixed, each saturated with traces of the other component. An attempt to combine the two phases requires energy that would establish water-oil association replacing the water-water/oil-oil contacts[4,5].

- Sonochemical synthesis: Sonochemistry is the application of ultrasound to chemical reactions and processes. The mechanism causing sonochemical effects in liquids is the phenomenon of acoustic cavitation.

- Template synthesis: Template-assisted electrodeposition is an important technique for synthesizing metallic nanomaterials with controlled shape and size. Arrays of nanostructured materials with specific arrangements can be prepared by this method, employing either an active or restrictive template as a cathode in an electrochemical cell.
- Biomimetic synthesis: Biomimetic synthesis is a branch of natural product synthesis that aims to synthesize a target molecule through a series of reactions, and passing through intermediate structures, that are closely related to those that occur during biosynthesis in its natural source.
- Hydrothermal/Solvothermal: Solvothermal synthesis is a method for preparing a variety of materials such as metals, semiconductors, ceramics, and polymers. The process involves the use of a solvent under moderate to high pressure and temperature that facilitates the interaction of precursors during synthesis. If water is used as the solvent, the method is called hydrothermal synthesis.

Reflux method for the synthesis of nanophotonic materials

Reflux method is one of the hydrothermal methods which is used to apply thermal energy to a chemical reaction. In this method, a liquid reaction mixture is placed in a vessel open only at the top and is connected to a condenser such that any vapours given off are cooled back to liquid, and fall back into the reaction vessel. To thermally accelerate the reaction, it is carried out at an elevated temperature. The main advantage of this technique is that it can be left for a long period of time without the need to add more solvent or fear of the reaction vessel boiling dry as any vapour is immediately condensed in the condenser. In order to boil the given solution at a certain temperature, one can be sure that the reaction will proceed at a constant temperature always. The choice of solvent is an important factor through which, one can control the temperature within a very narrow range. This technique is also useful for performing chemical reactions under controlled conditions that require substantial time for completion [6, 7]. Figure 2.1 shows a typical reflux apparatus for supplying thermal energy for the chemical reactions. It includes an optional beaker of water between the reactants

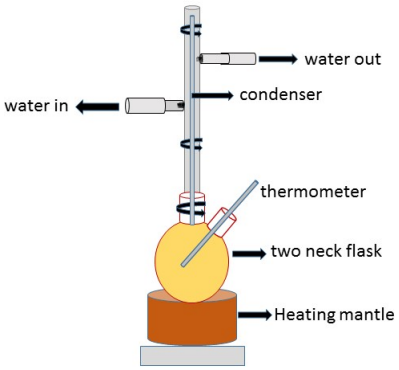

Figure 2.1: Laboratory reflux apparatus.

and the heat. In our experiments we used a two necked flask with one neck to keep the thermometer inside and the condenser is fit in the other neck. Inlet and outlet for water are included. Furthermore, a high boiling, thermally stable silicone oil is an option to immerse the reaction vessel, rather than water which evaporates too readily to be useful for lengthy reactions. Using an oil bath, temperatures of up to several hundred degrees can easily be achieved, which is higher than the boiling point of most commonly used solvents. If even higher temperatures are required, the oil bath can be replaced with a sand bath.

Microwave synthesis

In recent times, a microwave-assisted method has been widely applied in chemical reactions and synthesis of nanomaterials. It is an attractive method to promote reactions by effective heating compared to conventional heat conduction methods due to the direct heating of the reaction mixture. In conventional heating methods, the vessel is heated and subsequently transfers the heat by convection. In other words microwave heating is more efficient in terms of the energy used, produces higher temperature homogeneity, and is considerably more rapid than conventional heat sources. Microwave heating is a transfer of electromagnetic energy to thermal energy, and is an energy conversion phenomenon rather than the heat transfer. The electric component of an electromagnetic field causes heating by two main mechanisms, dipole

interaction mechanism and ionic conduction mechanism. Main features of these interactions between materials and microwaves are based on:-

- Both require effective coupling between target material and rapidly oscillating electromagnetic field of microwaves.
- Dipole interaction occurs with polar molecules.
- Polar end of the molecules reorient themselves and oscillates in steps with the oscillating electric field of microwaves.
- Heat is generated by molecular collision and friction.
- Generally, more polar the molecule the more effectively it will couple with microwave field.
- Nanostructures with smaller size distribution and higher degree of crystallization are obtained under microwave heating than in conventional heating.

In dipole interaction mechanism, for a substance to generate heat when irradiated with microwaves it must possess a dipole moment, as in water molecule which possess a very high dipole moment. The greater the polarity of a molecule, the more pronounced the microwave effect with regard to the rise in temperature [8, 9]. A dipole is sensitive to external electric fields and will attempt to align itself with the field by rotation. The applied field offers the energy for the molecules to collide with one another and heats the sample. High and low frequency radiation does not give rise to effective heating because in the first case, the field oscillates so well that there is no random motion generated and in the second case, the molecules follow the field so closely that there is no random motion generated [10, 11]. Second mechanism is the conduction process which is a much stronger interaction than the dipolar mechanism with regard to the heat-generating capacity. In this case mobile charge carriers like electrons, ions, etc. move relatively easily through the material under the influence of the microwave electric field. These induced currents will cause heating in the sample due to electrical resistance. In the same way as visible light, infrared irradiation, and UV irradiation, microwave energy is also delivered directly to the material through molecular interaction with the electromagnetic field. Since microwaves

can penetrate the material and supply energy, heat can be generated throughout the volume of the material resulting in volumetric heating [12]. Additionally, the method shows acceleration in reaction rate, yield improvement, short reaction time, small particle size, narrow particle size distribution, high purity materials, and enhanced physical-chemical properties [13-15].

2.2.2 Gas phase synthesis

This process involves super saturation achieved by vaporizing material into background gas and then cooling the gas. The gas phase method includes gas-phase evaporation method, chemical vapour reaction method, chemical vapor condensation and sputtering method. It can also be classified with the precursors used as:

- Methods using solid precursors

1. Inert gas condensation
2. Pulsed laser ablation
3. Spark discharge generation
4. Ion sputtering

- Methods using liquid or vapour precursors

1. Chemical vapour synthesis
2. Spray pyrolysis
3. Laser pyrolysis/photo chemical synthesis
4. Thermal plasma synthesis
5. Flame synthesis
6. Low temperature reactive synthesis

2.2.3 Vapour phase synthesis

This involves same mechanism as liquid phase reaction. Here, elevated temperature with vacuum is used for the reaction process. Vapour phase mixture rendered thermodynamically is unstable relative to formation of desired solid material.

Characterization techniques

Characterization techniques of materials are important to researchers as they are the basic tools in identifying the structure and thereby properties of materials synthesized, which help in determining whether the designed materials are suitable for particular applications. We present the experimental techniques to find out the structural, thermal, linear and nonlinear optical properties of samples and its applications as photonic materials.

2.3 Structural characterization techniques

X-ray diffraction (XRD), Fourier transform infrared spectroscopy (FTIR), Dynamic light scattering (DLS) method for particle size analysis, Transmission electron microscopy (TEM) and Scanning electron microscopy (SEM) are the main techniques used for the structural characterization of our samples in this thesis.

2.3.1 X-ray diffraction spectroscopy (XRD)

X-ray diffraction, often abbreviated as XRD, is extensively used to characterize the crystalline form of nanoparticles to estimate the crystalline sizes and for the study of crystal structures and atomic spacing. Since this method often utilizes X-ray diffraction from nanoparticles in powder form, it is called powder diffraction. This rapid analytical technique can provide information on unit cell dimensions and the crystalline nature of the sample. Max von Laue, in 1912, discovered that crystalline substances act as three-dimensional diffraction gratings for X-ray wavelengths similar to the spacing of planes in a crystal lattice. The basic principle behind XRD is the constructive interference of monochromatic X-rays from a crystalline sample. The interaction of the incident rays

with the sample produces constructive interference and a diffracted ray when conditions satisfy Bragg's Law [16].

$$2dsin(\theta) = n\lambda \tag{2.1}$$

This law relates the wavelength of electromagnetic radiation to the diffraction angle and the lattice spacing in a crystalline sample. These diffracted X-rays are then detected, processed and counted. By scanning the sample through a range of 2θ angles, all possible diffraction directions of the lattice could be attained due to the random orientation of the powdered material. Conversion of the diffraction peaks to d-spacing allows identification of the mineral because each mineral has a set of unique d-spacing. If a material does not show this diffraction peaks it confirms that the material is not a crystal and must be non-crystalline or amorphous. We used a Bruker AXS D8 Advance X-ray diffractometer with Ni-filtered Cu Kα (1.5406$\mathring{A}$) source to investigate the structural properties of the samples.

2.3.2 Fourier transform infrared spectroscopy (FTIR)

This non-destructive techniques provide extensive information about the structure and vibrational properties along with the characterizing covalent bonding information. FTIR is used to gather information about the structure of a compound and as an analytical tool to assess the purity of a compound. In the experimental section of IR spectroscopy, an organic molecule is exposed to infrared radiation and when the radiant energy matches the energy of a specific molecular vibration, absorption occurs. The wavenumber, plotted on the X-axis, is proportional to energy; therefore, the highest energy vibrations are on the left. The percent transmittance (%T) is plotted on the Y-axis. Absorption of radiant energy is therefore represented by a trough in the curve: zero transmittance corresponds to 100% absorption of light at that wavelength [17]. IR source emits an IR beam which is split into two identical beams; one goes through the sample and the other through a reference cell. IR spectroscopy is used to measure the amount of energy absorbed when the frequency of the infrared light is varied. In our works the FTIR spectra of the samples were recorded using Thermo NICOLET 380 FTIR Spectrometer by means of KBr pellet procedure[18].

2.3.3 Dynamic light scattering analysis (DLS)

DLS method is a well-established technique for measuring the size of particles and macromolecules typically in the sub micron region down to below 1 nanometer. It is sometimes referred to as Photon correlation spectroscopy (PCS) or quasi-elastic light scattering (QELS) method and is suitable to measure samples which consist of particles suspended in a liquid or emulsions. The basic mechanism behind is that, particles in suspension undergo Brownian motion caused by thermally induced collisions between the suspended particles and solvent molecules. If the particles are illuminated with a laser, the intensity of the scattered light fluctuates over very short time scales at a rate that is dependent upon the size of the particles; smaller particles are displaced further by the solvent molecules and move more rapidly. Analysis of these intensity fluctuations yields the velocity of the Brownian motion and hence the particle size using the Stokes-Einstein relationship.

The term hydrodynamic diameter is used to indicate the diameter measured in DLS method which refers to the way a particle diffuses within a fluid. This means that the particle size will be larger than measured by electron microscopy, and it is important to note that DLS produces an intensity weighted particle size distribution, which means that the presence of over sized particles can dominate the particle size result.

A conventional DLS instrument consists of a laser light source, which converges to a focus in the sample using a lens. Light is scattered by the particles at all angles and a single detector, traditionally placed at 90° to the laser beam, collects the scattered light intensity. Laser diffraction measures particle size distributions by measuring the angular variation in intensity of light scattered as a laser beam passes through a dispersed particulate sample. Large particles scatter light at small angles relative to the laser beam and small particles scatter light at large angles. The angular scattering intensity data is then analyzed to calculate the size of the particles responsible for creating the scattering pattern, using the Mie theory of light scattering. The particle size is reported as a volume equivalent sphere diameter[19]. We have used nanoparticle analyzer SZ-100 (Horiba)for the particle size measurement.

- **Measurement of Zeta potential**

It is one of the fundamental parameters known to affect dispersion stability. It is a measure of the magnitude of the electrostatic or charge repulsion or attraction between particles in a liquid suspension. It can also be done with Dynamic light scattering instrument system described above. Its measurement brings detailed insight into the causes of dispersion, aggregation or flocculation and can be applied to improve the formulation of dispersions, emulsions and suspensions [19, 20].

2.3.4 Transmission electron microscopy (TEM)

TEM is a tool utilized to analyze the structures of very thin specimens through which electrons as probes are transmitted. TEM image provides reliable information about the size and shapes of nanoparticles. The principle of operation in this instrument is similar to an optical microscope, where an electron beam, like light in a transmission microscope, travels through the sample and is affected by the structures in the specimen. Transmitted electron beam is projected onto a phosphor screen for imaging. A TEM consists of the following components:

1. An electron gun that produces a stream of monochromatic electrons
2. Electromagnetic condenser lenses that focus the electrons into a small beam
3. A condenser aperture to restrict the beam by eliminating the high-angle electrons
4. A sample stage on which the sample is placed
5. An objective lens to focus the transmitted beam
6. Optional objective and selected area metal apertures to enhance the contrast by blocking out high-angle diffraction, as well as to obtain electron diffraction
7. Subsequent intermediate and projector lenses to enlarge the image
8. Optical recording of the image carried by the transmitted electron beams

As the high energy electrons pass through the thin specimen, scattering occurs at the atoms because of Coulomb interactions. The degree of scattering depends on the constituent atoms of the specimen.The intensity distribution of the electrons reaching the fluorescent screen is determined by the number of electrons transmitted. This results in a relative darkness in the specimen image area, which is rich in heavy atoms and thus, TEM image provides reliable information about the size and shapes of nanoparticles. The electron micrograph images of our samples in colloidal form were obtained using transmission electron microscope of Philips Technai G2 at 120 kV [21].

2.3.5 Scanning electron microscopy (SEM)

SEM is a technique to obtain the image of a sample, by scanning of an electron beam across the surface of specially prepared specimens. It provides a greatly enlarged and highly resolved three-dimensional view of the specimen's exposed structure. An electron beam from an electron gun is focused onto the specimen surface by condenser lenses and this electron beam spot size determines the resolution of the image, which is finally obtained by scanning. A set of scanning coils deflects the electron beam which allows scanning of the surface in a grid fashion. There are several types of signals which are produced when the focused electron beam impinges on a specimen surface, to form an SEM image. They include back-scattered electrons, secondary electrons, cathode luminescence, and low-energy characteristic X rays generated by the impinging electrons. The signals obtained from specific emission volumes within the sample are used to measure composition, surface topography, crystallography, magnetic or electric character, etc. The secondary and back-scattered electrons are captured by a detector and are primarily responsible for topographic images. Thus, in principle, every point spot on a specimen is transposed to a corresponding point on the CRT and the brightness of a spot in a SEM image is a measure of the intensity of secondary electrons, which critically depends on the local surface topography. The advantage of SEM over TEM is that, it provides tremendous depth of focus [21]. Scanning electron microscopy (SEM) of our samples are performed on JEOL Model JSM-6390LV.

2.4 Linear Optical characterization

2.4.1 Absorption spectroscopy

JASCO V-570 UV/VIS/NIR Spectrophotometer was used for the absorption, transmission and reflectance measurements of the samples. The spectrometer consists of an optical system with single monochromatic, UV/VIS region (1200 lines/mm plane grating) and NIR region(300 lines/nm plane grating) of Czenry-Turner mount double beam type. The resolution is of 0.1 nm (UV/VIS region) and 0.5 nm (NIR region). Light source used are 30 mW deuterium discharge tube in 190 nm to 350 nm region and 20 W tungsten iodine lamp in 330 -2500 nm region. The total wavelength range for the analysis is 190 nm - 2500 nm. The beam from the light source is converged and enters in to the monochromator. It is dispersed by the grating in the monochromator and the light passes out through the exit slit. This light is split into two light paths by a sector mirror, one incident on the sample to be measured and the other on the reference sample such as solvent. The light that has passed through the sample or reference sample is incident on the photomultiplier tube and PbS photo conductive cell which act as the detectors.

In the reflectance measurement, the setup has to be changed. The Model SLM-468 single reflection attachment is designed to measure the relative reflectance of sample using the forward reflected light from the aluminum-deposited plane mirror as reference. It permits the measurement of the reflectance of metal deposited film, metal plating etc. The wavelength range is 220 nm to 2200 nm with a beam port diameter of 7 mm and angle of incidence approximately$\sim 5^{\circ}$[17]. For each wavelength of light passing through the spectrometer, the intensity of the light passing through the reference cell is measured as I_0. The intensity of the light I passing through the sample cell is also measured for that wavelength. If I is less than I_o, then obviously the sample has absorbed some of the light. By Beer-Lambert Law [22],the relationship between A (the absorbance) and the two intensities are given by $A = log\frac{I_0}{I}$ and the absorption coefficient, $\alpha = A/d$, d= thickness of the sample where α is given by the Taucs [23] relation to obtain the absorption edge as,

$$\alpha(\omega) = \beta \frac{(\frac{h}{2\pi}\omega - E_{opt})^n}{\frac{h}{2\pi}\omega} \tag{2.2}$$

where, β is a constant and n is an index which takes values of 2 and 1/2 for direct and indirect transitions. Band gap of CdSe QDs are calculated for direct transitions, using Tauc plot, with $(\alpha h\nu)^2$ along y-axis and E_{opt} along x-axis.

2.4.2 Fluorescence spectroscopy

The fluorescence excitation and emission spectrum of the samples were carried out using Cary eclipse fluorescence spectrophotometer of VARIAN [17]. It has a single cell holder for liquid sample analysis and a solid sample holder accessory to perform fluorescence measurements on solid samples. The solid sample holder accessory provides both rotational and translational adjustment of the sample. The angle of incidence of the excitation may be varied from $20°C - 35°C$. This is the angle between the exciting light and a line perpendicular to the surface of the sample mounting slide. The source of excitation is xenon lamp.

2.5 Photo-thermal characterization methods

Thermo-optic or photothermal (PT) spectroscopy belongs to a class of highly sensitive techniques, which can be used to measure optical absorption and thermal characteristics of a sample based on the change in thermal state of the sample resulting from the absorption of radiation. The basic principle of PT spectroscopies is the detection of the heat produced in the sample due to non-radiative de-excitation processes resulting from the absorption of intensity-modulated light by the sample. PT signals will not be affected by scattered or reflected light unlike conventional optical signal detection. Hence PT spectroscopy measures optical absorption more precisely in scattering solutions, solids and at interfaces. The large signal to noise ratio of thermo-optic techniques makes it an effective tool to study the surface and absorption properties of materials, particularly for solids. There are different PT mechanisms that can be used for the physical and chemical analyses of materials, such as photo acoustic spectroscopy, PT deflection, PT lens spectroscopy etc. Measurements of the temperature, pressure, and/ or density changes that occur due to optical absorption are ultimately the basis for these PT spectroscopic measurements. Each of these has a name indicating

the specific physical effect measured [24]. These are briefly described in the following sections.

1. Photo acoustic spectroscopy (PAS) is an indirect method for measuring optical absorption. Indirect methods do not measure light transmission or emission but rather measure an effect of sample absorption.

2. Photothermal lens spectroscopy (PTL)measures the thermal blooming that occurs when a beam of light heats a transparent sample. It is typically applied for measuring minute quantities of substances in homogeneous gas and liquid solutions.

3. Photothermal deflection (PTD) spectroscopy or the mirage effect measures the bending of light due to optical absorption. This technique is particularly useful for measuring surface absorption and for profiling thermal properties of layered materials.

4. PT diffraction, a type of four wave mixing, monitors the effect of transient diffraction gratings written into the sample with coherent lasers. It is a form of real time holography.

5. PT emission measures an increase in sample IR radiance resulting from absorption. Sample emission follows Stefan's law of thermal emission. These methods are used to measure the thermal properties of solids and layered materials.

2.5.1 Thermal lens effect

Thermal lens(TL) spectroscopy was the first PT spectroscopic method to be applied for sensitive chemical analysis. The TL effect was discovered by Gordon et al. in 1965. In this technique the sample is illuminated using a Gaussian beam having intensity distribution across the beam as

$$I_r = I_0 e^{\frac{-2r^2}{\omega^2}} \tag{2.3}$$

where ω is the beam radius. When energy from a laser beam passes through a sample, a part of the incident radiation is absorbed by the sample and subsequent nonradiative decay of excited state population results in local heating of the medium along the beam path. Heating

caused by absorption of a Gaussian beam has radial symmetry along the laser path which creates a corresponding radial temperature gradient in the sample and a blooming occurs, which is proportional to this temperature changes. Modification in refractive index causes the medium to mimic a lens, called thermal lens (TL). This lens causes beam divergence or convergence with the change in refractive index and the signal is detected as a time dependent decrease in power at the center of the beam. The thermal lens generally has a negative focal length since most materials expand upon heating and hence have negative temperature coefficient of refractive index which causes beam divergence and the signal is detected as a time dependent decrease in power at the center of the beam at far field using a probe beam.

Theory of thermal lens effect

Several experimental conditions have to be applied to derive TL theoretically [25-31]. Under pulsed and continuous wave(CW) excitation conditions, different pump or probe beam geometries and different sample conditions are some of the models applied. The theoretical procedure can be divided into three parts.
(1)The heat equation must be solved for the particular boundary conditions of the system to generate a temperature distribution within the sample.
(2)Temperature distribution must be converted into a refractive index profile.
(3)Interaction of the beam with the refractive index profile is used to predict a change in the beam intensity profile.

The different models differ primarily in the last step. A simple paraxial approximation theory is also usually used to predict changes in the beam center intensity and in the beam spot size[32, 33]. This paraxial approximation is a closed- form solution of ray tracing through a parabolic temperature rise near the beam axis. Following assumptions are involved in the model of the thermal lens.

- Beam cross section should be Gaussian and the spot of the laser beam remains constant over the length of the sample cell.
- The thermal conduction is the main mechanism of heat transfer

while the sample is homogeneous and satisfies Beer's law.

- Intensity profile of the laser beam detection is undertaken in the far field from the sample
- The strength of the thermal lens is not sufficient to induce a change in the beam profile within the sample where the refractive index change of the sample with temperature is constant over the sample.

Consider a Gaussian beam passing through an element of an absorbing sample in which the heat flow is radial and the beam is turned on during the time interval $0 \leq t \leq t_o$.
The heat generated per unit length [34]is given by

$$Q(r)dr = \frac{2\alpha E_0}{\pi\omega^2} e^{(\frac{-2r^2}{\omega^2})} \tag{2.4}$$

where α is the absorption coefficient of the medium. E_o is the total energy in each laser pulse and ω is the beam radius at time t = 0. The temperature rise of the laser-irradiated region [35, 36] is obtained as

$$T(r,t) = \frac{2\alpha E_0}{\pi\rho c_p(\omega^2 + 8Dt)} e^{[\frac{-2r^2}{(\omega^2+8Dt)}]} \tag{2.5}$$

Then thermal diffusivity D of the sample can be calculated from the equation

$$t_c = \frac{\omega^2}{4D} \tag{2.6}$$

where ω is the beam radius at the sample position and t_c, the time response to attain the steady state focal length. The solution of equation(2.5) for CW excitation is given as [29, 30]

$$T(r,t) = \frac{2\alpha P(1 + cos\omega t)}{\pi\rho c_p(\omega^2 + 8Dt)} e^{[\frac{-2r^2}{(\omega^2+8Dt)}]} \tag{2.7}$$

Due to non-uniform radial temperature distribution, time dependent refractive index gradient formed inside the sample can be expressed as

$$n(r,t) = n_0 + (\frac{\partial n}{\partial t}) T_{(r,t)} \tag{2.8}$$

where n_o is the refractive index at time t=0. Consequently, the irradiated sample acts like a lens, which affects the laser beam intensity

profile by altering the radius. The relative change in the beam intensity is proportional to the relative changes in power of the beam reaching the detector and hence is a direct measure of the thermal lens strength. The PT lens signal is obtained by monitoring the probe laser power that passes through a pinhole placed far from the sample. The photo TL will either focus or defocus the probe laser beam so that the power at the center of the beam will either increase or decrease.

Measurement approach of TL technique

- Single beam thermal lens configuration

In single-beam TL spectrometer, the same laser is used to excite the sample and to probe the thermal lens created. In single beam TL spectrometer, the laser beam is focused with a lens and modulated with a chopper or a shutter. After passing through the sample, the beam center intensity is usually measured in the far field with a photodiode .

- Dual beam thermal lens configuration

In this method the pump beam is used to generate the thermal lens in the medium and another laser of low intensity is used to probe the lens formed. Separate lenses are used to focus pump and prob beam on to a dichroic mirror. There are two types of dual beam instrumentation: Collinear and transverse configuration. In collinear configuration, good spatial overlapping of both beams is necessary for optimal sensitivity. In transverse thermal lens experiment, the excitation beam is focused on to the sample perpendicular to the probe beam[37]. This alignment is useful for samples, which are available in very low concentration and in small volume and for chromatographic detection. Prism can be used to ensure a good overlap and counter propagation between the pump and probe beams. Dual beam technique is more advantageous since only a single wavelength (probe) is always detected and no correction for the spectral response of the optical elements and detector are required.

Experimental methods

Schematic experimental set up for thermal lens study is shown in figure 2.2. The excitation source used is a CW, 532 nm diode pumped solid

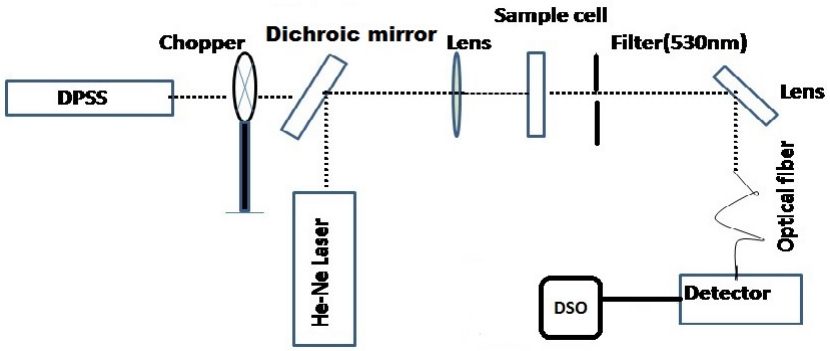

Figure 2.2: TL experimental setup using pump-probe method.

state(DPSS) laser with a maximum power of 150 mW. The power at the sample is suitably adjusted using attenuators so that the probe beam spot is free from aberrations. A 2mW He-Ne laser emitting at 632.8nm used as the probe and is arranged to be collinear with the pump using a dichroic mirror. The two beams are focused into the sample cell such that the beam area at the sample plane is the same for both pump and probe resulting in a mode matched TL arrangement. Sample was taken in a cuvette of 1 cm×1 cm path length for making the measurements. A low frequency mechanical chopper with 3 Hz is used to modulate the intensity of the pump, until the TL peak-to-peak signal is maximum. This also enables one to determine the thermal recovery of the sample. In the TL experiment the excitation laser must have Gaussian profile, so that when sample absorbs the beam with Gaussian intensity profile, the temperature distribution has a radial dependence. The temperature gradient causes refractive index gradient which behaves like a converging or diverging lens depending on whether rate of change of the refractive index with respect to temperature is positive or negative [38, 39]. The TL signal was collected using an optical fiber, which serves as the finite aperture and the same is mounted on an xyz translator. It is positioned at the center of the probe beam spot and connected to a photo detector-Digital Storage Oscilloscope (DSO) system. A filter to cut off 532 nm was used before the detector to remove the residual pump. The probe beam from the He-Ne laser which passes collinearly with pump beam experiences divergence and the beam shape expands in the presence of

a diverging thermal lens. The change in intensity of the probe beam is measured using a fast photodetector from which the relative intensity and intial slope is measured. The data are analyzed using the procedure described before[40]. Time dependent probe beam intensity follows the expression [41, 42]

$$I(t) = \frac{I_0}{1 - \theta(1 + \frac{t_c}{2t})^{-1} + \frac{1}{2}\theta^2(1 + \frac{t_c}{2t})^{-2}} \tag{2.9}$$

Here, the parameter θ is related to the thermal power radiated as heat and can be obtained with

$$I = \frac{I_0 - I_\infty}{I_\infty} \tag{2.10}$$

and

$$\theta = 1 - \sqrt{(1 + 2I)} \tag{2.11}$$

where I_0 is the initial intensity and I is the intensity after the steady state. A detailed curve fitting of this experimental data to equation (2.9) gives the time constant t_c of the thermal decay process. Finally the thermal diffusivity D of the sample can be calculated from the equation

$$t_c = \frac{\omega^2}{4D} \tag{2.12}$$

where ω is the beam radius at the sample position and t_c, the time response to attain the steady state focal length.

Advantages of thermal lens spectrometry

1. Linear PT signals are relatively independent of excitation and probe laser beam focus geometries.
2. Excitation energy or power dependent signals may be easily measured.
3. Yielding information regarding ground and excited state absorption cross sections and relaxation rate constants.
4. Data is complimentary to relaxation kinetic measurements but yield more information.
5. Sensitivity allows the use of thin optical cells.

2.5.2 Photo acoustic spectroscopy

Photo acoustic spectroscopy(PAS) is the oldest form of PT spectroscopy[43, 44]. To get a quantitative spectrum of a sample, the wavelength of excitation is scanned and the corresponding magnitude of the acoustic signal normalized by the excitation pulse energy is measured to provide an excitation spectrum called a PA spectrum[45]. This technique, called photo acoustic spectroscopy or PAS, is different from the conventional techniques. Even though the incident energy is in the form of optical photons, the interaction of these photons with the material under investigation is studied not through the subsequent detection and analysis of some of the photons, but rather through a direct measure of the energy absorbed by the material as a result of its interaction with the photon beam. The PA spectrum complements the fluorescence excitation spectrum in that, it responds to that part of the absorbed energy which is not radiated. The phase of the PA signal with respect to the phase of the input modulation can give information both on the lifetime of the excited state and on the heat energy transfer[46, 47].

Principle behind photo acoustic spectroscopy is that, when light of appropriate energy falls on a sample, a part of the absorbed energy will be degraded to random translational motion of the molecules which is in the form of heat, thus leading to a temperature rise in the cell. The absorbing sample warms and cools in a cycle if the incoming light is modulated. If the cycle is so fast that the sample does not have time to expand and contract in response to the modulated light, a change in pressure develops through the ideal gas equation PV= nRT for n moles of gas. This pressure wave can lead to the production of a sound wave. These sound waves can be detected by a sensitive microphone, piezoelectric devices, or optical methods. These techniques are more properly called PA techniques.

The magnitude of the acoustic signal depends on such properties of the sample as the absorption coefficient, the duration of the processes of conversion of absorbed radiation to heat, the thermo-physical properties, and the geometry [48, 49]. The acoustic oscillations also acquire a certain phase shift relative to the incident modulated radiation, mainly because of a considerable time lag of heat transfer processes [49-51].

Historical outlook

The PA effect in both non-gaseous and gaseous matter was first reported by Alexander Graham Bell in 1880 [50, 52]. According to him the PA effect in solids was dependent on the absorption of light and that the strength of the acoustic signal was in turn dependent on the strength of the absorption of incident light by the material in the cell. The earlier works on PA were done by Tyndall [53], Rntgen [51], Rayleigh [54] and Preece [55] et. al. The PA effect was completely undeveloped for nearly 50 years, until the advent of the microphone. The Rosencwaig-Gersho (RG) theory of the PA effect for a sample in PA cell provided a comprehensive theoretical framework which led to the rapid development and application of the effect. This led to the invention of numerous other detection schemes and to the current wide spread interest in PT science [56, 57].

General theory of the PA effect using CW excitation source in condensed media

The main source of a photo acoustic signal from a condensed sample, as measured by the gas-microphone method, arises from the periodic heat flow from the sample to the surrounding gas with the consequent change in the gas pressure within the cell. In the case of gas-microphone technique, it is often treated as an" indirect" PA generation method due to the measurements of the acoustic signals generated in the sample which are not"directly" observed.

Rosencwaig and Gersho formulated a general theory for the PA effect in condensed media [58, 59], now commonly referred to as the RG theory. It shows that in the gas-microphone measurement of a PA signal, the signal depends both on the generation of an acoustic pressure disturbance due to the periodic temperature of the sample-gas interface and on the transport of this disturbance through the gas to the microphone. The RG theory derives exact expressions for this temperature, while it considers the transport of the disturbance in the gas in an approximate experimental manner, which is, however, valid for most experimental conditions. In the following section we outline a simplified version of the salient features of the RG theory.

Indirect PA generation

Indirect PA generation is very valuable when the optical absorption is so strong that no light passes through the sample. It requires acoustic detection in a coupling fluid in contact with the sample. The main advantage of such experiment is that, spectra of totally opaque or highly light scattering materials can be measured.

- Experimental verification of the RG theory

One of the most obvious and important predictions of the RG theory is that the photo acoustic signal is linearly proportional to the power of the incident photon beam, irrespective of the sample or cell geometry. So it is possible to construct optical power meters based on the PA effect, and several of these have been described by various authors [60-62]. The variation of the PA signal amplitude as a function of sample thickness and modulation frequency for thin polymer films has been found to obey the RG theory except at very low modulation frequencies such as 10 Hz [63]. Wetsel and McDonald [64] have shown that the chopping frequency dependence of the PA signal is in agreement with the RG theory, and the predicted PA saturation has been demonstrated in aqueous solutions of the dye Methylene blue by HcClelland and Kniseley [65].

Direct PA generation by pulsed laser

Conventional PA spectroscopy utilizes a gas phase microphone which is in thermal contact with the sample of condensed matter that senses the heating and cooling of a gas layer. The acoustic signal generated in the sample with irradiated chopped light plays only a minor role in this case. Hence this technique has an inherently low sensitivity [66, 67] and is often only useful for observing absorptions typically exceeding 1%. The low coupling efficiency can be partially compensated for, however, by the use of high efficiency gas-phase microphones. It is also possible to improve the sensitivity by using piezoelectric transducers in contact with solid samples or liquid samples.

Attempts to use a pulsed laser source instead of CW modulation method seems to have been undertaken for the first time by Bonch-Bruevich et. al. [68]. However, the potential of pulsed PA spectroscopy has been

brought out and demonstrated by the pioneering work of Patel and Tam, wherein they have shown that pulsed PA spectroscopy technique, involving the use of pulsed lasers, a piezoelectric transducer in direct contact with the sample, and gated detection can have very high detection sensitivities. This technique is truly PA in character, because the original acoustic pulse generated in a condensed sample is directly detected by a piezoelectric transducer, where good acoustic impedance matching is also ensured.

Advantages of photo acoustics[48, 69]

- The main advantage of this methods is that, it can be performed on all states of matter.
- Transmitted, reflected or elastically scattered light by the sample is not detected rather a direct measure of the energy absorbed by the material as a result of its interaction with the photon beam is measured [70, 71]. This is of crucial importance when one is working with essentially transparent media, such as pollutant- containing gases, that have few absorbing centers [56] of the order of parts per trillion[48, 69].
- Optical absorption spectra of completely opaque materials can be obtained as PAS, which does not depend on the detection of photons [56]. So it can be applied to samples which are difficult to examine by conventional spectroscopic methods.
- PAS is a non-destructive method as the samples can be used as it is and depth profiles of analytes can be performed in optically transparent media.
- This non-destructive depth-profile analysis of absorption as a function of depth into a material is a unique advantage of the PAS.
- The PA effect resulting from nonradiative energy conversion process is a simple and sensitive spectroscopic tool for studying the phenomena of fluorescence and photo sensitivity in matter and is therefore complimentary to radiative and photochemical processes.

- Since the sample itself constitutes the electromagnetic radiation detector, no photoelectric device is necessary and a wide range of optical and electromagnetic wavelengths are possible for study.
- A direct measurement of non-radiative relaxation, lifetimes and the ability to gather information from sub-surface layers is possible in the method.
- One of the important advantages of this method is the scope for obtain information on thermal parameters like thermal diffusivity, thermal conductivity and thermal effusivity of the sample.
- An increase in S/N ratio with increase in input power is obtained in this method [72].

Basic requirements and experimental methods

The basic requirements of the PA detection technique are the light source, means of modulating light, appropriate photo acoustic cell, detection schemes and processing electronics equipments like DSO or lock in amplifier.

- *The light source:*
  Two m ajor classes of light sources that have been used for PA studies are the CW light sources and pulsed wave light sources. These sources can be xenon arc lamps or lasers. CW sources should possess broad wavelength output from UV to far IR and fast modulation capability while laser sources have high intensity, narrow spectral line width and modulation capability[72].
- *Modulation techniques:*
  Several methods have been employed to execute a temporal variation of the optical energy applied to a sample. The simplest form of modulating the light is using a chopper in the path of the light beam. It offers 100%modulation depths for frequencies from a few Hz to 5-8 kHz. The electro-optic modulation involves the changing of the plane of polarization of the incoming polarized laser beam in a non-linear crystal with the application of electric field on it. Acousto-optic (AO) modulation involves the spatial modulation of the laser by acoustic diffraction of the light in a crystal.

- *Photo acoustic cell:*
  PA cell contains the samples, and a fabricated piezoelectric transducer chamber to detect the acoustic signals [73]. The cell is of stainless steel body with an inner diameter of 2 cm and length 5 cm. Glass windows are fixed with flanges and O-rings to the cell for the entry and exit of the laser beam. One side of the cell has an opening in which the transducer chamber is fixed. A Lead Zirconate-Titanate -PZT- disc of 4 mm thickness and 15 mm diameter is the piezoelectric transducer that is contained in this chamber. The PZT disc is spring-loaded against the thin front diaphragm, with a thin layer of silicon grease applied between them to ensure good acoustic coupling. The PA signal is taken out through the BNC connector. Due to its high sensitivity a few μV of electrical signal could directly be obtained from the transducer with absorbing sample in the cell [73].

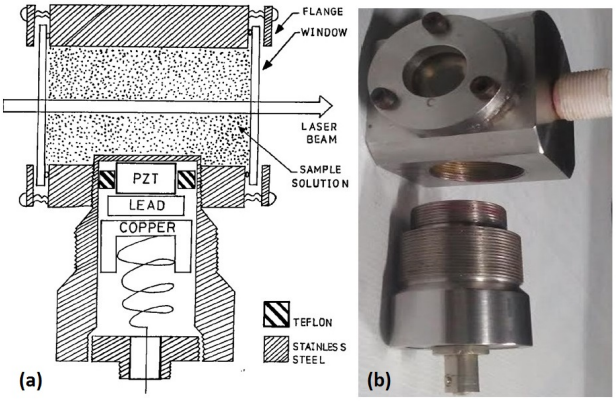

Figure 2.3: (a) Schematic representation and (b) Photograph of the PA cell used in the experiment.

- *Detection schemes and processing electronic equipments:*
  PA signal detection techniques employ either a gas condenser microphone for the detection of the pressure variations in air or a piezoelectric transducer for the detection of thermo-elastic waves in solid or liquid media[72,74]. For periodic modulation, phase-

sensitive detection (lock-in-amplifier) can be utilized to process the detected signal. The technique is extremely efficient for extracting very weak signals associated with noise. With pulsed laser sources, digital storage oscilloscope is used to store the data signal.

Experimental methods

1.CW laser source for excitation

Experimental set up for PA measurements in continuous wave light source as input is shown in figure 2.4. It consists of a light beam from a standard solar irradiation of 1000W Xe lamp (Oriel 6269). A water column kept after the Xenon lamp will effectively filter out the infrared portion of the spectrum. Light coming out of the Xe lamp is intensity modulated using a mechanical chopper(Ithaco HMS 230) and is focused on the sample within the PA cell. The acoustic signals generated are detected by the PZT, and processed on a lock in amplifier (Stanford Research Systems SR 510). The description of the PA cell is same given above. PA cell contains the samples, and a fabricated piezoelectric transducer chamber to detect the acoustic signals. In the

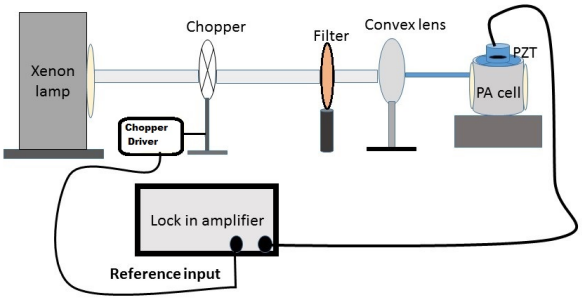

Figure 2.4: Experimental set up for PA study using Xe- lamp.

experimental section, the sample is taken in the PA cell which is firmly held on a holder, and properly aligned with the laser beam axis. After taking readings corresponding to one sample, it is pipetted out and the next sample is filled, without moving the PA cell. The experiment is repeated for sample at different wavelengths .

2.Pulsed laser source for excitation

In pulsed PA signal generation, Nd-YAG laser operating at 532 nm, at a pulse repeation frequency of 10Hz with 1 joule pulse energy is used as the excitation source, where signal detection was done with a digital storage oscilloscope (DSO-Tektronix; TDS 220,digital real time oscilloscope). Same PA cell was used for both the continuous wave and pulsed measurements. Here the synchronizing pulse from the laser is given as the reference signal to the DSO. The experimental setup is shown in figure 2.5.

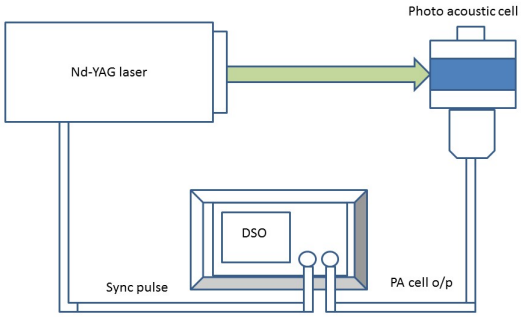

Figure 2.5: Experimental setup for PA signal generation by pulsed Laser.

2.6 Nonlinear optical studies by Z- Scan technique

For many photonic and optoelectronic applications like optical limiting and switching, the knowledge of the nonlinear optical properties of materials is necessary. There are a number of nano sized organic nonlinear optical materials and semiconductor structures of low dimension which have got new entry into the field of NL optics. There are many methods to study the NL properties of materials. Z-Scan is a fairly accurate and convenient method to study transparent samples.

2.6.1 Z-Scan technique

The Z-scan technique is a simple and effective experimental method to measure intensity dependent nonlinear optical susceptibilities of materials. Z-scan technique was originally introduced by Sheik Bahae et.al. [75]. In this method, the sample is translated in the Z-direction along the axis of a focused Gaussian beam, and the far field intensity is measured as function of sample position. This technique helps us to measure the sign and magnitude of both real and imaginary part of the third order nonlinear susceptibility coefficient $\chi^{(3)}$ of materials. When an incident beam propagates inside a NL medium it induces a self-phase change there by producing a wave front distortion of the beam. This can be studied by Z-Scan technique. Thus a laser beam propagating through a nonlinear medium will experience both amplitude and phase variations. Measurement of the transmission intensity of the focused laser beam as a function of distance from the sample, give information about nonlinear refraction and nonlinear absorption by the medium.

This technique has several advantages, some of which are:

- No complicated alignment except for keeping the beam centered on aperture.
- Simultaneous measurement of both sign and magnitude of nonlinearity.
- Data analysis is quick and simple except for some particular conditions.
- Possible to isolate the refractive and absorptive parts of nonlinearity unlike in DFWM.

Some of the disadvantage include:

- Requirement of high quality Gaussian beam for absolute measurements
- For non-Gaussian beams the analysis is completely different.
- Relative measurements against a standard samples allows relaxation on requirements of beam shape.
- Beam walk-off due to sample imperfections, tilt or distortions.

2.6.2 Theory of Z-scan technique

Two techniques employed in Z-Scan studies are:

1. Open aperture Z-Scan
2. Closed aperture Z-Scan.

In the open aperture Z- scan measurements nonlinear absorption of the sample is evaluated. For example, if nonlinear absorption like two-photon absorption (TPA) is present, it is manifested in the measurements as a transmission minimum at the focal point [76,77]. On the other hand, if the sample is a saturable absorber, transmission increases with increase in incident intensity and results in a transmission maximum at the focal region. A straight-line Z-scan graph is obtained in the case of samples with linear absorption. In closed aperture Z-scan technique the transmitted light is measured through an aperture placed in the far field with respect to focal region[75, 78]. In this case, the transmitted light is sensitive to both nonlinear absorption and nonlinear refraction. In a closed aperture z-scan experiment, phase distortion suffered by the beam while propagating through the nonlinear medium is converted into corresponding amplitude variations. If transmitted light is measured without an aperture, the mode of measurement is referred to as open aperture z-scan and with an aperture it is closed aperture Z-scan [78]. Closed and open aperture Z-scan graphs are always normalized to linear transmittance i.e.,transmittance at large values of $|z|$ and the real part and imaginary part of nonlinear susceptibility $\chi^{(3)}$ are obtained from the closed and open aperture z-scan methods respectively. Usually closed aperture Z- scan data is divided by open aperture data to cancel the effect of nonlinear absorption contained in the closed aperture measurements [78]. In a Z-scan measurement, it is assumed that the sample thickness is much less than Rayleighs range z_0 (diffraction length of the beam), defined as

$$z_0 = \frac{k\omega_0^2}{2} \tag{2.13}$$

where k is the wave vector and ω_0 is the beam waist radius given by

$$\omega_0 = \frac{f\lambda}{D} \tag{2.14}$$

where f is the focal length of the lens used, λ is the wavelength of the source and D is the beam radius at the lens. Z-scan technique is highly sensitive to the profile of the beam and also to the thickness of the sample. The sample thickness should always be kept less than the Rayleighs range for ensuring that the beam profile does not vary appreciably inside the sample.The sensitivity of this z-scan method is used to monitor nonlinear refraction at low irradiance levels, where a third order nonlinearity attributed to n_2 caused by bound electrons can be observed. At higher irradiance levels, the refraction caused by two photon absorption induced free charge carriers becomes significant. Thus the electronic Kerr effect will be dominant at low irradiance levels whereas TPA induced free carrier absorption (FCA) will be dominant at high irradiance levels. These are represented graphically in figure 2.6 where,nonlinear absorption like two-photon absorption (TPA) is present. It is manifested in the measurements as a transmission minimum at the focal point for reverse saturable absorption(RSA). On the other hand, if the sample is a saturable absorber,transmission increases with incident intensity and results in a transmission maximum at the focal region and the process is saturable absorption(SA). Both the curves are normalized to give a transmittance of one in the linear region (i.e. regions of large $|z|$). Sample positions are presented in units of z/z_o where z_o is the diffraction length.

Open aperture Z-scan technique

In the case of an open aperture z-scan, the transmitted light measured by the detector is sensitive only to the intensity variation. Therefore the phase variations of the beam can be neglected safely. The theory of Z-scan experiment outlined below is same as that given by M Sheik Bahae et.al.[75]. The intensity dependent nonlinear absorption coefficient α(I) can be written in terms of linear absorption coefficient α and TPA coefficient β as [75]

$$\alpha(I) = \alpha + \beta(I) \tag{2.15}$$

The irradiance distribution at the exit surface of the sample can be written as

$$I_r(z, r, t) = \frac{I(z, r, t)e^{-\alpha_0 L}}{1 + q(z, r, t)} \tag{2.16}$$

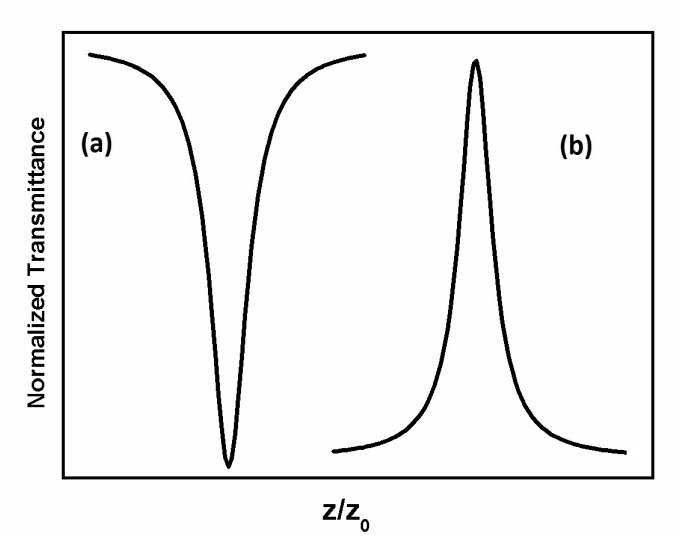

Figure 2.6: Open aperture z-scan curves for (a) Reverse saturable Absorption (b) Saturable absorption

$$q(z,r,t) = \beta I(z,r,t) L_{eff} \tag{2.17}$$

$$L_{eff} = \frac{1 - e^{-\alpha l}}{\alpha} \tag{2.18}$$

For a pulse of Gaussian temporal profile,equation (2.16) can be integrated to give the transmission as

$$T(Z, S = 1) = \frac{1}{\sqrt{\pi} q_0(z,0)} \int_{-\infty}^{+\infty} ln[1 + q_0(z,0) e^{-\tau^2}] d\tau \tag{2.19}$$

Nonlinear absorption coefficient is obtained from fitting the experimental results to the equation (2.19). If $q_0 < 1$ equation can be simplified as

$$T(z, S = 1) = \sum_{m=0}^{\infty} \frac{[-q_0(z,0)]^m}{(m+1)^{(3/2)}} \tag{2.20}$$

where m is an integer. The imaginary part of third order susceptibility (Im χ^3) determines the strength of the nonlinear absorption.

$$Im(\chi^{(3)}) = \frac{n_0^2 c^2 \beta}{240 \pi^2 \omega} (esu) \tag{2.21}$$

where λ is the excitation wavelength, n_0 is the linear refractive index, ϵ_0 is the permittivity of free space and c the velocity of light in vacuum.

Closed aperture z-scan technique

The basis of closed aperture z-scan is the self-refraction and self-phase modulation effects. The technique relies on the transmittance measurement of a nonlinear medium through a finite aperture in the far field as a function of the sample position z with respect to the focal plane using a single Gaussian beam in a tight focus geometry. Consider, for instance, a material with a negative nonlinear refraction and thickness smaller than the diffraction length

$$z_0 = \frac{\pi\omega_0^2}{\lambda} \tag{2.22}$$

of the focused beam being positioned at various points along the z-axis where

$$k = \frac{2\pi}{\lambda} \tag{2.23}$$

is the wave vector. This assumption implies that the sample acts as a thin lens of variable focal length due to the change in refractive index at each position ($n = n_0 + n_2 I$). Suppose that the sample is kept at a distance far away from the focus (-z). The irradiance is low and and there is negligible nonlinear refraction. Hence the transmittance characteristics are linear. As the sample is moved close to the focus, the beam irradiance increases, leading to self-lensing in the sample. A negative self-lensing prior to focus will tend to collimate the beam, causing a beam narrowing at the aperture which results in an increase in the measured transmittance. As the scan in z direction continues and passes the focal plane, the sample which acts as a negative lens increases the defocusing effect thus increasing the beam divergence, leading to beam broadening at the aperture. Hence the transmittance decreases. Thus there is a null as the sample crosses the focal plane (z_0). The z-scan is completed as the sample is moved away from focus (+z) such that the transmittance become linear since the irradiance is again low. A prefocal transmittance maxima (peak) followed by a post focal transmittance minima (valley) is the z-scan signature of negative refraction nonlinearity. The curves for closed z-scan in the case of positive nonlinearity

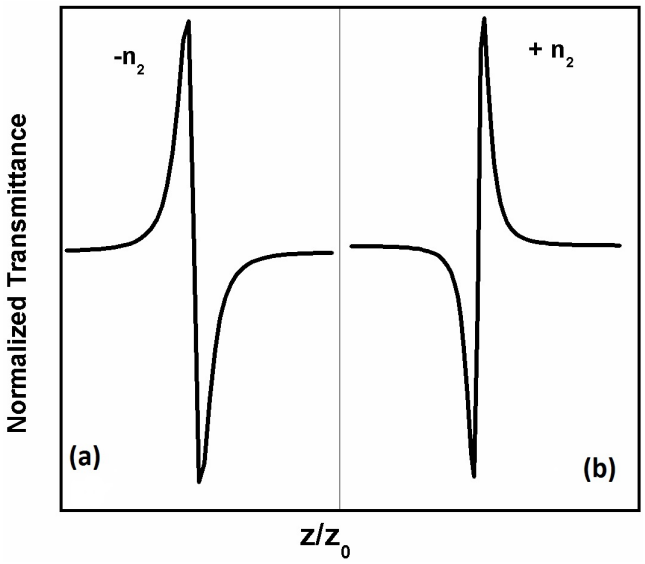

Figure 2.7: Typical closed aperture z-scan curves of samples having (a) Negative nonlinearity and (b) Positive nonlinearity.

and negative nonlinearity shows opposite effects as depicted in figure 2.7. This is the case of purely refractive nonlinearity where nonlinear absorption is absent. In the presence of multiphoton absorption, there is a suppression of the peak and enhancement of the valley, whereas the opposite effect occurs if there is a saturation of absorption [78]. In a cubic nonlinear medium the index of refraction (n) is expressed in terms of nonlinear index n_2 through

$$n = n_0 + n_2 I \tag{2.24}$$

where n_0 is the linear index of refraction,n_2 the intensity dependent refractive index and I denotes the irradiance of the laser beam within the sample [78]. Assume a TEM_{00} beam of waist radius ω_0 travelling in the +z direction. E is the peak electric field and can be written as

$$E(r,z) = E_0 \frac{\omega_0}{\omega(z)} e^{[-\frac{r^2}{\omega^2} + i\frac{kr^2}{2R}]} e^{-i\psi(z)} \tag{2.25}$$

$$= E(0,z)e^{-i\frac{kr^2}{2q}}$$

$$where \quad \omega^2(z) = \omega_0^2(1+\frac{z^2}{z_0^2}) \tag{2.26}$$

is the beam radius and

$$R(z) = z(1+\frac{z^2}{z_0^2}) \tag{2.27}$$

is the radius of curvature of the wave front at z .

E_0(t) denotes the radiation electric field at the focus and contains the temporal envelope of the laser pulse. The term $e^{i\phi(z,t)}$ contains all the radially uniform phase variations. For calculating the radial phase variations $\Delta\phi(r)$, the slowly varying envelope approximation (SVEA) is used and all other phase changes that are uniform in r are ignored. In the case of cubic nonlinearity and negligible nonlinear absorption, equation (2.28) and equation (2.29) can be solved to get the phase shift $\Delta\phi$ at the exit of the sample and is given by

$$\Delta\phi(z,r,t) = \Delta\phi(z,t)e^{[\frac{2r^2}{\omega^2(z)}]} \tag{2.28}$$

with

$$\Delta\phi(z,t) = \frac{\Delta\phi_0(t)}{(1+\frac{z^2}{z_0^2})} \tag{2.29}$$

where $\Delta\phi_0(t)$ is the on axis phase shift at the focus which is defined as

$$\Delta\phi(t) = k\Delta n_0(t)L_{eff} = \frac{2\pi}{\lambda}n_2 I_0(t)L_{eff} \tag{2.30}$$

Where $I_0(t)$ is the on axis irradiance at focus (i.e. at z=0). The complex electric field exiting the sample E now contains the nonlinear phase distribution

$$E(z,r,t) = E(z,r,t)e^{\frac{\alpha l}{2}}e^{i\Delta[z,r,t]} \tag{2.31}$$

By virtue of Huygens principle and making use of Gaussian decomposition method one can show that

$$\exp^{i\Delta[z,r,t]} = \sum_{k=0}^{\infty}\frac{[i\Delta\phi_0(z,r,t)]^m}{m!}e^{\frac{-2mr^2}{\omega_z^2}} \tag{2.32}$$

Each Gaussian beam can be simply propagated to the aperture plane and they will be resumed to reconstruct the beam. After including the initial beam curvature for the focused beam, the resultant electric field pattern at the aperture is

$$E(r,t) = E(z, r=0)e^{\frac{-\alpha l}{2}} \sum_{k=0}^{\infty} \frac{[i\Delta\phi_0(z,r,t)]^m}{m!} \frac{\omega_{m_0}}{\omega_m} e^{[\frac{-r^2}{\omega_m^2} - \frac{ikr^2}{2Rm} + i\theta_m]} \tag{2.33}$$

For a cubic nonlinearity, the peak and valley of the -scan transmittance can be calculated by solving the equation

$$\frac{d}{dz}T(z, \Delta\phi_0) = 0 \tag{2.34}$$

Solution to this equation (2.34) yields the peak valley separation as

$$\Delta z_{p-v} = 1.7 z_0 \tag{2.35}$$

Then the peak valley transmittance change is

$$\Delta T_{p-v} = 0.406\Delta\phi_0 \tag{2.36}$$

for $\Delta\phi_0 \leq \pi$.where S is the linear transmittance of the far field aperture. From the closed aperture Z-scan fit, $\Delta\phi_0$ can be obtained. Then the nonlinear refractive index n_2 can be determined using equation (2.30) and is given by

$$n_2(m^2/w) = \frac{\lambda}{2\pi I_0 L_{eff}}\Delta\phi_0 \tag{2.37}$$

$$n_2(e.s.u) = \frac{cn_0\lambda}{40\pi 2\pi I_0 L_{eff}}\Delta\phi_0 \tag{2.38}$$

The n_2 is related to Re($\chi^{(3)}$) by the relation

$$Re\chi^{(3)} = \frac{n_0 n_2}{3\pi}(e.s.u) \tag{2.39}$$

From the real and imaginary part of $\chi^{(3)}$, the modulus of third order nonlinear susceptibility can be found out as.

$$|\chi^{(3)}| = \sqrt{[Re(\chi^{(3)})]^2 + [Im(\chi^{(3)})]^2} \tag{2.40}$$

The magnitude of $\chi^{(3)}$ is significantly affected by the molecular orientation and it determines the strength of nonlinearity of the material.

Experimental methods

In the present investigation, we have employed the single-beam z-scan technique with nanosecond laser pulses to measure the nonlinear optical absorption properties of samples. A Q-switched Nd: YAG laser (Spectra Physics LAB-1760, 532 nm, 7 ns, 10 Hz) is used as the light source. The sample is moved in the direction of the light incidence near the focal spot of the lens which have a focal length of 20 cm. The beam waist ω_0 is calculated to be 42.56μm. The Rayleigh length, $z_0=\pi\omega_0^2/\lambda$, is estimated to be 10.06 mm, much greater than the thickness of the sample, which is an essential prerequisite for Z-scan experiments. The transmitted beam energy, reference beam energy, and their ratio are measured simultaneously by an energy ratio meter (Rj7620, Laser Probe Corp.) having two identical pyroelectric detector heads (Rjp735). The experimental set-up is shown in figure 2.8.

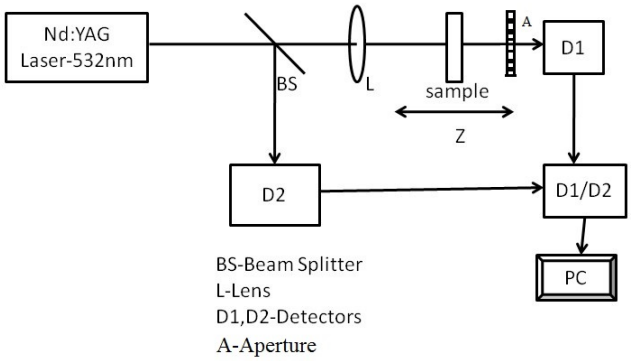

Figure 2.8: Experimental set-up of open/closed aperture Z- scan method.

The sample was moved along the z-axis by a motorized translational stage. The effect of fluctuations of laser power is eliminated by dividing the transmitted power by the power obtained at the reference detector[77]. Z-scan technique is highly sensitive to the profile of the beam and also to the thickness of the sample. Any deviation from Gaussian profile of the beam and also from thin sample approximation will give rise to erroneous results. For ensuring that the beam profile does not vary appreciably inside the sample, the sample thickness should always

be kept less than the Rayleighs range. The sensitivity of the Z-scan method is used to monitor nonlinear refraction at low irradiance levels, where a third order nonlinearity attributed to n_2 caused by bound electrons can be observed. At higher irradiance levels the refraction caused by two photon absorption induced free charge carriers becomes significant.

Optical limiting

To study the optical limiting property of the sample, the nonlinear transmission of the sample is measured as a function of input fluence. Optical power limiting is effected through the nonlinear optical processes of the sample. A schematic representation of transmission through an ideal optical limiter is shown in figure 2.9.

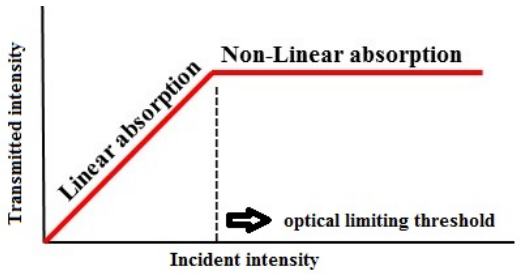

Figure 2.9: Schematic representation of transmission through an ideal optical limiter.

An important term in the optical limiting study is the optical limiting threshold. Optical limiters are essentially those systems which transmit light at low input fluence or intensities, but become opaque at high inputs. The optical limiting property is mainly found to be absorptive nonlinearity, which corresponds to the imaginary part of third order susceptibility [79, 80]. From the values of fluence at focus, the fluence values at other positions could be calculated using the standard equations for Gaussian beam waist. Such plots give a better comparison of the nonlinear absorption or transmission in the sample and are generated from z-scan trace. There are three basic requirements for a material to be good optical limiter: (1) An excited state absorption cross-section that exceeds the ground state absorption cross-section, (2)Fast response and

(3) High damage threshold. This phenomenon is exploited in passive optical power limiting to protect optical sensors, including human eye, from intense laser pulses.

2.7 Solar cells as the photonic material application of CdSe QDs

Traditional photovoltaic devices suffer from high costs of manufacturing and installation. Low-cost and high-performance solar cells are the main challenge to replace fossil for sustainable energy sources[81-83]. Semiconductor QD-sensitized solar cells (QDSSCs) have attracted considerable attention recently due to their cost-effective alternative to silicon-based photovoltaics, and have shown promising developments for the next generation of solar cells[83-88]. QDSSCs can be regarded as a derivative of dye-sensitized solar cells (DSSCs), which were first reported by O'Regan and Grtzel in 1991 [89]. The sensitizer commonly used in dye sensitized solar cells are organic dyes. To increase the efficiency, the light harvesting property in the visible region has to be increased, and have been made the focus on the development of high-performance sensitizers as quantum dots [89-92]. Narrow-band-gap semiconductor QDs, such as CdS [93, 94], CdSe[95, 96], PbS [97] and InAs [98] have been used as the photo sensitizers instead of organic dyes due to their versatile optical and electrical properties [99-101].

Background of three generations of solar cells

- Silicon solar cell

It is one of the most widely used solar cells which have efficiencies up to 24.4% reported for a commercial product[102]. But the main disadvantage of such solar cells are their relatively high cost for production. Even though amorphous silicon solar cell can be produced at lower temperature, this cell tends to degrade on longer duration of light exposure and hence efficiency decreases. Silicon solar cell can absorb a certain amount of energy greater than band gap and it can't absorb entire solar spectra, which is required to knock out an electron. Since silicon is a very shiny material having very high reflectance an anti-reflective coating is needed to reduce reflection losses.

- Polymer solar cells

These are flexible photovoltaic devices which are made of electron- donor and electron- acceptor materials. The main advantage of polymer solar cells over silicon cell-based devices are that they are being light weight [89,103], easily disposable and inexpensive. They acquire lower negative environmental impact, but are relatively unstable towards photochemical degradation. The photo induced charge transfer at polymer fullerene interfaces takes place within 15 fs [104]. The created charges have to be transported selectively to the contacts.

- Dye sensitized solar cells

DSSC [89, 105], a third generation photovoltaic cell, represents one of the most promising one that has been offered to challenge conventional silicon cells [106] over the past decade. These offer the lowest cost input and has an easy manufacturing process[107, 108]. The reported maximum overall power conversion efficiency is nearly 12.3%[109]. However, the main disadvantage of such types of cells is that, it absorsb light only in a particular region of solar spectrum.

- Quantum dot sensitized solar cell (QDSSC)

QDSSC is a third generation solar cell, with narrow band gap semiconductor quantum dots (QDs) as the sensitizer material used. The size-tunable band gap property of the QDs particularly makes this as attractive sensitizers. Several semiconductor QDs, such as PbS, CdS, CdSe and CdTe have been successfully verified as visible light sensitizers for Titanium Dioxide (TiO_2)-based working electrodes[95, 97, 110, 111]. In QDSCs the QDs generate excitons under illumination with sunlight and the excited electrons then are injected from the CB of QDs into the CB of TiO_2. At the same time, the photogenerated holes are donated to the electrolyte and thus the QDs are restored. The oxidation species of the electrolyte diffuses to the counter electrode and is reduced by the migrated electrons from the external circuit. The advantages of such types of solar cells are large QD extinction coefficients, the multiple exciton generation phenomenon and short excitonic path length which would lead to the enhancement of the conversion efficiency in QDSSCs[112].

2.7.1 Working principles of QDSSCs

The structure of a QDSSC consists of a wide-band-gap mesoporous oxide film (a photo electrode, such as the commonly used TiO_2 or ZnO), QDs (the sensitizer), an electrolyte, and a counter-electrode. During operation, photons are captured by QDs, yielding electron-hole pairs that are rapidly separated into electrons and holes at the interface between the nanocrystalline oxide and QDs. The electrons jump into the oxide film, and the holes are released by redox couples in the electrolyte for regeneration at the counter electrode.However, electron transport within the mesoporous TiO_2 film is slower than that of electron and hole transfers. So the recombination losses become a major factor in limiting the overall efficiency[81, 113]. Principle of operation of the QDSSCs is shown in figure 2.10.

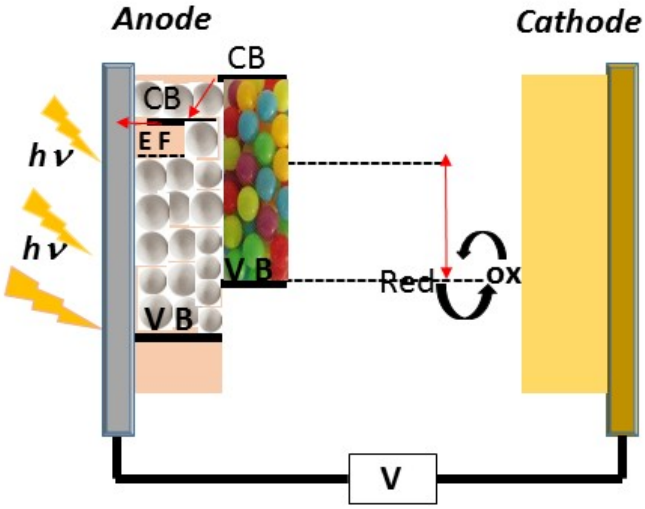

Figure 2.10: Principle of operation of the QDSSCs.

Photo excitation of the sensitizer is followed by electron injection into the conduction band of the wide-band-gap semiconductor. The sensitizer is regenerated by the redox system, which itself is regenerated at the counter electrode (cathode) by electrons passing through the load.

Methods of preparation of QDSSC

The synthesis of QDs and their incorporation into the QDSSC photo active electrode as sensitizers is carried out by several techniques:

- Chemical Bath deposition
  This technology is based on the slow controlled precipitation of the desired compound from its ions in a reaction bath solution [114].

- Successive ionic layer adsorption reaction (SILAR)
  SILAR method is mainly focused on the adsorption and reaction of the ions from the solutions and rinsing between every immersion with deionized water to avoid homogeneous precipitation in the solution[115].

- Deposition of Ex-Situ-Grown QDs
  In this method, mono disperse QDs are synthesized using organic capping ligands to control the shape and size of the QDs and are separated from the excess organic ligands and dissolved in an organic solvent; they are then ready to be attached to the TiO_2 electrodes with the help of a functional molecular linker [116, 117].

2.7.2 Factors influencing conversion efficiency of QDSSC

1. *Sensitizer materials*
   It is very important to select the appropriate materials to be not only cost-effective but also long lasting. The use of these quantum dots, which may produce more than one electron-hole pair per single absorbed photon (also known as multiple exciton generation (MEG)), is a promising solution to enhance power conversion efficiency. Furthermore, the creation of a type-II heterojunction greatly enhances charge separation, exciton concentration, quantum yield, and lifetime of hot electrons and therefore, the performance of QD-sensitized solar cells. [90, 118]

2. *The inherent triple junction of TiO_2/QDs/electrolyte*
   The mechanisms of charge-transfer processes occurring at the complex interfaces formed among the nanostructured Ti O_2, the sensitizing QDs, energy-level alignment among the materials constructing the triple junction and the aqueous electrolyte are the impor-

tant factors determining the overall performance of QDSSCs[113, 119, 120].

3. *Redox electrolyte*
   An efficient electrolyte solution, which is able to transfer electrons rapidly to regenerate the oxidized QD sensitizers while having good long-term stability under working conditions, constitutes one of the major challenges in the field of QDSSCs. It is because the V_{oc} of a QDSSC is determined by the energy difference between the TiO_2 Fermi level and the electrolyte redox potential.

4. *Counter electrode*
   Highly efficient counter electrode (CE), is able to catalyze the regeneration of the oxidized charge carrier ions ,so as to maximize the performance of QDSSCs[121, 122].

Other main features of QDSSCs

- **Quantum confinement effect for QDSSCs**
  QDs are extremely small semiconductor nanocrystals with a size comparable to the Bohr radius of an exciton [123]. For most semiconductors, the Bohr radius of an exciton is in the range of 1-10 nm. Due to the dimension effect, the behavior of electrons in QDs differs from that in the corresponding bulk material, which is called the quantum confinement effect. Because of the quantum confinement effect, the band gap energy (E_g) of QD increases with the decrease of particle size [124, 125]. So a range of optical absorption wavelengths of QD can be tuned by controlling the size of QD. Such a feature of QDs with tunable E_g has led to their application in LEDs for full-color displays [126], and in QD- sensitized solar cells for the generation of optical absorption at desired wavelengths [127, 128].

- **The multiple electron generation effect for QDSSCs**
  The multiple electron generation (MEG) effect is that two or more electron-hole pairs (excitons) are generated by one photon excitation, in contrast to the conventional case where one photon excitation can produce only a single exciton. In theory, the MEG effect requires a photon with energy at least twice that of the band gap

of the QDs.The possible reasons for the MEG effect, which can be achieved easily in QDs, have been attributed to the following [129]:
1) the electron- hole ($e^- - h^+$) pairs are correlated and thus exist as excitons rather than free carriers.
2) The rate of hot electron and hole cooling can be slowed because of the formation of discrete electronic states.
3)Momentum is not a good quantum number, and thus the need to conserve crystal momentum is relaxed.
4) Auger processes are greatly enhanced because of the increased $e^- - h^+$ Coulomb interaction.
So the production of multiple exciton pairs in QDs can be enhanced in comparison with bulk semiconductors. So the utilization of high-energy photons to generate multiple excitons or capture hot electrons before their thermalization can boost the operational efficiency of QDSSC[130].

2.7.3 Experimental methods

Current-voltage (J-V) characteristics of the cells were examined using a standard solar irradiation of 1000W Xe arc lamp (Oriel 6269) as the light source. The J-V curves were measured with a digital multimeter. Input intensity was measured using light meter (METRAVI 1332). In all the cases, input intensity was in the range of 1-10 Klux [131, 132]. The performance of a QSSC is assessed by determining the parameters such as the short-circuit current density (J_{sc}), the open-circuit voltage (V_{oc}), the fill factor (FF), and the overall power conversion efficiency (η). I-V curve of a typical solar cell in figure 2.11 shows the current drawn from a photovoltaic cell when illuminated.
The efficiency of a solar cell is defined as the ratio of maximum electrical power extracted to the incident radiation power illuminating the solar cell surface,

$$\eta = \frac{P_{max}}{P_{min}} = \frac{J_{sc}V_{oc}FF}{P_{in}} \tag{2.41}$$

The IPCE parameter of a QSSC is defined as the ratio of the number of electrons generated by light in the external circuit to the number of

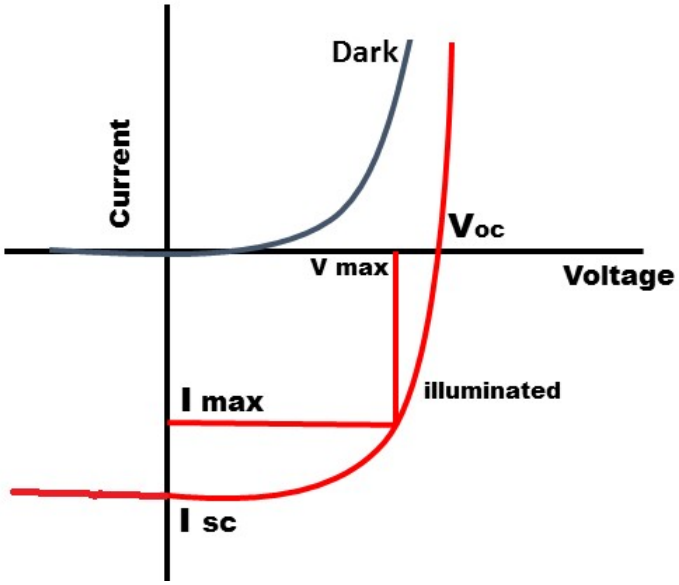

Figure 2.11: I-V curve of a typical solar cell.

incident photons, which can be expressed as

$$IPCE\% = \frac{1240 I_{sc}}{P_{in}\lambda} \tag{2.42}$$

where $P_{(in)}$ is the incident power and λ is the incident photon wavelength.

2.8 Random Lasers

Random Lasers (RL) differ from other conventional types of laser in that its cavity is formed not by mirrors but by multiple scattering in a disordered gain medium. In other words, a random laser is a non-conventional laser for which feedback mechanism is based on disorder-induced light scattering. The laser is random in the sense that the feedback for the photons generated in the dye is provided by the random multiple scattering of light from the particles. Fabry-Perot cavity is the

most common laser cavity made of two mirrors with one partially transmitting, and are placed on either side of the gain medium. Amplification of light occurs when it is bounced back and forth between two mirrors through the gain medium. Light that remains in the cavity interferes constructively after traveling a round trip between the mirrors and returning to its original position. When the population inversion occurs or the optical amplification is large enough to compensate the loss caused by mirror leakage and material absorption etc.,lasing oscillations occur at cavity resonant frequencies. The laser light transmitted through the partially reflecting mirror has well defined frequency, good directionality and a high degree of coherence. However, in RL, inside the cavity there are scatterers and the light can be scattered in other directions as well[133-137]. This results in additional loss and increases the lasing threshold. Therefore, in conventional laser cavities optical scattering is considered detrimental and we have to minimize the amount of scattering. In random lasers a disordered medium that contains a number of scattering centers scatter light many times before it escapes the gain medium [138, 139]. Multiple scattering increases the dwell time of light, enhancing light amplification. Light in the gain medium is trapped in the absence of mirrors as the scattering can do the job on its own[139-141]. Thus strong scattering in a disordered media can give rise to laser operation and produces random laser. The word random has been used to describe lasers that operate on the basis of these properties[142-145].

2.8.1 Classifications

The two classifications of random lasers :

1. ***Random laser with incoherent feedback***
   In this case the feedback is used simply to return part of energy or photons to the gain medium, i.e. it is energy or intensity feedback. Thus, in a laser with incoherent feedback or non resonant feedback the only resonant element is the amplification line of the gain medium. The mean frequency of emission does not depend on the dimensions of laser cavity but only on the center frequency of the amplification line[141].

2. ***Random laser with coherent feedback***
   In the case of RL with coherent feedback, the light can return to

its origin position in the disordered medium from which it was scattered. The process of making closed loops by light is called recurrent light scattering. When the amplification of light along each of the loop exceeds the loss, lasing oscillation occurs and this loops can serve as cavity analogous to ring cavity of conventional laser. If scattering light forms several loops, disordered medium lases at some determined frequencies and we receive some modes of coherent random laser very similar to that of a conventional laser. The major difference of coherent random laser from that of the normal laser is that the output is multi directional and the direction of each individual mode is different in coherent random laser while directional output is obtained in conventional laser.

2.8.2 Some salient features of random laser are:

- The output of random laser modes are multi directional, which means the modes have spatial distribution.
- When the pump intensity increases the output of modes and the number of modes increases with spectral narrowing of the emission lines.
- There is a mode competition between the random laser modes that results in the photon hopping effect, i.e. the hop of photon from one mode to the other modes and the field interaction effect between side modes.

2.8.3 Experimental methods

A Q-switched Nd: YAG laser (Spectra Physics LAB-1760,532 nm, 7ns,10 Hz) emitting pulses of 7 ns duration at 532 nm and 355 nm, at a repetition rate of 10 Hz is used as the light source. A cylindrical lens is used to focus the beam through the filter into the sample kept in a cuvette of 1 mm thickness. To collect the output a monochromatic-CCD system (Spectra Pro) with a resolution of 0.03 nm is used. The experimental setup for random laser study is shown in figure 2.12.

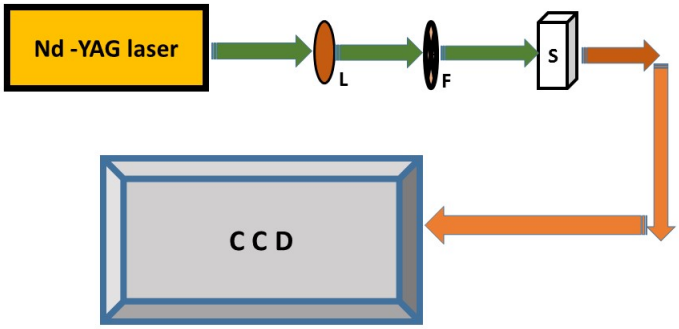

Figure 2.12: The experimental setup is shown with Nd-YAG Laser, L- cylindrical lens, F - filter, S- sample in cuvette, CCD spectrometer.

2.8.4 Applications of random lasers

- Lasing in a wide spectral regime from ultra-short wave (γ-ray, X-ray) to optical and radio waves obtained with random lasers and the construction of lasing is certainly cheaper and easier than conventional laser.
- Moreover multidirectional output of a random laser can be used in displays because a thin layer of random medium doped with emitter can be used to coat an arbitrarily shaped display panel.
- In the medical area, the random laser has potential application in photo dynamic therapy and tumor detection.
- The micro random laser may play the crucial role of an active element or miniature light source in integrated photonic circuit.
- It is possible to monitor the flow of liquids by adding a small number of nanoparticle clusters to the liquid and detecting their random laser emission over a large flow distance.
- Fast switching on and off of random laser can be used to create high speed display[142, 146].

2.9 Conclusion

- Preparation methods of the samples are discussed briefly along with the basic principle of microwave and reflux methods.
- Structural characterization methods including XRD,TEM,SEM,DLS and FTIR techniques are discussed.
- Linear optical characterization methods like U-V visible absorption and fluorescence methods have been discussed.
- Thermo-optic characterization methods - Thermal lens and Photo acoustic methods have been explained along with the basic theory.
- Nonlinear-optical studies using Z-scan methods - open and closed aperture are discussed along with the theory .
- Applications of the nanophotonic materials in the field of solar cell and random laser are discussed.

2.10 Refrences

[1] Horikoshi and N. Serpone,"Introduction to nanoparticles," Microwaves in Nanoparticle Synthesis: Fundamentals and Applications, Wiley-VCH Verlag, Weinheim, 2013.

[2] Y. Gogotsi, Nanomaterials Handbook. CRC press, 2006.

[3] L. Wang and R. Hong, Synthesis, Surface Modification and Characterisation of Nanoparticles. INTECH Open Access Publisher, 2011.

[4] Y. Li and C. Park, "Particle size distribution in the synthesis of nanoparticles using microemulsions," Langmuir, vol. 15, pp. 952-956, 1999.

[5] I. Capek,"Preparation of metal nanoparticles in water-in-oil (w/o) microemulsions," Adv. Colloid Interface Sci., vol. 110, pp. 49-74, 2004.

[6] X. Chen, J. L. Hutchison, P. J. Dobson and G. Wakefield,"Highly luminescent monodisperse CdSe nanoparticles synthesized in aqueous solution," J. Mater. Sci., vol. 44, pp. 285-292, 2009.

[7] B. Su, D. J. Fermn, J. Abid, N. Eugster and H. H. Girault,"Adsorption and photoreactivity of CdSe nanoparticles at liquid— liquid interfaces," J. Electro.anal. Chem, vol. 583, pp. 241-247, 2005.

[8] S. C. Motshekga, S. K. Pillai, S. S. Ray, K. Jalama and R. W. Krause, "Recent trends in the microwave-assisted synthesis of metal oxide nanoparticles supported on carbon nanotubes and their applications," Journal of Nanomaterials, vol. 2012, pp. 51, 2012.

[9] R. N. Gedye, F. E. Smith and K. C. Westaway,"The rapid synthesis of organic compounds in microwave ovens," Canadian Journal of Chemistry, vol. 66, pp. 17-26, 1988.

[10] P. Lidstrm, J. Tierney, B. Wathey and J. Westman,"Microwave assisted organic synthesis-a review," Tetrahedron, vol. 57, pp. 9225-9283, 2001.

[11] G. Whittaker, "Microwave chemistry," School Science Review, pp. 87-94, 2004.

[12] S. Das, A. Mukhopadhyay, S. Datta and D. Basu,"Prospects of microwave processing: An overview," Bull. Mater. Sci., vol. 32, pp. 1-13, 2009.

[13] L. Vovchenko,L.Matzui, M.Zakharenko, M.Babich and A.Brusilovetz, " Thermoexfoliated graphite as support for production of metal-graphite nanocomposites," Journal of Physics and Chemistry of Solids, vol. 65, pp. 171-175, 2004.

[14] J. Miyawaki, M. Yudasaka, H. Imai, H. Yorimitsu, H. Isobe, E. Nakamura and S. Iijima, "In Vivo Magnetic Resonance Imaging of Single-Walled Carbon Nanohorns by Labeling with Magnetite Nanoparticles," Adv Mater, vol. 18, pp. 1010-1014, 2006.

[15] Y. Li, E. J. Lee and S. O. Cho,"Superhydrophobic coatings on curved surfaces featuring remarkable supporting force," The Journal of Physical Chemistry C, vol. 111, pp. 14813-14817, 2007.

[16] A. Patterson,"The Scherrer formula for X-ray particle size determination," Physical Review, vol. 56, pp. 978, 1939.

[17] R. L. Thomas, Synthesis and Characterization of Tellurium Oxide Glasses for Photonic Applications, Ph. D. Thesis. CUSAT. Kochi,2013.

[18] K. W. Evanson and M. W. Urban, "Surface and interfacial FTIR spectroscopic studies of latexes. I. Surfactantcopolymer interactions," J Appl Polym Sci, vol. 42, pp. 2287-2296, 1991.

[19] W. Brown, Dynamic Light Scattering: The Method and some Applications. Oxford University Press, USA, 1993.

[20] J. Liaw, S. F. Chang and F. C. Hsiao, "In vivo gene delivery into ocular tissues by eye drops of poly(ethylene oxide)-poly(propylene oxide)-poly(ethylene oxide) (PEO-PPO-PEO) polymeric micelles," Gene Ther., vol. 8, pp. 999-1004, 2001.

[21] P. N. Prasad, Nanophotonics. John Wiley and Sons, 2004.

[22] W. K. Adams, C. E. Wieman, K. K. Perkins and J. Barbera, "Modifying and validating the Colorado Learning Attitudes about Science Survey for use in chemistry," J. Chem. Educ., vol. 85, pp. 1435, 2008.

[23] B. Balamurugan and B. Mehta, "Optical and structural properties of nanocrystalline copper oxide thin films prepared by activated reactive evaporation," Thin Solid Films, vol. 396, pp. 90-96, 2001.

[24] A. Mandelis, "Photoacoustic and thermal wave phenomena in semiconductors," NY (USA), Elsevier Science Pub. Co., Inc.,1987.

[25] S. Sheldon, L. Knight and J. Thorne, "Laser-induced thermal lens effect: a new theoretical model," Appl. Opt., vol. 21, pp. 1663-1669, 1982.

[26] S. Wu and N. J. Dovichi, "Fresnel diffraction theory for steady state thermal lens measurements in thin films," J. Appl. Phys., vol. 67, pp. 1170-1182, 1990.

[27] J. Shen, A. J. Soroka and R. D. Snook,"A model for cw laser induced mode mismatched dual beam thermal lens spectrometry based on probe beam profile image detection," J. Appl. Phys., vol. 78, pp. 700-708, 1995.

[28] A. E. Siegman, "Lasers University Science Books," Mill Valley, CA, vol. 37, 1986.

[29] R. T. Bailey, F. R. Cruickshank, D. Pugh and W. Johnstone, "Pulsed source thermal lens. Part 1.-Theoretical analysis," Journal of the Chemical Society, Faraday Transactions 2: Molecular and Chemical Physics, vol. 76, pp. 633-647, 1980.

[30] R. Vyas and R. Gupta,"Photothermal lensing spectroscopy in a flowing medium: theory," Appl. Opt., vol. 27, pp. 4701-4711, 1988.

[31] Q. He, R. Vyas and R. Gupta,"Theory of photothermal spectroscopy in an optically dense fluid," Appl. Opt., vol. 36, pp. 1841-1859, 1997.

[32] C. Hu and J. Whinnery,"New thermo-optical measurement method and a comparison with other methods," Appl. Opt., vol. 12, pp. 72-79, 1973.

[33] J. R. Whinnery,"Laser measurement of optical absorption in liquids," Acc. Chem. Res., vol. 7, pp. 225-231, 1974.

[34] F. L. Arbeloa, I. L. Gonzalez, P. R. Ojeda and I. L. Arbeloa,"Aggregate formation of rhodamine 6G in aqueous solution," Journal of the Chemical Society, Faraday Transactions 2: Molecular and Chemical Physics, vol. 78, pp. 989-994, 1982.

[35] J. Mialocq, P. Hbert, X. Armand, R. Bonneau and J. Morand, " Photophysical and photochemical properties of rhodamine 6G in alcoholic

and aqueous sodium dodecylsulphate micellar solutions," J. Photochem. Photobiol. A., vol. 56, pp. 323-338, 1991.

[36] D. Magde, G. E. Rojas and P. G. Seybold,"Solvent dependence of the fluorescence lifetimes of xanthene dyes," Photochem. Photobiol., vol. 70, pp. 737-744, 1999.

[37] A. Kurian, Characterization of Photonic Materials using Thermal Lens Technique, Ph. D. Thesis.CUSAT. Kochi,2002.

[38] J. Shen, R. D. Lowe and R. D. Snook, "A model for cw laser induced mode-mismatched dual-beam thermal lens spectrometry," Chem. Phys., vol. 165, pp. 385-396, 1992.

[39] C. Bindhu, S. Harilal, V. Nampoori and C. Vallabhan, "Thermal diffusivity measurements in organic liquids using transient thermal lens calorimetry," Optical Engineering, vol. 37, pp. 2791-2794, 1998.

[40] S. A. Joseph, M. Hari, S. Mathew, G. Sharma, V. Hadiya, P. Radhakrishnan and V. Nampoori,"Thermal diffusivity of rhodamine 6G incorporated in silver nanofluid measured using mode-matched thermal lens technique," Opt. Commun., vol. 283, pp. 313-317, 2010.

[41] A. Santhi, M. Umadevi, V. Ramakrishnan, P. Radhakrishnan and V. Nampoori, "Effect of silver nanoparticles on the fluorescence quantum yield of Rhodamine 6G determined using dual beam thermal lens method," Spectrochimica Acta Part A: Molecular and Biomolecular Spectroscopy, vol. 60, pp. 1077-1083, 2004.

[42] J. H. Brannon and D. Magde,"Absolute quantum yield determination by thermal blooming. Fluorescein," J. Phys. Chem., vol. 82, pp. 705-709, 1978.

[43] C. Sunandana,"Physical applications of photoacoustic spectroscopy, " Physica Status Solidi (a), vol. 105, pp. 11-43, 1988.

[44] G. H. Brilmyer, A. Fujishima, K. Santhanam and A. J. Bard, " Photothermal spectroscopy," Anal. Chem., vol. 49, pp. 2057-2062, 1977.

[45] A. Tam, "Overview of photothermal spectroscopy," Photothermal Investigation of Solids and Fluids, pp. 1-34, 1988.

[46] R. Philip,"Nonlinear optical properties of selected laser dyes investigated using photoacoustics, fluorescence and stimulated scattering", PhD.Thesis ,CUSAT,Kochi,1993.

[47] M. Colles, N. Geddes and E. Mehdizadeh,"The opto-acoustic effect," Contemporary Physics, vol. 20, pp. 11-36, 1979.

[48] D. W. Ball,"Photo-acoustic Spectroscopy," Spectroscopy-springfield then eugene then duluth-, vol. 21, pp. 14, 2006.

[49] S. Vinokurov,"Optoacoustic effect and the thermal diffusivity of solids," Journal of Engineering Physics and Thermo physics, vol. 44, pp. 50-55, 1983.

[50] A. G. Bell,"On the production and reproduction of sound by light," Am. J. Sci., pp. 305-324, 1880.

[51] W. C. Rntgen, "On tones produced by the intermittent irradiation of a gas," Taylor & Francis, pp. 308-311,1881.

[52] A. G. Bell," Upon the Production of Sound by Radiant Energy", Scientific American vol.11, pp.4471- 4475,1881.

[53] J. Tyndall,"Action of an intermittent beam of radiant heat upon gaseous matter," Proceedings of the Royal Society of London, vol. 31, pp. 307-317, 1880.

[54] L. Rayleigh,"The photophone," Nature, vol. 23, pp. 274-275, 1881.

[55] W. H. Preece, "On the conversion of radiant energy into sonorous vibrations," Proceedings of the Royal Society of London, vol. 31, pp. 506-520, 1880.

[56] A. Rosencwaig, Photoacoustics and Photoacoustic Spectroscopy. Wiley, 1980.

[57] Nibu A.George, "Photoacoustic and photothermal deflection studies on certain selected photonic materials"PhD.Thesis ,CUSAT,Kochi,2001

[58] A. Rosencwaig and A. Gersho,"Photoacoustic effect with solids: a theoretical treatment," Science, vol. 190, pp. 556-557, 1975.

[59] A. Rosencwaig and A. Gersho, "Theory of the photoacoustic effect with solids," J. Appl. Phys., vol. 47, pp. 64-69, 1976.

[60] A. Onokhov, T. Razumova and I. Starobogatov,"Photoacoustic method of detecting pulsed radiation energy," soviet journal of optical technology, vol. 47, pp. 36-37, 1980.

[61] M. Satheeshkumar and C. Vallabhan, "Use of a photoacoustic cell as a sensitive laser power meter," Journal of Physics E: Scientific Instruments, vol. 18, pp. 434, 1985.

[62] R. Guthrie and F. Medina, "Photoacoustic cell for use as an optical power meter," J. Appl. Phys., vol. 57, pp. 4485-4486, 1985.

[63] M. Adams, G. Kirkbright and K. Menon, "Effect of sample thickness on the magnitude of optoacoustic signals," Anal. Chem., vol. 51, pp. 508-511, 1979.

[64] G. Wetsel and F. McDonald, "Determination of absolute optical-absorption coefficient using photoacoustic effect," in bulletin of the american physical society, pp. 295-295, 1977.

[65] J. F. McClelland and R. N. Kniseley, "Signal saturation effects in photoacoustic spectroscopy with applicability to solid and liquid samples," Appl. Phys. Lett., vol. 28, pp. 467-469, 1976.

[66] A. Hordvik and H. Schlossberg, "Photoacoustic technique for determining optical absorption coefficients in solids," Appl. Opt., vol. 16, pp. 101-107, 1977.

[67] M. M. Farrow, R. K. Burnham, M. Auzanneau, S. L. Olsen, N. Purdie and E. M. Eyring, "Piezoelectric detection of photoacoustic signals," Appl. Opt., vol. 17, pp. 1093-1098, 1978.

[68] A. Bonch-Bruevich, T. Razumova and I. Starobogatov,"Single-and two-photon spectroscopy of liquid media using the pulsed acousto-optical effect," Optics and Spectroscopy, vol. 42, pp. 45-48, 1977.

[69] T. Schmid,"Photoacoustic spectroscopy for process analysis"Analy tical and Bioanalytical Chemistry, vol. 384, pp.1071-1086, 2006.

[70] C. Sunandana,"Physical applications of photoacoustic spectroscopy," Physica Status Solidi (a), vol. 105, pp.11-43, 1988.

[71] G. H. Brilmyer, A. Fujishima, K. Santhanam and A. J. Bard, "Photothermal spectroscopy"Anal. Chem., vol. 49, pp. 2057-2062, 1977.

[72] D. P. Almond and P. Patel, "Photothermal Science and Techniques", Springer Science and Business Media, 1996.

[73] R. Philip, P. Sathy, V. Nampoori, J. Philip and C. Vallabhan, " Characteristics of two-photon absorption in methanol solutions of Rhodamine 6G using laser induced pulsed photoacoustics," Journal of Physics B: Atomic, Molecular and Optical Physics, vol. 25, pp. 155, 1992.

[74] A. Rosencwaig, Solid State Photoacoustic Spectroscopy. Academic Press, New York, 1977.

[75] M. Sheik-Bahae, A. A. Said and E. W. Van Stryland, "High-sensitivity, single-beam n 2 measurements," Opt. Lett., vol. 14, pp. 955-957, 1989.

[76] M. Sheik-Bahae, A. A. Said, T. Wei, D. J. Hagan and E. W. Van Stryland,"Sensitive measurement of optical nonlinearities using a single beam," Quantum Electronics, IEEE Journal Of, vol. 26, pp. 760-769, 1990.

[77] L. M. Irimpan, Spectral and Nonlinear Optical Characterization of ZnO Nanocomposites,Ph. D. Thesis. CUSAT. Kochi, 2008.

[78] M. Sheik-Bahae, A. A. Said, T. Wei, D. J. Hagan and E. W. Van Stryland, "Sensitive measurement of optical nonlinearities using a single beam," Quantum Electronics, IEEE Journal Of, vol. 26, pp. 760-769, 1990.

[79] I. Sebastian, S. Divya, V. Nampoori, P. Radhakrishnan and S. Thomas, "Impact of intermediate localized states on nonlinear optical absorption of Ga-Ge-Se nanocolloidal solutions," Appl. Phys. Lett., vol. 102, pp. 031115, 2013.

[80] K. Tanaka, "Optical nonlinearity in photonic glasses," J. Mater. Sci. : Mater. Electron., vol. 16, pp. 633-643, 2005.

[81] I. Hod and A. Zaban, "Materials and interfaces in quantum dot sensitized solar cells: Challenges, advances and prospects," Langmuir, vol. 30, pp. 7264-7273, 2013.

[82] M. Graetzel, R. A. Janssen, D. B. Mitzi and E. H. Sargent, "Materials interface engineering for solution-processed photovoltaics," Nature, vol. 488, pp. 304-312, 2012.

[83] H. Tada, M. Fujishima and H. Kobayashi,"Photodeposition of metal sulfide quantum dots on titanium (IV) dioxide and the applications to solar energy conversion," Chem. Soc. Rev., vol. 40, pp. 4232-4243, 2011.

[84] P. K. Santra and P. V. Kamat,"Mn-doped quantum dot sensitized solar cells: a strategy to boost efficiency over 5%," J. Am. Chem. Soc., vol. 134, pp. 2508-2511, 2012.

[85] M. A. Hossain, J. R. Jennings, Z. Y. Koh and Q. Wang,"Carrier generation and collection in CdS/CdSe-sensitized SnO2 solar cells exhibiting unprecedented photocurrent densities," Acs Nano, vol. 5, pp. 3172-3181, 2011.

[86] J. Ryu, S. H. Lee, D. H. Nam and C. B. Park,"Rational Design and Engineering of QuantumDotSensitized TiO_2 Nanotube Arrays for Artificial Photosynthesis," Adv Mater, vol. 23, pp. 1883-1888, 2011.

[87] T. Sugaya, O. Numakami, R. Oshima, S. Furue, H. Komaki, T. Amano, K. Matsubara, Y. Okano and S. Niki, "Ultra-high stacks of InGaAs/GaAs quantum dots for high efficiency solar cells," Energy & Environmental Science, vol. 5, pp. 6233-6237, 2012.

[88] P. V. Kamat, "Quantum dot solar cells. The next big thing in photovoltaics," The Journal of Physical Chemistry Letters, vol. 4, pp. 908-918, 2013.

[89] B. Oregan and M. Grfitzeli, "A low-cost, high-efficiency solar cell based on dye-sensitized," Nature, vol. 353, pp. 24, 1991.

[90] P. G. Bomben, K. C. Robson, P. A. Sedach and C. P. Berlinguette,"On the viability of cyclometalated Ru (II) complexes for light-harvesting applications," Inorg. Chem., vol. 48, pp. 9631-9643, 2009.

[91] P. G. Johansson, J. G. Rowley, A. Taheri, G. J. Meyer, S. P. Singh, A. Islam and L. Han, "Long-Wavelength Sensitization of TiO2 by Ruthenium Diimine Compounds with Low-Lying * Orbitals," Langmuir, vol. 27, pp. 14522-14531, 2011.

[92] H. C. Zhao, J. P. Harney, Y. Huang, J. Yum, M. K. Nazeeruddin, M. Gratzel, M. Tsai and J. Rochford, "Evaluation of a ruthenium oxyquinolate architecture for dye-sensitized solar cells," Inorg. Chem., vol. 51, pp. 1-3, 2011.

[93] S. Kazemzadeh, A. Hassanjani-Roshan, M. Vaezi and A. Shokuhfar, " The effect of microwave irradiation time on appearance properties of silver nanoparticles," Transactions of the Indian Institute of Metals, vol. 64, pp. 261-264, 2011.

[94] S. Panigrahi and D. Basak, "Morphology driven ultraviolet photosensitivity in ZnOCdS composite," J. Colloid Interface Sci., vol. 364, pp. 10-17, 2011.

[95] I. Robel, V. Subramanian, M. Kuno and P. V. Kamat, "Quantum dot solar cells. Harvesting light energy with CdSe nanocrystals molecularly linked to mesoscopic TiO_2 films," J. Am. Chem. Soc., vol. 128, pp. 2385-2393, 2006.

[96] Q. Shen, J. Kobayashi, L. J. Diguna and T. Toyoda, "Effect of ZnS coating on the photovoltaic properties of CdSe quantum dot-sensitized solar cells," J. Appl. Phys., vol. 103, pp. 084304, 2008.

[97] R. Plass, S. Pelet, J. Krueger, M. Grtzel and U. Bach,"Quantum dot sensitization of organic-inorganic hybrid solar cells," The Journal of Physical Chemistry B, vol. 106, pp. 7578-7580, 2002.

[98] P. Yu, K. Zhu, A. G. Norman, S. Ferrere, A. J. Frank and A. J. Nozik, "Nanocrystalline TiO_2 solar cells sensitized with InAs quantum dots," The Journal of Physical Chemistry B, vol. 110, pp. 25451-25454, 2006.

[99] V. Gonzlez-Pedro, X. Xu, I. Mora-Sero and J. Bisquert, "Modeling high-efficiency quantum dot sensitized solar cells," ACS Nano, vol. 4, pp. 5783-5790, 2010.

[100] X. Yu, J. Liao, K. Qiu, D. Kuang and C. Su,"Dynamic study of highly efficient CdS/CdSe quantum dot-sensitized solar cells fabricated by electrodeposition," Acs Nano, vol. 5, pp. 9494-9500, 2011.

[101] C. Cheng, S. K. Karuturi, L. Liu, J. Liu, H. Li, L. T. Su, A. I. Y. Tok and H. J. Fan, "QuantumDotSensitized TiO2 Inverse Opals for Photoelectrochemical Hydrogen Generation," Small, vol. 8, pp. 37-42, 2012.

[102] J. Zhao, A. Wang, M. A. Green and F. Ferrazza,"19.8% efficient honeycomb textured multicrystalline and 24.4% monocrystalline silicon solar cells," Appl. Phys. Lett., vol. 73, pp. 1991-1993, 1998.

[103] C. J. Brabec, N. S. Sariciftci and J. C. Hummelen, "Plastic solar cells," Advanced Functional Materials, vol. 11, pp. 15-26, 2001.

[104] C. J. Brabec, G. Zerza, G. Cerullo, S. De Silvestri, S. Luzzati, J. C. Hummelen and S. Sariciftci, "Tracing photoinduced electron transfer process in conjugated polymer/fullerene bulk heterojunctions in real time," Chemical Physics Letters, vol. 340, pp. 232-236, 2001.

[105] M. Grtzel,"Solar energy conversion by dye-sensitized photovoltaic cells," Inorg. Chem., vol. 44, pp. 6841-6851, 2005.

[106] J. Zhao, A. Wang, P. Altermatt and M. Green,"Twentyfour percent efficient silicon solar cells with double layer antireflection coatings and reduced resistance loss," Appl. Phys. Lett., vol. 66, pp. 3636-3638, 1995.

[107] J. Kalowekamo and E. Baker,"Estimating the manufacturing cost of purely organic solar cells," Solar Energy, vol. 83, pp. 1224-1231, 2009.

[108] K. Shin, J. Ahn, H. Kang and Y. S. Eom, System and Method for Producing Flexible Dye-Sensitized Solar Cells by a Roll-to-Roll Printing Process, 2014.

[109] A. Yella, H. W. Lee, H. N. Tsao, C. Yi, A. K. Chandiran, M. K. Nazeeruddin, E. W. Diau, C. Y. Yeh, S. M. Zakeeruddin and M. Gratzel, "Porphyrin-sensitized solar cells with cobalt (II/III)-based redox electrolyte exceed 12 percent efficiency," Science, vol. 334, pp. 629-634, Nov 4, 2011.

[110] R. Vogel, P. Hoyer and H. Weller,"Quantum-sized PbS, CdS,Ag_2S, Sb_2S_3, and Bi_2S_3 particles as sensitizers for various nanoporous wide-bandgap semiconductors," J. Phys. Chem., vol. 98, pp. 3183-3188, 1994.

[111] Q. Shen, T. Sato, M. Hashimoto, C. Chen and T. Toyoda, "Photoacoustic and photoelectrochemical characterization of CdSe-sensitized TiO_2 electrodes composed of nanotubes and nanowires," Thin Solid Films, vol. 499, pp. 299-305, 2006.

[112] M. Afzaal and P. O'Brien, "Recent developments in II-VI and III-VI semiconductors and their applications in solar cells," Journal of Materials Chemistry, vol. 16, pp. 1597-1602, 2006.

[113] I. Hod, V. Gonzlez-Pedro, Z. Tachan, F. Fabregat-Santiago, I. Mora-Ser, J. Bisquert and A. Zaban,"Dye versus quantum dots in sensitized solar cells: participation of quantum dot absorber in the recombination

process," The Journal of Physical Chemistry Letters, vol. 2, pp. 3032-3035, 2011.

[114] S. Gorer and G. Hodes, "Quantum size effects in the study of chemical solution deposition mechanisms of semiconductor films," J. Phys. Chem., vol. 98, pp. 5338-5346, 1994.

[115] R. Vogel, K. Pohl and H. Weller,"Sensitization of highly porous, polycrystalline TiO_2 electrodes by quantum sized CdS," Chemical Physics Letters, vol. 174, pp. 241-246, 1990.

[116] A. Salant, M. Shalom, I. Hod, A. Faust, A. Zaban and U. Banin, "Quantum dot sensitized solar cells with improved efficiency prepared using electrophoretic deposition," Acs Nano, vol. 4, pp. 5962-5968, 2010.

[117] I. Mora-Ser, S. Gimenez, F. Fabregat-Santiago, R. Gomez, Q. Shen, T. Toyoda and J. Bisquert,"Recombination in quantum dot sensitized solar cells," Acc. Chem. Res., vol. 42, pp. 1848-1857, 2009.

[118] T. Bessho, E. Yoneda, J. Yum, M. Guglielmi, I. Tavernelli, H. Imai, U. Rothlisberger, M. K. Nazeeruddin and M. Gratzel,"New paradigm in molecular engineering of sensitizers for solar cell applications," J. Am. Chem. Soc., vol. 131, pp. 5930-5934, 2009.

[119] M. Shalom, Z. Tachan, Y. Bouhadana, H. Barad and A. Zaban, " Illumination intensity-dependent electronic properties in quantum dot sensitized solar cells," The Journal of Physical Chemistry Letters, vol. 2, pp. 1998-2003, 2011.

[120] V. Gonzlez-Pedro, X. Xu, I. Mora-Sero and J. Bisquert,"Modeling high-efficiency quantum dot sensitized solar cells," ACS Nano, vol. 4, pp. 5783-5790, 2010.

[121] J. Tian, Z. Liang, R. Gao, Q. Zhang and G. Cao,"CdS/CdSe co-sensitized quantum dots solar cells with different density of ZnO nanowire arrays," in Meeting Abstracts, pp. 424-424, 2012.

[122] J. Tian and G. Cao, "Semiconductor quantum dot-sensitized solar cells," Nano Reviews, vol. 4, pp. 18737-18753, 2013.

[123] Q. Zhang, E. Uchaker, S. L. Candelaria and G. Cao,"Nanomaterials for energy conversion and storage," Chem. Soc. Rev., vol. 42, pp. 3127-3171, 2013.

[124] S. Baskoutas and A. F. Terzis, "Size-dependent band gap of colloidal quantum dots," J. Appl. Phys., vol. 99, pp. 013708, 2006.

[125] D. Segets, J. M. Lucas, R. N. Klupp Taylor, M. Scheele, H. Zheng, A. P. Alivisatos and W. Peukert,"Determination of the quantum dot band gap dependence on particle size from optical absorbance and transmission

electron microscopy measurements," Acs Nano, vol. 6, pp. 9021-9032, 2012.

[126] Caruge, J. M., J. E. Halpert, V. Wood, V. Bulovi, and M. G. Bawendi., "Colloidal quantum-dot light-emitting diodes with metal-oxide charge transport layers", Nature Photonics vol.2, pp.247-250,2008.

[127] M. J. Panzer, K. E. Aidala and V. Bulovic, "Contact printing of colloidal nanocrystal thin films for hybrid organic/quantum dot optoelectronic devices," Nano Rev., vol. 3, pp. 10.3402, 2012.

[128] E. S. Shibu, A. Sonoda, Z. Tao, Q. Feng, A. Furube, S. Masuo, L. Wang, N. Tamai, M. Ishikawa and V. Biju,"Energy materials: supramolecular nanoparticles for solar energy harvesting," Nano Rev., vol. 4, pp. 10.3402, 2013.

[129] A. J. Nozik,"Nanoscience and nanostructures for photovoltaics and solar fuels," Nano Letters, vol. 10, pp. 2735-2741, 2010.

[130] P. V. Kamat, "Quantum dot solar cells. The next big thing in photovoltaics," The Journal of Physical Chemistry Letters, vol. 4, pp. 908-918, 2013.

[131] S. Divya, A. Thankappan, C. Vallabhan, V. Nampoori, P. Radhakrishnan and A. Mujeeb,"Electrolyte/photoanode engineered performance of TiO2 based dye sensitised solar cells," J. Appl. Phys., vol. 115, pp. 064501, 2014.

[132] Y. Li, L. Wei, R. Zhang, Y. Chen and J. Jiao, "Annealing effect on photovoltaic performance of CdSe quantum-dots-sensitized TiO_2 nanorod solar cells," Journal of Nanomaterials, vol.2012, pp.1-6, 2012.

[133] Y. Chen, J. Herrnsdorf, B. Guilhabert, Y. Zhang, I. M. Watson, E. Gu, N. Laurand and M. D. Dawson, "Colloidal quantum dot random laser," Optics Express, vol. 19, pp. 2996-3003, 2011.

[134] Z. Wu, Z. Mi, P. Bhattacharya, T. Zhu and J. Xu,"Enhanced spontaneous emission at 1.55 m from colloidal PbSe quantum dots in a Si photonic crystal microcavity," Appl. Phys. Lett., vol. 90, pp. 171105-171105, 2007.

[135] R. Bose, X. Yang, R. Chatterjee, J. Gao and C. W. Wong, "Weak coupling interactions of colloidal lead sulphide nanocrystals with silicon photonic crystal nanocavities near 1.55 m at room temperature," Appl. Phys. Lett., vol. 90, pp. 111-117, 2007.

[136] J. Xu and M. Xiao, "Lasing action in colloidal CdS/CdSe/CdS quantum wells," Appl. Phys. Lett., vol. 87, pp. 173117-173117-3, 2005.

[137] J. Yang, J. Heo, T. Zhu, J. Xu, J. Topolancik, F. Vollmer, R. Ilic and P. Bhattacharya, "Enhanced photoluminescence from embedded PbSe colloidal quantum dots in silicon-based random photonic crystal microcavities," Appl. Phys. Lett., vol. 92, pp. 261110, 2008.

[138] H. Cao, Y. Zhao, S. Ho, E. Seelig, Q. Wang and R. Chang,"Random laser action in semiconductor powder," Phys. Rev. Lett., vol. 82, pp. 2278, 1999.

[139] X. Zhao, Z. Wu, S. Ning, S. Liang, D. Wang and X. Hou, "Random lasing from granular surface of waveguide with blends of PS and PMMA," Optics Express, vol. 19, pp. 16126-16131, 2011.

[140] N. M. Lawandy, R. Balachandran, A. Gomes and E. Sauvain,"Laser action in strongly scattering media," Nature, vol. 368, pp. 436-438, 1994.

[141] H. Cao, Y. Zhao, S. Ho, E. Seelig, Q. Wang and R. Chang, "Random laser action in semiconductor powder," Phys. Rev. Lett., vol. 82, pp. 2278, 1999.

[142] R. C. Polson, M. E. Raikh and Z. V. Vardeny, "Universal properties of random lasers," Selected Topics in Quantum Electronics, IEEE Journal Of, vol. 9, pp. 120-123, 2003.

[143] Y. Boucher and P. Feron, "Generalized transfer function: A simple model applied to active single-mode microring resonators," Opt. Commun., vol. 282, pp. 3940-3947, 2009.

[144] V. I. Klimov VI, A. A. Mikhailovsky, D. W. McBranch, C. A. Leatherdale and M. G. Bawendi,"Quantization of multiparticle auger rates in semiconductor quantum dots," Science, vol. 287, pp. 1011-1013, 2000.

[145] D. Derkacs, W. Chen, P. Matheu, S. Lim, P. Yu and E. Yu, "Nanoparticle-induced light scattering for improved performance of quantum-well solar cells," Appl. Phys. Lett., vol. 93, pp. 091107, 2008.

[146] R. Polson, A. Chipouline and Z. Vardeny," Random Lasing in p-Conjugated Films and Infiltrated Opals," Adv Mater, vol. 13, pp. 760-764, 2001.

Chapter 3

Linear optical studies on CdSe quantum dots based materials

This chapter includes linear optical studies on the CdSe QDs and their dependence on various parameters like presence of capping agent, preparation methods, particle size, band gap, pH etc. Linear optical studies of CdSe-metal nanofluids has also been discussed in the present chapter. Discussion on photo induced studies on the samples give information about the photo darkening effect.

Results of this chapter are published in :

1. *Anju K Augustine et.al.,Asian Journal of Physics,vol.23, pp.683-686,2014.*

3.1 Introduction

During the last two decades, there has been an enormous interest in nanomaterials due to their novel physical and chemical properties which arise from quantum confinement of charge carriers[1, 2]. Luminescent semiconductor QDs are a promising alternative to organic dyes for fluorescence applications because of their stability against photo bleaching narrow and size-tunable multicolour emission as well as the functional advantages [3-5]. These materials hold potential applications in various fields including uses in fluorescent labels for photonic devices, sensor applications, biomedical science, solar cells etc. [6-8]. Core-shell QDs have been used as hetero nanocrystals, which allow optical amplification because of their stimulated emission of single-exciton states [9]. The most notable properties of such materials are, their high stability during and after growth[10], strong quantum confinement similar to atoms [11], different thermodynamically stable structures[12, 13] and a high surface to volume ratio, which means that most of the atoms are located on the surface.

For this reason, the passivating ligands contribute, a significant role in the properties of the total number of the atoms, so that the dispersing medium can dramatically affect their properties [14]. Therefore, the synthesis of stable nanoparticles via. colloidal aqueous solutions is extremely important because it prevents changes in dispersion media, thereby preserving the surface properties of the nanoparticles. Obtaining characteristic properties like thermodynamic stability, homogeneous dispersion, high radiative quantum efficiency, a very broad absorption spectrum, low levels of nonspecific links to biological compounds and, most importantly, stability in aqueous media simultaneously has been extremely difficult. Therefore, the fabrication of ideal QDs directly in an aqueous phase is of great interest because it would be highly reproducible, inexpensive, minimally toxic and capable of forming products that are easily dissolved in water.

Tuning of structural and optical properties of QDs, synthesized directly in a colloidal aqueous solution is also possible because these properties are strongly affected by various parameters of the synthesis process, such as the Cd/Se molar ratio[2], the cadmium precursor type [15], the

precursor concentration [16], reflux time[17], the stabilizer type [18-20], and the reaction medium [10, 21, 22]. Furthermore, inorganic QDs have several advantages over organic dyes, such as high molar absorption, a broad absorption spectrum, a narrow emission spectrum and high photo stability [23]. Among the various kinds of semiconductor NPs, colloidal CdSe is the most widely investigated one,because their emission can be easily tuned to cover from red (centered at 650 nm) to blue (centered at 450 nm) as the size of NPs decreases. CdSe having a band gap of 1.74 eV at 300K is a useful semiconductor material because of its strong size-dependent optical properties [24]. CdSe QDs can be prepared in either aqueous or organic solutions. It has thus been found that one of the successful methods to synthesize CdSe QDs are based on the trioctyl phosphine/trioctyl phosphine oxide (TOP/TOPO) non aqueous method. However, these CdSe QDs are only soluble in some nonpolar organic solvent, which raises problems if they have to be used for biological applications[25-27]. In this chapter we include linear optical studies of the as prepared CdSe QDs based photonic materials and their dependence on various parameters like capping agent, preparation methods, particle size, band gap, pH etc. Linear optical studies of CdSe-metal nanofluids has also been discussed in the present chapter. Discussion of photo induced effects on the samples gives information about the photo darkening effect. Samples for the investigations are prepared in aqueous medium and this approach yields a physiologically compatible medium that is useful in medical, biotechnological and photonic applications.

3.2 Synthesis of nanoparticles

3.2.1 Synthesis of CdSe QDs by reflux method

CdSe QDs are prepared by a modified aqueous method using reflux. Along with the precursors $CdCl_2.H_2O and Na_2SeO_3$, mercaptosuccinic acid (MSA) is used as the capping agent in a molar ratio 4:1:12. The buffer solution with pH$\sim$ 7 is prepared with sodium borate and citric acid in water [28]. The precursors are added in to the buffer with constant stirring. The pH of the corresponding colourless solution is adjusted by adding 1M NaOH. It was placed in a three-necked flask followed by reflux at 100°C in open-air conditions. Reflux process gives the required thermal energy to the reaction. The colour of the solution

turned to bright yellow after a few minutes reflux. The temperature of the reaction system was maintained at 100°C.

During the reflux, the colour of solution gradually changed and NPs started to form and aliquots were taken out of the flask at different times for the optical measurements to monitor the growth of the nanoparticles. The particles tend to form agglomerates due to the strong interaction of the carboxylic groups [29] leading to a possible over estimation of the mean size distribution. Also it is noted that the use of a suitable buffer solution is very crucial for a successful synthesis of highly luminescent CdSe QDs. During the formation of CdSe QDs , the following chemical reactions takes place [30].

$$(SeO_3)^{2-} + BH_4 \rightarrow Se^{2-} + B(OH)^3 + H_2O \tag{3.1}$$
$$CdL + Se^{2-} \rightarrow CdSe \quad where \;\; L = MSA.$$

Even though the Se^{2-} is very sensitive to oxygen, we did not preclude the oxygen dissolved in water. Here we assumed that the initially formed Se^{2-} may be re-oxidized to higher valance of Selenium which can be instantly reduced back to Se^{2-} by an excess $NaBH_4$ in water till the oxygen near Se^{2-} monomers were exhausted.

3.2.2 CdSe QDs by microwave irradiation method

In this method of synthesis, CdSe QDs are prepared by a rapid microwave irradiation. Along with the precursors $CdCl_2.H_2OandNa_2SeO_3$, mercaptosuccinic acid (MSA) is used as the capping agent in a molar ratio 4:1:12. The pH of the corresponding colourless solution is adjusted by adding 1M NaOH. It was placed in a conical flask followed by microwave irradiation. This gives the required thermal energy to the reaction. The colour of the solution turned to bright yellow after a few minutes of microwave irradiation. The power of the reaction system was maintained at 60W. During the reaction, the colour of solution gradually changed and NPs started to form and aliquots were taken out of the flask at different times for the optical measurements to monitor the growth of the NPs. Because of the shorter preparation time and formation of the good quality samples, we have selected this as the better synthesis

method for further applications.

3.2.3 Metal NPs by microwave irradiation method

Synthesis of silver nanoparticles, starts with boiling of 1mM $AgNO_3$ in aqueous solution followed by addition of 5 ml of 1% sodium citrate solution and 0.2 g of $NaBH_4$ during microwave irradiation. $NaBH_4$ act as the reducing agent while the sodium citrate takes the role of capping agent. For Au NPs, 0.5mM of $HAuCl_4$ in aqueous solution is allowed to boil by microwave rapid heating is followed by addition of 3.8 mM sodium citrate which takes the dual role of capping agent and reducing agent.

3.2.4 Effect of capping agent in the formation of CdSe QDs

The capping agent used in the formation of CdSe QDs in our experiment is mercaptosuccinic acid (MSA). The molecular structure of the MSA, a typical representation of MSA capped CdSe QDs and the photographs of the CdSe QDs synthesized by microwave irradiation method are shown in figure 3.1. The stability of the samples were studied by varying the pH

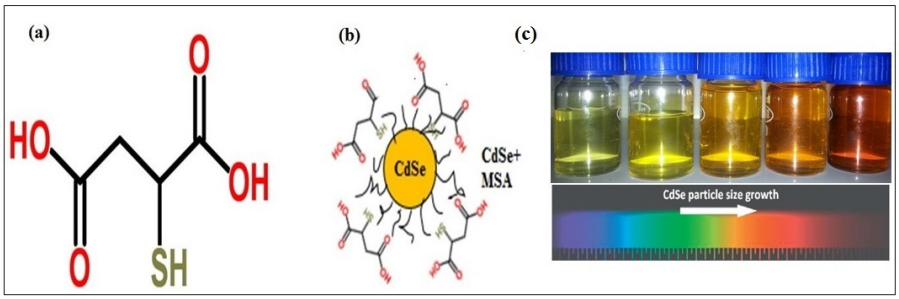

Figure 3.1: (a) Molecular structure of MSA, (b) Typical representation of the MSA capped CdSe QDs and (c) Photographs of the CdSe QDs synthesized by microwave irradiation method.

of the solution. Both the above mentioned methods of synthesis resulted in QDs with better stability with MSA as capping agent. It is observed that MSA - CdSe can be synthesized even in weak acidic solution, mostly because of the special structure of MSA with two carbonyl groups. In

our study, we obtained high-quality CdSe QDs in weak acid solution. One of the possible reason is the reduction in the number of trap sites on the CdSe surface after being covered with cadmiu-thiol complexes and the unique structure of MSA plays an important role in reducing the surface trap of CdSe QDs [31, 32]. The two carbonyl groups of MSA can provide better stability than other thiol compounds (MPA, GSH, etc.). Nevertheless, when the pH of the precursor solution was decreased further, it led to weakening of the protection abilities of MSA due to the protonation of MSA.

3.3 Linear optical studies of CdSe QDs

Linear optical studies mainly includes optical absorption and fluorescence studies of the samples. It reveals the absorption regions of the particles formed and the corresponding excitation energy and band gap. Particle size can also be calculated from the absorption spectra while fluorescence spectroscopy shows the emission at a particular excitation wavelength.

3.3.1 CdSe QDs with different particle size synthesized by reflux method

CdSe QDs are prepared by reflux method. Figure 3.2 shows the absorption spectra of the prepared CdSe QDs at room temperature. It can be clearly seen that the absorption and luminescence peaks of the CdSe QDs are red-shifted with increasing time of reflux, which in turn, decreases the energy gap of the resulting CdSe QDs . The absorption spectra from figure 3.3:(a) clearly shows a tunable change in absorption edge from 430nm-510nm. Sharp excitonic peaks in the spectra indicate mono dispersion of the CdSe QDs. Emission spectra of the CdSe QDs with different reflux time in figure 3.3:(b) shows that the spectra is extremely broad and the peak at 560 nm gets shifted to longer wavelengths (630nm) as the reflux time increases. This red-shift in emission peak arises due to the increase in size of the nanoparticles. These emissions are basically from exitonic ($1S_e - 1S_h$) transitions [29]. It is likely that there are a large number of surface defects at the early stages of NP nucleation, and the surface state density is high for small particles

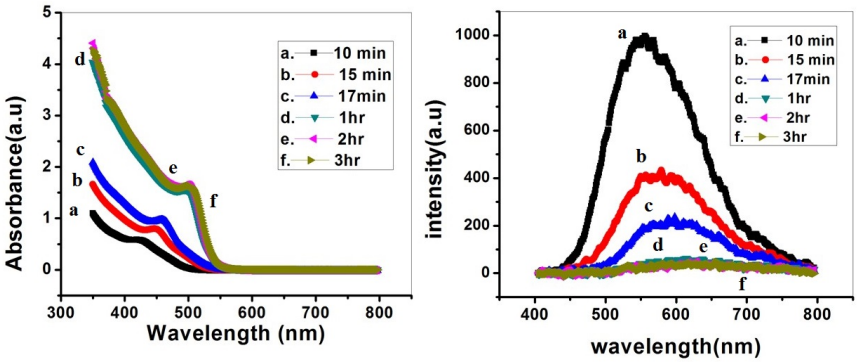

Figure 3.2: (a) Absorption spectra and (b) Emission spectra of the CdSe QDs with different reflux time.

[34] resulting in a rapid shift to lower energy region of free exciton emission[35].

For detailed study, we used samples with reflux time 10min, 1hr, 2hr and 3hr and are denoted as C_1, C_2, C_3 and C_4 respectively. During the reflux time from 10min to 3 hr, optical band gap of the NPs change from 2.52 eV-2.35 eV due to the increase in the particle size and is shown in figure 3.3. Particle size, shape and image of the as prepared CdSe QDs

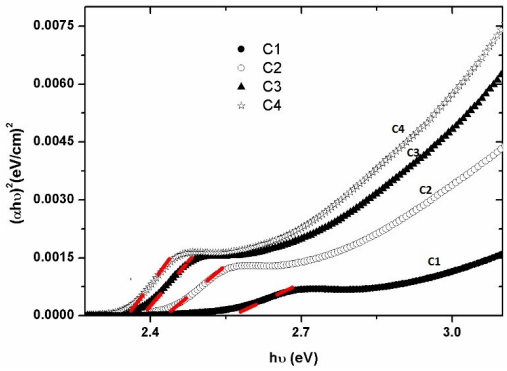

Figure 3.3: Optical energy band gap variation of the samples C_1, C_2, C_3,&C_4.

are shown from figure 3.4 where the spherical shaped particles are observed with average particle size $\sim$ 4-6nm.

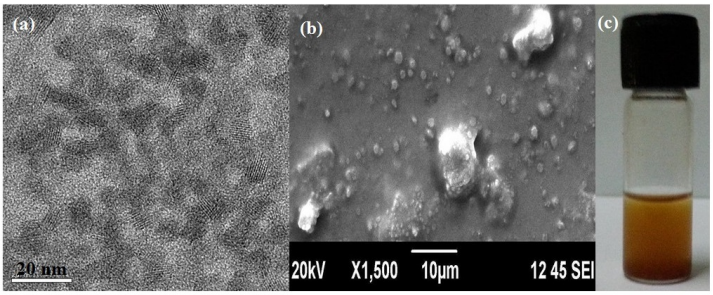

Figure 3.4: (a) TEM (b) SEM and (c) Photograph of the CdSe QDs (C_3)

The particle size is calculated with effective mass approximation[13]. For CdSe: E_{bulk}=1.74 eV, ϵ=10.6, m_e*=0.13, m_h*=0.45

$$E_{nano} = E_{bulk} + \frac{h^2}{2m_0 d^2}(\frac{1}{m_e^*} + \frac{1}{m_h^*}) - \frac{36e^2}{4\pi\epsilon\epsilon_0 d} \tag{3.2}$$

where d is the particle diameter. The calculated particle size by effective mass approximation method of the samples are presented in Table 3.1.

Sample	Particle size (nm)	Bandgap (eV)
C_1	4.62	2.516
C_2	4.88	2.384
C_3	4.96	2.348
C_4	5.16	2.345

Table 3.1: Particle size and band gap of CdSe QDs (C_1, C_2, C_3,&C_4).

3.3.2 CdSe QDs with different particle size by microwave irradiation method

For detailed study, we used samples prepared by different microwave irradiation times 10 seconds, 15 seconds, 20 seconds and 30 seconds which are denoted as C_1, C_2, C_3, and C_4 respectively. The images of as prepared samples of CdSe quantum dots showing visible emission on ultraviolet light irradiation are shown in figure 3.5. The different colours for the samples (C_1, C_2,&C_4) from yellow to red shows the confinement of the particle in the strong confinement regime. The absorption and

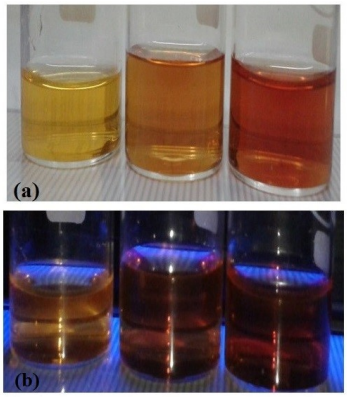

Figure 3.5: (a) True colour under visible light and (b) UV irradiated florescent images of C_1, C_2, andC_4 samples of CdSe QDs with different microwave irradiation time 10seconds, 15 seconds, 20 seconds and 30 seconds respectively.

fluorescent spectra of the CdSe QDs are given in figure 3.6:(a) & (b) respectively. Optical absorption studies show a red shift of absorption edge as the microwave irradiation time increases. Photoluminescence spectra of the prepared samples show a strong emission around 560nm wavelength in the case of CdSe QDs prepared by microwave irradiation for 10seconds. As the irradiation time of microwave increases, this emission get reduced due to the decrease in oscillator strength as a result of the aggregation of NPs. The particle size is calculated with effective mass approximation [36] using equation (3.2) above. As the particle size is increased, the absorption edge shifts to longer wavelength side and is given in Table 3.2.

Sample	Absorption edge(nm)	Particle size (nm)
C_1	529	2.29
C_2	572	2.68
C_3	635	3.64
C_4	650	4.03

Table 3.2: Data showing particle size and absorption edge of CdSe QDs irradiated by microwaves for different durations.

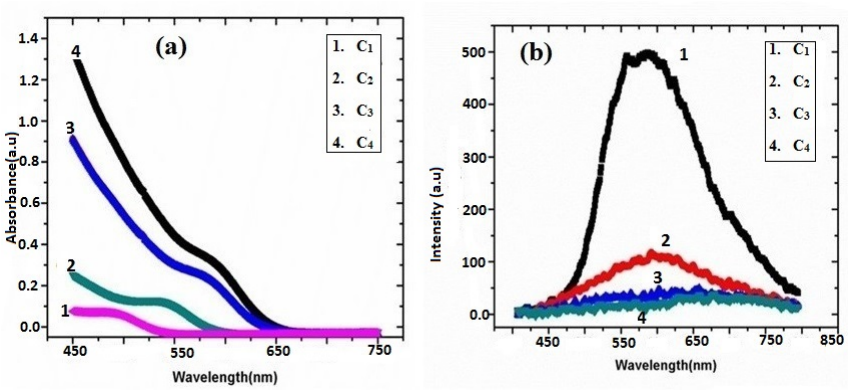

Figure 3.6: (a) Absorption and (b) fluorescence spectrum of C_1, C_2, C_3,&C_4 corresponding to different microwave irradiation time

3.3.3 Spectroscopic studies of CdSe nanofluids with different pH

CdSe QDs are prepared by a rapid microwave irradiation method. The pH of the corresponding colorless solution is adjusted by adding 1M NaOH. We have selected samples with different pH values. The samples taken for optical characterization are named as pH 3.7, pH 4.7, pH 7.6, and pH 8.9.

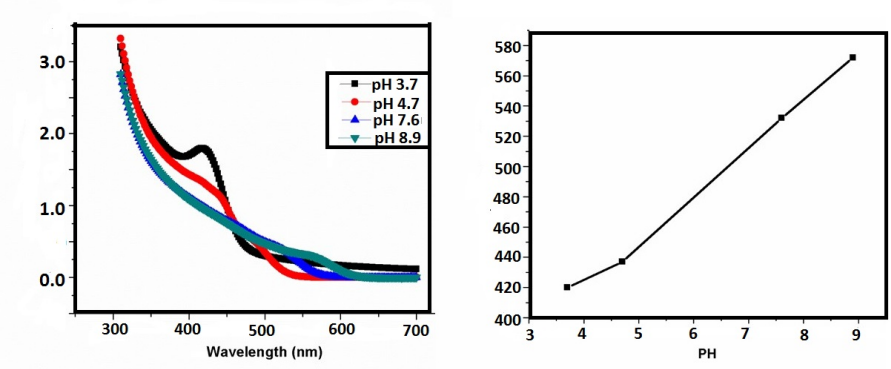

Figure 3.7: (a) Absorption spectra of the prepared CdSe nanofluids with pH (b) Red shift in wavelength of CdSe nanofluids with pH

Figure 3.7 and figure 3.8 shows the absorption and florescence spectra of the prepared CdSe QDs with different pH at room temperature. It can be clearly seen that the absorption and luminescence peaks of the CdSe QDs are red-shifted with increasing pH. It is observed that for sample with pH less than 4.7, a sign of agglomeration appears and with increasing the pH of the solution, the emission intensity is reduced. Figure 3.8

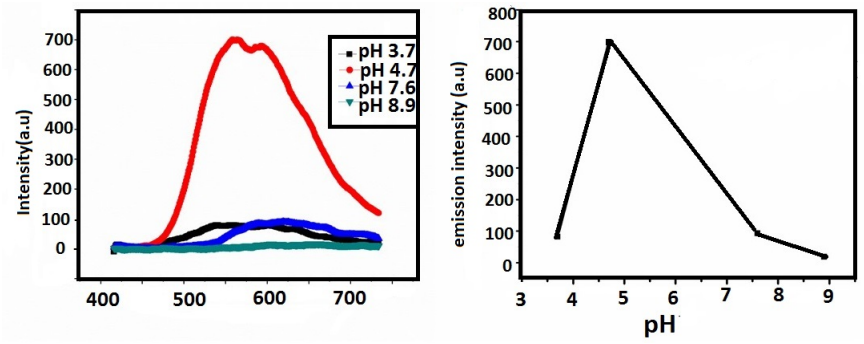

Figure 3.8: (a) Fluorescence spectra of the as prepared CdSe Quantum dots with different pH,(b) Change in the intensity of fluorescence peak CdSe QDs with pH value.

shows the effects of the reaction solution pH on the fluorescence properties of CdSe QDs. It can be seen that the pH in our synthesis is much lower than that with glutathione (GSH) ($\sim 11-12$) or MPA (≥ 8) as thiol stabilizers used in common aqueous synthesis. For example, when GSH was used as a stabilizer for CdSe QDs, the as-prepared colloid solution formed some white precipitate when the pH of the Cd precursor was reduced to acid or weakly basic, which restricted the preparation of CdSe QDs in a relatively lower pH aqueous solution. However, MSA-CdSe can be synthesized even in weak acidic solution, because of the special structure of MSA with two carbonyl groups. In this study, we also obtained high-quality CdSe QDs in weak acid solution and the possible reasons for which are as follows. First, previous studies indicated that thiols had strong complexation to CdSe QDs rather than to free cadmium ions. Under acidic conditions, this resulted in less trap sites on the CdSe surface. Second, a thick layer of cadmium thiol complexes under acidic conditions was also an important factor for determining high-quality QDs, because more trap sites on the CdSe surface are re-

moved after being covered with cadmium thiol complexes. Last, but not the least, the unique structure of MSA plays an important role in reducing the surface trap of CdSe QDs [17-19].

3.3.4 Linear optical studies of CdSe QDs based nanocomposites

Light- induced charge separation and energy transfer in nanostructures are two important mechanisms in photovoltaic and photo catalytic applications. Metal-semiconductor hybrid nanosystems play a crucial role in such applications owing to their complementary optical properties and the novel applications based on the exciton-plasmon interaction [37-42]. NPs of gold and silver have dielectric-confined electromagnetic modes which show tunable absorption and scattering properties controllable by varying the surface plasmon resonance (SPR), whereas semiconductor QDs like CdSe and CdTe possess optical and thermal properties through the control of energy gaps [43]. These controls are realized by tuning the sizes and shapes of these nanostructures. When a semiconductor QD is conjugated with a metal NP to form nanohybrid (NH), modification of optical and thermal properties of particular interest is obtained [44-46].

Light emissions of these NHs resemble the radiative behavior of organic molecules near metals [47-50], which can be effectively quenched. The influence of plasmon-exciton coupling on these phenomena depends on several parameters that play a decisive role in the quenching and enhancement mechanisms[51, 52]. Several metal-semiconductor hybrid nanoparticles(HNPs) consisting of various materials like Au-CdSe, Au-InAs, Au-PbS, Au-Cu_2O, Au-MnO, Ag-Fe_3O_4, Ag-Ag_2S, and Co-TiO_2 have been prepared by different methods[53]. Among these materials, Au-CdSe and Ag-CdSe systems have attracted specific consideration due to their ease of production, uniform morphology, effective charge separation, and potential applications in solar cells.

Experimental methods

In our study, microwave rapid heating is used for the synthesis of CdSe QDs and metal nanoparticles. For the preparation of hybrid CdSe-metal NPs , colloidal Ag/Au NPs are mixed to the colloidal CdSe QDs in fixed

volume ratio. Sharp excitonic peak in figure 3.9:(a) indicates mono dis-

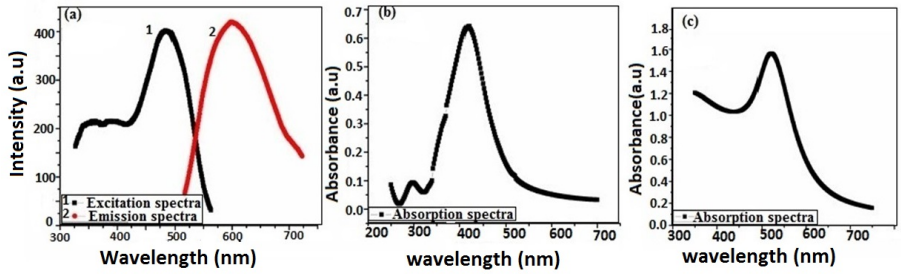

Figure 3.9: (a) Excitation and emission spectra of CdSe QDs, (b) Absorption spectra of AgNPs and (c) Absorption spectra of AuNPs.

persion of the CdSe QDs and these emissions are basically from exitonic ($1S_e - 1S_h$) transitions. SPR peaks around 415 nm from figure 3.9:(b) confirms the presence of Ag. The absorption peak at 520 nm in figure 3.9:(c) confirms the presence of Au NPs. The shape and position of surface plasmon absorption depend on particles size, shape and the dielectric constant of the surrounding medium. The sharpness of the peaks indicates that the particle sizes are fairly uniform and is confirmed from TEM images shown in figure 3.10.

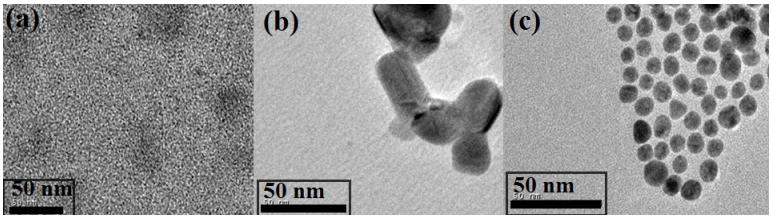

Figure 3.10: TEM images of mono dispersed (a) CdSe QDs, (b) Ag NPs and (c) Au NPs.

Absorption spectra of CdSe-Ag NPs and CdSe-Au NPs is shown in figure 3.11. It is also observed from figure 3.12 that at a particular volume fraction of metal NP (in both cases) a noticeable increase in the photoluminescence (PL) emission is observed from CdSe QDs due to metal induced surface plasmon.The emission relies on energy transfer from the

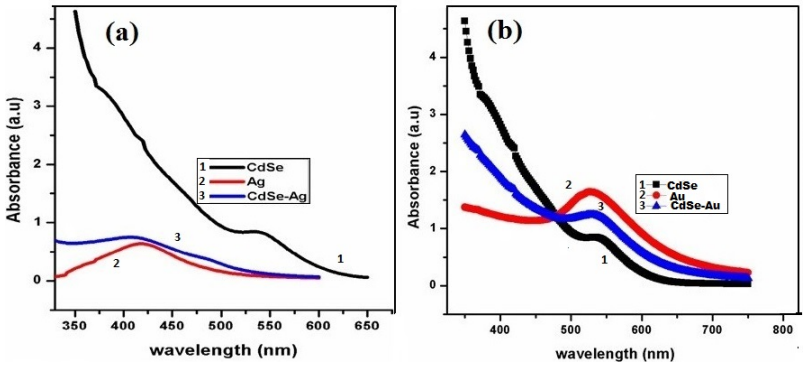

Figure 3.11: Absorption spectra of (a) CdSe-Ag NPs and (b) CdSe-Au NPs.

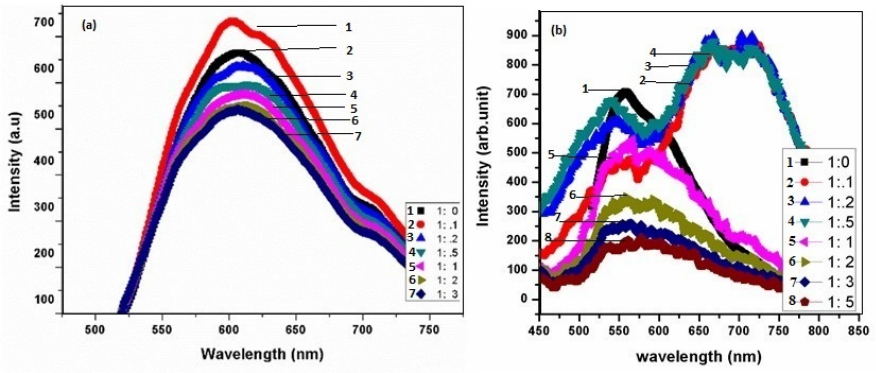

Figure 3.12: Florescence spectra of (a) CdSe-Ag NPs and (b) CdSe-Au NPs.

quantum dots to metal NPs which could be de-excited through radiative plasmon relaxation[54-56]. This exciton-plasmon interactions can give rise to modified emission properties like enhancement and quenching as seen from figure 3.12.

Generally, the interplay between metal NPs and QDs involves two major phenomena: first one is an enhancement of the local excitation field, and the second one is the modification of the radiative and nonradiative decay rates of the QDs, inducing a change of fluorescence lifetime and quantum yield. The competition between these processes results in two

contradictory observations as reported in the literature: quenching of luminescence or on the contrary it's enhancement. Different parameters play a determinant role in the quenching and enhancement mechanisms but their influence is still debated. Particularly, the spectral position and the influence of the localized surface plasmon resonance (LSPR) compared to the absorption and emission maximum of luminescent species is very decisive. Quenching of emission and shortening of exciton lifetime in the QD-NP superstructures can be explained using a typical model based on the exciton-plasmon resonance taking place when emission peak of excitons in QDs and absorption peak of the plasmons in NPs display a spectral overlap. In a QD-NP complex, oscillators corresponding to excitons in QDs and plasmons in metal NPs couple via simple Coulomb forces. Since QD-NP complexes are in liquid, they are randomly oriented with respect to the incident electric field which helps the additional mechanisms of energy transfer/quenching [57-60].

3.4 Photo induced studies on CdSe QDs based nanofluids

Photo induced phenomena has been characterized as photon mode, photo thermal mode and heat mode. In photon mode photo electronic excitation directly induces atomic structural changes and in PT mode photo electronic excitation induces structural changes with thermal activation while in heat mode, temperature rises by optical absorption is essential. Important photo induced processes are photo darkening, photo bleaching, photo-plastic effect, photochemical reactions, photo expansion, photo luminescence etc. Photo sensitivity of chalcogenide materials like Se/Te results changes in optical constants, electronic band gap, refractive index, optical absorption co-efficient and local atomic structure etc. These changes depend on the wavelength of the inducing light, the duration of exposure and the intensity of the light [61-62].

Experimental studies

Microwave rapid heating is used for the synthesis of CdSe QDs. Particle size of the CdSe sample (S_1) for the experiment is calculated as ~ 4 nm using effective mass approximation method [36]. Experimental set up

for the photo induced studies with exciting source of 403 nm blue laser with input power 100 mW,532 nm diode pumped solid state (DPSS) laser with input power100 mW and 632.8 nm He-Ne laser with input power 10 mW are shown in figure 3.13 below. Optical absorption, trans-

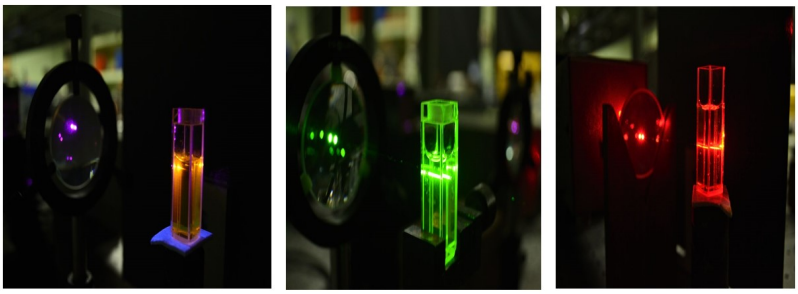

Figure 3.13: Experimental set up for the photo induced studies of CdSe nano fluid (sample-S_1) at different input excitations

mission and fluorescence spectra of the samples irradiated with different laser sources are studied and the corresponding changes at different time intervals are shown below, where 0,1,2,3 and 4 represents 0 min, 15 min, 45min, 1 hour and 1 day irradiation time respectively. As depicted in

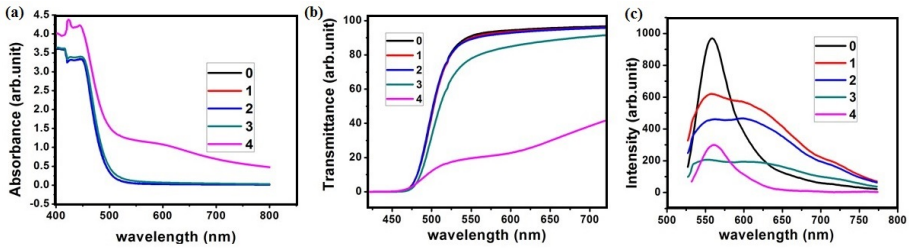

Figure 3.14: (a) Absorption, (b) Transmission and (c) Emission spectra of the CdSe nano fluid (S_1) irradiated with 403 nm wavelength for different time intervals.

figures 3.14. 3.15 and 3.16, we have observed photo darkening effect in our samples of CdSe at a time interval of one hour after irradiation; which refers to a shift of optical absorption edge to lower energies upon the application of light for which energy is near that of band gap energy.

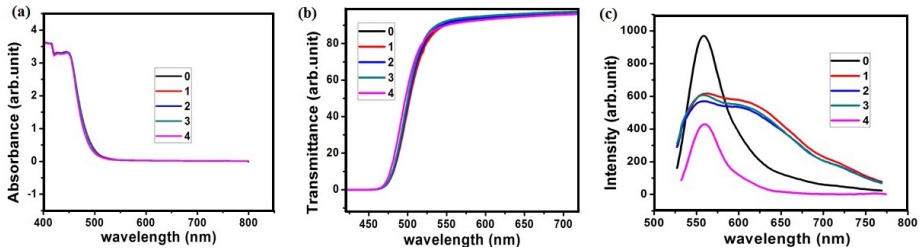

Figure 3.15: (a) Absorption, (b) Transmission and (c) Emission spectra of the CdSe nanofluid (S_1) irradiated with 532 nm wavelength for different time intervals.

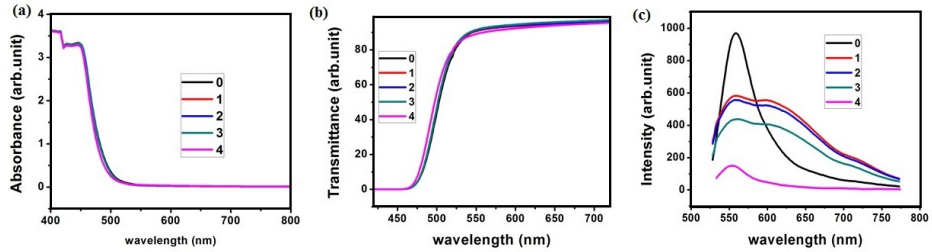

Figure 3.16: (a) Absorption, (b) Transmission and (c) Emission spectra of the CdSe nanofluid (S_1) irradiated with 632.8 nm wavelength for different time intervals.

An increase in the band tail absorption at corresponding change in optical transmission spectra can also be observed from the above figures. Since the above effects are reversed when kept at normal conditions after irradiation, this effect can thus be called as reverse photo darkening effect. Fluorescence spectra of the samples at different time intervals are also affected by these changes in optical constants and can be attributed to some photochemical changes occurring in the samples. The presence of new singlet and triplet states also arises which causes extra peak to be observed in the fluorescence spectrum. From these studies, it is concluded that the properties of the CdSe QDs based nanofluid can be controlled with light which makes them uniquely suitable for applications in optics and photonics [63].

3.5 Conclusion

- A simple synthetic route described in the chapter permits the synthesis of high-quality CdSe nanoparticles in aqueous solution.
- The as-synthesized MSA-capped CdSe QDs possess higher fluorescence, and better mono dispersity.
- The molecular structure of the capping agent - MSA, plays an important role in the formation of the mono dispersed QDs and the stability of the samples.
- These QDs show band gap tuning (2.52 eV-2.35 eV) and a strong fluorescence ranging from 560nm to 630nm for the prepared samples.
- CdSe QDs with narrow PL emissions and narrow size distributions have been synthesized in aqueous solution by microwave irradiation in the presence of MSA as an effective capping agent.
- The microwave irradiation time, power and pH of the reacting solution play important roles in controlling the optical properties of the CdSe QDs obtained.
- Optical absorption studies show a red shift of absorption edge as microwave irradiation time is increased and band gap can be tuned from 4.3 eV - 2.2 eV for the as prepared samples.
- Photoluminescence spectra of the prepared samples show a strong emission around 560nm wavelength and this emission gets decreased with irradiation time. This can be attributed to the decrease in oscillator strength due to the aggregation of QDs on microwave irradiation.
- CdSe QDs show red shifts in the absorption and luminescence peaks with increasing value of pH. Sample with pH less than 4.7 shows a sign of agglomeration and for higher pH, the intensity of emission gets decreased.

- To study the influence of plasmonic effect on CdSe nanofluids we have synthesized metal NPs of Au and Ag by microwave irradiation.
- With increasing volume of metal NPs, an enhancement in fluorescence spectrum followed by quenching is observed. The emission relies on energy transfer from the QDs to metal nanoparticles which could be de-excited through radiative plasmon relaxation.
- Photo induced studies of the samples show changes in absorption and transmission spectra with laser irradiating time. Reversible photo darkening effect is an interesting phenomenon observed from the samples.
- Fluorescence spectra of the corresponding samples also give information about the photochemical changes in the samples due to the formation of more excited levels.

3.6 References

[1] P. Gupta and M. Ramrakhiani, "Influence of the particle size on the optical properties of CdSe nanoparticles," Open Nanoscience Journal, vol. 3, pp. 15-19, 2009.

[2] L. Qu and X. Peng, "Control of photoluminescence properties of CdSe nanocrystals in growth," J. Am. Chem. Soc., vol. 124, pp. 2049-2055, 2002.

[3] P. Srivastava and K. Singh, "Synthesis of CdSe nanoparticles by solvothermal route: Structural, optical and spectroscopic properties," Advanced Materials Letters, vol. 3, pp. 340-344, 2012.

[4] A. F. Zedan, S. Sappal, S. Moussa and M. S. El-Shall,"Ligand-controlled microwave synthesis of cubic and hexagonal CdSe nanocrystals supported on graphene.Photoluminescence quenching by graphene," The Journal of Physical Chemistry C, vol. 114, pp. 19920-19927, 2010.

[5] V. Pilla, E.Munin, N.O. Dantas, A.C. Silva & A. A Andrade,"Photothermal spectroscopic characterization in CdSe/ZnS and CdSe/CdS quantum dots: a review and new applications," Quantum Dots-A Variety of New Applications, pp. 3-22, 2012.

[6] M. Bruchez Jr, M. Moronne, P. Gin, S. Weiss and A. P. Alivisatos, "Semiconductor nanocrystals as fluorescent biological labels," Science, vol. 281, pp. 2013-2016, Sep 25, 1998.

[7] P. N. Prasad, Nanophotonics. John Wiley & Sons, 2004. [8] N. Sounderya and Y. Zhang, "Use of core/shell structured nanoparticles for biomedical applications," Recent Patents on Biomedical Engineering, vol. 1, pp. 34-42, 2008.

[8] V. I. Klimov, S. A. Ivanov, J. Nanda, M. Achermann, I. Bezel, J. A. McGuire and A. Piryatinski,"Single-exciton optical gain in semiconductor nanocrystals," Nature, vol. 447, pp. 441-446, 2007.

[9] P. Dagtepe, V. Chikan, J. Jasinski and V. J. Leppert, "Quantized growth of CdTe quantum dots; observation of magic-sized CdTe quantum dots," The Journal of Physical Chemistry C, vol. 111, pp. 14977-14983, 2007.

[10] V. Soloviev, A. Eichhfer, D. Fenske and U. Banin, "Molecular limit of a bulk semiconductor: Size dependence of the band gap in CdSe cluster molecules," J. Am. Chem. Soc., vol. 122, pp. 2673-2674, 2000.

[11] R. Jose, N. U. Zhanpeisov, H. Fukumura, Y. Baba and M. Ishikawa, "Structure-property correlation of CdSe clusters using experimental results and first-principles DFT calculations," J. Am. Chem. Soc., vol. 128, pp. 629-636, 2006.

[12] K. A. Nguyen, P. N. Day and R. Pachter, "Understanding structural and optical properties of nanoscale CdSe magic-size quantum dots: Insight from computational prediction," The Journal of Physical Chemistry C, vol. 114, pp. 16197-16209, 2010.

[13] L. Brus,"Zero-dimensional excitons in semiconductor clusters," Quantum Electronics, IEEE Journal Of, vol. 22, pp. 1909-1914, 1986.

[14] Z. A. Peng and X. Peng, "Nearly monodisperse and shape-controlled CdSe nanocrystals via alternative routes: nucleation and growth," J. Am. Chem. Soc., vol. 124, pp. 3343-3353, 2002.

[15] J. Ouyang, M. B. Zaman, F. J. Yan, D. Johnston, G. Li, X. Wu, D. Leek, C. I. Ratcliffe, J. A. Ripmeester and K. Yu, "Multiple families of magic-sized CdSe nanocrystals with strong bandgap photoluminescence via noninjection one-pot syntheses," The Journal of Physical Chemistry C, vol. 112, pp. 13805-13811, 2008.

[16] R. Jose, Z. Zhelev, R. Bakalova, Y. Baba and M. Ishikawa,"White-light-emitting CdSe quantum dots synthesized at room temperature," Appl. Phys. Lett., vol. 89, pp. 013115-013115-3, 2006.

[17] S. Kilina, S. Ivanov and S. Tretiak,"Effect of surface ligands on optical and electronic spectra of semiconductor nanoclusters," J. Am. Chem. Soc., vol. 131, pp. 7717-7726, 2009.

[18] Y. Park, A. Dmytruk, I. Dmitruk, A. Kasuya, M. Takeda, N. Ohuchi, Y. Okamoto, N. Kaji, M. Tokeshi and Y. Baba,"Size-selective growth

and stabilization of small CdSe nanoparticles in aqueous solution," ACS Nano, vol. 4, pp. 121-128, 2009.

[19] W. U. Huynh, J. J. Dittmer and A. P. Alivisatos,"Hybrid nanorod-polymer solar cells," Science, vol. 295, pp. 2425-2427, 2002.

[20] D. R. Baker and P. V. Kamat, "Tuning the emission of CdSe quantum dots by controlled trap enhancement," Langmuir, vol. 26, pp. 11272-11276, 2010.

[21] K. Yu, M. Z. Hu, R. Wang, M. L. Piolet, M. Frotey, M. B. Zaman, X. Wu, D. M. Leek, Y. Tao and D. Wilkinson,"Thermodynamic equilibrium-driven formation of single-sized nanocrystals: reaction media tuning CdSe magic-sized versus regular quantum dots," The Journal of Physical Chemistry C, vol. 114, pp. 3329-3339, 2010.

[22] U. Resch-Genger, M. Grabolle, S. Cavaliere-Jaricot, R. Nitschke and T. Nann, "Quantum dots versus organic dyes as fluorescent labels," Nature Methods, vol. 5, pp. 763-775, 2008.

[23] S. S. Ashtaputre, A. Deshpande, S. Marathe, M. Wankhede, J. Chimanpure, R. Pasricha, J. Urban, S. Haram, S. Gosavi and S. Kulkarni, "Synthesis and analysis of ZnO and CdSe nanoparticles," Pramana, vol. 65, pp. 615-620, 2005.

[24] W. Y. William, E. Chang, R. Drezek and V. L. Colvin, "Water-soluble quantum dots for biomedical applications," Biochem. Biophys. Res. Commun., vol. 348, pp. 781-786, 2006.

[25] X. Peng, L. Manna, W. Yang, J. Wickham, E. Scher, A. Kadavanich and A. P. Alivisatos, "Shape control of CdSe nanocrystals," Nature, vol. 404, pp. 59-61, 2000.

[26] Y. Wang, J. P. Lu and Z. F. Tong, "Rapid synthesis of CdSe nanocrystals in aqueous solution at room temperature," Bull. Mater. Sci., vol. 33, pp. 543-546, 2010.

[27] S. Xu, C. Wang, Q. Xu, H. Zhang, R. Li, H. Shao, W. Lei and Y. Cui,"Key roles of solution pH and ligands in the synthesis of aqueous ZnTe nanoparticles," Chemistry of Materials, vol. 22, pp. 5838-5844, 2010.

[28] A. L. Rogach, A. Kornowski, M. Gao, A. Eychmller and H. Weller, " Synthesis and characterization of a size series of extremely small thiol-stabilized CdSe nanocrystals," The Journal of Physical Chemistry B, vol. 103, pp. 3065-3069, 1999.

[29] E. Ying, D. Li, S. Guo, S. Dong and J. Wang, "Synthesis and bio-imaging application of highly luminescent mercaptosuccinic acid-coated CdTe nanocrystals," PloS One, vol. 3, pp. e2222, 2008.

[30] M. Dong, J. Xu, S. Liu, Y. Zhou and C. Huang,"Synthesis of highly luminescent mercaptosuccinic acidcoated CdSe nanocrystals under atmospheric conditions," Luminescence, vol. 29, pp. 818-823, 2014.

[31] H. Zhang, Z. Zhou, B. Yang and M. Gao,"The influence of carboxyl groups on the photoluminescence of mercaptocarboxylic acid-stabilized CdTe nanoparticles," The Journal of Physical Chemistry B, vol. 107, pp. 8-13, 2003.

[32] J. R. McBride, A. D. Dukes, M. A. Schreuder and S. J. Rosenthal,"On ultrasmall nanocrystals," Chemical Physics Letters, vol. 498, pp. 1-9, 2010.

[33] Z. A. Peng and X. Peng, "Nearly monodisperse and shape-controlled CdSe nanocrystals via alternative routes: nucleation and growth," J. Am. Chem. Soc., vol. 124, pp. 3343-3353, 2002.

[34] W. Hong, G. Jo, M. Choe, T. Lee, J. I. Sohn and M. E. Welland, "Influence of surface structure on the phonon-assisted emission process in the ZnO nanowires grown on homoepitaxial films," Appl. Phys. Lett., vol. 94, pp. 043103, 2009.

[35] Anju K Augustine, V P N Nampoori and M Kailasnath, "Tuning of particle size and bandgap of CdSe nanoparticles prepared by reflux method", Asian Journal of physics vol. 23, pp. 683-686,2014

[36] S. A. Maier, Plasmonics: Fundamentals and Applications, Springer Science & Business Media, 2007.

[37] M. Pelton, J. Aizpurua and G. Bryant, "Metalnanoparticle plasmonics," Laser & Photonics Reviews, vol. 2, pp. 136-159, 2008.

[38] H. I. El Ahrach, R. Bachelot, A. Vial, G. Lrondel, J. Plain, P. Royer and O. Soppera, "Spectral degeneracy breaking of the plasmon resonance of single metal nanoparticles by nanoscale near-field photopolymerization," Phys. Rev. Lett., vol. 98, pp. 107402, 2007.

[39] E. Cohen-Hoshen, G. W. Bryant, I. Pinkas, J. Sperling and I. Bar-Joseph, "Excitonplasmon interactions in quantum dotgold nanoparticle structures," Nano Letters, vol. 12, pp. 4260-4264, 2012.

[40] W. Zhang, A. O. Govorov and G. W. Bryant, "Semiconductor-metal nanoparticle molecules: Hybrid excitons and the nonlinear Fano effect," Phys. Rev. Lett., vol. 97, pp. 146804, 2006.

[41] J. Yan, W. Zhang, S. Duan, X. Zhao and A. O. Govorov,"Optical properties of coupled metal-semiconductor and metal-molecule nano crystal complexes: role of multipole effects," Physical Review B, vol. 77, pp. 165301, 2008.

[42] G. C. Schatz and R. P. Van Duyne, "Electromagnetic mechanism of surface enhanced spectroscopy," Handbook of Vibrational Spectroscopy, 2002.

[43] J. Lakowicz and Y. Fu,"Modification of single molecule fluorescence near metallic nanostructures," Laser & Photonics Reviews, vol. 3, pp. 221-232, 2009.

[44] D. J. Bergman and M. I. Stockman, "Surface plasmon amplification by stimulated emission of radiation: quantum generation of coherent surface plasmons in nanosystems," Phys. Rev. Lett., vol. 90, pp. 027402, 2003.

[45] M. I. Stockman, "Spasers explained," Nature Photonics, vol. 2, pp. 327-329, 2008.

[46] M. Noginov, G. Zhu, A. Belgrave, R. Bakker, V. Shalaev, E. Narimanov, S. Stout, E. Herz, T. Suteewong and U. Wiesner, "Demonstration of a spaser-based nanolaser," Nature, vol. 460, pp. 1110-1112, 2009.

[47] E. Dulkeith, A. Morteani, T. Niedereichholz, T. Klar, J. Feldmann, S. Levi, F. Van Veggel, D. Reinhoudt, M. Mller and D. Gittins,"Fluorescence quenching of dye molecules near gold nanoparticles: radiative and non-radiative effects," Phys. Rev. Lett., vol. 89, pp. 203002, 2002.

[48] P. Anger, P. Bharadwaj and L. Novotny, "Enhancement and quenching of single-molecule fluorescence," Phys. Rev. Lett., vol. 96, pp. 113002, 2006.

[49] F. Tam, G. P. Goodrich, B. R. Johnson and N. J. Halas, "Plasmonic enhancement of molecular fluorescence," Nano Letters, vol. 7, pp. 496-501, 2007.

[50] S. Khn, U. Hkanson, L. Rogobete and V. Sandoghdar, "Enhancement of single-molecule fluorescence using a gold nanoparticle as an optical nanoantenna," Phys. Rev. Lett., vol. 97, pp. 017402, 2006.

[51] Y. Wang, T. Yang, M. T. Tuominen and M. Achermann,"Radiative rate enhancements in ensembles of hybrid metal-semiconductor nanostructures," Phys. Rev. Lett., vol. 102, pp. 163001, 2009.

[52] C. Rao, H. R. Matte, R. Voggu and A. Govindaraj, "Recent progress in the synthesis of inorganic nanoparticles," Dalton Transactions, vol. 41, pp. 5089-5120, 2012.

[53] M. Achermann, "Exciton- plasmon interactions in metal-semiconductor nanostructures," The Journal of Physical Chemistry Letters, vol. 1, pp. 2837-2843, 2010.

[54] J. Bellessa, C. Bonnand, J. Plenet and J. Mugnier, "Strong coupling between surface plasmons and excitons in an organic semiconductor," Phys. Rev. Lett., vol. 93, pp. 036404, 2004.

[55] A. O. Govorov, G. W. Bryant, W. Zhang, T. Skeini, J. Lee, N. A. Kotov, J. M. Slocik and R. R. Naik, "Exciton-plasmon interaction and hybrid excitons in semiconductor-metal nanoparticle assemblies," Nano Letters, vol. 6, pp. 984-994, 2006.

[56] P. Viste, J. Plain, R. Jaffiol, A. Vial, P. M. Adam and P. Royer," Enhancement and Quenching Regimes in Metal-Semiconductor Hybrid Optical Nanosources," ACS Nano, vol. 4, pp. 759-764, 2010.

[57] D. Melnikau, D. Savateeva, A. Susha, A. L. Rogach and Y. P. Rakovich, "Strong plasmon-exciton coupling in a hybrid system of gold nanostars and J-aggregates," Nanoscale Research Letters, vol. 8, pp. 1-6, 2013.

[58] A. Agarwal, G. D. Lilly, A. O. Govorov and N. A. Kotov, "Optical Emission and Energy Transfer in Nanoparticle Nanorod Assemblies: Potential Energy Pump System for Negative Refractive Index Materials," The Journal of Physical Chemistry C, vol. 112, pp. 18314-18320, 2008.

[59] G. Pfeiffer, M. Paesler and S. Agarwal,"Reversible photodarkening of amorphous arsenic chalcogens," J. Non Cryst. Solids, vol. 130, pp. 111-143, 1991.

[60] Anju K Augustine, C P Girijavallabhan, V P N Nampoori and M Kailasnath, " Influence of pH on the thermo-optic properties of CdSe QDs prepared by a microwave irradiation method" Laser Phys. Lett. vol.11, 115901 (6pp),2014.

[61] K. Tanaka, "Photoinduced processes in chalcogenide glasses," Current Opinion in Solid State and Materials Science, vol. 1, pp. 567-571, 1996.

[62] L. Tichy, H. Ticha, P. Nagels and R. Callaerts,"Photoinduced optical changes in amorphous Se and GeSe films," J. Non Cryst. Solids, vol. 240, pp. 177-181, 1998.

Chapter 4

Thermo-optic studies on CdSe quantum dots based materials

Details of the thermo-optic studies of CdSe based nanomaterials are described in this chapter. We have applied two thermo-optic methods for the characterization of the samples in which thermal lens study give information about thermal diffusivity property of the material. Characterization of the samples has also been carried out using Photo acoustic technique. Both of these studies give the details about the nonradiative property of the samples.

Results of this chapter are published in :

1. *Anju. K. Augustine et.al., J Opt. vol.44,pp.8591,2015.*
2. *Anju. K. Augustine et.al., Laser Phys. Lett. vol.11,115901,6pp,2014.*
3. *Anju. K. Augustine et.al., Journal of electronic materials,2015.*

4.1 Introduction

In recent years, thermo-optic method has emerged as an effective research and analytical tool for the characterization of materials due to its dependence on optical absorption coefficient. This study includes group of techniques used to measure the optical absorption and thermal properties of the samples. The basic idea behind these techniques is the change in thermal state of the sample resulting from nonradiative relaxation following the absorption of a pulsed or chopped optical radiation [1-9].

The detected PT signal depends on the optical absorption coefficient at the incident wavelength as well as on how heat diffuses through the sample [10-14]. Dependence of PT signal on how heat diffuses through the specimen allows the investigation of transport and structural properties such as thermal diffusivity, thermal effusivity, thermal conductivity, voids, etc. The unique feature of PT methods is that the detected PT signal depends only on the absorbed light and it is independent of transmitted or scattered light. Among the two relaxation processes for the de excitation of the states, nonradiative relaxation occurs in thermo-optic methods while radiative emission leads to the studies on conventional spectroscopy. Nonradiative process leads to the heating of the sample and the corresponding thermodynamic properties can be studied [13-15]. The merit of these methods also lies in the extremely sensitive detection technique used here in comparison with conventional transmission methods.

PT methods based on the measurement of the strength of the lens formed due to the refractive index changes are called thermal lens spectroscopy (TLS). This technique has proven to be an appreciated method to study the thermo-optical properties of transparent materials such as glasses, liquid crystals and polymers. TLS method is useful for the determination of thermal diffusivity, thermal conductivity, the temperature coefficient of the refractive index leading to change in the optical path length, optical absorption coefficient and fluorescence quantum efficiency. Since this is an isolated sensing technique, measurement of samples in isolated environment presents no extra difficulties.

In PT methods another important parameter that can be exploited is the pressure change associated with the transient temperature change in the specimen. Pressure transducers such as microphones and piezo-electric crystals are commonly used for the detection of pressure waves associated with a rapid sample heating. The branch of PT method based on the detection of these pressure waves is known as opto acoustic or photo acoustic (PA) technique [16-19]. A detailed description of this technique is given in the 2^{nd} chapter.

Our interest is to study the thermo-optic changes which occurs in the QDs since they are highly sensitive to the light- matter interactions. The measurement of the heat transfer through diffusion in a liquid medium containing CdSe QDs and its composites at different conditions is also done.

4.2 Thermal lens study of CdSe QDs based samples

Thermal lens spectrometry (TLS) is one of the important PT techniques which depends on temperature gradient generated by absorption of electromagnetic radiation and subsequent non-radiative relaxation of the excited molecules. For thermal lens studies, the schematic experimental set up and explanations are same as described in the 2^{nd} chapter in figure 2.2. Sample was taken in a cuvette of 1 cm path length for making the measurements. A low frequency mechanical chopper with 3 Hz is used to modulate the intensity of the pump beam until the abbreviate free TL peak-to-peak signal is maximum [20-21]. The probe beam from the He-Ne laser which passes collinearly with pump beam(532nm) experiences divergence due to thermally induced negative refractive index gradient in the sample and the beam shape expands in the presence of thermal lens. The change in intensity at the centre of the probe beam spot in the far field is measured using a fast photo detector from which the relative intensity and initial slope is measured. Photograph showing the thermal blooming of the probe beam is given in figure 4.1. The data are analyzed by using the procedure reported earlier [22]. Time

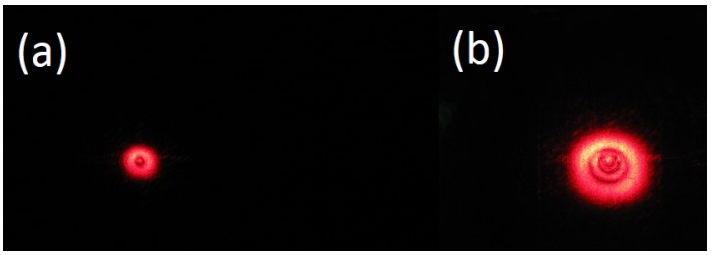

Figure 4.1: Photograph showing probe beam cross -section (a) without pump beam and (b) with pump beam.

dependent probe beam intensity follows the expression [23-24].

$$I(t) = I_0[1 - \theta(1 + \frac{t_c}{2t})^{-1} + \frac{\theta^2}{2}(1 + \frac{t_c}{2t})^{-2}]^{-1} \tag{4.1}$$

Here, the parameter θ is related to the thermal power radiated as heat and can be obtained with

$$I = \frac{I_0 - I_\infty}{I_\infty} \tag{4.2}$$

and

$$\theta = 1 - \sqrt{(1 + 2I)} \tag{4.3}$$

where I_0 is the initial intensity and I_∞ is the intensity after the steady state. A detailed curve fitting of this experimental data to equation (4.1) gives the time constant t_c of the thermal decay process. Finally the thermal diffusivity D of the sample can be calculated from the equation

$$t_c = \frac{\omega^2}{4D} \tag{4.4}$$

where ω is the beam radius at the sample position and t_c is the time response to attain the steady state TL signal.

4.2.1 Size dependent variation of thermal diffusivity of CdSe based QDs

CdSe QDs are prepared by a modified aqueous method using reflux.We have selected four samples with different particle sizes for the study,

namely C_1=4.62nm, C_2=4.88nm, C_3 =4.96nm and C_4=5.16nm. Figure 4.2 represents a typical TL pulse train measured at 3Hz and figure 4.3 represents the thermal decay of CdSe sample (C_2) at an input power of 136 mW.

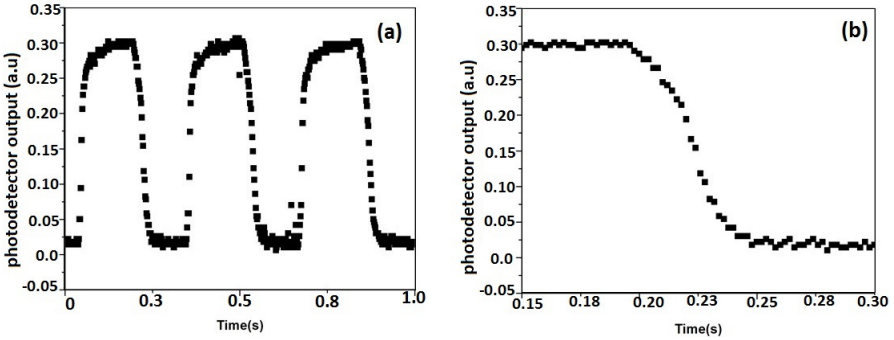

Figure 4.2: (a) Time dependent TL signal of CdSe sample (C_2) and (b) One of the peaks for visual clarification.

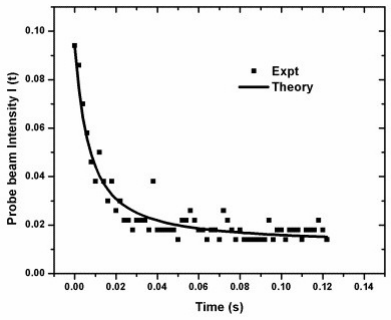

Figure 4.3: Fitting of the data with probe beam intensity as a function of time with fit parameters $I_0 = 0.094$, & $\theta = 2.88$ and t_c =0.05 s.

Similar TL signal evolution obtained for CdSe QDs of different sizes (C_1, C_2, C_3 and C_4) and their corresponding t_c θ, and D are tabulated in Table 4.1. Thermal diffusivity plotted against the size of the CdSe QDs is shown in figure 4.4. Thermal diffusivity is mainly controlled by the size and shape of the NPs. Particle size is an important parameter controlling thermal properties of nanofluids. There are reports based

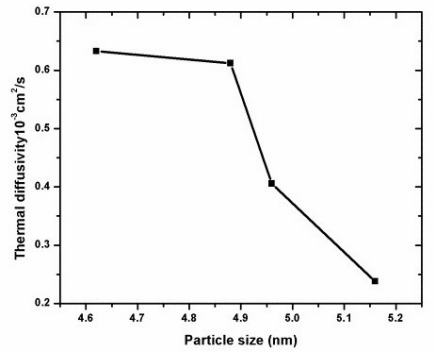

Figure 4.4: Plot of thermal diffusivity versus particle size.

on variation of thermal diffusivity with particle size[25-26]. The range of particle size in our experiment lies between 4nm-6 nm. The general trend in our experimental data is that the thermal diffusivity of CdSe nanofluid decreases with increasing particle size in the fluid. This trend is theoretically supported by Brownian motion of NPs and liquid layering around these. The reduction of D in our experiment with increased particle size is attributed to the convection velocity

$$V = \sqrt{\frac{18k_BT}{\pi\rho d^3}} \tag{4.5}$$

which drops drastically due to the cube dependence on particle size. Where d=particle size, ρ=density of the medium, and K_BT=thermal energy. Therefore if the particle size is very small, Brownian motion is strong and if the particles are large, Brownian motion is severely arrested [22]. Thus the observed decrease in the thermal diffusivity with

sample	Particle size(nm)	θ	t_c (s)	$D \times 10^{-3}(cm^2/s)$
C_1	4.62	-2.07	0.05	0.63
C_2	4.88	-2.89	0.05	0.61
C_3	4.96	-12.65	0.08	0.41
C_4	5.16	-5.70	0.13	0.24

Table 4.1: Particle size, time constant and diffusivity of CdSe QDs prepared by reflux method

increased particle size can be attributed due to the increase in Brownian velocity. Also it can be concluded that CdSe with very small particle size, transports heat rapidly through it and cause high thermal diffusivity.

4.2.2 Thermal lens studies of CdSe based nanofluids with different pH.

In this experiment, CdSe nanofluids are prepared by rapid microwave irradiation method 2*nd* chapter. The pH of the corresponding colourless solution was adjusted by adding 1M NaOH. We have selected samples with different pH values. The samples taken for optical characterization were named as pH 3.7, pH 4.7, pH 7.6, and pH 8.9. Figures 4.5 & 4.6 show the absorption and florescence spectra of the prepared CdSe samples with different pH at room temperature. It can be clearly seen that the absorption and luminescence peaks of the CdSe QDs were red-shifted with increasing value of pH. It is observed that sample with pH less than 4.7, there is a sign of agglomeration and for higher pH sample shows much less intensity with large FWHM.

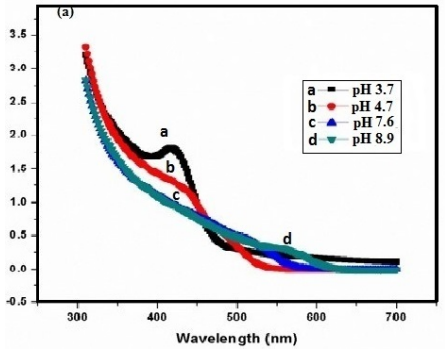

Figure 4.5: Absorption spectra of the prepared CdSe QDs with different pH.

Figure 4.6 shows the pH effects of the reaction solution on the fluorescent properties of CdSe QDs. The unique structure of MSA plays an important role in reducing the surface trap states of CdSe QDs and the two carbonyl groups of MSA can provide better stability than other thiol compounds [27-28].
Figure 4.7 represents the Particle size distribution and auto correlation function g2(T) vs. delay time for the measurement of hydro dynamic

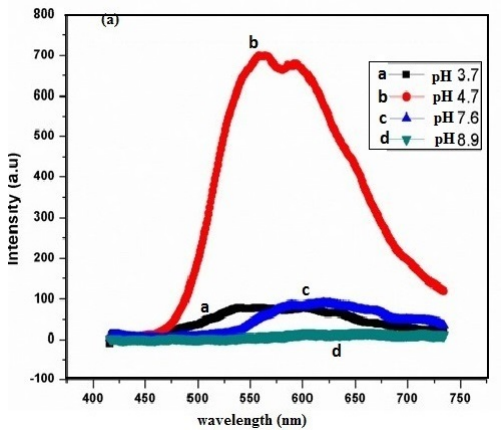

Figure 4.6: Fluorescence spectra of the prepared CdSe Quantum dots with different pH.

particle size (d) of CdSe sample by DLS method.

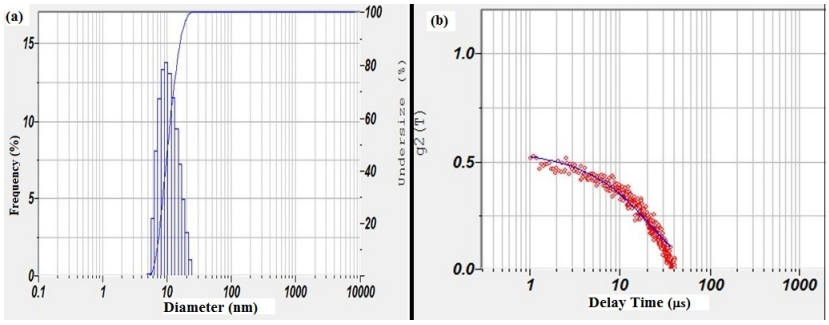

Figure 4.7: (a) Particle size distribution and (b) Auto correlation function g2(T) vs. delay time by DLS method.

It shows that the average size of the nanoparticles formed are within 10 nm range. Figure 4.8 represents the thermal decay at an input power of 136mW. The experiment was repeated for CdSe nanofluids with various pH values. Typical results are shown in figure 4.9. The beam spot size at the sample position is 0.225mm. Finally,the thermal diffusivity D of the sample was calculated from the equation(4.4). Similarly TL signal evolution were obtained for CdSe QDs of different pH values and their

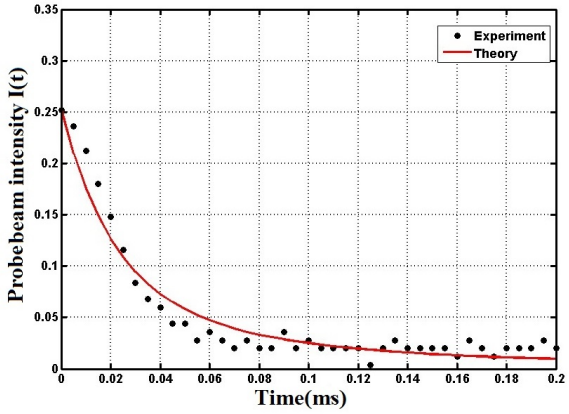

Figure 4.8: Fitting of the data of sample (PH- 9.6) with probe beam intensity as a function of time with fit parameters $I_0 = 0.252, \theta = 36.22$ and t_c=1.94 s.

corresponding cluster size or hydro dynamic particle size (d),t_c, θ, and diffusivity(D) with an error ± 0 .03 were obtained and are tabulated in Table 4.2.

pH	d (nm)	θ	t_c (ms)	$D \times 10^{-5} cm^2/s$
3.7	8.4	467.97	12.907	0.24
4.7	10	0.98	0.01	4520
7.6	10.1	13.24	0.79	3.98
8.9	10.3	103.10	4.9	0.64
9.6	8.5	36.22	1.94	1.62
10	9.2	463.52	48.23	0.06
11	7.9	465.01	30.07	0.10

Table 4.2: Observations of thermal diffusivity changes of CdSe QDs prepared at different pH

The observed (figure 4.10) reduction in t_c at optimum pH can be the effect of shortening of the mean free path of the phonons which is confirmed from Table 4.2. As the pH value is increased continuously, the mean free path of the phonon in the solid increases the value of t_c and thermal diffusivity get reduced. From the figure it is observed that, at an optimum pH, t_c value is very small compared to that at other

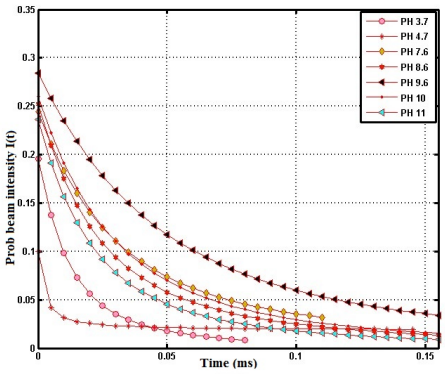

Figure 4.9: TL fitting of data of CdSe QDs with different pH values.

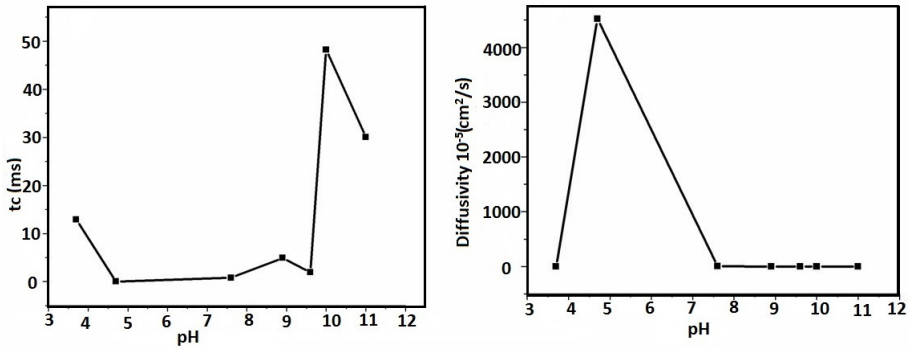

Figure 4.10: (a) Observed t_c of CdSe QDs plotted against pH and (b) Thermal diffusivity of CdSe QDs plotted against pH.

pH values. A large enhancement of thermal diffusivity is also observed (from figure 4.10.(b)) with sample pH $\sim$ 4.7. When the QDs are dispersed into water, the overall behaviour of the particle-water interaction depends on the properties of the particle surface. Experimental results also indicate that the stabilities of these nanofluids are influenced by pH values. Derjaguin theory [29-30] explains the aggregation of aqueous dispersions quantitatively and describes the force between charged surfaces interacting through a liquid medium. It combines the effects of the van-der Waals attraction and the electrostatic repulsion due to the so called double layer of counter ions. According to this, when the pH is increased

to the optimized value, (~ 4.7) the surface charge increases because of the more frequent attacking of the surface hydroxyl groups and phenyl sulfonic group by potential-determining ions (H^+, OH^- and phenyl sulfonic group). This leads to an increase of the electrostatic repulsion force between the particles, and the suspensions show significantly reduced agglomeration and enhanced mobility, ultimately improving the heat transport [31-32]. When the pH is equal to the isoelectric point (IEP), which is the optimized pH(~ 4.7) in our case the QDs tend to be unstable, form clusters, and precipitate, where IEP, is the pH at which a particular molecule or surface carries no net charge. The repulsive forces among metal oxides are zero and QDs coagulate together at this pH value.The resulting big clusters formed at IEP will trap water and the structures of trapped water are varied due to the strong atomic force among QDs. Water is packed well inside and volume fraction of the QDs will be larger.

In addition, shapes of clusters containing trapped water will not be spherical but rather has irregular structure like chains. Such structure favors thermal transport because they provide a long link [33]. Therefore, the overall thermal conductivity and hence thermal diffusivity of nanofluids are enhanced. When the pH is too large, the concentration of the pH adjustment reagent (NaOH) in the system increases, which causes the compression of the electrical double-layer. At pH$\geq$ 10, surface charge of QDs increases, which creates repulsive forces between QDs. As a result of this effect, substantial clustering of QDs is prevented.

Zeta (ζ) potential studies based on different pH of CdSe nanofluids

Zeta (ζ) potential is a measure of the magnitude of the electrostatic or charge repulsion or attraction between particles in a liquid suspension. We calculated the variation of ζ potential and cluster radius or hydro dynamic particle size (d) of the QDs (table 4.2) as a function of pH by using DLS measurement. The effect of charge on the clustering process with varying pH has also been plotted in figure 4.11,which shows that an almost neutral charge is obtained at optimum pH. Therefore, it looks reasonable to infer that optimizing pH or high surface charge facilitates heat transport through increased transport efficiency. We also attempt

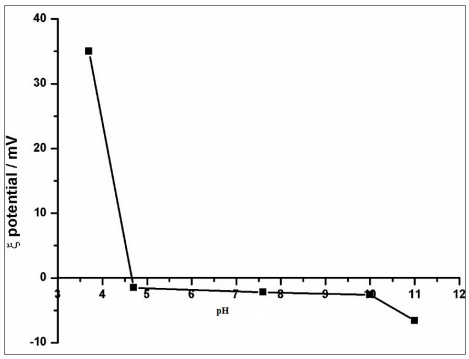

Figure 4.11: Variation of ζ -potential with pH.

to link the concept of this interesting phenomena of change in thermal diffusivity with pH from the emission intensity in figure 4.6. We have the total relaxation cross section $\sigma_T = \sigma_R + \sigma_{NR}$,where σ_R is the radiative relaxation and σ_{NR} is the nonradiative relaxation crosssection so that $\sigma_{NR} = \sigma_T - \sigma_R$. From figure 4.6: (b) the observation of maximum fluorescence intensity at optimum pH value indicating maximum fluorescence quantum yield and minimum thermal energy generated in the medium. Our calculation showed that maximum fluorescence quantum yield is obtained at pH $\sim$4.7, where the probe beam (TL signal) intensity is minimum. It is also observed from figure 4.6. This enhanced radiative process will reduce the heat evolved through nonradiative process. This may cause reduction of t_c, which is the time taken to transport heat, and hence enhancement of the magnitude of diffusion coefficient. The major advantages of such materials is that they can be used both as coolant and insulator by adjusting the corresponding pH values. At low pH ($\sim$4.7), it acts as a good coolant which can be used to diffuse heat energy to the surroundings, and at high pH they can be efficient materials to trap thermal energy and act as good insulators.

4.2.3 Thermal lens studies on CdSe-metal nanofluids

Microwave rapid heating is used for the synthesis of CdSe QDs and metal NPs. For the preparation of hybrid CdSe-metal NPs, different volume ratios of colloidal Ag/Au NPs are mixed with fixed volume of colloidal

CdSe QDs. Sharp excitonic peak in figure 4.12:(a)indicates mono disper-

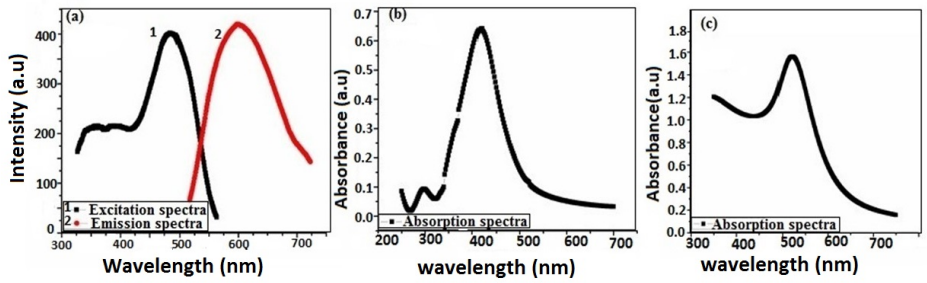

Figure 4.12: (a) Excitation and emission spectra of CdSe QDs , (b) Absorption spectra of Ag NPs and (c) Absorption spectra of Au NPs.

sion of the CdSe QDs and these emissions are basically from excitonic $(1S_e - 1S_h)$ transitions. Surface plasmon resonance (SPR) peaks around 415 nm confirm the presence of Ag. The 520 nm peak in figure 4.12: (c) confirms the presence of Au NPs. The shape and position of surface plasmon (SP) absorption depend on particle size, shape and the dielectric constant of the surrounding medium. The sharpness of the peaks indicates that the particle size is fairly uniform.

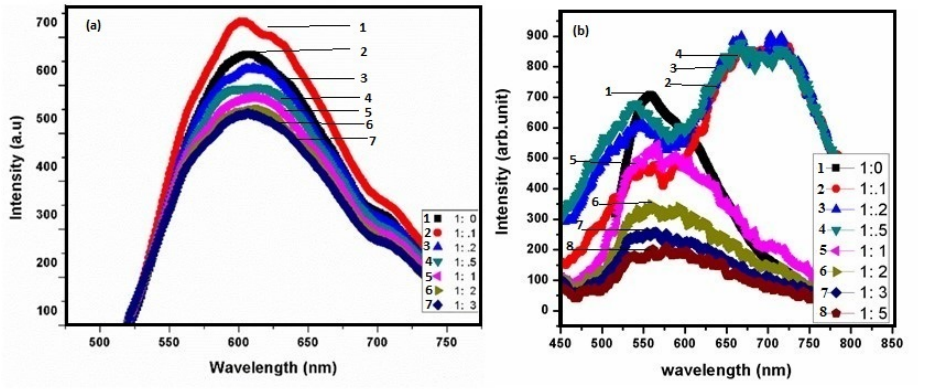

Figure 4.13: (a) Florescence spectra of CdSe-Ag NPs and (b) CdSe-Au NPs.

From figure 4.13, it is clear that by adding a particular volume fraction of metal NPs to the CdSe nanofluid, an increase in the PL emission is

observed. This emission may relies on energy transfer from the QDs to metal NPs which could be de-excited through radiative plasmon relaxation [34-36].From figure 4.13:(b) it is clear that, at low values of volume ratio of Au NPs an additional strong band is observed in $\sim$ 700nm spectral region and at higher ratio this is quenched and the emission peak coincide with that of CdSe QDs. This exciton-plasmon interactions can give rise to modified emission properties like enhancement and quenching as seen in figure 4.13. Generally, the interplay between metal NPs and QDs involves two major phenomena: the first one is an enhancement of the local excitation field, and the second one is the modification of the radiative and nonradiative decay rates of the QDs, inducing a change of fluorescence lifetime and quantum yield. The competition between these processes results in two contradictory observations as reported in the literature: quenching of luminescence or on the contrary it's enhancement. Different parameters play a determinant role in the quenching and enhancement mechanisms but their influence is still debated. Particularly, the spectral position and the influence of the localized surface plasmon resonance (LSPR) compared to the absorption and emission maximum of luminescent species is very decisive.

Quenching of emission and shortening of exciton lifetime in the QD - NP superstructures can be explained using a typical model based on the exciton-plasmon resonance taking place when emission peak of excitons in QDs and absorption peak of the plasmons in NPs display a spectral overlap. In a QD- NP complex, oscillators corresponding to excitons in QDs and plasmons in metal NPs couple via. simple Coulomb forces. Since QD - NP complexes are in liquid, they are randomly oriented with respect to the incident electric eld [37-38]. Figure 4.14 shows TEM images of monodispersed CdSe QDs, AgNPs and Au NPs. By using the non-contact TL technique with optical interactions of material we are able to extract the thermal properties of material mainly the thermal diffusivity. The theoretical curves in figure 4.15 calculated using equation (4.1) agree very well with experimental data, which give the thermal diffusivity value for the sample at an input power of 136 mW. Finally the thermal diffusivity D of the sample can be calculated using the equation (4.2). Similarly TL signal evolution were obtained for CdSe-metal nanofluid of different volume ratios and their corresponding diffusion

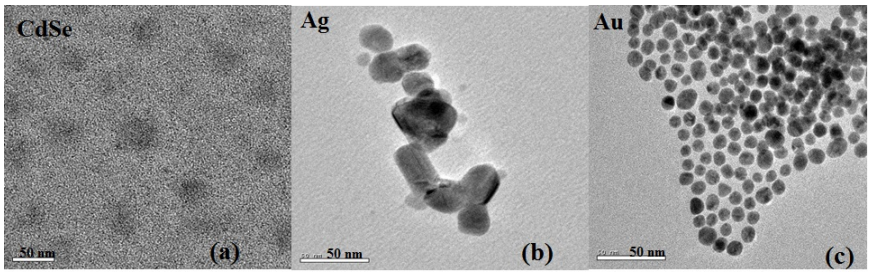

Figure 4.14: TEM images of (a) mono dispersed CdSe QDs, (b) Ag NPs and(c) Au NPs.

coefficients are obtained and plotted in figure 4.15. From figure 4.16, it is clear that the heat diffusion constant has enhanced at an optimum volume of metal NPs and it gets reduced with further addition of it. NPs composed of various materials (such as Au, Ag, and semiconductors) can efficiently release heat under optical excitation.

The mechanism of heat release under laser excitation can be explained as follows: the laser electric field strongly drives mobile carriers inside the QDs, and the energy gained by carriers gets converted into heat. Then the heat diffuses away from the QDs and leads to an elevated temperature of the surrounding medium making the nanofluid an effective coolant. Heat generation becomes especially strong in the case of metal NPs in the regime of plasmon resonance where a collective motion of a large number of electrons occur. In the case of semiconductor QDs, the heat generation rate is much weaker since heat dissipation occurs through an interband absorption process with the creation of mobile electron and hole (exciton) pairs followed by possible radiative process [39-40]. The heating effect can be strongly enhanced in the presence of several NPs. Mechanisms of interaction between NPs that could enhance the heating process are accumulative effect and Coulomb interaction. The accumulative effect comes from the addition of heat fluxes generated by single NPs [41-42]. Coulomb interaction effects leads to the partial screening of electric fields inside the NP. The total heat dissipation can increase or decrease, depending on the incident light polarization. If the NPs are in solution and randomly oriented, the average heat generation can be enhanced or reduced depending on the screening effect which

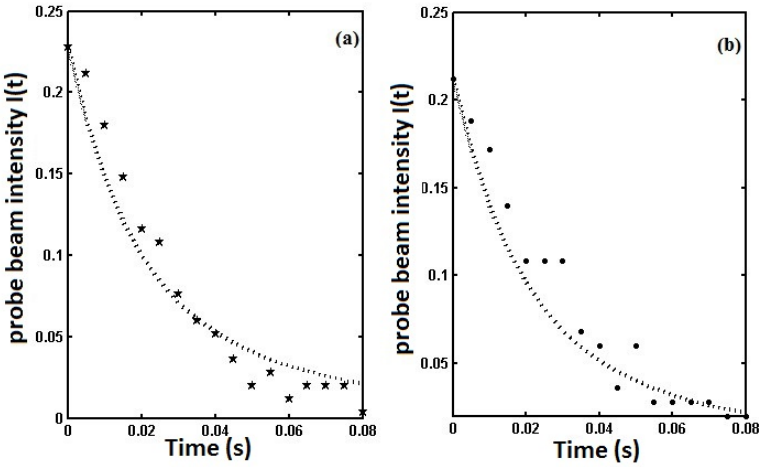

Figure 4.15: Fitting of the data with probe beam intensity as a function of time for (a) CdSe-Ag and (b) CdSe-Au.

become concentration dependent. It is also suggested that, clustering of metal NPs can significantly affect the total heat generation and diffusion. This effect may also cause the variation of thermal diffusivity of CdSe-Au /CdSe-Ag complexes. Most of the studies based on the measurement of thermal diffusivity of metal nanofluids using TLS [23-24, 43-44] reported the enhancement of thermal diffusivity with metal NP in dye colloidal system. In our study we report, the heat and charge transport mechanism of QD-metal nanohybrid (NH)which can be optimized with properties of QDs and metal. The emission properties of the QD-metal nanofluid can be tuned and can also be used as an effective coolant under optimum conditions.

4.3 Photo acoustic measurements of CdSe QDs based nanofluids

Over the years numerous techniques have been developed for the optical investigation of highly scattering and opaque materials, the most common of which are diffuse reflectance [45], attenuated total reflection, internal reflection spectroscopy [46] and scattering [47]. But all these

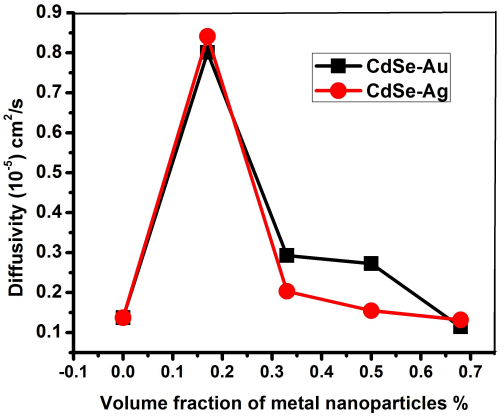

Figure 4.16: Thermal diffusivity of CdSe with different volume fraction of metal NPs.

methods have their specific limitations. During the past few years, another optical technique has been developed to investigate the optical properties of those materials that are unsuitable with the conventional transmission or reflection methodologies. This technique, called photo acoustic spectroscopy (PAS), deals with the effect of generation of acoustic waves in the specimen after illumination with a chopped or pulsed optical radiation.

PA effect was discovered by Graham Bell in 1880, when he noticed that the incidence of modulated light on a diaphragm connected to a tube produced sound [47-49]. Extensive study of photo acoustic effect in liquids and gases showed that the intensity of acoustic signal depends on the absorption of light by the material. Thereafter in the nineteenth century, it was known that the heat of a gas in a closed chamber produces pressure and volume change in this gas and during the next years many theories were developed to explain the PA effect [50-53]. According to Rayleigh this effect was due to the movement of the solid diaphragm, and Bell believed that the incidence of light on a porous sample expanded its particles, producing a cycle of air expulsion and re absorption in the sample pores. These ideas were opposed by Preece by pointing that the expansion/contraction of the gas layer inside the photo acoustic cell is the cause of the phenomenon. Mercadier explained the effect correlated

with the thermal diffusion mechanism in which the periodic heating of the sample is transferred to the surrounding gas layer, generating pressure fluctuations. At present, the invention of sensitive and compact microphone made this area of study an interesting one. Ever since the theory of PA effect in solids was developed by Rosencwaig and Gersho, this technique has been effectively used in diverse areas of physics, chemistry and medicine [52-55].

Main difference of PA effect from other spectroscopic methods is that this is an indirect method wherein the incident energy is in the form of optical photons, which interacts with the material under investigation. The measurement is not through the subsequent detection and analysis of some of the photons, but rather through a direct measure of the energy absorbed by the material. Local warming of the sample matrix arises due to the non-radiative relaxation processes such as collisions with other molecules. Pressure fluctuations are then generated by thermal expansion, which can be detected in the form of acoustic or ultrasonic waves. In a typical experiment the sample is illuminated with an intensity modulated monochromatic radiation. If any of the incident photons are absorbed by the sample, internal energy levels within the sample are excited. Upon subsequent de-excitation of these energy levels, all or part of the absorbed photon energy is transformed into heat energy through nonradiative de-excitation processes. In PAS, we measure the acoustic signal produced by the pressure variations due to this internal heating of the sample. Hence PAS is clearly a form of optical spectroscopy.

Usual temperature sensors such as thermistors and thermopiles have inherent disadvantages for being used in PAS in terms of sensitivity, detector rise time and the speed at which measurements can be made. A more appropriate method is the measurement of heat production through volume and pressure changes produced in the sample or in an appropriate transducing material in contact with the sample. In this aspect piezoelectric transducers are employed in many cases for the detection of ultrasonic pulses in liquid and solid samples. Quartz crystals, piezoelectric ceramics such as lead zirconate titanate (PZT), lead metaniobate, and lithium niobate as well as piezoelectric polymer films can be applied

to the detection of laser- induced shock pulses.[49,56-58]

4.3.1 Calibration of PA cell

Experimental set up for the calibration of PA cell by finding velocity of sound in aluminum sheet as shown below. A Q-switched Nd-YAG laser with second harmonic frequency of 532 nm and output power of one joule has been used as the laser source. PA signal amplitude at different locations of the aluminium sheet is taken for the input pulse. Distance vs. time delay of the samples are measured and the average velocity of the PA signal was calculated. It is observed from the experiment that velocity of sound in Aluminum sheet is $\sim$ 2600 m/s whereas it can change from 2000m/s to 2600m/s theoretically. The experimetal set up is shown in figure 4.17.

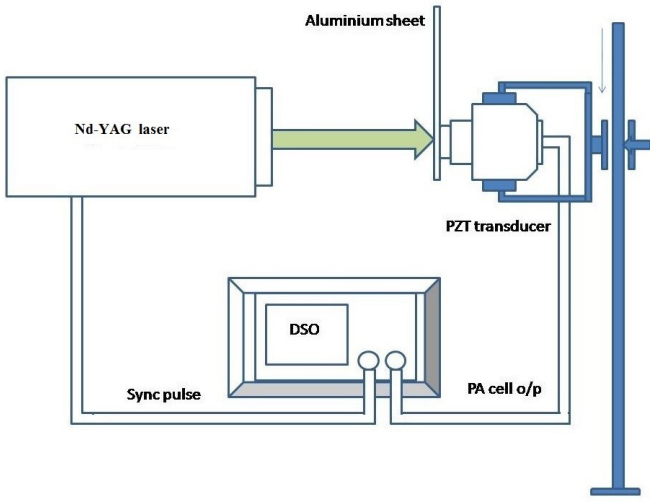

Figure 4.17: Experimental set up for the calibration of PA cell by finding velocity of sound in aluminum sheet.

Typical photographs of the selected output signals are given in figure 4.18.

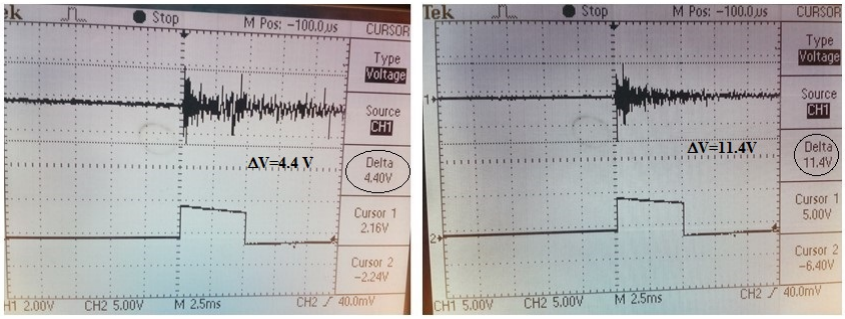

Figure 4.18: Typical photographs of output PA signal for the calibration of PA cell.

4.3.2 Measurement of Photo acoustic signal by pulsed Nd: YAG laser

For the generation of efficient PA signals, laser pulse durations in the range of tens to hundreds of nanoseconds are required. To obtain adequate penetration depth, it is also desirable to use a wavelength suitable to the samples. These requirements can be met, in part, by using the second harmonic frequency from the Q-switched Nd: YAG laser operating at 532nm, at a pulse repetition frequency of 10 Hz, with one joule pulse energy.

Measurements of PA signal amplitude with different input laser intensity

We have observed PA signal variation at different input power levels for samples using pulsed Nd-YAG laser with 532 nm wavelength. Experimental set up for the study of variation of PA signal amplitude with different input power for CdSe QDs based samples is described inthe 2^{nd} chapter(figure 2.5). The synthesis of the metal NPs and CdSe QDs for the study were carried out by microwave rapid-heating method. Absorption spectra of the prepared CdSe QDs were recorded using UV-Visible spectrophotometer. The samples are labelled as S_1 ,S_2 and S_3 where S_1 is CdSe nanofluid incorporated with Rh-6G dye solution of 10^{-4} M and S_2 is a mixture of sample S_1 with Au nanofluid in volume ratio 1:0.5 and S_3 is sample S_1 with Ag nanofluid mixture in volume ratio

1:0.5. CdSe QDs based nanofluid with Rh-6G dye is taken as the reference sample (S_1) and sample S_2 shows maximum PA signal output where Au NPs are incorporated to S_1. It is observed from figure 4.19 that as power increases, amplitude of the PA signal also increases and an abrupt change occurs at a threshold. It is also observed that the

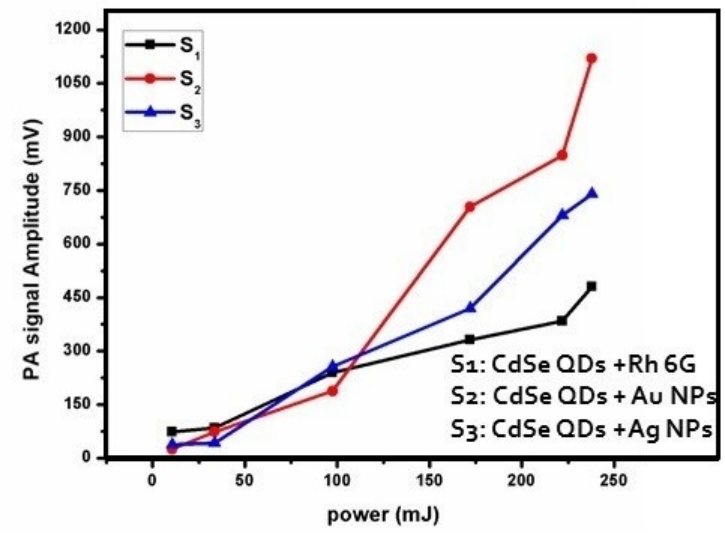

Figure 4.19: Variation of PA signal amplitude at different input power for S_1, S_2 and S_3 samples

output of the PA signal varies differently for samples and it is higher in the case of samples incorporated with Au metal NPs. Generation of PA signal, on introducing metal NPs is a nonlinear function of pump beam intensity as clearly seen in the figure 4.19. This enhancement can be attributed to Brownian motion, nano convection, and heat diffusion on addition of Au metal NPs to the fluid. The Variation of PA signal amplitude of CdSe QDs based samples with different input energies are tabulated in Table 4.3. The introduction of metal NPs in CdSe enhance thermal diffusivity which reduce the depletion of pump in the coupling medium thereby enhancing the PA signal amplitude with pump power. It can be seen that in CdSe sample (S_1) the PA signal propagation is linear with pump power while it is nonlinear in samples with metal NPs (S_2andS_3) added. The observation is also supported by the enhanced

thermal diffusivity of metal incorporated CdSe samples. Typical images of the PA signal output from DSO for different samples (S_1, S_2 and S_3) are shown in figure 4.20.

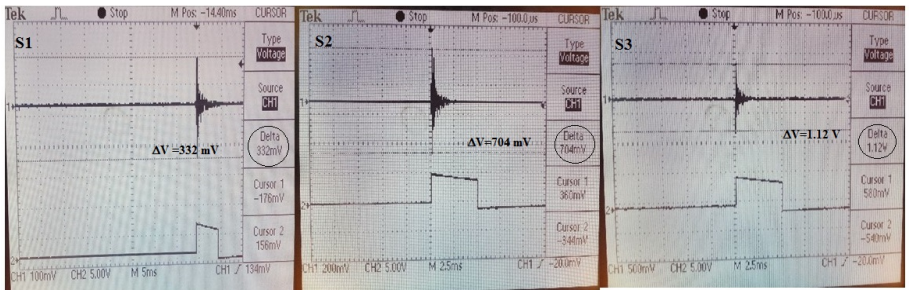

Figure 4.20: Typical images of the PA signal of samples(S_1, S_2 and S_3)

4.3.3 Measurement of photo acoustic spectrum using continuous wave light source

PA signal generation has also been done with modulated chopped light from the continuous wave using a Xenon lamp. The synthesis of the samples were carried out by microwave rapid-heating method. The products were collected for size characterizations after being cooled down to room temperature. Absorption spectra of the prepared CdSe QDs were recorded using UV-Visible Spectrophotometer. The samples are labeled as S_1,S_2 and S_3 where S_1 is CdSe nanofluid incorporated with Rh-6G

Energy (m J)	PA signal voltage (mV)		
	S_1	S_2	S_3
10.6	73.6	24.8	38.4
33.5	84.8	74	43.2
97.5	240	188	256
172	332	704	420
222	384	848	680
238	480	1120	740

Table 4.3: Variation of PA signal amplitude with different power in CdSe QDs based samples

dye solution of 10^{-4} M and S_1 is mixture of sample S_1 with Au nanofluid in volume ratio 1:0.5 and S_3 is a mixture of sample S_1 with Ag nanofluid in volume ratio 1:0.5.

In the experimental section, the sample is taken in the PA cell which is firmly held on a holder, and properly aligned with the laser beam axis. The modulated chopped light from the Xenon lamp is focused and passed through the sample in the PA cell. The acoustic signals generated are detected by the PZT, and recorded using a lock in amplifier. When readings are taken for one sample, it is pipetted out and the next sample is filled, without moving the PA cell. The experiment is repeated for different samples by varying wavelengths using filters. The experimental arrangement of the PA study is shown in 2^{nd} chapter(figure 2.4). It consists of a light beam from a standard solar irradiation of 1000W Xe lamp (Oriel 6269). A water column kept after the Xenon lamp will effectively filter out the infrared portion of the spectrum. Light coming out of the Xe lamp is intensity modulated using a mechanical chopper(Ithaco HMS 230) and is focused to the PA cell. The acoustic signal is processed using a lock-in-amplifier (Stanford Research Systems SR 510).

PA cell contains the samples, and a fabricated piezoelectric transducer chamber to detect the acoustic signals [58]. The cell is of stainless steel body with an inner diameter of 2 cm and length 5 cm. Glass windows are fixed with flanges and O-rings to the cell for the entry and exit of the laser beam. One side of the cell has an opening in which the transducer chamber is fixed. A Lead Zirconate-Titanate (PZT) disc of 4 mm thickness and 15 mm diameter is the piezoelectric transducer that is contained in this chamber. The PZT disc is spring-loaded against the thin front diaphragm as shown, with a thin layer of silicon grease applied between them to ensure good acoustic coupling. The PA signal is taken out through the BNC connector. Due to its high sensitivity a few μV of electrical signal could directly be obtained from the transducer with absorbing sample in the cell [55].

Absorption spectra and the corresponding PA spectra of the samplesS_1, S_2 andS_3 are shown below in figure 4.21.

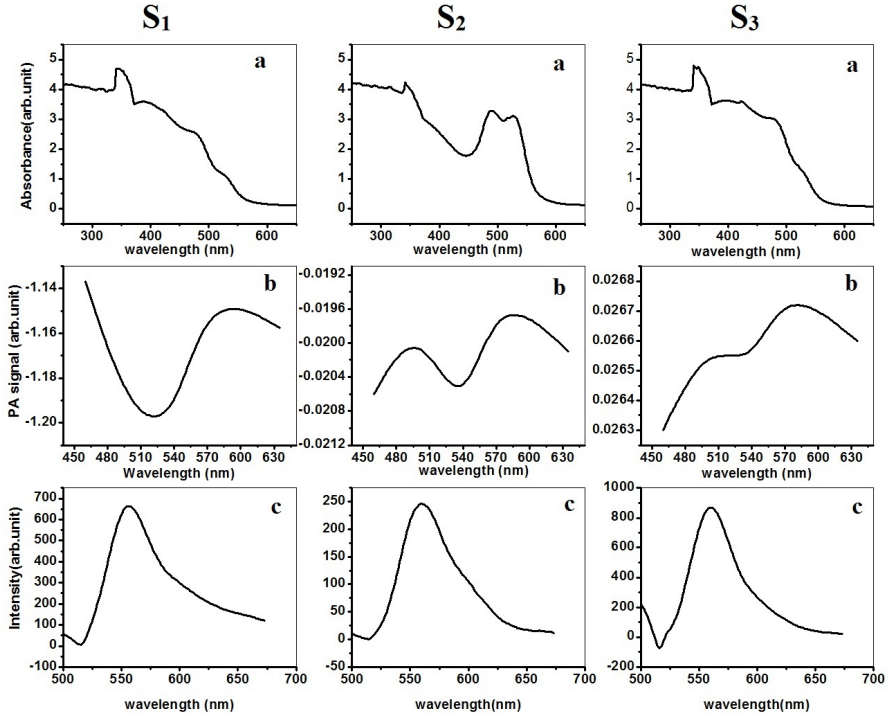

Figure 4.21: (a) Absorption spectra,(b) PA spectra and (c) Emission spectra of the CdSe based samples,S_1, S_2 and S_3 .

It is observed that the output PA spectrum is similar to the absorption spectrum and can be used to identify the absorbing energy levels of the samples. We observed that the change from optics signal to PA signal indicates the transformation of transverse wave to longitudinal wave where direct measurement of absorbed energy is observed. We also observed from the spectrum that there is a transfer of energy due to the exciton-plasmon interactions especially in the case of CdSe QDs based nanofluid incorporated with Ag NPs. This enhancement can be attributed to Brownian motion, nano convection, and heat diffusion on addition of Ag metal NPs to the fluid. Depending on the sample and the pump flux at different wavelengths nonlinear and/or excited state absorption can occur in a typical nanofluid medium.Various non-radiative relaxation channels are active in a highly excited large molecule, which

will lead to the generation of photo acoustic signals. Analysis of these PA signals can yield valuable information about the nature of absorption and the distribution of various energy levels of the molecule. Using the same experimental setup in figure 2.4 a relation ship between the amplitude and modulation frequency of samples S_1, S_2 andS_3 are studied and the results are shown in figure 2.4. The linear nature for plot of

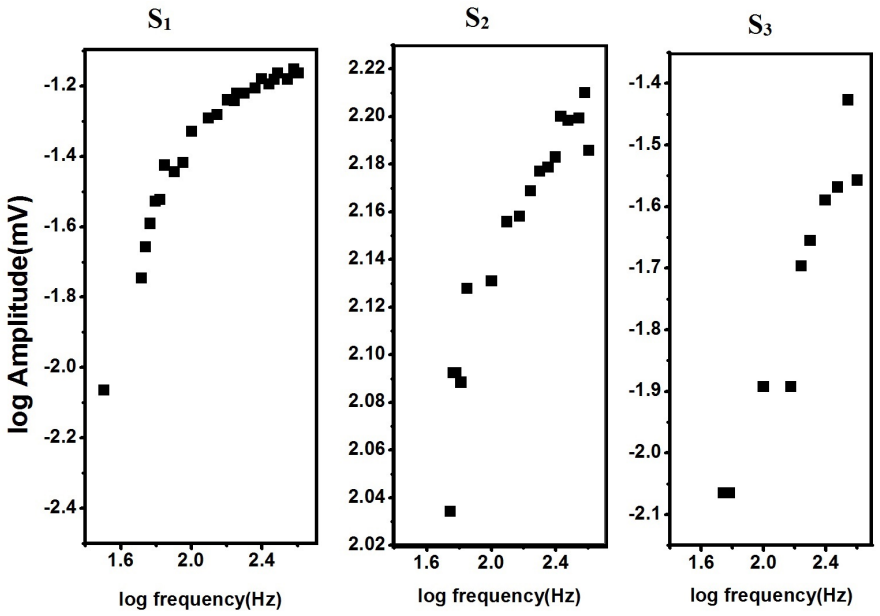

Figure 4.22: Log frequency versus log amplitude of S_1 and S_2 andS_3 samples.

samples S_1 and S_2 and S_3 indicates that, due to the relatively high thermal diffusivity, the heat generated at the sample interface is transmitted instantaneously to other side without leaving any temperature gradient inside the sample. But for materials of very low thermal diffusivity,this cannot be applied [59-62].

4.4 Conclusion

- CdSe QDs prepared by reflux method shows variation of energy band gap of the NPs from 2.56 eV to 2.35 eV as the particle size increased during the reflux period.

- Studies on size dependent variation of thermal diffusivity of CdSe QDs based nanofluid using laser induced mode matched thermal lens technique shows a decrease in thermal diffusivity with particle size. This trend is theoretically supported by Brownian motion of NPs and liquid layering around NPs, where rapid heat transports in smaller particles cause high thermal diffusivity.

- Influence of pH on thermo optic properties of MSA capped CdSe QDs prepared by microwave irradiation method shows a significant increase in thermal diffusivity with optimum pH.

- At this optimum value of pH, increase in surface charge of NPs increases repulsive forces thus resulting in reduced agglomeration of QDs which enhances mobility and heat transport. The major advantages of such material is that they can be used as both coolant and insulator by adjusting the corresponding pH values.

- A study on charge and heat energy transfer dynamics of directly coupled mixtures of CdSe QDs with metal NPs using TL and photoluminescence techniques shows an effective increase of the absorption cross section of the semiconductor nanostructure and modified emission properties due to the exciton-plasmon interactions.

- Quenching of emission and shortening of exciton lifetime in the QD-NP superstructures can be explained using a typical model, based on the exciton-plasmon resonance occurring due to the overlap of the emission peak of excitons in QDs and absorption peak of the plasmons in NPs.

- In our study the heat and charge transport mechanism of QD with metal NPs can be optimized with properties of QDs and metal. The emission properties of the QD with metal nanofluid can be tuned and it's potential to be used as a coolant is also discussed.

- Calibration of PA cell by finding the velocity of sound in aluminium sheet using pulsed Nd-YAG laser with 532 nm wavelength laser source shows that velocity of sound in aluminum sheet is ∼2600 m/s in experiment whereas it can vary from 2000m/s to 2600m/s theoretically.

- Variation of PA signal amplitude with different input energies are studied. Output of the PA signal varies differently for samples and it is higher in the case of samples incorporated with metal NPs.
- Enhancement of PA signal with CdSe QDs based nanofluid sample incorporated with Au NP can be attributed to Brownian motion, nano convection, and heat diffusion on the addition of metal NPs to the fluid.
- Measurement of Photo acoustic spectrum using chopped optical radiation at different wavelength from a Xenon lamp gives information about the absorption regions of the CdSe QDs based nanofluids.
- The linear nature of the log frquency vs. log amplitude curve indicates that at relatively high thermal diffusivity value of the sample, the heat generated at the sample interface is transmitted instantaneously to other side without leaving any temperature gradient inside the sample.

4.5 Refrences

[1] Gurevich, Yu G., G. Gonzalez de la Cruz, G. N. Logvinov, and M. N. Kasyanchuk. "Effect of electron-phonon energy exchange on thermal wave propagation in semiconductors." Semiconductors ,vol.32 ,pp.1179-1184, 1998

[2] Mandelis, Andreas. "Diffusion waves and their uses." Physics today, vol. 53, Pp.29-34,2007

[3] Nandini, T. "Photohermal investigations on certain organic molecules and their plasma polymerised thin films" PhD diss., Cochin University of Science and Technology, 2005.

[4] Klzer, J., E. Oesterschulze, and G. Deboy."Thermal imaging and measurement techniques for electronic materials and devices." Microelectronic Engineering ,vol. 31 ,pp.251-270, 1996.

[5] Bozki, Zoltn, Andrea Pogany, and Gabor Szabo. "Photoacoustic instruments for practical applications: present, potentials, and future challenges." Applied Spectroscopy Reviews ,vol. 46,pp. 1-37,2011 .

[6] Kurian Achamma, K. P.Unnikrishnan, D.Sajan George, Pramod Gopinath, V. P. N. Nampoori, and C. P. G.Vallabhan,"Thermal lens spectrum of organic dyes using optical parametric oscillator." Spectrochimica Acta Part A: Molecular and Biomolecular Spectroscopy,vol.59, pp.487-491,2003.

[7] Ristovski, Zoran D., and Miroslav D. Dramcanin. "Photoacoustic measurement of internal quantum efficiency and observation of the exciton effect in GaSe with photoacoustic phase spectra." Applied optics ,vol.36,pp. 648-654 ,1997 .

[8] Fukuyama, A., T. Ikari, K. Miyazaki, K. Maeda, and K. Futagami. "Near Infrared Photoacoustic Spectra of Deep Levels in GaAs Grown by Liquid Encapsulated Czochralski Method." Japanese Journal of Applied Physics ,vol.31 ,pp. 20, 1992.

[9] Fukuyama, Atsuhiko,Tetsuo Ikari, Kouji Maeda, and Koji Futagami, "Spatial distribution of EL2 in GaAs wafer determined by photoacoustic spectroscopy."Japanese journal of applied physics ,vol.32 ,pp. 2567, 1993.

[10] Nibu A George,"Photoacoustic and photothermal deflection studies on certain selected photonic materials", PhD.Thesis, CUSAT,Kochi 2001.

[11] Balderas-Lopez, J. A., A. Mandelis, and J. A. Garca. "Normalized photoacoustic techniques for thermal diffusivity measurements of buried layers in multilayered systems." Journal of applied physics ,vol.92, no. 6,pp.3047-3055, 2002.

[12] Zhou, Weiya, Sishen Xie, Shengfa Qian, Gang Wang, Luxi Qian, Lianfeng Sun, Dongsheng Tang, and Zuqin Liu."Photothermal deflection spectra of crystalline C 60 S x and RbC 60." Journal of Physics and Chemistry of Solids ,vol.61 ,pp. 1165-1169,2000.

[13] Shi, B. X., C. W. Ong, and K. L. Tam."Measurements of thermal diffusivity of boron-silicon film-on-glass structure using phase detection method of photothermal deflection spectroscopy." Journal of materials science ,vol.34 ,pp. 5169-5173, 1999.

[14] Khuen, Q. E., W. Faubel, and H. J. Ache. "cw and pulsed photothermal deflection spectroscopy on textile dyes solutions." Le Journal de Physique IV4 ,pp. C7-361, 1994.

[15] Fukuyama, Atsuhiko, Yoshito Akashi, Kenji Yoshino, Kouji Maeda, and Tetsuo Ikari."Piezoelectric photoacoustic studies of optical recovery of metastable states related to EL2 and EL6 levels in semi-insulating GaAs." Physical Review B ,vol.58,pp.12868,1998 .

[16] Kurian, Achamma."Characterization of photonic materials using thermal lens technique." PhD diss., Cochin University of SCience and Tech-

nology, 2002.

[17] Mansanares, A. M., A. C. Bento, H. Vargas, N. F. Leite, and L. C. M. Miranda. "Photoacoustic measurement of the thermal properties of two-layer systems."Physical Review B ,vol.42 ,pp. 4477,1990.

[18] Song, K., H. Cha, J. Lee, and I. A. Veselovskii. "Application of optical parametric oscillators to photoacoustic studies in semiconductors." Applied Physics B ,vol.61 ,pp. 547-552,1995.

[19] Gulbinas, K., V. Grivickas, P. Grivickas, and J. Linnros."Conversion of Laser Pulse Optical Energy to Photo-acoustic Wave in nm-Scale Layered TlGaSe2 Crystals." In IOP Conference Series: Materials Science and Engineering, vol. 68, p. 01 ,2004.

[20] Shen, Jun, Roger D. Lowe, and Richard D. Snook. "A model for cw laser induced mode-mismatched dual-beam thermal lens spectrometry." Chemical physics ,vol.165,pp. 385-396,1992 .

[21] Bindhu, C. V., S. S. Harilal, V. P. N. Nampoori, and C. P. G. Vallabhan, "Thermal diffusivity measurements in organic liquids using transient thermal lens calorimetry." Optical Engineering ,vol.37 ,pp. 2791-2794, 1998.

[22] Joseph, Santhi Ani, Misha Hari, S. Mathew, Gaurav Sharma, V. M. Hadiya, P. Radhakrishnan, and V. P. N. Nampoori"Thermal diffusivity of rhodamine 6G incorporated in silver nanofluid measured using mode-matched thermal lens technique." Optics Communications ,vol.283,pp.313-317, 2010 .

[23] Brannon, James H., and Douglas Magde. "Absolute quantum yield determination by thermal blooming. Fluorescein." The Journal of Physical Chemistry,vol. 82 ,pp.705-709, 1978.

[24] Santhi, A., M. Umadevi, V. Ramakrishnan, P. Radhakrishnan, and V. P. N. Nampoori."Effect of silver nanoparticles on the fluorescence quantum yield of Rhodamine 6G determined using dual beam thermal lens method."Spectrochimica Acta Part A: Molecular and Biomolecular Spectroscopy ,vol.60 ,pp.1077-1083,2004.

[25] Beck, Michael P., Yanhui Yuan, Pramod Warrier, and Amyn S. Teja."The effect of particle size on the thermal conductivity of alumina nanofluids." Journal of Nanoparticle Research,vol. 11 ,pp.1129-1136,2009.

[26] Wang, Xiang-Qi, and Arun S. Mujumdar."Heat transfer characteristics of nanofluids: a review." International journal of thermal sciences, vol. 46 ,pp.1-19,2007.

[27] Dong, Meiting, Jingyi Xu, Shuxian Liu, Ying Zhou, and Chaobiao Huang. "Synthesis of highly luminescent mercaptosuccinic acid coated CdSe nano

crystals under atmospheric conditions."Luminescence vol.29,pp. 818-823, 2014 .

[28] Zhang, Hao, Zhen Zhou, Bai Yang, and Mingyuan Gao. "The influence of carboxyl groups on the photoluminescence of mercaptocarboxylic acid-stabilized CdTe nanoparticles." The Journal of Physical Chemistry B ,vol.107,pp. 8-13,2003 .

[29] Derjaguin , B.V. and Landau, L., "Theory of the stability of strongly charged lyophobic sols and the adhesion of strongly charged particles in solution of electrolytes", Acta Phys. Chim,vol.14, pp.733 ,1941.

[30] Hunter, R.J. "Zeta potential in Colloid Science", Academic Press, NY,1981

[31] Xu, Shuhong, Chunlei Wang, Qinying Xu, Haisheng Zhang, Rongqing Li, Haibao Shao, Wei Lei, and Yiping Cui."Key roles of solution pH and ligands in the synthesis of aqueous ZnTe nanoparticles". Chemistry of Materials ,vol.22 ,pp. 5838-5844, 2010.

[32] Younes, Hammad, Greg Christensen, Xinning Luan, Haiping Hong, and Pauline Smith."Effects of alignment, pH, surfactant, and solvent on heat transfer nanofluids containing Fe_2O_3 and CuO nanoparticles." Journal of Applied Physics ,vol.111 ,pp. 064308, 2012.

[33] Xian-Ju, Wang, and Li Xin-Fang."Influence of pH on nanofluids' viscosity and thermal conductivity." Chinese Physics Letters ,vol.26 ,pp. 056601,2009.

[34] Achermann, Marc,"Exciton-plasmon interactions in metal-semiconductor nanostructures".The Journal of Physical Chemistry Letters ,pp.2837-2843, 2010.

[35] Bellessa, J., C. Bonnand, J. C. Plenet, and J. Mugnier."Strong coupling between surface plasmons and excitons in an organic semiconductor."Physical review letters,vol. 93, pp.036404,2004 .

[36] Govorov, Alexander O., Garnett W. Bryant, Wei Zhang, Timur Skeini, Jaebeom Lee, Nicholas A. Kotov, Joseph M. Slocik, and Rajesh R. Naik."Exciton-plasmon interaction and hybrid excitons in semiconductor-metal nanoparticle assemblies." Nano letters ,vol.6 ,pp. 984-994,2006.

[37] Viste, Pierre, Jrome Plain, Rodolphe Jaffiol, Alexandre Vial, Pierre Michel Adam, and Pascal Royer. "Enhancement and Quenching Regimes in Metal- Semiconductor Hybrid Optical Nanosources." ACS nano ,vol.4,pp. 759-764, 2010 .

[38] Melnikau, Dzmitry, Diana Savateeva, Andrey Susha, Andrey L. Rogach, and Yury P. Rakovich."Strong plasmon-exciton coupling in a hybrid system of gold nanostars and J-aggregates." Nanoscale research letters ,vol.8 ,pp.1-6, 2013.

[39] Govorov, Alexander O., and Hugh H. Richardson. "Generating heat with metal nanoparticles." Nano today vol.2 ,pp.30-38, 2007.

[40] Vasa, P., R. Pomraenke, S. Schwieger, Yu I. Mazur, Vas Kunets, P. Srinivasan, E. Johnson et al. "Coherent exciton-surface-plasmon-polariton interaction in hybrid metal-semiconductor nanostructures." Physical review letters ,vol.101 ,pp.116801,2008.

[41] Gomez, D. E., K. C. Vernon, Paul Mulvaney, and T. J. Davis. "Surface Plasmon Mediated Strong Exciton - Photon Coupling in Semiconductor Nanocrystals." Nano letters,vol. 10 ,pp. 274-278,2009.

[42] Barnes, William L., Alain Dereux, and Thomas W. Ebbesen. "Surface plasmon subwavelength optics." Nature ,vol.424 ,pp. 824-830,2003.

[43] Jimnez Prez, J. L., J. F. Snchez Ramrez, R. Gutirrez Fuentes, A. Cruz-Orea, and J. L. Herrera Prez."Enhanced of the Rh-6G thermal diffusivity on aggregated small gold particles." Brazilian journal of physics ,vol.36 ,pp.1025-1028, 2006.

[44] Moreira, Lyane M., E. A. Carvalho, M. J. V. Bell, V. Anjos, A. C. SantAna, Ana Paula P. Alves, B. Fragneaud, L. A. Sena, B. S. Archanjo, and C. A. Achete. "Thermo-optical properties of silver and gold nanofluids." Journal of thermal analysis and calorimetry,vol. 114 ,pp. 557-564, 2013.

[45] Schmid, Thomas, " Photoacoustic spectroscopy for process analysis. "Analytical and bioanalytical chemistry,vol.384, pp.1071-1086,2006.

[46] Kirkbright, G. F. "Some applications of photoacoustic spectroscopy to the study of chemical systems in the condensed phase-a tutorial review." Le Journal de Physique Colloques ,vol.44 ,pp. 96-99,1983.

[47] Bell, Alexander Graham."On the production and reproduction of sound by light." American Journal of Science,vol.118 ,pp.305-324,1880.

[48] Zackrisson, Sophia, S. M. W. Y. van de Ven, and S. S. Gambhir. "Light in and sound out: emerging translational strategies for photo acoustic imaging". Cancer research ,vol.74 ,pp. 979-1004, 2014.

[49] Bell, Alexander Graham."LXVIII. Upon the production of sound by radiant energy." The London, Edinburgh, and Dublin Philosophical Magazine and Journal of Science,vol. 11,pp. 510-528, 1881 .

[50] Rosencwaig, Allan. "Photoacoustic spectroscopy of solids." Review of Scientific Instruments ,vol.48,pp. 1133-1137,1977 .

[51] Afromowitz, Martin A., PenShu Yeh, and Sinclair Yee."Photoacoustic measurements of spatially varying optical absorption in solids: A theoretical treatment." Journal of Applied Physics,vol. 48 ,pp. 209-211, 1977.

[52] Rosencwaig, Allan, and Allen Gersho. "Theory of the photoacoustic effect with solids." Journal of Applied Physics ,vol.47 ,pp. 64-69, 1976.

[53] Rosencwaig, Allan. "Photoacoustic spectroscopy. New tool for investigation of solids." Analytical Chemistry ,vol.47 ,pp. 592-604, 1975.

[54] Thomas, R. L."Reflections of a Thermal Wave Imager: Two Decades of Research in Photoacoustics and Photothermal Phenomena." Analytical Sciences/Supplements ,vol.17 ,pp. s1-s4,2002.

[55] Faubel, Werner, Stefan Heissler, Ute Pyell, and Natalia Ragozina. "Photothermal trace detection in capillary electrophoresis for biomedical diagnostics and toxic materials." Review of scientific instruments,vol. 74 ,pp. 491-494,2003.

[56] Tam, A. C., and H. Coufal. "Pulsed opto-acoustics: theory and applications."Le Journal de Physique Colloques ,vol.44, pp. C6-C9,1983.

[57] Bageshwar, Deepak V., Avinash S. Pawar, Vineeta V. Khanvilkar, and Vilasrao J. Kadam. "Photoacoustic Spectroscopy and Its ApplicationsA Tutorial Review." Eurasian Journal of Analytical Chemistry ,vol.50 ,pp. 187-203, 2001.

[58] Philip, Reji, P. Sathy, V. P. N. Nampoori, J. Philip, and C. P. G. Vallabhan. "Characteristics of two-photon absorption in methanol solutions of Rhodamine 6G using laser induced pulsed photoacoustics." Journal of Physics B: Atomic, Molecular and Optical Physics ,vol.25 ,pp. 155,1992.

[59] Patel, C. K. N., and A. C. Tam."Pulsed optoacoustic spectroscopy of condensed matter." Reviews of Modern Physics ,vol.53 ,pp.517, 1981.

[60] Kinney, John B., and Ralph H. Staley."Applications of photoacoustic spectroscopy." Annual Review of Materials Science ,vol.12 ,pp. 295-321,1982.

[61] Almond, Darryl P., and Pravin Patel. Photothermal science and techniques. Vol. 10. Springer Science& Business Media, 1996.

[62] George, Sajan D., Achamma Kurian, Martin Lase, V. P. N. Nampoori, and C. P. G. Vallabhan. "Thermal characterization of doped InP using photoacoustic technique." In International Symposium on Photonics and Applications, pp.183-191,2001.

Chapter 5

Nonlinear-optical studies on CdSe QDs based photonic materials

---

In the present chapter, we focus on the evaluation of nonlinear optical characteristics of CdSe based nano colloids employing the technique of single beam z-scan. The effect of various experimental parameters like input laser fluence, pH, particle size and presence of NP on the reverse saturable absorption property of the CdSe nano colloid have been studied. These studies show the application of colloidal CdSe QDs based samples as a promising nonlinear optical material.

Results of this chapter are published in :

1. *Anju. K. Augustine et.al.,Journal of Nanoscience,vol.2014,pp.7,2014.*
2. *Anju. K. Augustine et.al., Optik vol.125, pp.6696-6699,2014.*

5.1 Introduction

Before the advent of lasers, transparent optical materials were assumed to be essentially passive unaffected by the light travelling through them. The high powers of laser beams made it possible, to observe that the effect of light on a medium can indeed change its properties such as refractive index or absorption.These are optical non-linear phenomena. When this happens, the light itself gets affected by this change in a non-linear way; for example the non-linear response of the material can convert the laser light into new colours, both harmonics of the optical frequency and sum and difference frequencies. With the development of optical communication networks; various nonlinear optical (NLO) devices such as optical switches, optical limiters, optical detectors and optical sensors have attracted considerable attention because of their widespread usage for scientific and industrial purposes.

Among all the nonlinear optical properties, optical limiting is one of the most promising practical applications, as it can protect the human eye and photosensitive components from damage caused by intense optical radiation[1, 2]. Optical limiting results from irradiance-dependent NLO responses of materials in which the incoming intense light alters the refractive and absorptive properties, resulting in a greatly reduced transmitted intensity. It is important to select suitable materials as optical limiting media by determining the magnitude of their nonlinearity. Organic materials characterized by large NLO responses are of major interest owing to their large NLO susceptibilities, fast response time, architectural flexibility, low cost and ease of fabrication [3, 4].

In recent years, interest in the synthesis, characterization, and application of colloidal QD semiconductor materials has grown markedly. QDs of CdSe are by far the most studied system among all the semiconducting NCs. The bulk CdSe has a direct band gap of 1.74 eV at 300 K, and a typical Bohr exciton diameter of around 5.6 nm[5]; Consequently, CdSe QDs show quantum confinement effects with remarkably different optical properties. The size dependent, unusual optical and electronic properties of these QDs have been studied in detail using a wide variety of experimental and theoretical techniques. The linear optical properties of CdSe QDs depend strongly on particle size, for example,

the blue shift of excitonic absorption and emission peaks with decreasing particle size is a well- known observation. The unusual properties of the QDs, in the quantum-confined regime, have led to numerous technological applications.

In the past decade, there has been increasing interest in the luminescent and nonlinear optical properties of these nanometer-sized QDs. Large optical nonlinearities in CdSe QDs have been reported using different techniques. These techniques include degenerate four wave mixing and z-scan techniques with nanosecond and picosecond laser pulses. Z- scan, especially, is an effective technique to investigate nonlinear absorption and nonlinear refraction. An ideal optical limiter, by definition, is a device that exhibits a linear transmittance below a threshold and clamps the output to a constant value above it, thus providing safety to sensors and the eyes. A wide range of materials contributing to the optical limiting and nonlinear absorption has been investigated. It is well known that optical limiting devices rely on one or more of the nonlinear optical mechanisms such as excited state absorption, free carrier absorption, two-photon absorption (TPA), photo-refraction, nonlinear refraction and induced scattering with enhancement in limiting performance by coupling two or more of such mechanisms [6-8].

5.2 Z- scan method for nonlinear optical studies

The nonlinear optical characterization of the samples was carried out by the Z-scan technique using 532 nm [9, 10]. The experimental set up is described in chapter 2. The samples to be investigated were translated through the focal point of a lens of focal length 20 cm.The beam waist radius ω_0 was estimated to be 35.4μm. The Rayleigh length

$$z_0 = \frac{k\omega_0^2}{2} \tag{5.1}$$

was calculated to be 7.4 mm.The samples were taken in a 1mm thickness cuvette which is much less than z_0 which is an essential prerequisite for Z-scan experiment. The normalized transmittance for TPA in the open aperture condition is given by [11]

$$T(Z, S = 1) = \frac{1}{\sqrt{\pi q_0(z,0)}} \int_{-\infty}^{+\infty} ln[1 + q_0(z,0)e^{-\tau^2}]d\tau \tag{5.2}$$

where

$$q_0(z,0) = \frac{\beta I_0 L_{eff}}{1+(\frac{z}{z_0})^2} \tag{5.3}$$

The parameter q_0 is the depth of the open aperture Z- scan curve obtained from the theoretical fit and it is the measure of the intensity dependent absorption. Here, I_0 is the laser intensity in the focal plane,β is the nonlinear optical absorption coefficient, L_{eff} is the effective thickness with linear absorption coefficient α. L_{eff} is given by

$$L_{eff} = \frac{(1-e^{-\alpha l})}{\alpha} \tag{5.4}$$

The open-aperture curve exhibits a normalized transmittance valley at the focal point, indicating the presence of reverse saturable absorption (RSA) in the nano colloidal solutions. The open z-scan scheme was also used to measure $\mathrm{Im}\chi^{(3)}$.The imaginary part of third order susceptibility, $\mathrm{Im}\chi^{(3)}$ is related to β through the equation,

$$Im\chi^{(3)} = \frac{n_0^2 c^2 \beta}{240\pi^2\omega} \tag{5.5}$$

From the closed aperture z-scan scheme the nonlinear refractive index n_2 and the real part of the third order nonlinear susceptibility, $\mathrm{Re}(\chi^{(3)})$ are given, respectively,by equations (5.6) and (5.7).

$$n_2(e.s.u) = \frac{cn_0\lambda}{40\pi 2\pi I_0(t) L_{effe}}\Delta\Phi_0 \tag{5.6}$$

n_2 is related to $\mathrm{Re}(\chi_{(3)})$ by the relation

$$Re\chi^{(3)} = \frac{n_0 n_2(e.s.u)}{3\pi^2} \tag{5.7}$$

From the real and imaginary part of $\chi^{(3)}$, the modulus of third order nonlinear susceptibility can be found out.

$$\sqrt{Re(\chi^{(3)})^2 + Im(\chi^{(3)})^2} \tag{5.8}$$

To study the optical limiting property of the sample, the nonlinear transmission of the sample is measured as a function of input fluence. Optical

power limiting is effected through the nonlinear optical processes of the sample. An important term in the optical limiting study is the optical limiting threshold.Optical limiters are essentially those systems which transmit light at low input fluence or intensities, but become opaque at high inputs. The optical limiting property is mainly found to be absorptive nonlinearity, which corresponds to the imaginary part of third order susceptibility[12]. From the values of fluence at focus, the fluence values at other positions could be calculated using the standard equations for Gaussian beam waist.

5.3 Size dependent nonlinearity of CdSe QDs

For detailed study, we used samples taken after reflux times of 10min, 1hr and 3hr and are denoted as $C_1, C_2 \& C_3$ respectively. The variation in absorption peak, and the corresponding optical energy band gap (inset) of samples ($C_1, C_2 \& C_3$) are shown in figure 5.1:(a), (b) and (c).

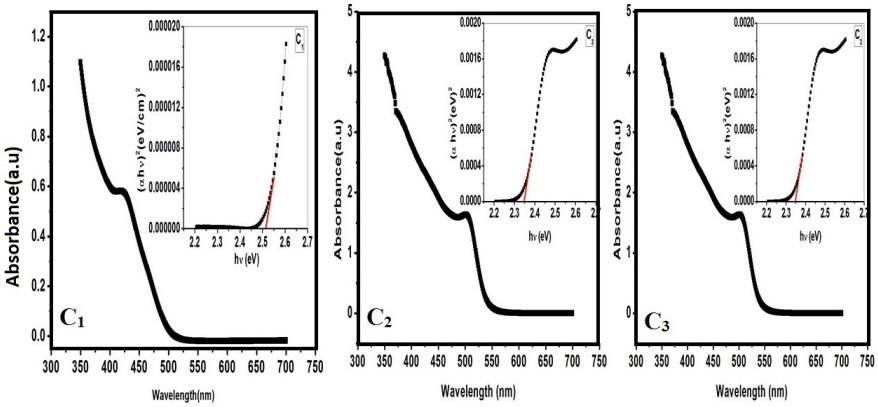

Figure 5.1: (a),(b) and(c) shows the variation in absorption peak, and the corresponding optical energy band gap (inset) of samples C_1,$C_2 \& C_3$.

Energy band gap of the QDs shows a variation from 2.51eV-2.34eV as the particle size increased during the reflux time from 10minute to 3 hour. It is observed that as particle size increases, absorption peak shifts to higher wavelength side and the band gap is enhanced with decrease in particle size. The emission spectra of the C_1, C_2, and C_3 samples also shown in figure 5.2. The particle size is calculated with

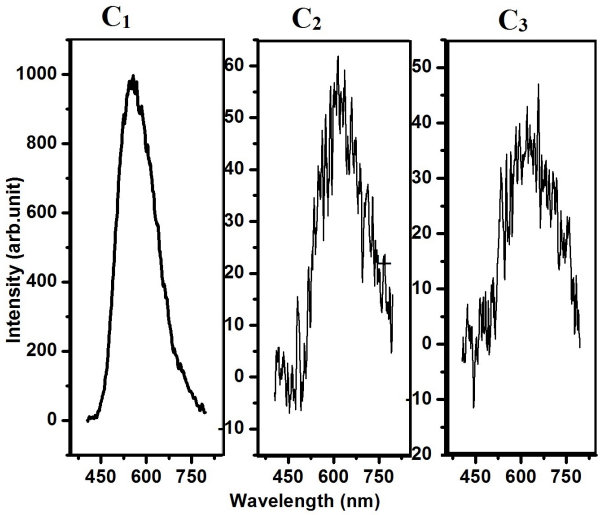

Figure 5.2: The emission spectra of $C_1, C_2 \& C_3$ sample under the excitation wavelength of 390nm.

effective mass approximation [13]. For CdSe:Eg_{bulk}=1.74 eV, ϵ=10.6, m_e^*=0.13,m_h^*=0.45

$$E_{nano} = E_{bulk} + \frac{h^2}{2m_0 d^2}(\frac{1}{m_e^*} + \frac{1}{m_h^*}) - \frac{36e^2}{4\pi\epsilon\epsilon_0 d} \tag{5.9}$$

where d is the particle diameter. The calculated particle size of these QDs are presented in Table 5.1. The nonlinear optical characterization of the samples was carried out using the Z-scan technique and the normalized transmittance for two photon absorption (TPA) in the open aperture condition is given by equation 5.2 above. The open-aperture curve exhibits a normalized transmittance valley at the focal point, indicating the presence of RSA in the nano colloidal solutions. The open aperture Z- scan plot for samples having different particle size is depicted in figure 5.6. The fits of equation (5.2) to experimental data are shown as solid curves.The data can be fitted well by assuming TPA in the nonlinear optical absorption process. From this fit, we can confirm that the basic mechanism involved in the nonlinear absorption of nano colloidal solutions of CdSe QDs is TPA process because the photon energy of the 532 nm laser is within the range $E_g \leq 2h\nu \leq 2E_g$, where $h\nu$ =2.33 eV[11].

The nonlinear absorption coefficient (β) is calculated from the above fits shows a dependence on the particle size of the QDs. The experimental data show that β value increases with increasing particle size. With a small decrease in the band gap a significant increase in the nonlinear absorption is observed. In order to explain the optical nonlinearity, we mainly consider the band gap variation of CdSe QDs samples ($C_1, C_2, and C_3$).Sample $C_1 and C_2$ have band gap very near to 2.4 (2.39 $\pm$.02) and 2.5 (2.52$\pm$ 0.02) respectively which is more than one photon energy corresponding to 532nm. The data fitting shows that the nonlinear optical absorption is through TPA process in these samples. Our studies show that sample C_3 has large optical nonlinearity (2.47×10^{-10} m/W) enhancement, compared to other samples as seen in figure 5.3. Band gap corresponding to sample C_3 is 2.33eV to 2.33 $\pm$ .02 eV which

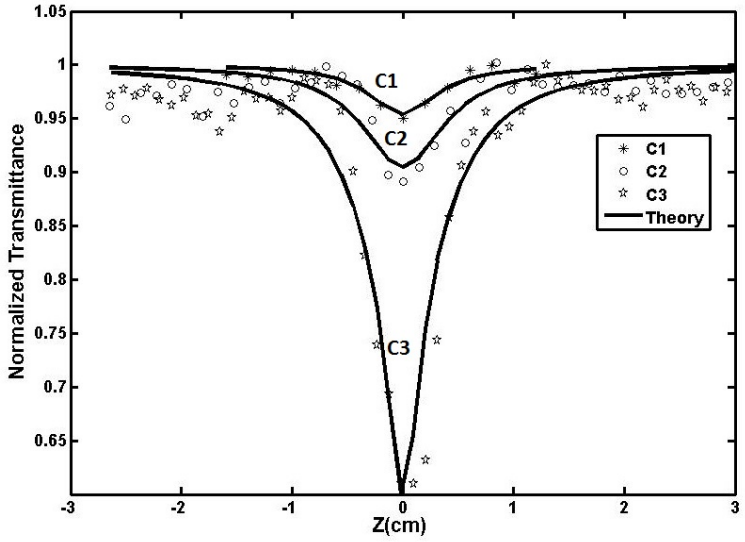

Figure 5.3: The open aperture Z- scan plot for different particle sizes of CdSe QDs (C_1, C_2, and C_3).

is very near to the one photon energy corresponding to 532nm (2.33 eV).The fact that optical nonlinearity in this case is also due to the two photon absorption reveals that, two photon excitation cross section is enhanced due to resonant one photon absorption level. A small

mismatch between band gap of sample C_3 and the one photon energy will be compensated by phonon assisted excitation. The enhancement also arises due to increased optical nonlinear interaction between the radiation and the particles.This can be explained by the fact that with increase in particle size, there is an increase in the multiple scattering from the QDs. This increase in multiple scattering leads to large effective interaction length which in turn results in an enhancement in NL absorption [10].

The open z-scan scheme was also used to measure Im$\chi^{(3)}$ from the equation(5) where $n_0 = 2.34$ is the linear refractive index of CdSe, C is the velocity of light in vacuum, ω is the angular frequency of the radiation used. The measured values of optical band gap for different particle size and nonlinear absorption coefficient at a wavelength of 532 nm for input laser power density of 0.54 GW/cm^2, are given in the Table 5.1.

S	d(nm)	B.G(eV)	β(m/W)	OLT(GW/cm^2)	Im$\chi^{(3)}$(e.s.u)
C1	4.17	2.52	0.27×10^{-10}	0.57	0.16×10^{-11}
C2	4.96	2.38	0.69×10^{-10}	0.48	0.41×10^{-11}
C3	5.25	2.34	2.47×10^{-10}	0.35	1.45×10^{-11}

Table 5.1: Data showing particle size, energy band gap, nonlinear absorption coefficient(β),optical limiting threshold(OLT) and imaginary part of susceptibility(Im $\chi_{(3)}$) of the samples C_1, C_2, andC_3.

To study the optical limiting property of the sample, the nonlinear transmission of the sample is measured as a function of input fluence. Such plots give a better comparison of the nonlinear absorption or transmission in the sample and are generated from Z-scan trace[14, 15]. Figure 5.4 illustrates the optical limiting response of the samples (C_1, C_2, andC_3). The line in the figure indicates the approximate fluence at which the normalized transmission begins to deviate from linearity. The fluence value corresponding to the onset of optical limiting (optical limiting threshold) is found to vary from 0.35 GW/cm^2 to 0.572 GW/cm^2 for the samples with input fluence 0.54 GW/cm^2. Our works show that the semiconductor nanomaterial which has got a one photon resonant absorption can be employed for third order optical nonlinear material in which two photon absorption will get enhanced by the one photon

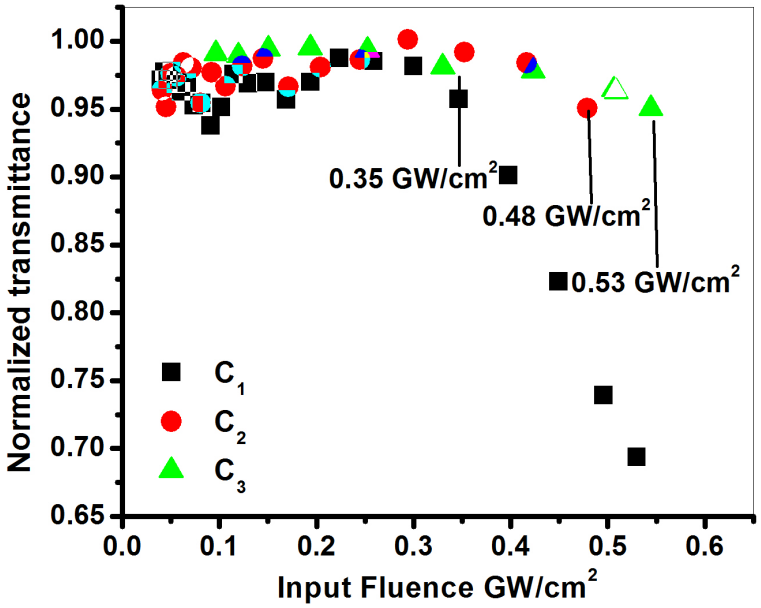

Figure 5.4: Optical limiting response of the samples ($C_1, C_2, and C_3$).

resonance energy level (Table 5.1). Such materials are useful as optical limiters with low threshold energy. Thus it is clear from figure 5.4 that the CdSe QDs with large particle size can be used for optical power limiting at high laser fluences. Thus, size of QDs has a significant effect on limiting performance. Closed-aperture Z-scan trace of the CdSe QDs for input fluence of 436 MW/cm^2 is shown in figure 5.5. The solid line shows the theoretical fit. The closed-aperture curve of CdSenano fluid displayed a peak to valley shape, indicating a negative value of the nonlinear refractive index n_2 and it is the self-defocusing nonlinearity. It is observed that the peak-valley of the closed-aperture Z-scan satisfies the condition

$$\Delta z = 1.7 z_0 \tag{5.10}$$

thus confirming the presence of cubic nonlinearity. The value of ΔT_{p-v} which is the difference between the peak and valley transmittance, could

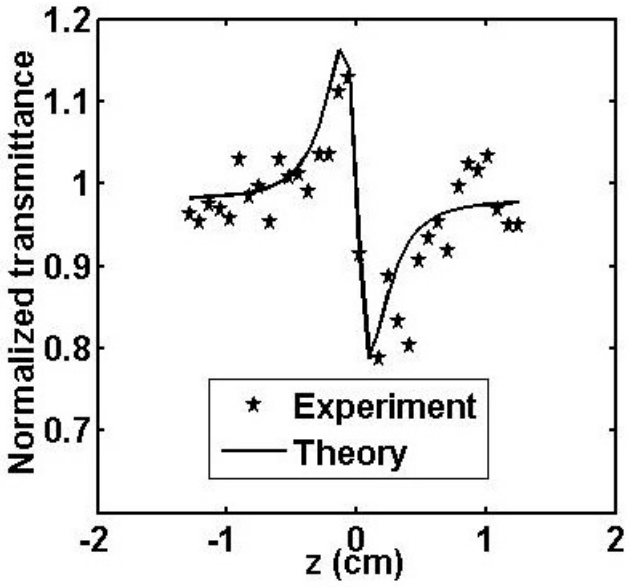

Figure 5.5: Closed-aperture z-scan trace of the CdSe QDs (C_3) for input fluence of 436 MW/cm^2.

be obtained by the best theoretical fit from the results. The peak valley transmittance change is

$$\Delta T_{p-v} = 0.406\Delta\phi_0 \tag{5.11}$$

Numerical calculations show that this relation is accurate to 0.5%for $\Delta\phi_0 \leq \pi$ =0.406. For large aperture, this equation is modified within a $\pm 2\%$ accuracy and is given by

$$\Delta T_{p-v} = 0.406(1-s)^{.25}\Delta\phi_0 \tag{5.12}$$

for $\Delta\phi_0 \leq \pi$ where S is the linear transmittance of the far field aperture. From the closed aperture z-scan fit, $\Delta\phi_0$ can be obtained and from this the nonlinear refractive index n_2 is calculated as 0.79×10^{-10} (e.s.u) with the corresponding β value as 0.432×10^{-10} m/W.

5.4 Nonlinear studies of CdSe nanofluids with different pH.

The absorption and emission spectrum of the CdSe nanofluids with different pH is given in figure 5.6.

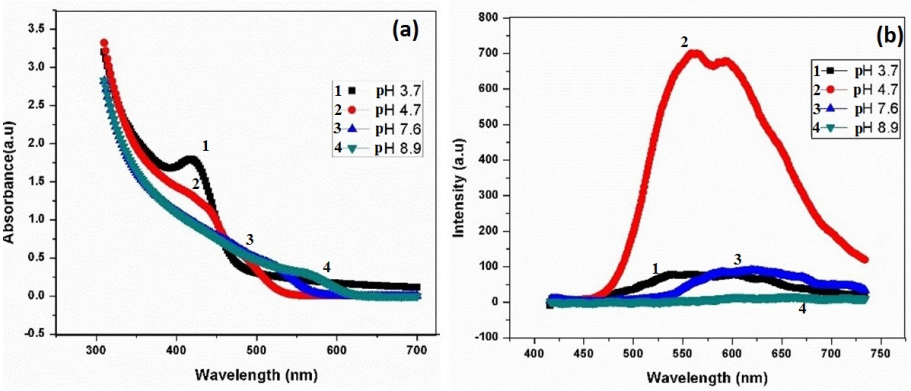

Figure 5.6: (a) Absorption and (b) Fluorescence spectra of the CdSe QDs for different pH.

It is clear from the spectrum that the first exciton peak is sharp which indicates a narrow size distribution. Due to the narrow size distribution, the differences in band gap energy of different sized particles will be very small and hence most of the electrons will get excited over a smaller range of wavelengths. As the pH increases absorption spectrum shows a red shift in wavelength. This can be explained on the basis of the dynamic growth process of the QDs with pH. It is clear from figure 5.6:(b) that, the fluorescence spectra of CdSe QDs having pH 4.7 shows an intense emission around 560 nm which is attributed to the inter-band transition. The full width half maximum (FWHM) around 150 nm for this emission at pH 4.7 is primarily attributed to the optimum size distribution of these nanofluids. In this case, there is a chance that radiative relaxation effect may be more significant so that band to band transition give significant width for the fluorescence emission process. At the same time high fluorescence quenching is also observed when pH varied from the optimum value. When the pH of the precursor solution is far away from the optimum value, it led to weakening of the protection abilities

of MSA due to the protonation and deprotonation of MSA[16].

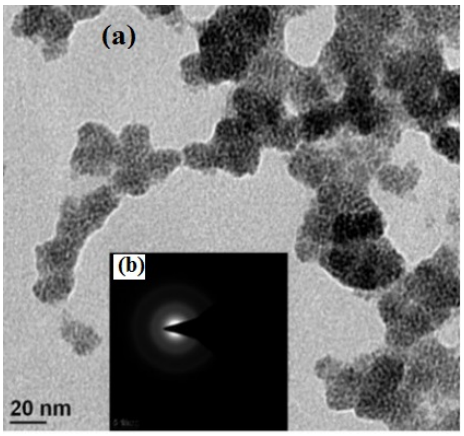

Figure 5.7: (a) TEM image and (b) SAED of CdSe sample.

TEM image and selected area electron diffraction(SAED) image of CdSe sample with pH 7.6 is shown in figure 5.7. For Z-scan studies we have selected samples named pH 3.7, pH 4.7 and pH 9.7. The open-aperture z-scan scheme was used to measure nonlinear absorption coefficient (β), and the imaginary part of the third-order NLO susceptibility (Im $\chi^{(3)}$). The data are analyzed by using the procedure described by Sheik-Bahae et al. The NL absorption coefficient is obtained by fitting the experimental z-scan plot to equations (5.2).Figure 5.8:(a) gives the open aperture z-scan trace of CdSe QDs having different pH at a typical fluence of 199 MW/cm^2, carried out using the Z-scan technique at 532 nm. The theory of the two photon absorption process that fitted well with the experimental curve infers that TPA is the basic mechanism involved in the nonlinear absorption process, but the possibility of a higher order nonlinear process such as free carrier absorption that contributes to induced absorption cannot be ruled out. We observed that at the off resonance wavelength of 532nm, the CdSe nanofluid of pH4.7 showed a minimum of RSA behavior compared to other pH values.

In order to investigate the influence of fluence in the nonlinear optical response, similar Z-scan measurements were carried out for the CdSe nanofluid at a different fluence (436 MW/cm^2) with varying pHs and

is shown in figure 5.8:(b). The measured values of nonlinear absorption

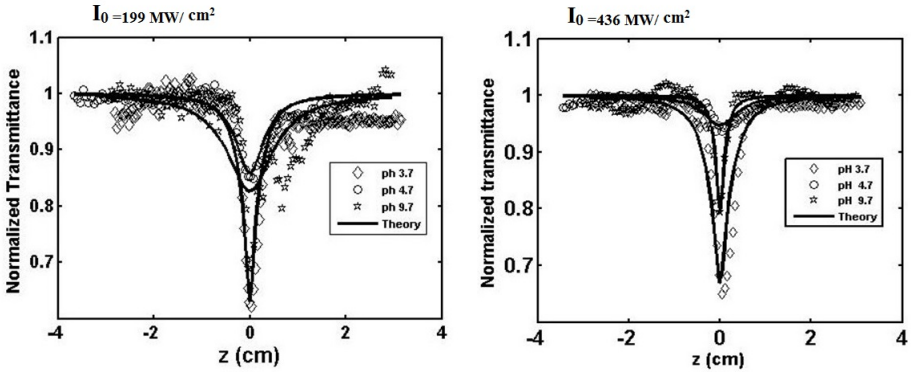

Figure 5.8: Open aperture z-scan trace of CdSe QDs having different pH at a typical fluence of (a) 199 MW/cm^2 and (b) 436 MW/cm^2.

coefficient at a wavelength of 532 nm for different laser power densities and the corresponding value of $Im\chi^{(3)}$ are given in the Table 5.2. The origin of the optical nonlinearity of the quantum dots, can be mainly attributed to the enhanced exciton oscillator strength of the quantum dots due to quantum confinement effect [17-19]. From figure 5.6 and figure 5.8, it's cleare that the linear and nonlinear absorption property of the CdSe QDs are highly influenced by the pH of the medium. Maximum radiative transition and minimum nonlinearity at pH 4.7 can be attributed to the ability of the protonation or deprotonation of the MSA capped CdSe QDs. We also attempt to link the concept of surface charge and phonon transport mechanism to this phenomena. As the pH value diverges from the optimum value, the particles acquire larger charge and the particle-particle repulsion increases, thus facilitating phonon transport through increase of transport efficiency. Thus nonradiative transitions enhanced at these pH values and the nonlinear scattering due to thermally induced- phonon assisted- nonlinearity is an alternative process that can mimic nonlinear absorption. The photon energy will be compensated by phonon assisted excitation in the case where pH diverges from optimum value and lead to enhanced nonlinearity. This is not in the case of CdSe QDs with optimum pH (4.7) where the assistance of nonradiative-phonon transport is less.

An interesting phenomena obtained in the open aperture Z-scan measurement from the samples are the unusual ‘ hump′ flanking the valley in figure 5.8:(a) with pH 4.7. We observed that they arise from the trend of bleaching of the ground-state- atomic band prior to free-carrier absorption as reported earlier[20]. In the case of sample solution with pH 4.7, at the far field of the Gaussian beam, where $|Z| \geq Z_0$, the beam fluence is too weak to elicit nonlinear RSA effects and at a higher fluence purely RSA occurs as shown in figure 5.6:(b). From figure 5.9, it is observed that nonlinear absorption of CdSe QDs with optimum pH (4.7) is highly fluence-dependent and this optimized pH is also the evidence of sensitivity of the optical interaction of the material to dipole moment. Optical interactions are very much influenced by hydrogen ion concentration as can be seen from the data in Table 5.1. This method can also be applied to optimize the pH of the nanofluid. The decrease in $\beta$and Im$\chi^{(3)}$ at high input fluence shows the probability of bleaching of free charge carriers and can be attributed to the decrease in ground state free carrier density with increased input intensity. This happens predominantly in CdSe QDs with optimum pH (4.7) which shows an 80% decrease in Im$\chi^{(3)}$,while it is 50% in other cases. The open aperture z-scan curves of the CdSe QDs with optimum pH (4.7) at different input fluences are shown in figure 5.9.

Closed-aperture z-scan trace of the CdSe QDs for input fluence of 436 MW/cm^2 is shown in figure 5.10. The solid line shows the theoretical fit. The closed-aperture curve of nano fluid with pH 3.7 and 9.7 displayed a peak to valley shape, indicating a negative value of the nonlinear refractive index n_2 and it is the self-defocusing nonlinearity. In the case of CdSe QDs based nano fluid sample with pH 4.7, the molecular reorientated Kerr effect becomes the dominant mechanism for nonlinear refraction, indicating a positive value of the nonlinear refractive index n_2 and it is the self-focusing nonlinearity. It is observed that the valley-peak of the closed-aperture z-scan satisfied the condition Δ z=1.7 z_0, thus confirming the presence of cubic nonlinearity. The value of ΔT_{p-v} the difference between the peak and valley transmittance, could be obtained by the best theoretical fit from the results. From the real and imaginary part of $\chi^{(3)}$, the modulus of third order nonlinear susceptibility can be found out. The magnitude of$\chi^{(3)}$ is significantly affected by

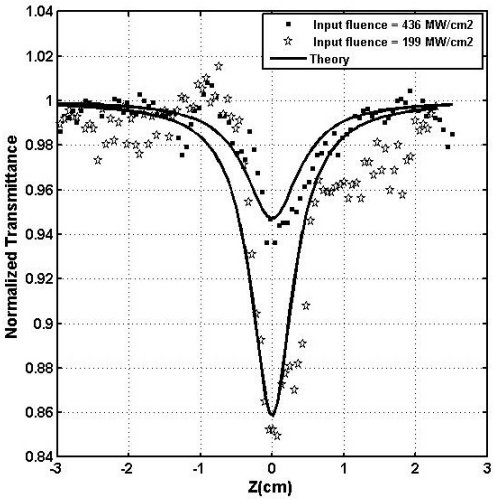

Figure 5.9: Open aperture z-scan curves of the CdSe QDs with pH 4.7 at different input fluences.

the molecular orientation and it determines the strength of nonlinearity of the material. Its figure of merit

$$F = \frac{\chi^{(3)}}{\alpha} \tag{5.13}$$

is found to vary from 24.9 $\times 10^{-12}$ (esu. m) to 63.8 $\times 10^{-12}$(esu. m).The calculated values are shown in Table 5-2.

To study the optical limiting property of the sample, the nonlinear transmission of the sample is measured as a function of input fluence. Optical power limiting is effected through the nonlinear optical processes of the sample[21, 22]. From figure 5.11 the fluence value corresponding to the onset of optical limiting is found to vary from 0.39 GW/$cm^2$to 0.51 GW/cm^2 for the samples having different pH with input fluence 0.199 GW/cm^2. A careful comparison of figure 5.11 shows that the limiting capability of the optimized CdSe sample with pH 4.7 shows good optical nonlinear behavior which is somewhat better than that of other samples by virtue of their early onset of limiting and larger reduction in transmittance. The onset of limiting occurs around an input uence of

pH	$I_0(MW/cm^2)$	$\beta(m/W)$	$Im\chi^{(3)}$ (e.s.u)	$\Delta\phi_0$	n_2(e.s.u)	Re$\chi^{(3)}$ $(e.s.u)$	$\chi^{(3)}$	F (esu.m)
3.7	199	6.47 $\times10^{-10}$	3.30 $\times10^{-11}$	-	-	-	-	
	436	2.78 $\times10^{-10}$	1.64 $\times10^{-11}$	0.94	1.04 $\times10^{-10}$	2.57 $\times10^{-11}$	2.98 $\times10^{-11}$	24.9 $\times10^{-12}$
4.7	199	2.68 $\times10^{-10}$	1.58 $\times10^{-11}$	-	-	-	-	
	436	0.39 $\times10^{-10}$	0.23 $\times10^{-11}$	1.00	1.09 $\times10^{-10}$	2.72 $\times10^{-11}$	2.73 $\times10^{-11}$	22.8 $\times10^{-12}$
9.7	199	3.42 $\times10^{-10}$	2.02 $\times10^{-11}$	-	-	-	-	
	436	1.93 $\times10^{-10}$	1.14 $\times10^{-11}$	0.73	- 0.79 $\times10^{-10}$	1.97 $\times10^{-11}$	2.28 $\times10^{-11}$	63.2 $\times10^{-12}$

Table 5.2: The measured values of nonlinear absorption coefficient at a wavelength of 532 nm for different laser intensity and the corresponding value of $\chi^{(3)}$ and figure of merit (F).

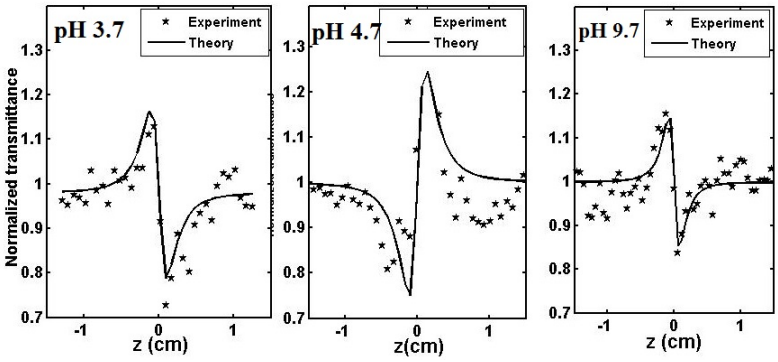

Figure 5.10: Closed-aperture z-scan trace of the CdSe QDs for input fluence of 436 MW/cm^2

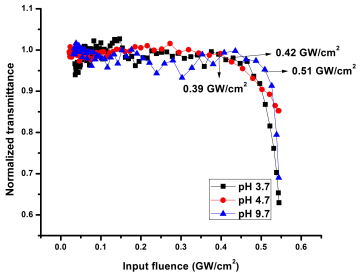

Figure 5.11: Optical limiting response of the samples with $I_0 = 199$ MW/cm^2

0.39 GW/cm^2 in this case and this value compares favorably with that observed in earlier reports.

5.5 Nonlinear studies on metal - semiconductor nanoparticles

Metal NPs, specially gold(Au) and silver(Ag) NPs have received much attention as potentially useful materials, showing novel electronic, optical, magnetic and thermal properties derived from the quantum-sized effect.Optical and electronic properties of metal NPs were shown to affect by both the size and the shape.

During the last decade, a wide variety of methods were used for the preparation of such NPs. Recently, the thermal factor has also been proven to affect the size of NPs during the synthesis[23-28]. Controlling the particle growth rate is possible through knowledge of the temperature history of reaction. In the past, the hot-plate heating method was widely applied to synthesize gold NPs in aqueous solution [29]. Since 1986, the microwave synthesis, which is quite fast, simple and very energy efficient, has been developed for a lot of applications in chemistry [30,31,32]. It is well known that the interaction of dielectric materials, liquids or solids, with microwave leads to what is generally known as dielectric heating. Many experiments with microwave heating reveal results different from those obtained from conventional heating.Thus, many developments are bound to occur and enhance the advantage associated with microwave heating. To our knowledge, the heating is created by the interaction of the dipole moment of molecules with high-frequency electromagnetic radiation. Water has a very high dipole moment, which makes it one of the best solvents for microwave heating. In addition, the precise temperature controlling program is a built-in function of a commercial microwave instrument, therefore, microwave heating seems to be a convenient approach to study the thermal effect on the size or the shape of NPs [33,34].

Nonlinear optics is one of the mature research fields relevant to fundamentals and applications of light matter interaction. Several nonlinear optical processes such as second harmonic generation (SHG),two-photon resonances, four-wave mixing etc., have played critical role in realizing various optical devices. Plasmonic metals such as gold and silver exhibit inherent non-linear optical behaviour. The NLO property of plasmonic nanostructures can be varied, modulated and eventually controlled by optimizing geometric features such as size, shape and arrangement of the nanostructures. One such plasmonic geometry that has captured the attention in recent times is the plasmonic NPs. Optical power limiting is effected through the nonlinear optical processes of the sample. Optical limiters are eventually those systems which transmit light at low input fluence or intensities, but become opaque at high inputs.

5.5.1 Synthesis and Z-scan studies on Au NPs.

In this study, microwave rapid heating is used for the synthesis of gold NPs. For detailed linear optical study we have selected four samples with decreasing concentration as (C_1,C_2,C_3,C_4), where C_1-0.5mM ; C_2-0.15mM; C_3-0.05mM ;C_4-0.005mM. Linear and nonlinear optical characteristics of the samples were discussed and optical limiting threshold of the sample C_1 was calculated using open aperture Z-scan technique using a Nd-YAG laser (532 nm, 7 ns, 10Hz). Nonlinearity varies with concentration of gold NPs within the range of our investigations which in turn may depend on the particle size. The nonlinear absorption and the RSA behavior in metal NPs were usually believed to be due to free carrier absorption or excited state absorption[35-38].

- **Results and discussion**

Figure 5.12 shows the UV-Vis absorption spectra and emission spectra of gold NPs (C_1,C_2,C_3,C_4) prepared by microwave irradiation method using citric acid as the reducing agent. Surface plasmon resonance (SPR)

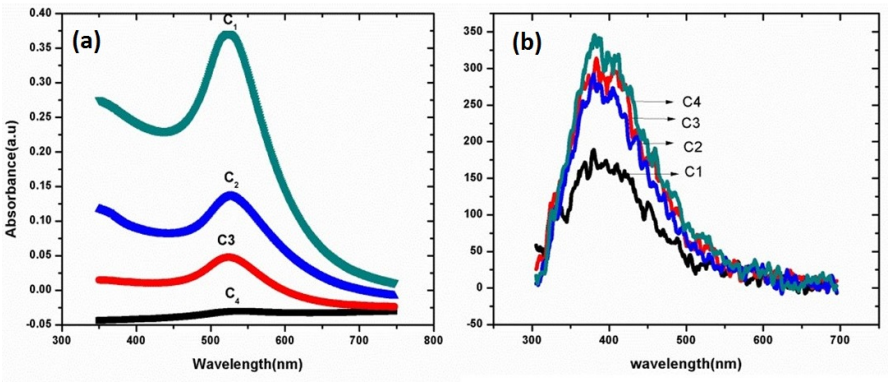

Figure 5.12: (a) UV-Vis absorption spectra and (b) Emission spectra of gold NPs (C_1,C_2,C_3,C_4).

peaks around 520 nm from Figure 5.12:(a)confirm the presence of gold NPs. The shape and position of SP absorption depends on particle size, particle shape and the dielectric constant of the surrounding medium. Sharp peak indicates that the particle sizes are uniform. The SPR plays a major role in the determination of optical absorption spectra of metal

NPs, which slightly shifts to longer wavelength with decrease in concentration of Au NPs. From SPR peak it is also clear that as the concentration decreases, there decrease in absorbance. From figure 5.12:(b) it is observed that highest value of concentration lies in the region of concentration dependent florescent quenching which is due to nonradiative relaxation through collisional process between the molecules. This phenomenon of concentration dependent florescent quenching takes place due to small mean free path. At very low concentration ,such a collisional nonradiative relaxation process will not takes place due to larger mean free path. As the concentration increases, fluorescence emission intensity will get enhanced till the optimum concentration is reached. Figure 5.13 shows, change in colour of Au NPs with decrease in concentration ie.the wine red color of Au NPs changes to purple and the absorbance decreased with a red shift in the SPR band. The observed spectral and colour changes were attributed to the aggregation of Au NPs.

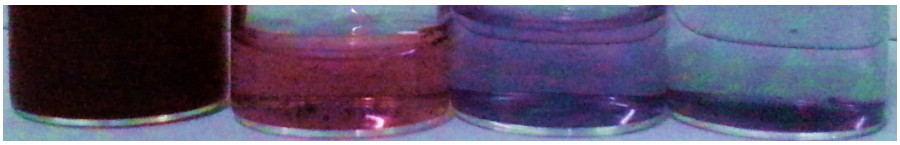

Figure 5.13: Change in colour of Au NPs with decrease in concentration.

Figure 5.14:(a)&(b) gives the TEM image and histogram of C_1 sample with particle size 7.7 nm. It shows that the particles formed are mono dispersed and spherical in shape. The FTIR spectra shown in figure 5.14:(c) suggests the formation of coordination bond between carboxylate group and gold. The main peaks at 1603 cm^{-1} and 1406 $cm^{-1}$are due to the symmetric stretching of -COO^{-}, the antisymmetric stretching of -COO^{-} of citrate ligand in Au NPs spectra, respectively. The band at 3439 cm^{-1} is due to stretching vibration of -OH. The stability of capped Au NPs is confirmed from the symmetric and antisymmetric stretching of-COO^{-} of citrate ligand in FTIR spectra. The nonlinear optical characterization of the sample was carried out using the Z-scan technique at 532 nm [11, 39].The samples were taken in 1mm thickness cuvette which is much lesser than z_0; therefore, the essential prerequisite for Z-scan experiment is satisfied. The open aperture Z-scan plot for

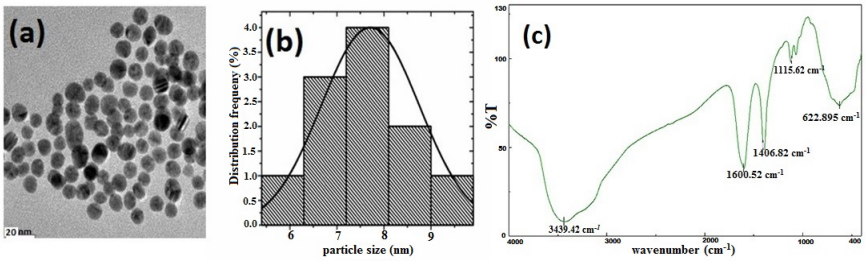

Figure 5.14: (a) TEM image (b) Histogram & (c) FTIR spectra of of C_1 sample with particle size 7.7 nm.

samples of different concentrations (C_1 and C_2) of Au NPs with same input energy is depicted in figure 5.15. The fits of equation (5.2)to experimental data are shown as solid curves.

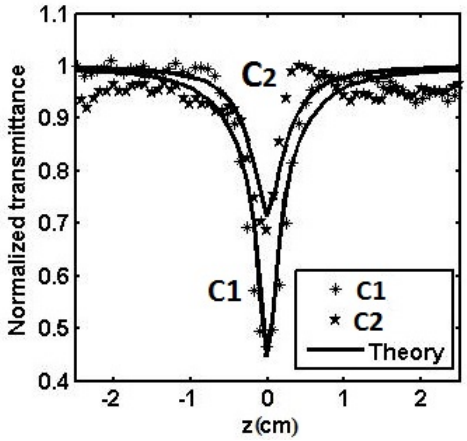

Figure 5.15: The open aperture Z- scan plot for different concentration of Au NPs with theoretical fit.

The nonlinear absorption and the RSA behavior in metal NPs were usually believed to be due to free carrier absorption or excited state absorption. The data fitting shows that the nonlinear optical absorption is through two-photon absorption process in the samples. It is also observed from figure 5.15 that, sample C_1 has large optical nonlinearity enhancement, compared to C_2. An enhancement in optical nonlinearity with increased input energy has been observed for sample C_1 and

is given in figure 5.16. I_0 values for the C_1 sample corresponding to

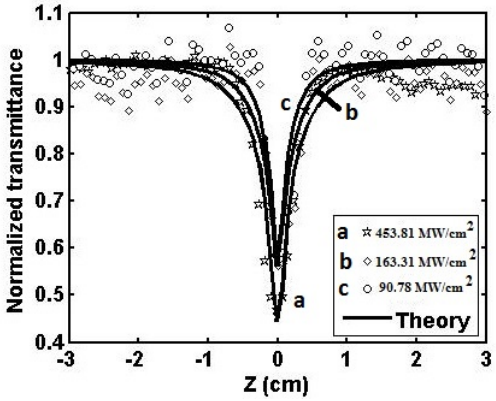

Figure 5.16: The open aperture Z- scan plot for C_1 concentrations of Au NPs with different input energies.

input energies of 125 μJ,45 μJ and 25 μJ are 453.81 MW/cm^2,163.39 MW/cm^2 and 90.78 MW/cm^2 respectively. Figure 5.17 illustrates the optical limiting response of the C_1 sample with input power density 0.453 GW/cm^2 [9, 21]. The line in the figure indicates the approximate fluence

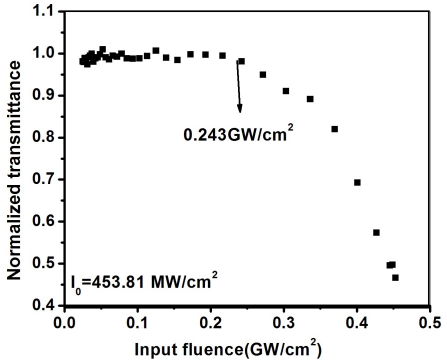

Figure 5.17: Optical limiting response of the C_1 sample.

at which the normalized transmission begins to deviate from linearity. The fluence value corresponding to the onset of optical limiting (optical limiting threshold) is found to be 0.243GW/cm^2 for the C_1 sample with

input fluence 453.81 MW/cm^2. Thus it is clear from figure 5.17 that the Au NPs can be used as good optical power limiters at high laser fluences. Closed-aperture Z-scan trace of the Au NPs for input fluence of 436 MW/cm^2 is shown in figure 5.18. From the closed aperture Z-scan

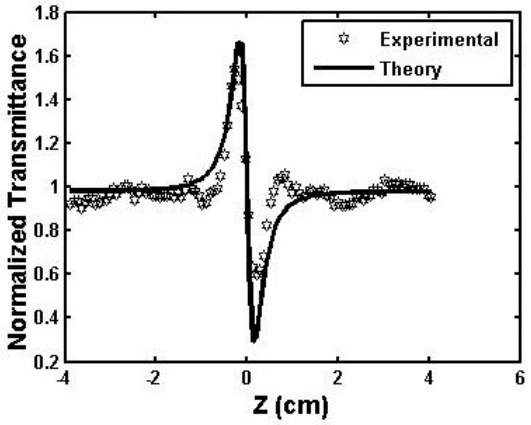

Figure 5.18: Closed-aperture Z-scan trace of the Au NPs for input fluence of 436 MW/cm^2.

fit, $\Delta\phi_0$ can be obtained as 1.74. The nonlinear absorption coefficient β =2.04×10^{-10} m/W and nonlinear refractive index n_2 as 1.90×10^{-10} (e.s.u) is obtained for C_1 sample .

5.6 Synthesis and Z-Scan studies on Ag NPs.

Noble metal NPs have attracted a lot of interest for applications in optical devices due to their enhanced third order nonlinear optical response near the surface plasmon resonance (SPR)[40, 41]. The third order optical nonlinear response of gold and silver NPs dispersed in the liquid host of toluene demonstrates a low threshold for optical nonlinearity and large two-photon absorption cross sections for monolayer protected gold clusters are also observed [42, 43].Silver NPs are of particular interest because they are known to have optical absorption transitions with high oscillator strengths due to the lesser s-d hybridization pronounced than

for gold clusters of the same size [43-45].Thus,higher nonlinear absorption coefficients are expected for Ag.

- **Results and discussions**

UV-Vis absorption spectra of Ag NPs prepared by microwave irradiation method is shown in figure 5.19.

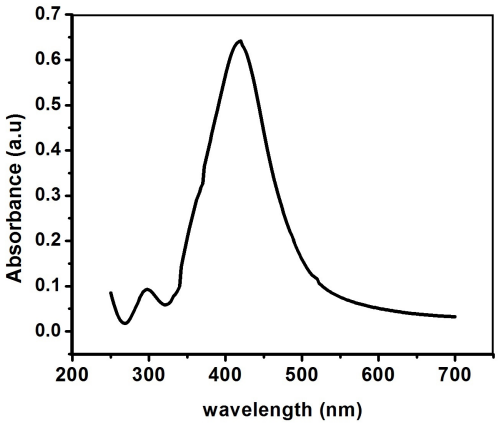

Figure 5.19: UV-Vis absorption spectra of samples of Ag NPs prepared by microwave irradiation method.

The stable position of absorbance peak indicates that new particles do not aggregate. One can understand that since the silver colloidal particles possess a negative charge due to the adsorbed citrate ions, a repulsive force works along particles and prevents aggregation[46-48]. UV-Vis absorption results confirmed the formation of silver NPs as seen, from the SPR peaks around 420 nm. TEM images of the sample in figure 5.20:(a) shows that the particles formed are around 28nm. As in well-known that small size of nanoparticles means they exhibit enhanced or different properties when compared with the bulk material. The FTIR spectra of of Ag NPs in figure 5.20:(b) suggests the formation of coordination bond between carboxylate group and silver. The main peaks at 1595 cm^{-1} and 1393 cm^{-1} are due to the symmetric stretching of -COO^{-}, the antisymmetric stretching of -COO^{-} of citrate ligand in Ag NPs spectra, respectively. A band at 3330 cm^{-1} is observed due to stretching vibration of -OH. The stability of capped Ag NPs is confirmed from the symmetric and antisymmetric stretching of -COO^{-} of

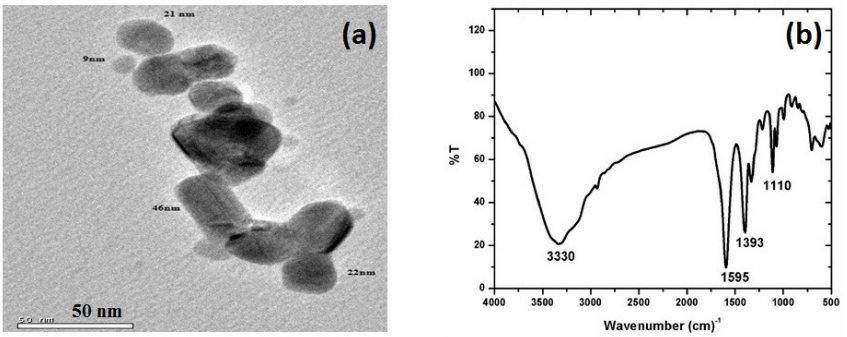

Figure 5.20: (a) TEM image & (b) FTIR spectra of Ag NPs prepared by microwave irradiation method with average size 28nm.

citrate legend in FTIR spectra. The nonlinear optical characterization of the samples was carried out using the Z-scan technique at 532 nm [11, 39].The parameter q_0 is the depth of the open aperture Z-scan curve obtained from the theoretical fit and it is a the measure of the intensity dependent absorption. Here, I_0 is the laser intensity in the focal plane, β is the NL optical absorption coefficient, L_{eff} is the effective thickness with linear absorption coefficient α. The open aperture Z- scan plot for Ag NP samples at different power density is depicted in figure 5.21. By

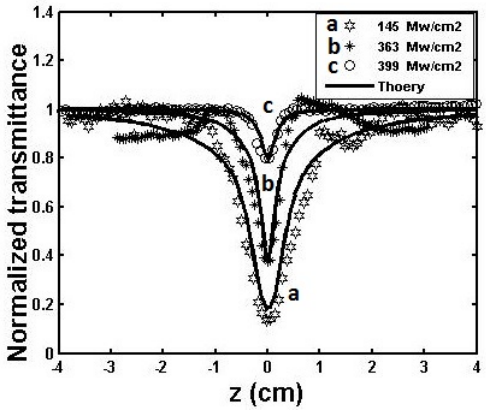

Figure 5.21: Open aperture z-scan trace of the Ag NPs for different input fluence.

fitting of equation(5.2), experimental data are shown as solid curves and the NLO absorption coefficient are tabulated in Table 5.3. The effective TPA cross section of Ag NPs are quenched at higher input power densities which can be attributed to bleaching of the ground state at higher input intensities. Closed aperture Z-scan trace of the Ag NPs for input

Power (Gw/cm^2)	q	$\beta \times 10^{-12}$ (m/W)
0.145	1.72	11.88
0.36	1.58	4.36
0.39	0.84	2.12

Table 5.3: Nonlinear absorption coefficient of Ag NPs at different power densities.

fluence of 399 MW/cm^2 is shown in figure 5.22. It is observed that the peak- valley of the closed-aperture Z-scan confirms the presence of cubic nonlinearity with $\Delta\phi_0$ obtained as 1.37. The NL absorption coefficient β =1.10 $\times 10^{-10}$ m/W and nonlinear refractive index n_2 as 1.50$\times 10^{-10}$ (e.s.u) is obtained for the sample.

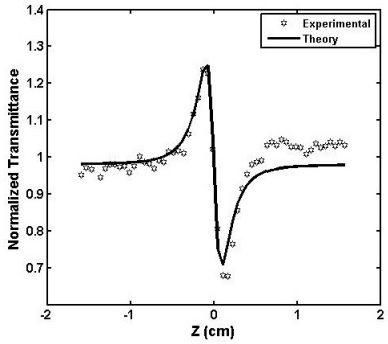

Figure 5.22: Closed-aperture Z-scan trace of the Ag NPs for input fluence of 399 MW/cm^2.

5.7 Z-scan studies on metal-semiconductor nano fluid

The complementary optical properties of metal and semiconductor NPs make them attractive components for many applications that require controlled flow of electromagnetic energy on nanometer regime. Interactions between quantum confined electronic states in semiconductor nano structures and dielectric confined electromagnetic modes in the metal are the main effects obtained when such exciton-plasmon interactions occurs. This can be attributed to increase in optical nonlinearities,control of nanoscale energy-transfer process etc. This phenomenan also amplifies optical nonlinearities and leads to an enhanced optical Stark effect ie,a change of energy levels in the presence of an optical light field which can induce a spin splitting of electrons that then allows spin manipulation in the CdSe component of the hybrid nanostructures[49]. Hence these metal-semiconductor NPs are attractive for quantum information applications that require spin manipulation as one of the key processes.

5.7.1 Open and closed aperture Z-scan study on Au-CdSe nanofluids

Microwave rapid heating is used for the synthesis of metal NPs and CdSe QDs described earlier. After being cooled down to room temperature, products were collected for size characterizations. All the above samples remained transparent without precipitation for three to ten months. For the preparation of hybrid CdSe-metal nanofluids, colloidal Au NPs mixed to the colloidal CdSe QDs in the volume ratio 1:1. Samples named as S_1 and S_2 where S_1 is the bare CdSe nanofluid and S_2 is the Au NPs induced CdSe nanofluid respectively. Absorption spectra of the prepared NPs is recorded in figure 5.23. The nonlinear optical properties of CdSe QDs and CdSe-Au nanocomposites are investigated using Z-scan technique at 532 nm employing Nd-YAG laser pulses with input fluence of 0.435 GW/cm^2 and is shown in figure 5.24. The effective two-photon absorption cross section of CdSe-Au nanostructures is enhanced and can be attributed to charge transfer between CdSe and Au NPs. We observed that the optical nonlinear absorption coefficient (β) varies from 0.432 $\times$ 10^{-10} m/W to 2.53 $\times$ 10^{-10} m/W and the nonlinear refractive index n_2 varies from $0.795\times10^{-10}(e.s.u)$ to 0.832

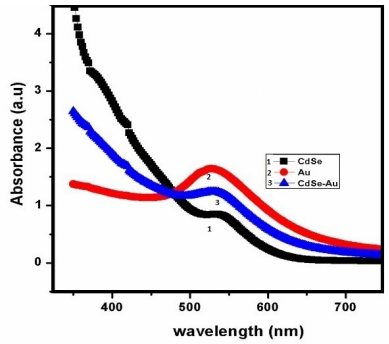

Figure 5.23: Absorption spectra of CdSe, Au and CdSe-Au NPs

$\times 10^{-10}$(e.s.u). Also,Optical limiting properties of the samples are im-

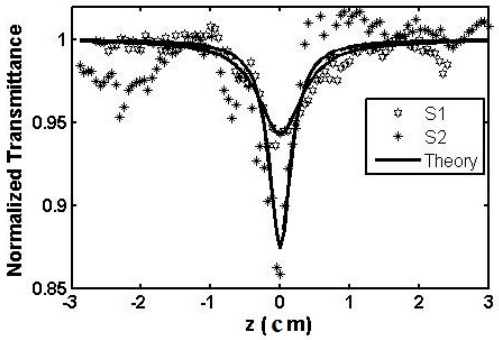

Figure 5.24: Open aperture Z-scan trace of the CdSe QDs and CdSe-Au nanofluid for input fluence of 0.43 GW/cm^2.

proved from 0.35 GW/cm^2 to 0.17 GW/cm^2 by inducing metal NPs as shown in figure 5.25. Closed-aperture Z-scan trace of the CdSe - Au nanofluid for input fluence of $436MW/cm^2$ is shown in figure 5.26. Figure shows that the peak-valley of the closed-aperture Z-scan satisfied the condition Δz=1.7 z_0, thus confirming the presence of cubic nonlinearity. The value of ΔT_{p-v} i.e., the difference between the peak and valley transmittance, could be obtained by the best theoretical fit from the results and $\Delta\phi_0$can be obtained as 0.76.

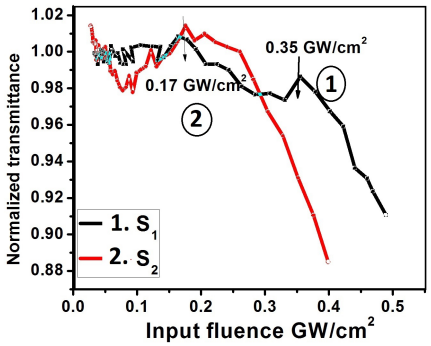

Figure 5.25: Optical limiting property of the samples $S_1$and S_2.

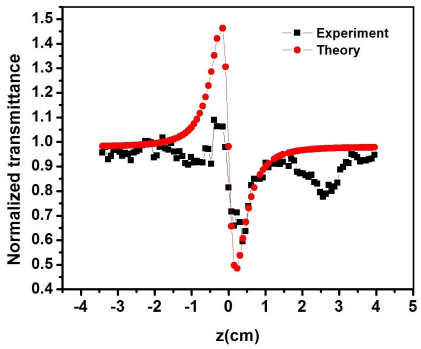

Figure 5.26: Closed-aperture Z-scan trace of the CdSe - Au nanofluid for input fluence of 436 MWcm^2.

5.7.2 Open and closed aperture Z-scan studies on Ag-CdSe nanofluids

Microwave rapid heating is used for the synthesis of metal NPs and CdSe QDs as described earlier. Absorption spectra of the prepared NPs and that of colloidal CdSe-Ag NPs in the volume ratio 1:1 is recorded. UV-Visible absorption spectra of prepared nanofluids of CdSe and CdSe-Ag are shown below in figure 5.27. The absorption peak of the samples confirms the formation of the particles. We observed a charge transfer from CdSe QDs to Ag nanofluids from this absorption spectra and we expected this system consisting of mono dispersed NPs to enhance the local field. It has been shown that nanofluids consisting of mono dis-

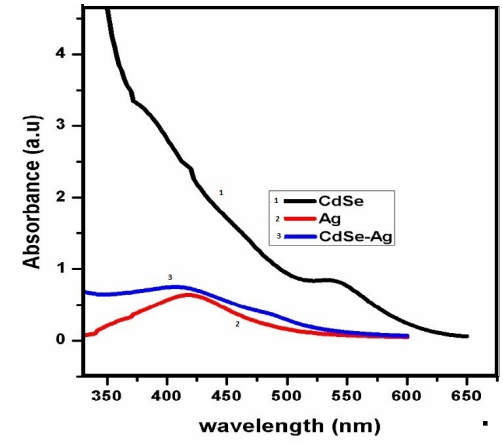

Figure 5.27: UV-Visible absorption spectra of prepared nanofluids .

persed metal NPs have a sharp SPR peak around 410 nm [50] created in part by the strong and coherent local field around the nanostructures. Hence, it is expected that mono dispersed NPs will boost the NLO response of the metal NPs [51]. The nonlinear optical properties of CdSe QDs and Ag-CdSe nanocomposites are investigated using Z-scan technique at 532 nm employing Nd-YAG laser pulses with input fluence of 0.435 GW/cm^2 as shown in figure 5.28. The higher NLO response ob-

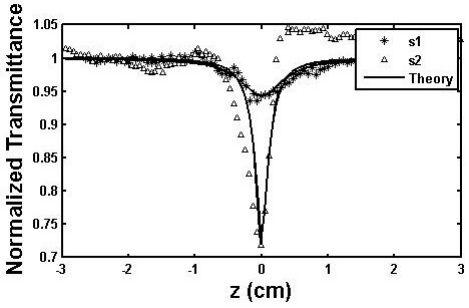

Figure 5.28: Open aperture Z-scan trace of the CdSe QDs and CdSe-Ag nanofluid for input fluence of 0.43 GW/cm^2.

served from the metal induced nanofluids is explained in terms of an electric field enhancement near the SPR.The effective two-photon ab-

sorption cross section of CdSe-Ag nanostructures is enhanced and can be attributed to charge transfer between CdSe and Ag NPs. We observed that the optical nonlinear absorption coefficient (β) varies from 0.432 $\times$ 10^{-10} m/W to 2.53 $\times$ 10^{-10} m/W and the optical limiting property of the samples(figure 5.29) are also improved with this nanofluid from 0.42 GW/cm^2 to 0.30 GW/cm^2.Closed-aperture Z-scan trace of the CdSe-Ag nanofluid for input fluence of 436 MW/cm^2 is shown in figure 5.30.

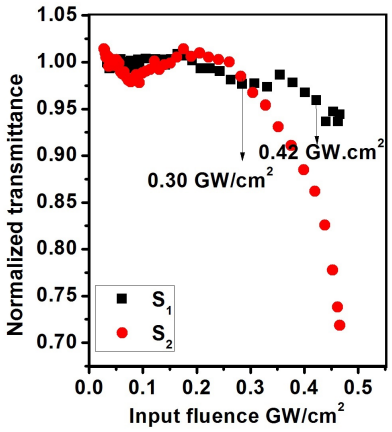

Figure 5.29: Optical limiting property of the samples $S_1$and S_2

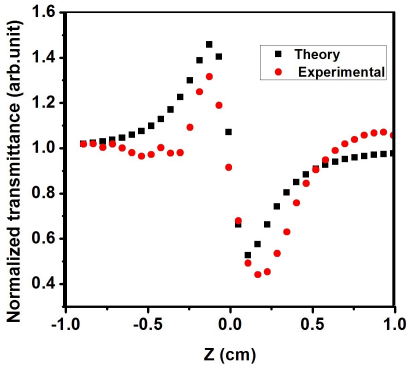

Figure 5.30: Closed-aperture Z-scan trace of the CdSe - Ag nanofluid for input fluence of 436 MW/cm^2

From the closed aperture Z-scan fit, $\Delta\phi_0$can be obtained as 2.049 and it is observed that the peak- valley of the closed-aperture z-scan confirms the presence of cubic nonlinearity and the nonlinear refractive index n_2 varies from 0.795×10^{-10}(e.s.u) to 2.24×10^{-10} (e.s.u)as the sample changes from S_1 to S_2.

5.8 Conclusion

- Third-order optical nonlinear absorption in CdSe QDs synthesized by microwave rapid heating with particle sizes in the range 4.16-5.25 nm has been evaluated by the Z-scan technique.
- At an excitation irradiance of 0.54 GW/cm^2, CdSe QDs exhibit reverse saturation indicating a clear nonlinear behavior and this nonlinearity increases with particle size in CdSe QDs within the range of our investigations.
- The nonlinear absorption in the nano colloidal solution can be attributed to the phenomenon of two photon absorption. The measured β values were found to enhance with decrease in optical energy gap.
- Our works show that the semiconductor nanomaterial which has got a one photon resonant absorption can be employed as a third order optical nonlinear material in which two photon absorption will get enhanced by the one photon resonance energy level.
- The optical limiting threshold of the QDs varies from 0.35 GW/cm^2 to 0.57 GW/cm^2 which makes CdSe QDs a promising candidate for reverse-saturable absorption based devices at high laser intensities such as optical limiters.
- Third order optical nonlinear absorption in CdSe QDs capped with mercaptosuccinic acid with variable pH has been evaluated by the Z- scan method
- Results exhibits an optimal pH value with lowest nonlinearity and the highest fluorescence emission for CdSe nanofluids.

- Observation of change in negative to a positive value of the nonlinear refractive index n_2 indicates the molecular representational Kerr effect which becomes the dominant mechanism for nonlinear refraction in optimized sample .
- The optical limiting threshold of the samples shows the possibility of tuning of nonlinear behavior by changing the pH value of medium.
- The closed-aperture curve of CdSe nano fluid displayed a peak to valley shape, indicating a negative value of the nonlinear refractive index n_2 and it is the self-defocusing nonlinearity
- RSA at longitudinal SPR in gold (Au) and silver(Ag) NPs have been observed using Z-scan and transient absorption techniques with 532nm laser pulses.
- The nonlinear absorption and the RSA behavior in metal NPs were usually believed to be due to free carrier absorption or excited state absorption.
- Our observations show that metal induced CdSe nanofluids exhibit enhanced nonlinearity and optical limiting properties which can be attributed to the charge transfer mechanism from colloidal CdSe QDs to metal NP and the enhancement of the electromagnetic field in the presence of semiconductor QDs.
- Closed-aperture z-scan trace of the CdSe metal nanofluid for input fluence of 0.436 GW/cm^2 is fitted with the theoretical Z-scan curve and it follows that the peak to valley shape, indicating a negative value of the nonlinear refractive index n_2 and confirming the presence of cubic nonlinearity.

5.9 References

[1] H. Fan, X. Wang, Q. Ren, X. Zhao, G. Zhang, J. Chen, D. Xu, G. Yu and Z. Sun, "Investigation of the nonlinear absorption and optical limiting properties of two [Q] 2 [Cu (C 3 S 5) 2] compounds," Optics & Laser Technology, vol. 42, pp. 732-736, 2010.

[2] I. Gerdova and A. Hach, "Third-order non-linear spectroscopy of CdSe and CdSe/ZnS core shell quantum dots," Opt. Commun., vol. 246, pp. 205-212, 2005.

[3] D. Maikhuri, S. Purohit and K. Mathur, "Linear and nonlinear intraband optical properties of ZnO quantum dots embedded in SiO_2 matrix," AIP Advances, vol. 2, pp. 012160, 2012.

[4] N. Venkatram, R. S. S. Kumar and D. N. Rao, "Nonlinear absorption and scattering properties of cadmium sulphide nanocrystals with its application as a potential optical limiter," J. Appl. Phys., vol. 100, pp. 074309, 2006.

[5] R. W. Meulenberg, J. R. Lee, A. Wolcott, J. Z. Zhang, L. J. Terminello and T. Van Buuren, "Determination of the exciton binding energy in CdSe quantum dots," ACS Nano, vol. 3, pp. 325-330, 2009.

[6] A. Patra, N. Venkatram, D. N. Rao and T. Radhakrishnan,"Optical limiting in organic molecular nano/microcrystals: nonlinear optical effects dependent on size distribution," The Journal of Physical Chemistry C, vol. 112, pp. 16269-16274, 2008.

[7] W. Sun, C. M. Lawson, G. M. Gray, C. Zhan and D. Wang,"Degenerate four-wave mixing and Z-scan measurements of stilbazolium derivatives," Appl. Phys. Lett., vol. 78, pp. 1817-1819, 2001.

[8] S. Mathew, A. D. Saran, S. A. Joseph, B. S. Bhardwaj, D. Punj, P. Radhakrishnan, V. Nampoori, C. Vallabhan and J. R. Bellare, "Nonlinear optical characterization and measurement of optical limiting threshold of CdSe quantum dots prepared by a microemulsion technique," J. Mater. Sci. : Mater. Electron., vol. 23, pp. 739-745, 2012.

[9] A. Thankappan, S. Thomas and V. Nampoori, "Effect of betanin natural dye extracted from red beet root on the nonlinear optical properties ZnO nanoplates embedded in polymeric matrices," J. Appl. Phys., vol. 112, pp. 123104, 2012.

[10] I. Sebastian, S. Divya, V. Nampoori, P. Radhakrishnan and S. Thomas, "Impact of intermediate localized states on nonlinear optical absorption of Ga-Ge-Se nanocolloidal solutions," Appl. Phys. Lett., vol. 102, pp. 031115, 2013.

[11] M. Sheik-Bahae, A. A. Said, T. Wei, D. J. Hagan and E. W. Van Stryland,"Sensitive measurement of optical nonlinearities using a single beam," Quantum Electronics, IEEE Journal Of, vol. 26, pp. 760-769, 1990.

[12] F. Qureshi, S. Martin, X. Long, D. Bradley, F. Henari, W. Blau, E. Smith, C. Wang, A. Kar and H. Anderson, "Optical limiting properties

of a zinc porphyrin polymer and its dimer and monomer model compounds," Chem. Phys., vol. 231, pp. 87-94, 1998.

[13] L. Brus,"Zero-dimensional excitons in semiconductor clusters," Quantum Electronics, IEEE Journal Of, vol. 22, pp. 1909-1914, 1986.

[14] Anju K. Augustine, S.Mathew, P. Radhakrishnan, V. P. N. Nampoori, and M. Kailasnath, "Size Dependent Optical Nonlinearity and Optical Limiting Properties of Water Soluble CdSe Quantum Dots" ,Journal of Nanoscience, vol.2014, pp.1-7,2014.

[15] C. Pradeep, S. Mathew, B. Nithyaja, P. Radhakrishnan, V.P.N. Nampoori, "Studies of nonlinear optical properties of PicoGreen dye using Z-scan technique," Appl Phys A,vol.115, pp. 291-295,2014.

[16] M. Gogoi, P. Deb and A. Kostka, "Differential tunability effect on the optical properties of doped and undoped quantum dots," Physica Status Solidi (a), vol. 209, pp. 1543-1551, 2012.

[17] W. Zhang, X. Qiao and J. Chen, "Formation of silver nanoparticles in SDS inverse microemulsions," Mater. Chem. Phys., vol. 109, pp. 411-416, 2008.

[18] M. Chu, Y. Sun and S. Xu,"Silica-coated quantum dots fluorescent spheres synthesized using a quaternary water-in-oilmicroemulsion system," Journal of Nanoparticle Research, vol. 10, pp. 613-624, 2008.

[19] C. Y. Tai and C. Chen, "Particle morphology, habit, and size control of $CaCO_3$ using reverse microemulsion technique," Chemical Engineering Science, vol. 63, pp. 3632-3642, 2008.

[20] S. Divya, V. Nampoori, P. Radhakrishnan and A. Mujeeb,"Origin of optical non-linear response in TiN owing to excitation dynamics of surface plasmon resonance electronic oscillations," Laser Physics Letters, vol. 11, pp. 085401, 2014.

[21] Aparna Thankappan, Sheenu Thomas and V.P.N. Nampoori, "Solvent effect on the third order optical nonlinearity and optical limiting ability of betanin natural dye extracted from red beet root" ,Optical Materials vol.35, pp.23322337, 2013.

[22] K. Tanaka, "Optical nonlinearity in photonic glasses," J. Mater. Sci. : Mater. Electron., vol. 16, pp. 633-643, 2005.

[23] F. Liu, Y. Chang, F. Ko and T. Chu, "Microwave rapid heating for the synthesis of gold nanorods," Mater Lett, vol. 58, pp. 373-377, 2004.

[24] R. Ashayer, M. Green and S. H. Mannan,"Synthesis of palladium nanoshell using a layer-by-layer technique," Journal of Nanoparticle Research, vol. 12, pp. 1489-1494, 2010.

[25] F. Liu, C. Ker, Y. Chang, F. Ko, T. Chu and B. Dai, "Microwave heating for the preparation of nanometer gold particles," Japanese Journal of Applied Physics, vol. 42, pp. 4152, 2003.

[26] W. K. Leutwyler, S. L. Brgi and H. Burgl,"Semiconductor clusters, nanocrystals, and quantum dots," Science, vol. 271, pp. 933-937, 1996.

[27] T. Teranishi, I. Kiyokawa and M. Miyake, "Synthesis of monodisperse gold nanoparticles using linear polymers as protective agents," Adv Mater, vol. 10, pp. 596-599, 1998.

[28] Y. Zhou, H. Itoh, T. Uemura, K. Naka and Y. Chujo,"Synthesis of novel stable nanometer-sized metal (M= Pd, Au, Pt) colloids protected by a -conjugated polymer," Langmuir, vol. 18, pp. 277-283, 2002.

[29] K. C.Grabar, R. G. Freeman,M. B. Hommer and M. J. Natan,"Preparation and characterization of Au colloid monolayers," Anal. Chem., vol. 67, pp. 735-743, 1995.

[30] R. Al-Gaashani, S. Radiman, N. Tabet and A. R. Daud, "Effect of microwave power on the morphology and optical property of zinc oxide nano-structures prepared via a microwave-assisted aqueous solution method," Mater. Chem. Phys., vol. 125, pp. 846-852, 2011.

[31] I. Bilecka and M. Niederberger,"Microwave chemistry for inorganic nanomaterials synthesis," Nanoscale, vol. 2, pp. 1358-1374, 2010.

[32] K. Rao, B. Vaidhyanathan, M. Ganguli and P. Ramakrishnan,"Synthesis of inorganic solids using microwaves," Chemistry of Materials, vol. 11, pp. 882-895, 1999.

[33] M. Chu, X. Shen and G. Liu, "Microwave irradiation method for the synthesis of water-soluble CdSe nanoparticles with narrow photoluminescent emission in aqueous solution," Nanotechnology, vol. 17, pp. 444, 2006.

[34] C. Louis, R. Bazzi, C. A. Marquette, J. Bridot, S. Roux, G. Ledoux, B. Mercier, L. Blum, P. Perriat and O. Tillement, "Nanosized hybrid particles with double luminescence for biological labeling," Chemistry of Materials, vol. 17, pp. 1673-1682, 2005.

[35] Anju K. Augustine, V.P.N. Nampoori, M. Kailasnath,"Rapid synthesize of gold nanoparticles by microwave irradiationmethod and its application as an optical limiting material," Optik,vol.125, pp. 6696-6699,2014.

[36] I. Gerdova and A. Hach, "Third-order non-linear spectroscopy of CdSe and CdSe/ZnS core shell quantum dots," Opt. Commun., vol. 246, pp. 205-212, 2005.

[37] L. De Boni, E. L. Wood, C. Toro and F. E. Hernandez, "Optical saturable absorption in gold nanoparticles," Plasmonics, vol. 3, pp. 171-176, 2008.

[38] M. A. K. Abdelhalim, M. M. Mady, M. M. Ghannam, M. S. Al-Ayed and A. Alhomida, "The effects of gold nanoparticles size and concentration on viscosity, flow activation energy, dielectric and optical properties," African Journal of Biotechnology, vol. 10, pp. 13121-13127, 2013.

[39] S. Mathew, A. D. Saran, B. S. Bhardwaj, S. A. Joseph, P. Radhakrishnan, V. Nampoori, C. Vallabhan and J. R. Bellare, "Size dependent optical properties of the CdSe-CdS core-shell quantum dots in the strong confinement regime," J. Appl. Phys., vol. 111, pp. 074312, 2012.

[40] H. H. Mai, V. E. Kaydashev, V. K. Tikhomirov, E. Janssens, M. V. Shestakov, M. Meledina, S. Turner, G. Van Tendeloo, V. V. Moshchalkov and P. Lievens, "Nonlinear Optical Properties of Ag Nanoclusters and Nanoparticles Dispersed in a Glass Host," The Journal of Physical Chemistry C, vol. 118, pp. 15995-16002, 2014.

[41] G. Banfi, V. Degiorgio and D. Ricard,"Nonlinear optical properties of semiconductor nanocrystals," Adv. Phys., vol. 47, pp. 447-510, 1998.

[42] R. Philip, P. Chantharasupawong, H. Qian, R. Jin and J. Thomas, "Evolution of nonlinear optical properties: from gold atomic clusters to plasmonic nanocrystals," Nano Letters, vol. 12, pp. 4661-4667, 2012.

[43] S. H. Yau, O. Varnavski and T. Goodson III, "An ultrafast look at Au nanoclusters," Acc. Chem. Res., vol. 46, pp. 1506-1516, 2013.

[44] K. Baishya, J. C. Idrobo, S. gt, M. Yang, K. Jackson and J. Jellinek, "Optical absorption spectra of intermediate-size silver clusters from first principles," Physical Review B, vol. 78, pp. 075439, 2008.

[45] S. Fedrigo, W. Harbich and J. Buttet,"Collective dipole oscillations in small silver clusters embedded in rare-gas matrices," Physical Review B, vol. 47, pp. 10706, 1993.

[46] S. Kazemzadeh, A. Hassanjani-Roshan, M. Vaezi and A. Shokuhfar, "The effect of microwave irradiation time on appearance properties of silver nanoparticles," Transactions of the Indian Institute of Metals, vol. 64, pp. 261-264, 2011.

[47] M. Hari, S. Mathew, B. Nithyaja, S. A. Joseph, V. Nampoori and P. Radhakrishnan, "Saturable and reverse saturable absorption in aqueous silver nanoparticles at off-resonant wavelength," Opt. Quant. Electron., vol. 43, pp. 49-58, 2012.

[48] Ratyakshi and R. Chauhan,"Colloidal synthesis of silver nanoparticles," Asian Journal of Chemistry, vol. 21, pp. 113-116, 2009.

[49] M. Achermann, "Exciton- plasmon interactions in metal- semiconductor nanostructures," The Journal of Physical Chemistry Letters, vol. 1, pp. 2837-2843, 2010.

[50] A. Suslov, P. Lama and R. Dorsinville, "Fabrication of monodispersed silver nanoparticles and their collective sharp plasmonic response," Plasmonics, vol. 9, pp. 493-497, 2014.

[51] P. Lama, A. Suslov, A. D. Walser and R. Dorsinville,"Plasmon assisted enhanced nonlinear refraction of monodispersed silver nanoparticles and their tunability," Optics Express, vol. 22, pp. 14014-14021, 2014.

Chapter 6

Applications of CdSe quantum dots based photonic materials in the fabrication of solar cells and Random lasers.

This chapter includes the applications of CdSe quantum dots as the potential photonic material in the fabrication of solar cells and random lasers.The effects of annealing and incorporation of metal nanoparticles on the efficiency of CdSe QDs based solar cells have been studied.

Results of this chapter are published in :

1. *Anju. K. Augustine et.al.,Laser Phys. Lett.,vol.12, 025006,(4pp),2015.*

6.1 Introduction

The size-dependent optical and electrical properties of semiconductor quantum dots have been widely studied in recent years [1]. Colloidal QDs are of much interest in the field of photonics as they are inexpensive, easy to synthesize, manipulate and incorporate into device structures etc. In addition to the scientific interests, tunable emission and band gap properties of CdSe QDs open a variety of potential applications in the field of photonics [2-4]. These materials can be useful in photonic devices such as emitters for color displays, light emitting diodes, optical fiber amplifiers, low threshold lasers, photovoltaic (PV) devices, optical sensors and probes, high speed signal processing filters, random lasers etc. This is also an interesting material in the field of bio medical imaging. All these applications prefer photoluminescence emission peaks that are narrow and bright [5-8]. In this chapter we have studied two main interesting applications of CdSe based systems viz. QDSSCs and random lasers using the properties of CdSe QDs based materials.

Energy crisis is one of the important issues in this new era, which leads to the utilization of abundant solar energy employing several technologies. New types of energy storage materials with the desired electrical and optical properties are the greatest challenge in the PV field. Nowadays different PV systems are available. However the efficiency and the costs are the two main factors which prevent these systems being available to the public. Presently solar panels are used in combining with a storage unit to provide effective energy storage for the "offline" use but the expense of the combined system is too high. Now researchers are developing methods to overcome these drawbacks and capable of simultaneous photo energy generation and storage; by which both cost and size can be reduced.

Silicon Solar cell is a semiconducting device that converts light to electricity. It belongs to first generation PV cells which account for $\sim$ 80%-90 % of solar cell market [9, 10]. These solar cells are leading in market due to their high efficiency and stability, but their manufacturing cost is very high. Silicon solar cell is basically a p-n junction diode; sun light generates an electron-hole pairs on both sides of the junction. The generated holes and electrons diffuse to the junction and are swept away by

the electric field, thus producing an electric current through the device. Second generation cells, also called thin-film solar cells, are significantly cheaper to produce than first generation cells but have lower efficiencies. The great advantage of second generation thin-film solar cells, along with low cost is their flexibility. Third generation solar cells are the cutting edge of solar technology. New third generation PV systems including dye-sensitized solar cell (DSSCs), organic solar cells and multifunction solar cells are introduced as the advanced PV devices in this era[11-14]. Among the different types of third generation solar cells, DSSCs can reach light-to-electric conversion efficiencies of up to 11% but this type of cells are still not feasible for practical applications. This necessitates to select appropriate materials which are not only cost-effective but also quite lasting for practical purposes.

Another application in this photonic era is random lasers which have received great attention due to their low cost and easy fabrication without the need for extra cavities. There are many challenges to obtain random lasing as high optical gain and strong scattering have to be achieved simultaneously. In random lasers light generation and subsequent stimulated emission take place within a multiple-scattering medium with optical gain. In this system of random lasers, QDs can act as coherent light sources for amplified laser emission above a particular light threshold. For the amplification of the emitted light we do not use any of the conventional optical resonators employed in a laser system[15-19]. In this era, random laser phenomena have been studied in many systems including organic and inorganic QDs, such as rhodamine 640 with TiO_2 particles [20], ZnO powder in Polystyrine and PMMA film etc. [21-23]. Due to its direct band gap,good absorption abilities and excellent photo sensitivity, CdSe QD is recognized as a promising material in this field .

6.2 Solar cell studies on CdSe QD based materials

Important advantages of inorganic semiconductors over conventional dyes are connected with their optical and electrical properties. The band gap of semiconductor QDs can be tuned by size to match the solar spectrum. Their large intrinsic dipole moments can lead to rapid

charge separation and a large extinction coefficient, which is known to reduce the dark current and increase the overall efficiency. In addition, semiconductor QD sensitizers provide new chances to utilize hot electrons or generate multiple charge carriers with a single photon. Hence, the nano sized, tuned band gap semiconductor materials have proved to be the ideal sensitizers for high PV performance. Some of the materials exhibiting these properties are CdS, CdSe, CdTe, PbS, PbSe and they have been studied by various groups for photo catalyst and solar cell applications [14, 24, 25]. CdS and CdSe have shown much promise and impressive qualities among these sensitizers due to their appropriate band gap of about 2.7eV and 1.70 eV respectively, which show strong absorption of the solar spectrum. The use of these QDs, which may produce more than one electron-hole pair per single absorbed photon (also known as multiple exciton generation (MEG)), is a promising solution to enhance power conversion efficiency. Furthermore, the creation of anode by growing CdS/CdSe QDs on TiO_2 surface greatly enhances charge separation properties too. To date, CdSe-TiO_2 - or CdS/CdSe-TiO_2 nanostructured solar cells have been reported by several groups [26, 27]. In this section we have discussed the study on enhancing solar cell efficiency by applying different methods.

6.2.1 Thermo-optic studies on CdSe based QDSSc

Charge transport rate in the sensitizer and at the TiO_2/sensitizer interface has an important role in the performance in energy conversion of a semiconductor-sensitized photo electrode. Any structural defect in the sensitizer layer, as well as mismatch between structures of TiO_2 and sensitizer, can trigger barriers to the charge transport. A well-known method to perform structural reorganization in bulk materials is the heat annealing and is able to eliminate structural defects present in an as prepared material. Appropriate heat annealing was also shown to be effective in enhancing the performance of thin film solar cells. In this study a heat treatment method is used to differentiate the efficiencies of QDSSCs. The composite form of the CdS /CdSe semiconductor sensitizers assembled on mesoporous TiO_2 films for extending the light harvest region. Furthermore, heat annealing was utilized to eliminate structural defects present in an as-prepared material and to enhance the performance of semiconductor-sensitized TiO_2 photoelectrodes for

photovoltaic performance.This strategy was shown to be effective not only for CdS and CdSe-sensitized electrodes, but also for CdS/CdSe co-sensitized electrode. [28, 29]

Experimental methods

In this work, TiO_2 /CdS/CdSe films are prepared as the anode and Platinum was used as the counter electrode for solar cell fabrication. Both anode and cathode are coated on the conductive side of an ITO glass (Aldrich, 812 /sq). Pure TiO_2 of$\sim$ 18nm size with anatase phase was prepared by surfactant (P_{123}) assisted hydrothermal technique using weak acidic medium followed by calcination at 500°C. CdS nanoparticle of $\sim$28 nm has been prepared by using cadmium acetate ($CdAc_2$) and thiourea with triethanolamine as the capping agent. CdSe QDs with particle size $\sim$10nm are prepared by aqueous microwave irradiation method. Platinum in ethanol was used as the counter electrode prepared from $H_2PtCl_6.6H_2O$ and I_2 solution acts as the electrolyte. TiO_2 powder mixed with ethanol and Mercapto propanoic acid (MPA) is coated on the conductive side of ITO by drop casting method. Above this ,a layer of CdS/CdSe nanoparticle is coated where MPA acts as the linking molecule between semiconductor chalcogenide nanoparticles(CdS/CdSe) and TiO_2. The annealing temperature is controlled and the anode is prepared at different temperatures. In all the cases TiO_2 paste is annealed at 150°C and CdS QDs at 25°C, while the CdSe QDs are coated on the latter with 50°C, 65°C, 75°C and 100°C and named as S_1, S_2, S_3 and S_4 respectively. A colour change from (yellow-orange red-brown) has been obtained with increasing temperature. The ITO coated counter electrode(platinum) was placed on the top so that the conductive side of the counter electrode faced the QDS adsorbed TiO_2 film. Electrolyte placed at the edges was drawn into the space between the electrodes by capillary action. Binder clips were used to hold the electrodes together. UV-visible absorption measurements were carried out using a Jasco spectrophotometer. Current-voltage (J-V) characteristics of the cells were examined where a standard solar irradiation of 1000W Xe arc lamp (Oriel 6269) is used as the light source. Incident monochromatic photo-to-current conversion efficiency (IPCE) measurements were carried out using small band-pass filters to create monochromatic light. Input intensity was measured using light meter (METRAVI 1332). In

all the cases, input intensity was in the range of 1-10 k lux [23, 30].

Results and discussions

UV-vis absorption spectra of CdS and CdSe QDs are shown in figure 6.1.

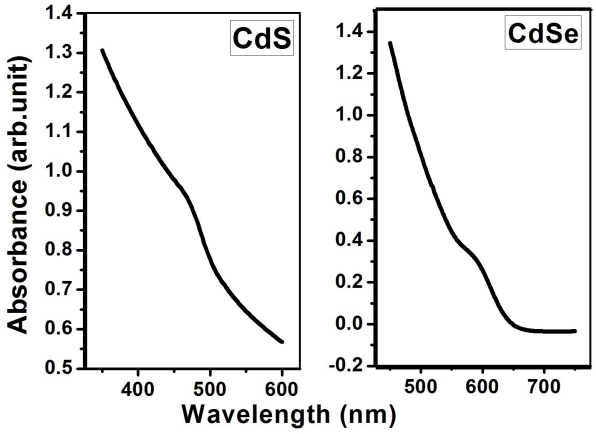

Figure 6.1: UV-vis absorption spectra of CdS and CdSe QDs.

The ability to harvest a portion of the visible region of the suns spectrum and their good charge separation properties for better QDSSC conversion efficiencies make CdS and CdSe QDs to be chosen as the sensitizer materials in this study. In this double layered QDSSC the layer order TiO_2/ CdS/ CdSe is arranged such that the electrons will be injected to theTiO_2 by the appropriate band edge alignments, while only a part of the electrons were transferred to the TiO_2 when the layer order was opposite[31]. Also the bi-functional molecular linker MPA enables the mesoporous TiO_2 layer to adhere with the QDs. Images of the NPs in figure 6.2 shows the shape of the particles and information about the high interior crystal quality of the NPs which is conducive to reduce the recombination of the excited electron-hole pairs and increase the photocurrent of the solar cells. UV-vis absorption spectra of the TiO_2/CdS /CdSe electrodes by heat annealing at various temperatures is shown in figure 6.3. Thermal annealing triggers a slight redshift of the absorption spectrum and this effect is more significant at a higher

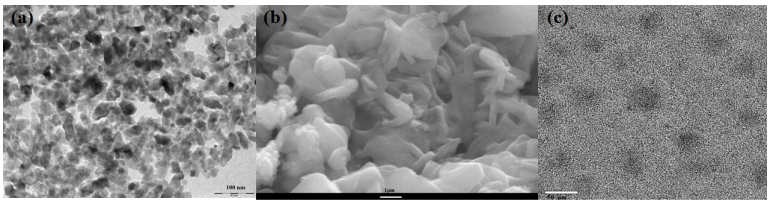

Figure 6.2: (a) TEM image ofTiO_2 NPs, (b) SEM of CdS NPs and (c) TEM image of CdSe QDs.

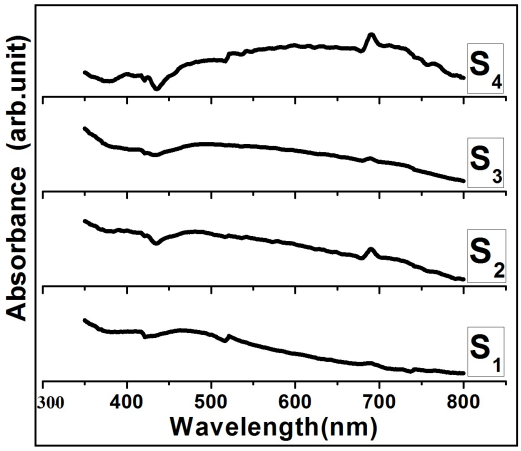

Figure 6.3: UV-vis absorption spectra of the electrodes($S_1, S_2, S_3 and S_4$)

annealing temperature. From the figure 6.3, it is clear that a higher thermal annealing temperature triggers larger particle sizes of CdS /CdSe nanocomposites, and therefore results in a smaller band gap. The obtained colour changes (yellow-orange red) with increase in annealing can be due to partial decomposition and phase transformation of nanocomposites at higher treatment temperatures. The possible decomposition of CdS/CdSe may lead to the formation of a vacancy, which can also contribute to the smaller band gap at high annealing temperature. The performance of a QDSSC is assessed by determining the parameters such as the short-circuit current density (J_{sc}), the open-circuit voltage (V_{oc}), the fill factor (FF), and the overall power conversion efficiency (η). The efficiency of a solar cell is defined as the ratio of maximum electrical power extracted to, the incident radiation power illuminating the solar

cell surface.

$$\eta = \frac{P_{max}}{P_{min}} = \frac{J_{sc}V_{oc}FF}{P_{in}} \tag{6.1}$$

The internal photo conversion efficiency(IPCE) parameter of a QDSSC is defined as the ratio of the number of electrons generated by light in the external circuit to, the number of incident photons, which can be expressed as

$$IPCE\% = \frac{1240I_{sc}}{P_{in}\lambda} \tag{6.2}$$

where P_{in} is the incident power and λ is the incident wavelength. J-V

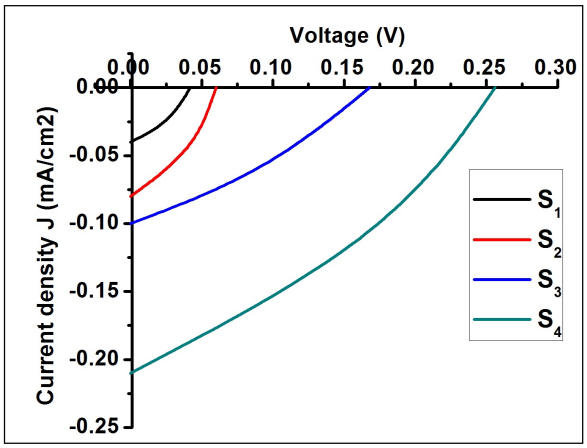

Figure 6.4: J-V characteristics of the QDSSCs (TiO_2/CdS /CdSe) at various annealing temperatures.

characteristics of the QDSSCs (TiO_2/CdS /CdSe-anode) at various annealing temperatures is shown in figure 6.4. An open - circuit voltage (V_{oc}) of 0.042 and a short circuit current 0.04 and an overall efficiency of 0.069 % is observed for the S_1 sample. As the annealing temperature is increased the $V_{(oc)}$ is improved to 0.06V and the short circuit current density increased to 0.08 mA/cm^2. An overall efficiency of 2.1% was observed for S_4, indicating an increase of efficiency by elevating the temperature of the electrode. The performance of the QDSSCs at different annealing temperatures is shown in Table 6.1.

The IPCE characteristics of the sample S_4 which shows maximum photo conversion efficiency $\sim 54\%$ is shown in figure 6.5.

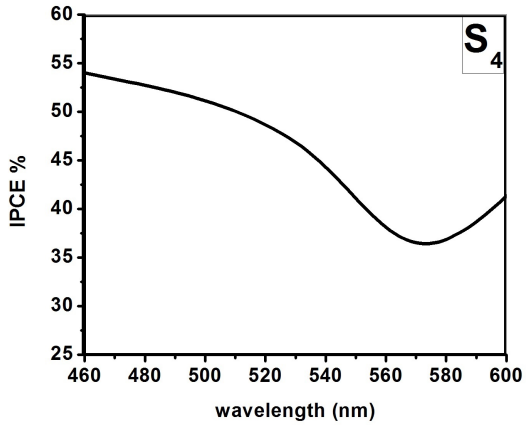

Figure 6.5: IPCE characteristics of the sample S_4 which shows maximum efficiency.

We can assume that, this enhanced power conversion efficiency is due to these CdS/CdSe QDs, which may produce more than one electron-hole pair per single absorbed photon. This significant improvement of the PV performance obtained for QDSSC based on annealed TiO_2/ CdS /CdSe nanostructure can be ascribed to the following reasons. The absorption spectra in figure 6.3 which confirms that as the annealing temperature is increased the absorption cross section gets increased and the current -voltage performance shows improvement. This is due to the changes happening in the crystal structure of NP due to the annealing process which helps to improve the better photo conversion efficiency as shown

Sample	J_{sc} (mA/cm^2)	V_{oc} (V)	FF	$\eta\%$
S_1	0.04	0.042	0.34	0.069
S_2	0.08	0.06	0.36	0.2
S_3	0.10	0.168	0.29	0.6
S_4	0.21	0.256	0.32	2.1

Table 6.1: The performance of the QDSSCs at different annealing temperatures

in the sample S_4.

The annealing treatment will decrease the internal defects, which can reduce the recombination of photo excited carriers and thereby result in a higher power conversion efficiency. Another benefit of annealing at high temperature is a good contact between the sensitizer QDs and theTiO_2 nano rod [30]. The two-step annealing process, which is more effective to decrease the counter-diffusion effect in the PV performance is done here. The improved performance is attributed to the high crystallization state of the semiconductor sensitizers as well as a better connection at the sensitizer/sensitizer interface. Such a superior interface between TiO_2 and QDs can inhibit the interfacial recombination of the injected electrons from TiO_2 to the electrolyte, which is also responsible for its higher efficiency [28].

6.2.2 Enhanced conversion efficiency of metal NP doped-CdSe QDSSCs.

In particular, QDSSCs are of great interest because of their excellent performance, low-cost, photo stability, high molar extinction coefficients and size-dependent optical properties. Inspite of the progress in research and development of QDSSCs, their efficiency level is still lower than that of the dye-sensitized solar cells (DSSCs). This is mainly a result of the high electron loss between electrolyte and electrodes (photo electrode and counter electrode) and the relatively narrow absorption spectra of most of the efficient QDs. Thus, to increase the conversion efficiency, much effort has been concentrated to develop properties of QDs referring to electron transport rate, light harvesting ability, the catalytic ability of counter electrode and decrease of charge recombination. QDSSCs have also shown potential in further improving the performance of the most efficient multi-junction solar cell devices due to the flexibility in band gap tuning. This enables better current-matching and hence the improved output current of the entire device, leading to higher efficiencies [30, 32-36].

One of the other aspect for improving efficiency of such solar cells are to incorporate with metal NPs. In recent decades there has been a great deal of work related to such particles with reference to their funda-

mental properties and applications of plasmonic resonances, especially in integrated optics and biosensing. Novel works have been done in the area of plasmonic solar cell devices where an enhancement in the photocurrent could be achieved using silver NPs on the surface of the material device[37-40]. In particular, works related to plasmonic solar cells showed enhanced photoluminescence, due to plasmon-enhanced absorption of the QDs. It is also possible to enhance the long wavelength photon absorption of the QDSSCs by employing light trapping phenomena [41]. This plasmonic light can be achieved by depositing metal NPs on the solar cell surface[23, 42-44]. In this part of the thesis we study the enhanced performance of CdSe QD based solar cells, modified with metal NPs.

Experimental methods

In this work TiO_2 /CdSe/metal films are prepared as the anode and platinum was used as the counter electrode for solar cell fabrication. Both anode and cathode are coated on the conductive side of an ITO glass (Aldrich, 8-12Ω/sq). Pure TiO_2 of $\sim$ 18nm size with anatase phase was prepared by surfactant (P_{123}) assisted hydrothermal technique using weak acidic medium followed by calcination at 500°C. As described in the 2^{nd} chapter, CdSe QDs with particle size $\sim$10nm are prepared by an microwave irradiation method. Au NPs with size$\sim$10nm and silver NPs with size$\sim$ 28 nm, prepared by microwave irradiation method are used as the metal NPs. Platinum in ethanol was used as the counter electrode prepared from $H_2PtCl_6.6H_2O$ and I_2 solution acts as the electrolyte. TiO_2 powder, mixing with ethanol and MPA is coated on the conductive side of ITO by drop casting method. Above this, a layer of CdSe QDs followed by metal NPs are coated. MPA acts as the linking molecule between semiconductor chalcogenide materials(CdSe QDs) and TiO_2 paste. Prepared electrodes are named as T(TiO_2), TCS(TiO_2-CdSe), TCS-G(TiO_2/CdSe/Gold), TCS-S(TiO_2/CdSe/Silver) respectively. The ITO coated counter electrode (platinum) was placed on the top, so that the conductive side of the counter electrode faced the QDS adsorbed TiO_2 film. Electrolyte placed at the edges was drawn into the space between the electrodes by capillary action. UV-visible absorption measurements and J-V characteristics of the cells were examined. The J-V curves were measured and photon-to-current conversion efficiency or

IPCE measurements were carried out by allowing monochromatic radiation to fall on the cell provided by small band pass filters. Input intensity was measured using light meter (METRAVI 1332) and is in the range of 1-10 K lux in all the cases[23].

Results and discussions

UV-vis absorption spectra of CdSe QDs,Ag NPs and Au NPs are shown in figure 6.6. The ability to harvest a portion of the visible region of the suns spectrum and their good charge separation properties for better QDSSC conversion efficiencies make CdSe QDs-Metal NPs to be chosen as the sensitizer materials in this study. The bi-functional molecular linker-MPA enables to the mesoporous TiO_2 layer to adhere with the QDs.TiO_2 was chosen as the spacer layer material because of its higher refractive index, necessary for tuning the particle plasmon resonance closer to the band edge of QDs, without increasing the NP size.

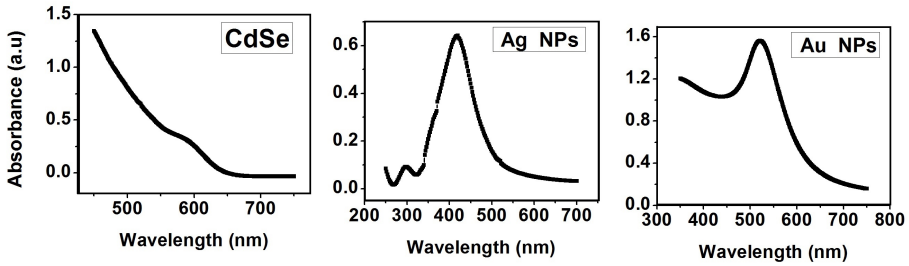

Figure 6.6: UV-vis absorption spectra of CdSe QDs, Ag NPs and Au NPs.

TEM image of (a)TiO_2,(b)CdSe QDs,(c)Gold and (d)Silver NPs is shown in figure 6.7. UV-vis absorption spectra of the electrodes T, TCS, TCS-G,TCS-S in figure 6.8 shows the increase in the absorption cross section of anodes, by incorporating metal NPs. Graphic presentation for the working principle of the anode with ITO as the substrate is shown in figure 6.9. When light hits the metal nanoparticles at their surface plasmon resonance, the light is scattered in many different directions. This allows light to travel along the active layer of the solar cell and bounce between the substrate and the nanoparticles enabling the solar cell to absorb more light. The performance of a QSSC is assessed by equa-

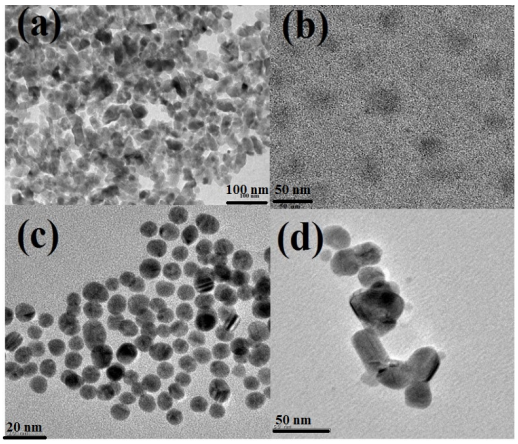

Figure 6.7: TEM image of (a) TiO_2,(b) CdSe QDs,(c) Gold and (d) Silver NPs.

tions (6.1) & (6.2) described above. J-V characteristics of the quantum dot sensitized solar cells based on various electrodes of T, TCS, TCS-G,TCS-S are shown in figure 6.10. It is observed that the short circuit current and an overall efficiency of QDSS cell have improved with metal NPs. As seen from the Table 6.2, there has been better characteristics properties obtained for solar cell embedded with Ag NPs. This signif-

Sample	J_{sc} (mA/cm^2)	V_{oc}(V)	FF	η%
TCS	0.312	0.23	0.34	1.94
TCS-G	0.58	0.22	0.29	2.99
TCS-S	0.65	0.29	0.26	3.93

Table 6.2: The performance of the QDSSCs for different electrodes.

icant improvement of the PV performance obtained for QDSSC, based on the IPCE characteristics of the anode with TiO_2/CdSe/Silver (TCS-S) which shows maximum photo conversion efficiency $\sim$ 63% obtained for wavelength $\sim$ 525 nm as shown in figure 6.11. We can assume that, this enhanced power conversion efficiency is due to Ag doped CdSe QDs, which may produce MEG. The importance of QDSSC having plasmonic NPs such as gold and silver mixed in QDSSC solar cell technology include scattering and absorption of light due to the deposition of metal

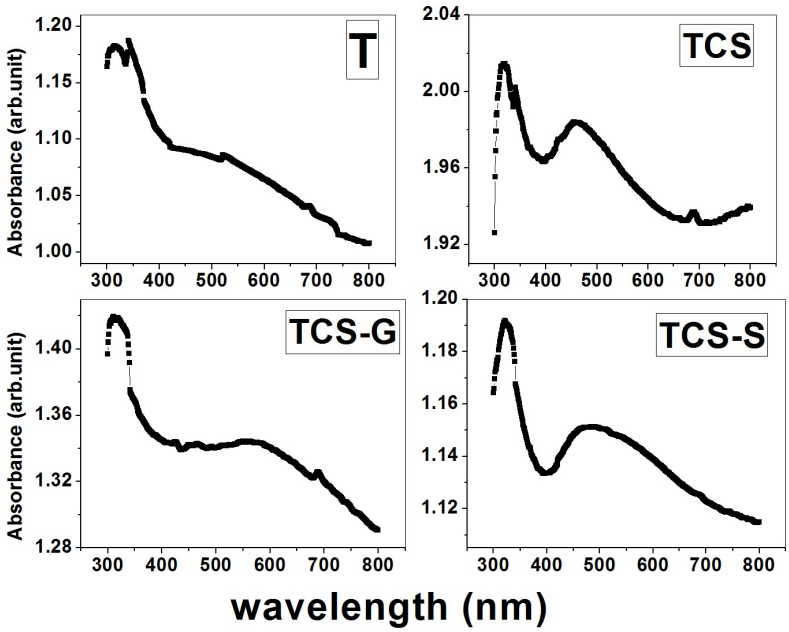

Figure 6.8: UV-vis absorption spectra of the electrodes T,TCS,TCS-G,TCS-S

nanoparticles as shown in figure 6.9. It can be done by trapping light inside the solar cell so that the absorbance can be increased. The main reason involved is that,the plasmonic NPs which have very high electromagnetic field around will increase absorption of photons and thereby give some more enhancement in photo current. The scattering of electrons from noble metal NPs excited at their localized surface plasmon resonance (LSPR) is used for this purpose. When photons of high energy hit the surface of a solar cell, the energy they carry is absorbed by the atoms of a metal NP at a desired frequency which may be tuned with the particle size of the QDs and the surface enhanced plasmon resonance. It also depends on the near-field concentration of light and the absorption cross section of the nanoparticle used. For particles with diameters well below the wavelength of light, a point dipole model describes the absorption and scattering of light well [42, 45, 46].

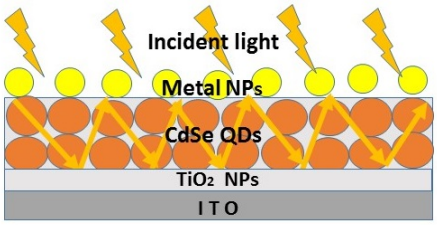

Figure 6.9: Graphic presentation for the working principle of anode with ITO as the substrate.

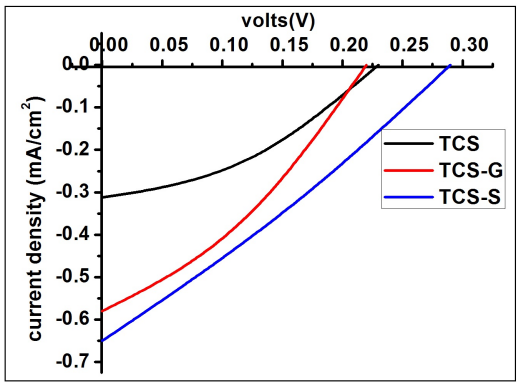

Figure 6.10: J-V characteristics of the quantum dot sensitized solar cells with anodes T, TCS, TCS-G,TCS-S.

In our works it is shown from figure 6.11 that the photo current and the conversion efficiency can be improved by using metal NPs. QDSSC with silver NP shows much higher efficiency (3.9 %) than with gold (2.9%) NPs, indicates that the main origin of the improved J_{sc} in our system results from an enhanced absorption of active layer through strongly enhanced local electromagnetic field in the vicinity of Ag nanoparticles, leading to an increase in excition generation. The enhanced IPCE characteristics of theTiO_2/CdSe/Silver(TCS-S) electrode which shows maximum efficiency and photocurrent can be attributed to the increased excition generation leading to higher incident photon to current conversion efficiency as shown in figure 6.11. An enhancement over the entire excitation spectral range longer than 400 nm, which is related to the

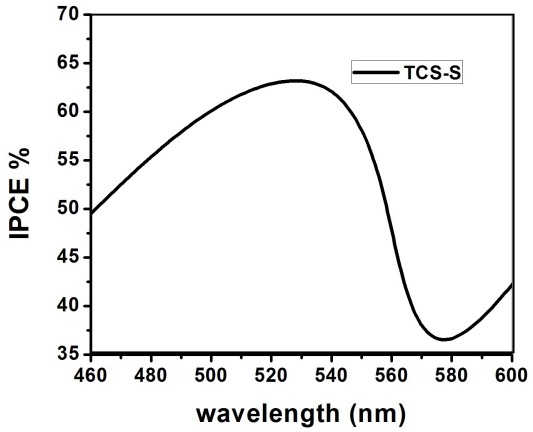

Figure 6.11: IPCE characteristics of the TiO_2/CdSe/Silver (TCS-S) electrodes which shows maximum efficiency

SPR band of Ag NPs, was observed for the cell with Ag NPs. These results indicate that LSPR might induce more photo generated charge carriers by stronger absorption of an active layer, resulting from the stronger enhancement in electromagnetic field near the metal surface [47, 48].

6.3 Random lasing from colloidal CdSe quantum dots - Rh6G system.

The unique properties of random lasers provide applications in areas such as new generation display devices, sensors, optical coding of objects, random number generators and medical diagnostics etc. Many systems including organic and inorganic QDs have applications in this area[20, 49]. This optical size dependent emission properties offer great potential for fabricating new types of laser devices using these materials. As random laser action relies on the combined effects of multiple scattering and optical amplification, colloidal quantum dots (CQDs) especially CdSe CQDs provide an attractive material system for such applications. In this work, we report random laser action in CQDs with rhodamine-6G (Rh-6G) where CdSe QD is used as the optical gain medium as well as strong scattering centers. In this section we report random laser action

in a system where optical amplification is provided by CQDs of CdSe. Such lasing opens the door to practical applications of QD random laser. Feedback for the photons generated by Rh-6G is provided by the random multiple scattering by CdSe QDs.

Experimental method

Colloidal solutions of CdSe QDs were prepared by microwave irradiation method described in the 2*nd* chapter. About 50% of a dye solution of Rh-6G(10^{-4}M) is added to it and allowed to mix. Sample is taken in a one mm thickness cuvette for the experiment. For the random laser experiments, the CQDs sample was photo-pumped by a frequency-doubled Q-switched Nd:YAG laser system emitting 7-ns pump pulses at an excitation wavelength of 532 nm. A cylindrical lens was aligned to shape the pump beam as a stripe and it was parallel to the colloidal CdSe QD sample (inside the cuvett of 1mm thickness) and the pump fluence could be adjusted through a neutral density filter. Emission from the sample could be collected and recorded with an optical fiber connected to a multi - channel grating-CCD spectrometer. The spectrometer had the detection channel with a spectral resolution of 0.03 nm. The laser is random in the sense that the feedback for the photons generated in the dye is provided by the random multiple scattering of light from the particles. The experimental setup is shown in chapter 2 (figure 2.13). A schematic representation of the random lasing action in CdSe QDs-Rh 6G system is shown in figure 6.12. Multiple light scattering with gain is observed here. A random collection of CdSe QDs containing Rh 6G dye is excited (for example, by an external light source) to obtain population inversion. The QDs then scatter light and amplify it in the process. The propagation of the light waves becomes that of an amplified random walk. Specifically, for the detailed studies we have used Rh-6G dye (10^{-4} M) and sample S_1 andS_2. R-S_1 and R-S_2 refers Rh-6G mixed with CdSe QDs of size $\sim$3 nm and $\sim$2.5 nm respectively while R refers bare Rh-6G. For the lasing action studies, a comparative data of the typical emission spectrum of R and R-S_2 collected from a single excitation spot for varying excitation intensities is provided.

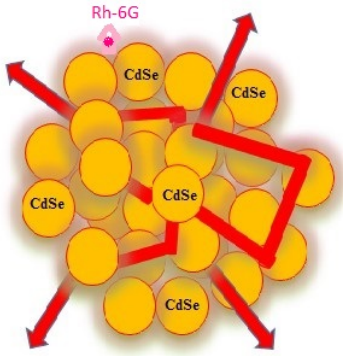

Figure 6.12: A schematic representation of the random lasing action in CdSe QDs-Rh 6G system

Results and Discussions

U-V visible absorption spectra of CdSe colloidal QDs used for samples R-S_1 and R-S_2 are denoted as Q1-R$S_1$and Q2-RS_2 with sizes 3nm and 2.5 nm respectively are shown in figure 6.13. Figure 6.14 shows typical

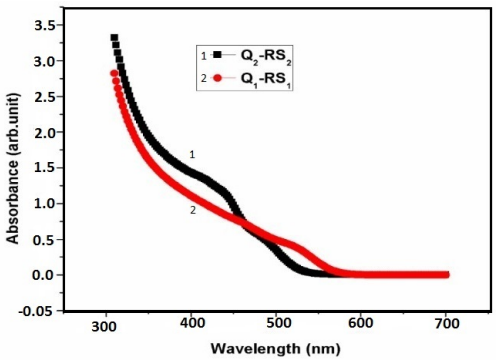

Figure 6.13: U-V visible absorption spectra of Q_1-RS_1 and Q_2-RS_2.

emission spectrum of R and R-S_2 collected from a single excitation spot for varying excitation intensities. As seen, the intensity of the emission get highly enhanced by the addition of CQDs to the Rh 6-G dye solution. Varying the input power also increases the emission intensity and it is depicted in figure 6.15. Figure 6.15 and figure 6.16 shows a typical emission spectrum of R-S_1 and R-S_2 respectively collected from a single

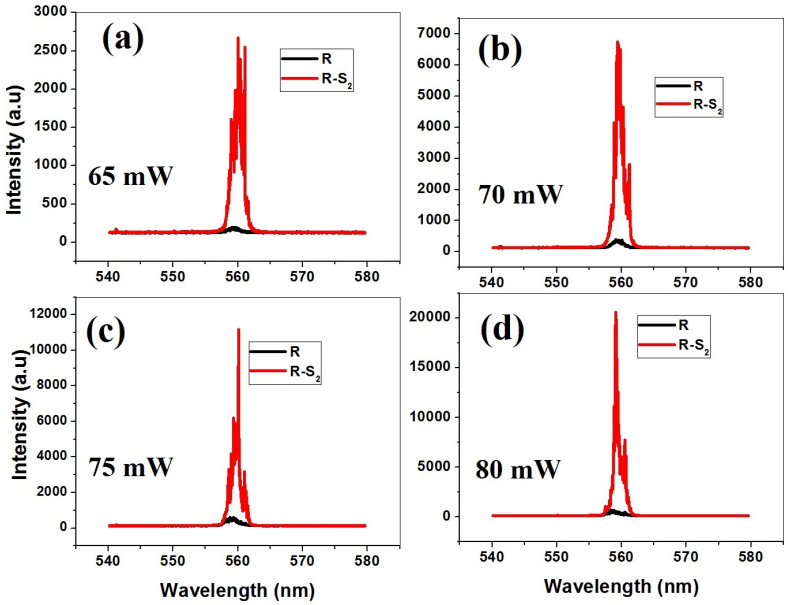

Figure 6.14: Typical emission spectrum of R and R-S_2 collected from a single excitation spot for varying excitation intensities.

excitation spot for varying excitation intensities. From figures 6.14 ,6.15 and 6.16, we observe that at relatively low excitation intensities, the spectrum exhibits a broad spontaneous emission($\sim$3 nm). By increasing the pumping intensities narrow discrete spikes with a line width of $\sim$ 0.03 nm appear. More and more intense spikes turn up at higher excitation intensity. Once the pump intensity exceeds a certain threshold, a much narrower emission peak begins. We observe a 0.3 nm of FWHM at this narrower emission which is shown in figure 6.16. The abrupt increase of the integrated intensity indicates the achievement of random lasing with a threshold of 240 mW. In order to explain the random lasing action from such a material we could classify them into two categories viz. incoherent random lasing and coherent random lasing, based on the feedback mechanism. In the case of incoherent random lasing, there is only intensity or energy feedback and the spectral shape is attributed to a narrowing peak at the gain maximum with a line width of several nanometers while the feedback for coherent random lasing is provided by field or amplitude mechanism, where closed optical loops would be

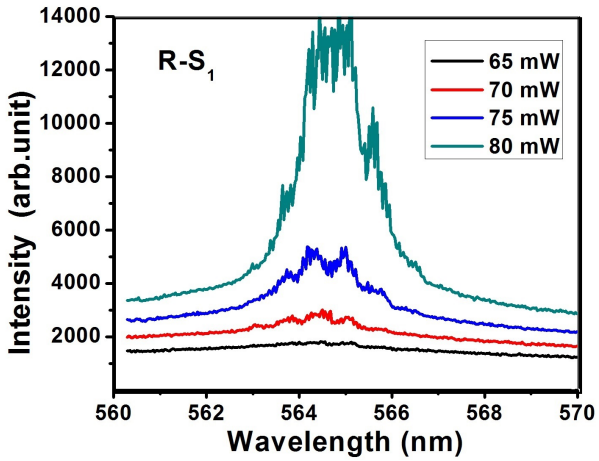

Figure 6.15: Typical emission spectrum of R-S_2 $\sim$ 3 nm size with variation of power.

formed by the interference of multiple scattering and this acts as ring cavities. Discrete super-narrow peaks or spikes with a line width of usually less than 1 nm will appear in coherent random lasing [50-53]. Based on this, we can attribute the lasing action from our system of colloidal CdSe QDs with Rh-6G to be coherent random lasing. Due to different losses of these random ring cavities, the threshold for the laser action in individual cavities are different. Under higher pumping intensities, more ring cavities can meet the threshold requirements, and thus more spikes are developed, which agrees with our results. The feedback for lasing in this system is expected to be due to scattering from CdSe QDs. Many of the clusters with sizes of tens of nanometers are formed during the mixing of CQDs with the dye. These clusters act as scattering centers for the emitted photo luminescent light to form optically closed loops, and is the main factor in the lasing action of such a random medium[54-56]. Here, colloidal CdSe QDs serve as both gain medium and scattering centers. It is possible to find the path length in terms of the excitation wavelength

$$(\Delta\lambda) = \frac{\lambda^2}{2nL} \tag{6.3}$$

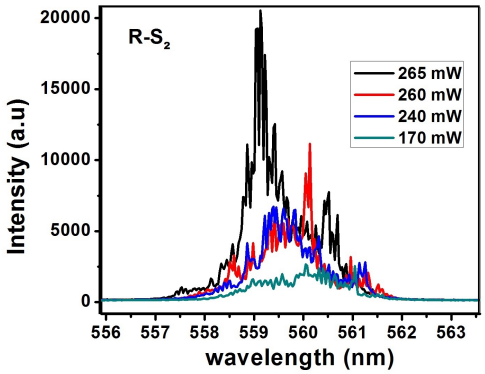

Figure 6.16: Typical emission spectrum of R-S_2 $\sim$ 2.5 nm size with variation of power.

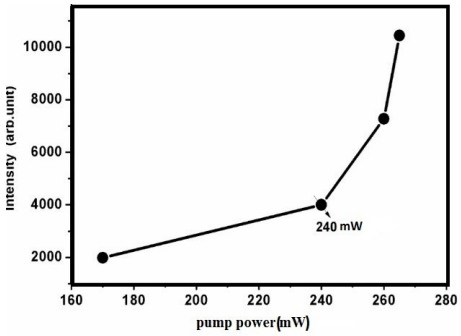

Figure 6.17: Input power vs. intensity of R-S_2 sample with threshold power 240 mW.

where n is the refractive index and L is the cavity length and$\Delta\lambda$ is the small change in wavelength obtained. We find the cavity length as 0.5mm while the cavity length of the cuvette used for our sample is 1 mm thickness. Here, we assume, multiple random resonances being excited by the non-Lorentzian line shape of emission peak [57] and not from the resonating cavity formed by the cuvette. The plot of the peak emission intensity versus the pump intensity shown in inset of figure 6.17 exhibits a soft threshold curve at 240 mW,which is due to a significant amount of spontaneous emission coupled into the laser mode. The FWHM of the emission peak drops from $\sim$ 3 nm below threshold to 0.3 nm above

240mW indicating laser action.

6.4 Conclusion

- In this chapter we have studied applications of CdSe QDs based nanofluids as quantum dot sensitized solar cells and random lasers.
- The obtained colour changes(yellow-orange red)with increase in annealing temperature is due to the formation of larger particles sizes of CdS /CdSe and, therefore, resulting in a smaller band gap.
- The absorption cross section of the solar irradiation increases with the annealing temperature and the current -voltage performance improves.
- The enhanced photo conversion efficiency of $\sim 54\%$ of the S_4 sample reveals that CdS/CdSe QDs produce more than one electron-hole pair per single absorbed photon (also known as multiple exciton generation).
- Surface plasmon enhanced TiO_2 CdSe quantum dot solar cells are fabricated by incorporating Ag, Au metal nanoparticles and the performance are studied.
- Light trapping by metallic nano structures offers the potential to realize better performance in CdSe QDs based solar cells.
- It is observed that conversion efficiency of the solar cells has been increased by the deposition of Au and Ag NPs and it is better with Ag (3.93%). This enhanced efficiency can be attributed to the improved photocurrent due to enhanced forward scattering from the plasmonic nanostructures.
- Random laser action is observed in a CdSe-Rh 6G based colloidal QD system.
- The laser is random in the sense that the feedback for the photons generated in the Rh- 6G dye is provided by the random multiple scattering of light from the CdSe QDs.

- Single-shot spectra were recorded to study the process of the laser emission from this system and the results show enhanced laser emission from the CdSe CQDs compared to that from the bare dye.
- Observations could open the door for unconventional lasers to be used in a wider range of commercial applications such as document security, remote sensing, ultra-fast displays and diagnostic imaging.
- Single-shot spectra were recorded to study the process of the laser emission from this system and the results show enhanced emission of laser occurred from the CdSe colloidal QDs compared to that from bare dye.
- The FWHM of the emission peak drops from ∼3 nm below threshold to 0.3 nm above threshold indicating laser action.
- Observations could open the door for unconventional lasers to be used in a wider range of commercial applications such as document security, remote sensing, ultra-fast displays and diagnostic imaging.

6.5 References

[1] D. Bimberg, M. Grundmann and N. N. Ledentsov, Quantum Dot Heterostructures. John Wiley & Sons, 1999.

[2] V. I. Klimov,"Nanocrystal quantum dots-From fundamental photophysics to multicolor lasing," Los Alamos Science, vol. 28, pp. 214-220, 2003.

[3] J. Wang, M. S. Gudiksen, X. Duan, Y. Cui and C. M. Lieber,"Highly polarized photoluminescence and photodetection from single indium phosphide nanowires," Science, vol. 293, pp. 1455-1457, 2001.

[4] X. Peng, L. Manna, W. Yang, J. Wickham, E. Scher, A. Kadavanich and A. P. Alivisatos, "Shape control of CdSe nanocrystals," Nature, vol. 404, pp. 59-61, 2000.

[5] J. Hu, L. Li, W. Yang, L. Manna, L. Wang and A. P. Alivisatos,"Linearly polarized emission from colloidal semiconductor quantum rods," Science, vol. 292, pp. 2060-2063,2001.

[6] W. U. Huynh, J. J. Dittmer and A. P. Alivisatos,"Hybrid nanorod-polymer solar cells," Science, vol. 295, pp. 2425-2427, Mar 29, 2002.

[7] J. Lee, V. C. Sundar, J. R. Heine, M. G. Bawendi and K. F. Jensen, "Full color emission from IIVI semiconductor quantum dotpolymer composites," Adv Mater, vol. 12, pp. 1102-1105, 2000.

[8] M. Bruchez Jr, M. Moronne, P. Gin, S. Weiss and A. P. Alivisatos, "Semiconductor nanocrystals as fluorescent biological labels," Science, vol. 281, pp. 2013-2016,1998.

[9] J. Halls, C. Walsh, N. Greenham, E. Marseglia, R. Friend, S. Moratti and A. Holmes,"Efficient photodiodes from interpenetrating polymer networks," nature,498-500,1995.

[10] M. Grtzel, "Photoelectrochemical cells," Nature, vol. 414, pp. 338-344, 2001.

[11] H. Chen, C. Su, J. Chen, T. Yang, N. Hsu and W. Li, "Preparation and characterization of pure rutile TiO_2 nanoparticles for photocatalytic study and thin films for dye-sensitized solar cells," Journal of Nanomaterials, vol. 2011, pp. 47, 2011.

[12] F. A. de Castro, F. Nesch, C. Walder and R. Hany,"Challenges found when patterning semiconducting polymers with electric fields for organic solar cell applications," Journal of Nanomaterials, vol. 2012, pp. 10, 2012.

[13] T. Zdanowicz, T. Rodziewicz and M. Zabkowska-Waclawek,"Theoretical analysis of the optimum energy band gap of semiconductors for fabrication of solar cells for applications in higher latitudes locations," Solar Energy Mater. Solar Cells, vol. 87, pp. 757-769, 2005.

[14] J. Tian, R. Gao, Q. Zhang, S. Zhang, Y. Li, J. Lan, X. Qu and G. Cao,"Enhanced performance of CdS/CdSe quantum dot cosensitized solar cells via homogeneous distribution of quantum dots inTiO_2film," The Journal of Physical Chemistry C, vol. 116, pp. 18655-18662, 2012.

[15] D. S. Wiersma, "The physics and applications of random lasers," Nature Physics, vol. 4, pp. 359-367, 2008.

[16] S. Gottardo, R. Sapienza, P. D. Garcia, A. Blanco, D. S. Wiersma and C. Lpez, "Resonance-driven random lasing," Nature Photonics, vol. 2, pp. 429-432, 2008.

[17] H. E. Tureci, L. Ge, S. Rotter and A. D. Stone, "Strong interactions in multimode random lasers," Science, vol. 320, pp. 643-646, 2008.

[18] A. Uchida, K. Amano, M. Inoue, K. Hirano, S. Naito, H. Someya, I. Oowada, T. Kurashige, M. Shiki and S. Yoshimori,"Fast physical random

bit generation with chaotic semiconductor lasers," Nature Photonics, vol. 2, pp. 728-732, 2008.

[19] N. M. Lawandy, R. Balachandran, A. Gomes and E. Sauvain,"Laser action in strongly scattering media," Nature, vol.368, pp.436-438, 1994.

[20] H. Cao, Y. Zhao, S. Ho, E. Seelig, Q. Wang and R. Chang,"Random laser action in semiconductor powder," Phys. Rev. Lett., vol. 82, pp. 2278, 1999.

[21] R. Polson, A. Chipouline and Z. Vardeny,"Random Lasing in p-Conjugated Films and Infiltrated Opals," Adv Mater, vol. 13, pp. 760-764, 2001.

[22] X. Meng, K. Fujita, S. Murai and K. Tanaka, "Coherent random lasers in weakly scattering polymer films containing silver nanoparticles," Physical Review A, vol. 79, pp. 053817, 2009.

[23] S. Divya, A. Thankappan, C. Vallabhan, V. Nampoori, P. Radhakrishnan and A. Mujeeb, "Electrolyte/photoanode engineered performance of TiO_2 based dye sensitised solar cells," J. Appl. Phys., vol. 115, pp. 064501, 2014.

[24] J. A. Chang, J. H. Rhee, S. H. Im, Y. H. Lee, H. Kim, S. I. Seok, M. K. Nazeeruddin and M. Gratzel, "High-performance nanostructured inorganic organic heterojunction solar cells," Nano Letters, vol. 10, pp. 2609-2612, 2010.

[25] P. V. Kamat, "Quantum dot solar cells. Semiconductor nanocrystals as light harvesters," The Journal of Physical Chemistry C, vol. 112, pp. 18737-18753, 2008.

[26] I. Hod and A. Zaban, Materials and interfaces in quantum dot sensitized solar cells: Challenges, advances and prospects," Langmuir, vol. 30, pp. 7264-7273, 2013.

[27] J. A. Christians, R. C. Fung and P. V. Kamat,"An inorganic hole conductor for organo-lead halide perovskite solar cells. Improved hole conductivity with copper iodide," J. Am.Chem. Soc., vol.136, pp.758-764, 2013.

[28] C. Chi, S. Liau and Y. Lee, "The heat annealing effect on the performance of CdS/CdSe-sensitized TiO_2photoelectrodes in photochemical hydrogen generation," Nanotechnology, vol. 21, pp. 025202, 2010.

[29] M. Rincon, M. Sanchez, A. Olea, I. Ayala and P. Nair,"Photo-electrochemical behavior of chemically deposited CdSe and coupled CdS/CdSe semiconductor films," Solar Energy Mater.Solar Cells, vol. 52, pp.399-411,1998.

[30] Y. Li, L. Wei, R. Zhang, Y. Chen and J. Jiao, "Annealing effect on photovoltaic performance of CdSe quantum-dots-sensitized TiO_2 nanorod solar cells," Journal of Nanomaterials, vol. 2012, pp.1, 2012.

[31] N. Osada, T. Oshima, S. Kuwahara, T. Toyoda, Q. Shen and K. Katayama, "Photoexcited carrier dynamics of double-layered CdS/CdSe quantum dot sensitized solar cells measured by heterodyne transient grating and transient absorption methods," Physical Chemistry Chemical Physics, vol. 16, pp. 5774-5778, 2014.

[32] B. O'regan and M. Grtzel, "A low-cost, high-efficiency solar cell based on dye-sensitized colloidal TiO_2films,"nature vol. 24 , Pp.353 1991.

[33] C. Hgglund, M. Zch and B. Kasemo,"Enhanced charge carrier generation in dye sensitized solar cells by nanoparticle plasmons," Appl. Phys. Lett., vol. 92, pp. 013113, 2008.

[34] I. Hod and A. Zaban,"Materials and interfaces in quantum dot sensitized solar cells: Challenges, advances and prospects," Langmuir, vol. 30, pp. 7264-7273, 2013.

[35] M. Yamaguchi, "Multi-junction solar cells and novel structures for solar cell applications," Physica E: Low-Dimensional Systems and Nanostructures, vol. 14, pp. 84-90, 2002.

[36] J. Tian, R. Gao, Q. Zhang, S. Zhang, Y. Li, J. Lan, X. Qu and G. Cao, "Enhanced performance of CdS/CdSe quantum dot cosensitized solar cells via homogeneous distribution of quantum dots in TiO_2 film," The Journal of Physical Chemistry C, vol. 116, pp. 18655-18662, 2012.

[37] H. R. Stuart and D. G. Hall, "Absorption enhancement in silicononinsulator waveguides using metal island films," Appl. Phys. Lett., vol. 69, pp. 2327-2329, 1996.

[38] C. M. Chuang, P. R. Brown, V. Bulovi and M. G. Bawendi, "Improved performance and stability in quantum dot solar cells through band alignment engineering," Nature Materials, vol. 13, pp. 796-801, 2014.

[39] M. J. Mendes, E. Hernndez, E. Lpez, P. Garca-Linares, I. Ramiro, I. Artacho, E. Antoln, I. Tobas, A. Mart and A. Luque, "Self-organized colloidal quantum dots and metal nanoparticles for plasmon-enhanced intermediate-band solar cells," Nanotechnology, vol.24, pp.345-402,2013.

[40] V. E. Ferry, J. N. Munday and H. A. Atwater,"Design considerations for plasmonic photovoltaics," Adv Mater, vol. 22, pp. 4794 - 4808, 2010.

[41] H. A. Atwater and A. Polman, "Plasmonics for improved photovoltaic devices," Nature Materials, vol. 9, pp. 205-213, 2010.

[42] K. Catchpole and A. Polman, "Plasmonic solar cells," Optics Express, vol. 16, pp. 21793-21800, 2008.

[43] S. Fahr, C. Rockstuhl and F. Lederer, "Metallic nanoparticles as intermediate reflectors in tandem solar cells," Appl. Phys. Lett., vol. 95, pp. 121105, 2009.

[44] K. Catchpole and A. Polman, "Plasmonic solar cells," Optics Express, vol. 16, pp. 21793-21800, 2008.

[45] C. Martella, D. Chiappe, C. Mennucci and F. B. de Mongeot, "Tailoring broadband light trapping of GaAs and Si substrates by self-organised nanopatterning," J. Appl. Phys., vol. 115, pp. 194308, 2014.

[46] K. Nakayama, K. Tanabe and H. A. Atwater, "Plasmonic nanoparticle enhanced light absorption in GaAs solar cells," Appl. Phys. Lett., vol. 93, pp. 121904, 2008.

[47] D. Derkacs,W. Chen, P. Matheu, S. Lim, P. Yu and E. Yu,"Nanoparticle-induced light scattering for improved performance of quantum-well solar cells," Appl. Phys. Lett., vol. 93, pp. 091107, 2008.

[48] S. Kim, S. Na, J. Jo, D. Kim and Y. Nah, "Plasmon enhanced performance of organic solar cells using electrodeposited Ag nanoparticles," Appl. Phys. Lett., vol. 93, pp. 073307, 2008.

[49] X. Zhao, Z. Wu, S. Ning, S. Liang, D. Wang and X. Hou, "Random lasing from granular surface of waveguide with blends of PS and PMMA," Optics Express, vol. 19, pp. 16126-16131, 2011.

[50] Y. Wang, V. D. Ta, Y. Gao, T. C. He, R. Chen, E. Mutlugun, H. V. Demir and H. D. Sun, "Stimulated Emission and Lasing from CdSe/CdS/ZnS CoreMultiShell Quantum Dots by Simultaneous ThreePhoton Absorption," Adv Mater, vol. 26, pp. 2954-2961, 2014.

[51] L. Cerdn, E. Enciso, V. Martn, J. Bauelos, I. Lpez-Arbeloa, A. Costela and I. Garca-Moreno, "FRET-assisted laser emission in colloidal suspensions of dye-doped latex nanoparticles," Nature Photonics, vol. 6, pp. 621-626, 2012.

[52] H. Cao, Y. Zhao, S. Ho, E. Seelig, Q. Wang and R. Chang,"Random laser action in semiconductor powder," Phys. Rev. Lett., vol. 82, pp. 2278, 1999.

[53] D. S. Wiersma, "The physics and applications of random lasers," Nature Physics, vol. 4, pp. 359-367, 2008.

[54] R. C. Polson, M. E. Raikh and Z. V. Vardeny,"Universal properties of random lasers," Selected Topics in Quantum Electronics, IEEE Journal Of, vol. 9, pp. 120-123, 2003.

[55] Y. Boucher and P. Feron, "Generalized transfer function: A simple model applied to active single-mode microring resonators," Opt. Commun., vol. 282, pp. 3940-3947, 2009.

[56] V. I. Klimov VI, A. A. Mikhailovsky, D. W. McBranch, C. A. Leatherdale and M. G. Bawendi, "Quantization of multiparticle auger rates in semi-

conductor quantum dots," Science, vol. 287, pp. 1011-1013, Feb 11, 2000.

[57] D. S. Wiersma,"The physics and applications of random lasers," Nature Physics, vol. 4, pp. 359-367, 2008.

[58] Anju K Augustine, P Radhakrishnan, V P N Nampoori and M Kailasnath" Enhanced random lasing from a colloidal CdSe quantum dot-Rh6G system", Laser Phys. Lett.vol.12 pp.025006 (4pp), 2015.

Chapter 7

General Conclusions and Future Work

This chapter deals with the significant conclusions of the present work and the few observations regarding future prospects.

In general, linear- optic, thermo- optic and nonlinear- optical studies on CdSe QDs based nanofluids and their special applications in solar cells and random lasers have been studied in this thesis. Photo acoustic and thermal lens studies are the two characterization methods used for thermo- optic studies whereas Z- scan method is used for nonlinear-optical charecterization. In all these cases we have selected CdSe QDs based nanofluid as potential photonic material and studied the effect of metal NPs on its properties.

Linear optical studies on these materials have been done using various characterization methods and photo induced studies is one of them. Thermal lens studies on these materials give information about heat transport properties of these materials and their suitability for applications such as coolant and insulators. Photo acoustic studies shows the effect of light on the absorption energy levels of the materials. We have also observed that these materials can be used as optical limiters in the field of nonlinear optics. Special applications of these materials have been studied in the field of solar cell such as QDSSCs, where CdSe QDs act as the sensitizing materials for light harvesting. Random lasers have many applications in the field of laser technology, in which CdSe QDs act as scattering media for the gain.

- *In the first chapter we have included the literature review on thermo-optic and nonlinear-optical methods as the characterization methods for our study. The importance of QDs as photonic materials and the specialty of CdSe QDs is also discussed. Thermal lens, Photoaccoustics and Z- scan methods are described with experimental setup and theoretical background in the second chapter. Synthesis and analysis methods on CdSe QDs and metal NPs are also included in this section. Methods for the synthesis of high-quality, monodispersed, MSA capped CdSe nanoparticles in aqueous solution, and formation of the plasmonic NPs like Ag and Au are discussed. Particle size calculation methods, basics on zeta potential studies and other structural and optical characterization methods are also described.*

- *Liner optical studies on CdSe QDs based nanofluids reveal properties of band gap tuning and varying fluorescence at different conditions. Presence of MSA can act as an effective capping agent in the formation of monodispersed CdSe QDs with tunable particle size and has an important role in its optical properties. Linear optical output of the samples are also influenced by the reaction time, input irradiation power, pH of the solution medium and the effect of the presence of metal NPs etc. Energy transfer from the quantum dots to metal NPs have been observed with our samples along with the enhancement and quenching. Photo induced studies on the samples show changes in absorption and transmission spectra for different time intervals of laser irradiating time. Reversible photo darkening effect is another phenomena observed in this regard. Laser induced photo luminescence spectra of the corresponding samples give information about the photochemical changes in the samples due to the formation of highly exited levels.*

- *Size dependent variation of thermal diffusivity is observed from CdSe QDs based nanofluid. Influence of pH on thermo-optic properties of these MSA capped CdSe QD's show a significant increases in thermal diffusivity for an optimum pH. Major advantages of such materials are that they can be used as both coolant and insulator by adjusting the corresponding pH values and particle size. An effective increase of the absorption cross section of the semiconductor nanostructure and modified emission properties due to the exciton-plasmon interactions also causes variation in the thermal diffusivity properties. Studies of variation of photoacoustic signal amplitude with different input power show that samples which are incorporated with metal NPs exhibit better characteristics. PA spectrum of CdSe QDs based nanofluids using Xenon lamp is also studied.*

- *The nonlinear optical characterization by Z-scan technique shows a third-order optical nonlinear absorption in CdSe QDs which increases with particle size and can be attributed to the phenomenon of two photon absorption. The optical limiting threshold of the QDs also varies with particle size which makes CdSe QDs a promising candidate for RSA based devices at high laser intensities such as*

optical limiters. Third order optical nonlinear absorption in CdSe QDs with variable pH has also been evaluated and the results exhibit an optimal pH value with lowest nonlinearity. A change in negative to a positive value of the nonlinear refractive index n_2 indicating the molecular representational Kerr effect is observed with the optimized sample which becomes the dominant mechanism for nonlinear refraction. RSA is observed in Au,Ag NPs which is due to free carrier absorption or excited state absorption. Our observations show that metal induced nanofluids exhibit enhanced nonlinearity and optical limiting properties which can be attributed to the charge transfer mechanism from colloidal CdSe QDs to metal nanoparticle and the enhancement of the electromagnetic field in the presence of semiconductor QDs.

- *Special applications of CdSe QDs based nanofluids as quantum dot sensitized Solar cells include studies on the performance of the CdS/CdSe QDSSCs based on different annealing temperature performance of the photo anode. Annealing temperature increases the absorption cross section of the solar irradiation and the current-voltage performance. Surface plasmon enhanced TiO_2/ CdSe QD solar cells are fabricated by incorporating Ag, Au metal NPs and it offers the potential to realize better performance from quantum dot based solar cells. Conversion efficiency of the solar cells has been increased by the deposition of Au and Ag NPs and it is better with Ag NPs (3.93%) and is attributed to the improved photocurrent due to enhanced forward scattering from the plasmon nanostructures. Random laser action is observed in a CdSe- Rh 6G, system which is provided by the random multiple scattering of light from the CdSe QDs. Enhanced laser emission occurred from the CdSe QDs comparable to that of bare dye and this could open the door for unconventional lasers to be used in a wider range of commercial applications such as document security, remote sensing, ultra-fast displays and diagnostic imaging.*

In short,the versatility and utility of linear-optic,thermo-optic and nonlinear-optical techniques for the measurement of characteristic properties of the CdSe QDs based photonic materials have been experimentally demonstrated and applied to QDSSCs and random lasers. There are different areas where further investigations can be carried out in the field.

Studies on further enhancement of solar cell efficiency can be conducted with different electrolytes, different cathodes and varying input conditions.

Photo acoustic and solar cell study can be investigated with varying size of the CdSe samples.

Electro-optic and dielectric properties of the samples have not been studied which is useful in the area of solar cell studies.

Studies based on random lasers with different dyes can be performed. It may open us new areas of research based on CdSe QDs.

All the above mentioned investigations can be carried out in samples prepared in the form of thin film.

Appendix

* Selected published papers

IOP Publishing | Astro Ltd Laser Physics Letters

Laser Phys. Lett. **11** (2014) 115901 (6pp) doi:10.1088/1612-2011/11/11/115901

Influence of pH on the thermo-optic properties of CdSe QDs prepared by a microwave irradiation method

Anju K Augustine, C P Girijavallabhan, V P N Nampoori and M Kailasnath

International School of Photonics, Cochin University of Science and Technology, Kochi-682022, Kerala, India

E-mail: srrosmin2009@gmail.com

Received 8 May 2014, revised 30 July 2014
Accepted for publication 8 September 2014
Published 29 September 2014

Abstract

In this letter the optical behavior as well as the thermal properties of CdSe quantum dots (QDs) capped with mercapto succinic acid (MSA) are studied and analyzed. CdSe QDs with an average particle size of 7.0 nm are prepared by a microwave irradiation method. The unique structure of MSA plays an important role in determining the PL intensity and better stability by controlling the pH of the medium. A significant increase in thermal diffusivity with pH values is observed with a mode matched thermal lens method. At the optimum value of pH, the surface charge of nanoparticles increases, which increases the repulsive forces. The resulting reduced agglomeration of QDs enhances mobility and improves heat transport. There is a clear correlation between luminous intensity and thermal diffusivity in these nano fluids containing CdSe QDs.

Keywords: MSA, CdSe QDs, luminous intensity, thermal diffusivity

(Some figures may appear in colour only in the online journal)

1. Introduction

During the last two decades, there has been an enormous interest in nanomaterials due to their novel physical and chemical properties, which arise from quantum confinement of charge carriers that differ clearly from those of bulk materials [1–5]. Among the various kinds of quantum dot (QD) semiconductors, colloidal CdSe is the most widely investigated kind, because their emission can be easily tuned to cover from red (centred at 650 nm) to blue (centred at 450 nm) as the size of QDs decrease because of their strong size-dependent optical properties [6–8]. CdSe QDs, prepared in a non aqueous method are only soluble in some nonpolar organic solvents, which creates problems if they have to be used for thermal or biological applications [9, 10]. In the present work, CdSe QDs are prepared by a microwave irradiation (MWI) method in an aqueous medium [11, 12].

However, due to the high surface energy of QDs, they can easily coagulate and are difficult to disperse in the base fluid. This leads to changes of the morphology and of the volume fraction resulting in low fluidity. Therefore, controlling the coagulation of QDs in the nanofluid becomes the primary issue in order to exploit their potential benefits and applications. In the case of nanofluids, it is an important evaluation for understanding the dispersion stability behavior [13, 14]. However, to our knowledge, recent efforts have mainly focused on optical behavior and there are few reports regarding the nanofluid thermal diffusivity changes with pH. In this letter, by measuring the optical changes as well as the thermal diffusivity changes of nanofluids with pH, we investigate the effect of pH value on the dispersive stability and the heat transfer enhancement of the nanosuspension. The high sensitivity character of the thermal lens (TL) technique makes it very appropriate for measuring the thermal diffusivity in the samples that are dispersed in a fluid medium. It is expected to provide a means for designing nanofluids with desirable thermal and optical properties.

2. Experimental details

CdSe QDs were prepared by a rapid MWI method. The precursors used were $CdCl_2.H_2O$ and Na_2SeO_3. The capping

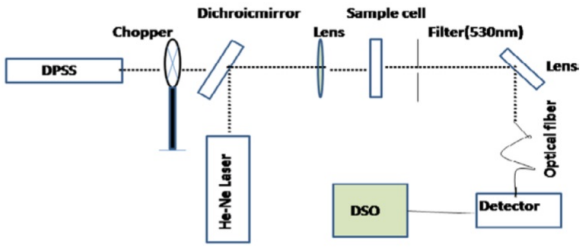

Figure 1. TL experimental setup with a DSO.

agent used was mercaptosuccinic acid (MSA). The pH of the corresponding colourless solution was adjusted by adding 1 M NaOH. We have selected samples with different pH values. MWI provided the required thermal energy to the reaction. The power level of the reaction system was maintained at 60 W. During the reaction, the colour of the solution gradually changed and QDs began to form. Aliquots were taken out of the flask for the optical measurements to monitor the growth of the QDs. The samples taken for optical characterization are named as pH 3.7, pH 4.7, pH 7.6, and pH 8.9.

Absorption spectra of the prepared CdSe QDs were recorded using a UV–Visible Spectrophotometer (Jasco V-570 UV/VIS/IR). Fluorescence spectra of the nanoparticles were obtained on a Cary Eclipse fluorescence spectrophotometer (Varian). The excitation wavelength was kept at 390 nm, and the emission spectra were recorded. All absorption and fluorescence spectra were measured without any post preparative size separation. The Electron micrograph images of CdSe QDs in colloidal form were taken using a Transmission electron microscope (Philips Technai G2 at 120 kV).

TL spectrometry (TLS) is one of the important photothermal techniques that depends on a temperature gradient generated by the absorption of electromagnetic radiation and subsequent non-radiative relaxation of the excited molecules. For TL studies, the schematic experimental setup is shown in figure 1.

The excitation source used was a continuous wave (cw), 532 nm diode pumped solid state laser (DPSS) with a maximum power of 150 mW. The power at the sample was suitably adjusted using attenuators so that the probe beam spot was free from aberrations. A 2 mW He–Ne gas laser emitting at 632.8 nm used as the probe was arranged to be collinear with the pump using a dichroic mirror. The two beams were focused into the sample cell such that the beam area at the sample plane was the same for both pump and probe resulting in a mode matched TL arrangement.

A sample was taken in a cuvette of 1 cm path length for making the measurements. A low frequency mechanical chopper with 3 Hz was used to modulate the intensity of the pump, until the TL peak-to-peak signal reached its maximum. This also enabled us to determine the thermal recovery of the sample. In the TL experiment the excitation laser must have a Gaussian profile, so that when the sample absorbs the beam with a Gaussian intensity profile, the temperature distribution has a radial dependence. The temperature gradient causes a refractive index gradient which behaves like a converging or diverging lens depending on whether the rate of change of the refractive index with respect to temperature is positive or negative [15, 16]. The TL signal was collected using an optical fiber, which serves as the finite aperture and the same was mounted on the xyz translator. It was positioned at the centre of the probe beam spot and connected to a photo detector–digital storage oscilloscope (DSO) system. A filter to cut off 532 nm was used before the detector to remove the residual pump. The probe beam from the He–Ne laser which passes collinearly with the pump beam experienced divergence and the beam shape expanded in the presence of the TL. The change in intensity of the probe beam was measured using a fast photodetector from which the relative intensity and initial slope was measured. The data was analyzed by using the procedure reported earlier [17].

3. Results and discussion

Figures 2 and 3 show the absorption and florescence spectra of the prepared CdSe QDs with a different pH at room temperature. It can be clearly seen that the absorption and luminescence peaks of the CdSe QDs were red-shifted with increasing value of pH. It is observed that, for the sample with pH of less than 4.7 there are signs of agglomeration and for a higher pH the intensity of emission is decreased, and it shows much less intensity with a large FWHM.

Figure 3 shows the pH effects of the reaction solution on the fluorescent properties of CdSe QDs. It can be seen that the pH in our synthesis is much lower than with glutathione (GSH) (~11.0–12.0) or MPA (>8.0) as thiol stabilizers used in common aqueous synthesis. For example, when GSH was used as a stabilizer for CdSe QDs, the prepared colloid solution formed some white precipitates if the pH of the Cd precursor was reduced to acid or was weakly basic, which restricted the preparation of the CdSe QDs in a relatively lower pH aqueous solution. However, MSA–CdSe can be synthesized even in a weak acidic solution, mostly because of the special structure of MSA with two carbonyl groups. In this study, we also obtained high-quality CdSe QDs in a weak acid solution, the possible reasons for which are as follows. First, previous studies indicated that thiols had a strong complexation to CdS particles rather than to free cadmium ions under acidic conditions, which resulted in a smaller trap site on the

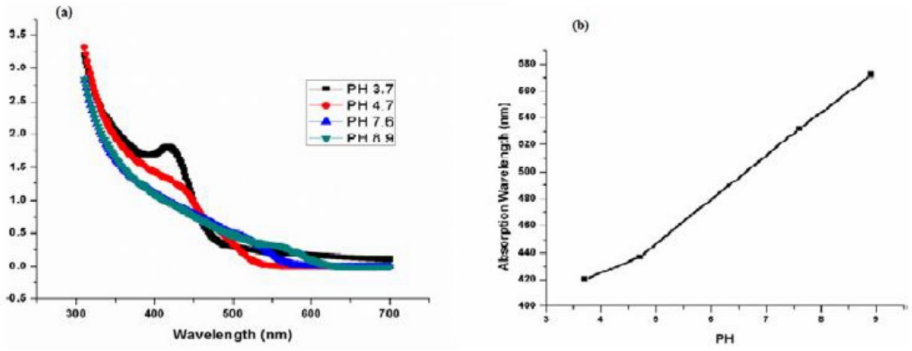

Figure 2. (*a*) Absorption spectra of the prepared CdSe QDs with different pH. (*b*) Red shift in wavelength of CdSe QDs with pH.

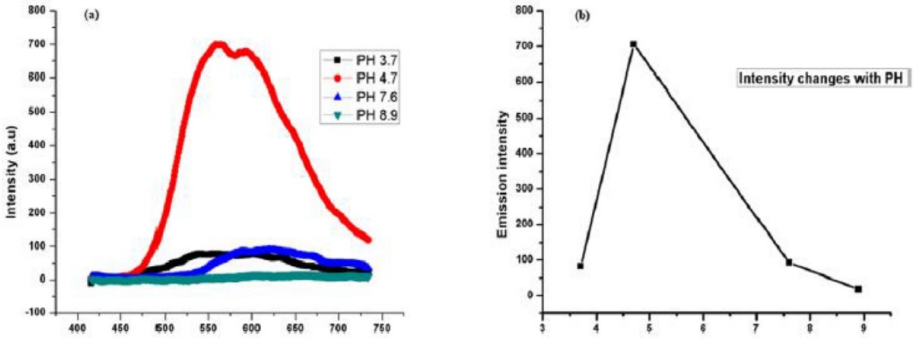

Figure 3. (*a*) Fluorescence spectra of the prepared CdSe QDs with different pH. (*b*) Change in intensity of CdSe QDs with pH.

CdSe surface. Secondly, a thick layer of cadmium thiol complexes under acidic conditions was also an important factor for determining high-quality QDs, because more trap sites on the CdSe surface are removed after being covered with cadmium thiol complexes. Last, but not least, the unique structure of MSA plays an important role in reducing the surface trap of CdSe QDs [18–20]. The two carbonyl groups of MSA can provide better stability than other thiol compounds (MPA, GSH, etc), as seen from figure 2. Nevertheless, when the pH of the precursor solution was decreased further, it led to weakening of the protection abilities of MSA due to the protonation of MSA. Because the strong acidic solution was unfavorable for the formation of a defect-free surface, we choose pH ~ 4.7 for the synthesis of CdSe QDs. Figure 4 represents the TEM image and SAED of the CdSe sample. It shows that the nanoparticles formed are spherical in shape.

Figure 5 represents the thermal decay at an input power of 136 mW.

Under the same experimental conditions, the experiment was repeated for various pH conditions of CdSe QDs dissolved in water. Two typical results are shown in figure 6

The time dependent probe beam intensity follows the expression [20, 21].

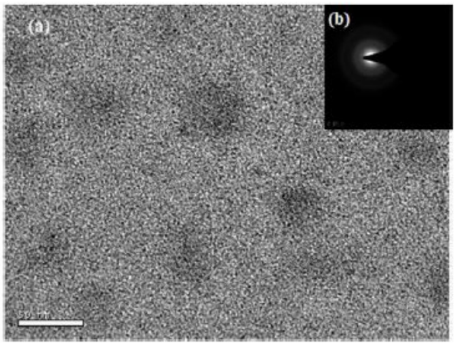

Figure 4. (*a*) TEM image and (*b*) SAED of the CdSe sample.

$$I(t) = I_0 \Big/ \left[1 - \theta\left(1 + {}^{t_c}/_{2t}\right)^{-1} + \left({}^{1}/_{2}\right)\theta^2\left(1 + {}^{t_c}/_{2t}\right)^{-2}\right]. \quad (1)$$

Here, the parameter θ is related to the thermal power radiated as heat, P_{ath}, and can be obtained with $I = (I_0 - I_\infty)/I_\infty$

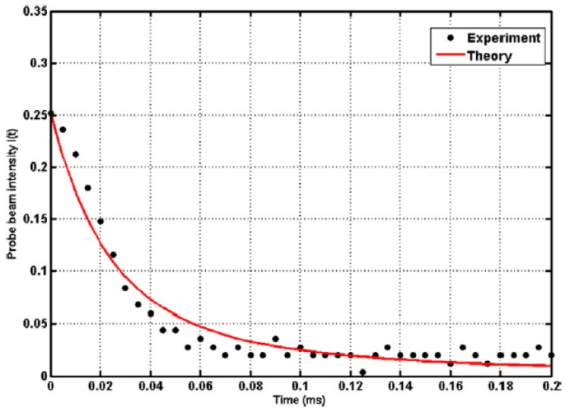

Figure 5. Fitting of the data (pH –9.6) using equation (1) with the probe beam intensity as a function of time with fit parameters $I_0 = 0.25$, $\theta = 36.22$ and $t_c = 1.94$ s The beam spot size at the sample position is 0.225 mm.

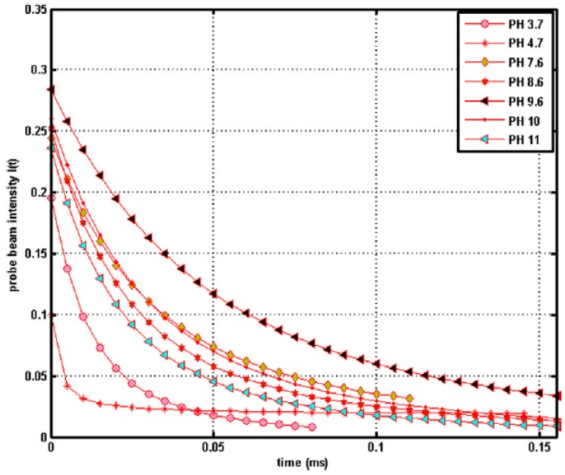

Figure 6. TL fitting of the CdSe QD data with different pH using equation (1) with the probe beam intensity as a function of time with error ±0.03. The beam spot size at the sample position is 0.22 mm.

and $\theta = 1 - \sqrt{(1+2I)}$, where I_0 is the initial intensity and I_∞ is the intensity after the steady state. A detailed curve fitting of this experimental data to equation (1) gives the time constant t_c of the thermal decay process. Finally the thermal diffusivity D of the sample can be calculated from the equation $t_c = \omega^2 / 4D$ where ω is the beam radius at the sample position and t_c, the time response to attain the steady state focal length. Similarly TL signal evolution was obtained for CdSe QDs of different pH values and their corresponding cluster size (d) or hydro dynamic particle size, t_c's, θ's, and diffusivity(D)s were obtained and are tabulated in table 1.

Table 1. Data showing pH, θ, time constant and diffusivity of CdSe QDs with error ±0.03.

pH	Hydro dynamic particle size (d) (nm)	θ	t_c (ms)	Diffusivity 10^{-5} cm^2 s^{-1}
3.7	8.4	467.9730	12.9078	0.2451
4.7	10	0.9801	0.0007	4520
7.6	10.1	13.2410	0.7934	3.987
8.9	10.3	103.1097	4.9154	0.6436
9.6	8.5	36.2265	1.9444	1.6272
10	9.2	463.5255	48.2313	0.0656
11	7.9	465.0139	30.0740	0.1052

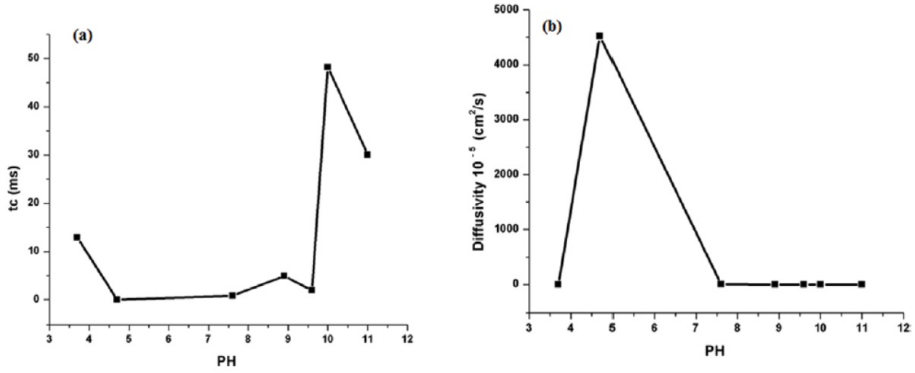

Figure 7. (*a*) t_c of CdSe QDs plotted against pH and (*b*) thermal diffusivity of CdSe QDs plotted against pH.

The observed reduction (from figure 7(*a*)) in t_c at optimum pH could be the effect of shortening the mean free path of the phonons. It has to be noted from table 1. As the pH increased continuously the mean free path of the phonon in the solid increases the value of t_c and thermal diffusivity was reduced. From the figure it is observed that at optimum pH, the t_c value is very small compared to pH other than this. A large enhancement of thermal diffusivity is observed (from figure 7(*b*)) with the sample of pH in the region of ~4.7 Note that thermal diffusivity of the base fluid is nearly constant at different doses of electrolyte salt and acid or base. The enhancement seems to be related only to the particles. When the QDs are dispersed into water, the overall behavior of the particle-water interaction depends on the properties of the particle surface. Experimental results also indicate that the stabilities of these nanofluids are influenced by pH values.

The Derjaguin theory explains the aggregation of aqueous dispersions quantitatively and describes the force between charged surfaces interacting through a liquid medium. It combines the effects of the van der Waals attraction and the electrostatic repulsion due to the so-called double layer of counter ions. According to this, when the pH is increased to the optimized value, (pH less than 4.7) the surface charge increases because of the more frequent attacking of the surface hydroxyl groups and the phenyl sulfonic group by potential-determining ions (H^+, OH^- and the phenyl sulfonic group). This leads to an increase of the electrostatic repulsion force between the particles, and the suspensions show significantly reduced agglomeration and enhanced mobility, ultimately improving the heat transport [21]. When the pH is equal to the isoelectric point (IEP), which is the optimized pH(~4.7) in our case the QDs tend to be unstable, form clusters, and precipitate where IEP is the pH at which a particular molecule or surface carries no net charge. The repulsive forces among metal oxides are zero and QDs coagulate together at this pH value. The resulting big clusters formed at the IEP will trap water and the structures of trapped water vary due to the strong atomic force among QDs. Water is packed well inside and the volume fraction of the QDs will be larger. In addition, the shapes of clusters containing trapped water will not be spherical but rather will have an

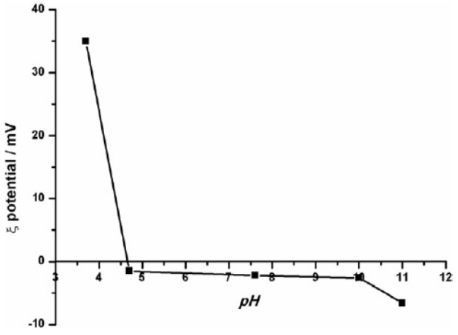

Figure 8. Variation of ξ-potential with pH.

irregular structure like chains. Such a structure favors thermal transport because they provide a long link [22]. Therefore, the overall thermal conductivity and hence the thermal diffusivity of nanofluids are enhanced. When the pH is too large, the concentration of the pH adjustment reagent (NaOH) in the system increases, which causes compression of the electrical double-layer. At pH > 10, the surface charge of QDs increases, which creates repulsive forces between the QDs. As a result of this effect, substantial clustering of Quantum dots is prevented. We calculated the variation of ξ-potential and the cluster radius of the QDs (table 1) as a function of pH by using dynamic light scattering (DLS) measurement. The effect of charge on the clustering process with varying pH has also been plotted in figure 8 which shows an almost neutral charge at optimum pH.

Therefore, it is reasonable to infer that optimizing the pH or a high surface charge facilitates heat transport through increases in transport efficiency. We also attempt to link the concept of this interesting phenomenon of change in thermal diffusivity with pH from the emission intensity in figure 4. The total relaxation cross section (σ_T) = σ_R + σ_{NR}; where σ_R is radiative relaxation and σ_{NR} is the nonradiative relaxation cross section. So that $\sigma_{NR} = \sigma_T - \sigma_R$. From figure 4, at optimum pH value, the fluorescence intensity maximum indicating

maximum fluorescence quantum yield and minimum thermal energy is generated in the medium. Our calculation showed that maximum fluorescence quantum yield is obtained at pH ~ 4.7 where the probe beam (TL signal) intensity is at a minimum. It is also observed in figure 6. This enhanced radiative process will reduce the heat evolved through the nonradiative process. This may cause reduction of t_c which is the time taken to transport heat and hence enhance the magnitude of the diffusion coefficient. The major advantages of such materials are that they can be used as both a coolant and an insulator by adjusting the corresponding pH values. At a low pH (~4.7), they act as a good coolant which can be used to diffuse heat energy to the surroundings, and at a greater pH they can be an efficient material to trap thermal energy and act as good insulators.

4. Conclusion

A thermo-optic study of MSA capped CdSe QDs synthesized by a MWI method shows a significant increase in thermal diffusivity at optimum pH value. It was observed that QDs become unstable and aggregated at pH equal to or close to the isoelectric point and the resulting big clusters that are formed trap water molecules and form long chain like structures. This may be the reason for large enhancement in the thermal diffusivity of nanofluids at optimum pH. When the pH is too large, the repulsive force of the QDs prevents agglomeration and causes a decrease in thermal diffusivity. The reduced nonradiative process at pH ~ 4.7 may also be the reason for the highest diffusion coefficient.

Acknowledgment

The authors acknowledge DST for financial assistance.

References

[1] Gupta P and Ramrakhiani M 2009 *Open Nanosci. J.* **3** 15
[2] Qu L and Peng X 2002 *J. Am. Chem. Soc*. **124** 2049
[3] Srivastava P and Singh K 2012 *Adv. Mater. Lett*. **3** 340
[4] Zedan A F, Sappal S, Moussa S and El-Shall M S 2010 *J. Phys. Chem.* C **114** 19920
[5] Zhu J, Palchik O, Chen S and Gedanken A 2000 *J. Phys. Chem.* B **104** 7344
[6] Ashtaputre S S, Deshpande A, Marathe S, Wankhede M E, Chimanpure J, Pasricha R, Urban J, Haram S K, Gosavi S W and Kulkarni S K 2005 *Pramana J. Phys.* **65** 615
[7] Ganapathy Raman S, Selvarajan P and Ratnam Chidambaradhanu K 2010 *Recent Res. Sci. Technol.* **2** 72
[8] Yu W W, Chang E,Drezek R and Colvin V L 2006 *Biochem. Biophys. Res. Commun.* **348** 781
[9] Peng X, Manna L, Yang W, Wickham J, Scher E, Kadavanich A and Alivisatos A P 2000 *Nature* **404** 59
[10] Wang Y, Lu J-P and Tong Z-F 2010 *Mater. Sci*. **33** 543
[11] Chu M, Shen X and Liu G 2006 *Nanotechnology* **17** 444–9
[12] Rogach A L, Nattatri R, Ostrander J W, Giersig M and Kotov N A 2000 *Chem. Mater.* **12** 2676
[13] Li X F, Zhu D S and Wang X J 2007 *J. Colloid Interface Sci.* **310** 456
[14] Nguyen C T, Desgranges F, Roy G, Galanis N, Mare T, Boucher S and Angue M H 2007 *Int. J. Heat Fluid Flow* **28** 1492
[15] Shen J, Lowe R D and Snook R D 1992 *Chem. Phys*. **165** 385
[16] Bindhu C V, Harilal S S, Nampoori V P N and Vallabhan C P G 1998 *Opt. Eng*. **37** 2791–4
[17] Ani Joseph S, Hari M, Mathew S, Sharma G, Soumya V M, Hadiya P, Radhakrishnan P and Nampoori V P N 2010 *Opt. Commun.* **283** 313
[18] Dong M, Xu J, Liu S, Zhou Y and Huang C 2014 *Luminescence* at press (doi:10.1002/bio.2626)
[19] Zhang H, Zhou Z and Yang B 2003 *J. Phys. Chem.* B **107** 8–13
[20] Xu S, Wang C, Xu Q, Zhang H, Li R, Shao H, Lei W and Cui Y 2010 *Chem. Mater*. **22** 5838–44
[21] Younes H, Christensen G, Luan X, Hong H and Smith P 2012 *J. Appl. Phys.* **111** 064308
[22] Xian-Ju W and Xin-Fang L 2009 *Chin. Phys. Lett*. **26** 056601

IOP Publishing | Astro Ltd Laser Physics Letters

Laser Phys. Lett. **12** (2015) 025006 (4pp) doi:10.1088/1612-2011/12/2/025006

Enhanced random lasing from a colloidal CdSe quantum dot-Rh6G system

Anju K Augustine, P Radhakrishnan, V P N Nampoori and M Kailasnath

International School of Photonics, Cochin University of Science and Technology, Kochi-682022, India

E-mail: srrosmin2009@gmail.com

Received 19 November 2014
Accepted for publication 19 December 2014
Published 9 January 2015

Abstract

In this letter, we report random laser action in a system where optical amplification is provided by colloidal CdSe quantum dots (CQDs) triggered by the emission from Rhodamine 6G. The laser emission from CdSe QDs is optically excited by Rh-6G which in turn is photo-pumped by a frequency-doubled Q-switched Nd:YAG laser system at an excitation wavelength of 532 nm. At intensities greater than the threshold value, laser emission is characterized by narrowing peaks.

Keywords: colloidal quantum dots, threshold, random laser

(Some figures may appear in colour only in the online journal)

1. Introduction

In this photonic era, random lasers have received great attention due to their low cost and easy fabrication without the need for extra cavities. There are many challenges in obtaining random lasing as high optical gain and strong scattering have to be achieved simultaneously. In random lasers, light generation and subsequent stimulated emission takes place within a multiple-scattering medium with optical gain. In this system of random lasers, QDs can act as coherent light sources for amplified laser emission above a particular light threshold. For the amplification of the emitted light we do not use any of the conventional optical resonators employed in a laser system [1–5]. The unique properties of such random lasers provide applications in areas such as new generation display devices, sensors, optical coding of objects, random number generators and medical diagnostics, etc. In this era, random laser phenomena have been studied in many systems including organic and inorganic QDs, such as Rhodamine 640 with TiO_2 particles [6], ZnO powder in polystyrene and polymethyl methacrylate film etc [7, 8]. CdSe QDs exhibit tunable emission characteristics with particle size. These optical size-dependent emission properties offer great potential for fabricating new types of laser devices using these materials. As random laser action relies on the combined effects of multiple scattering and optical amplification, colloidal quantum dots (CQDs), particularly CdSe CQDs, provide an attractive material system for such applications. In this work, we report random laser action in CQDs of CdSe with Rhodamine 6G where CdSe QDs are used as the optical gain media as well as strong scattering centers. Feedback for the photons generated by Rh6G is provided by the random multiple scattering by CdSe QDs.

2. Experimental details

Colloidal solutions of CdSe QDs were prepared by the microwave irradiation method. The precursors used are $CdCl_2{\cdot}H_2O$ and Na_2SeO_3. The capping agent used is mercaptosuccinic acid (MSA). Microwave irradiation gives the required thermal energy to the reaction. The power of the reaction system is maintained at 60 W. The buffer solution with pH ~7 is prepared with sodium borate and citric acid in water. The precursors are added into the buffer with constant stirring. The PH of the corresponding colorless solution is adjusted by adding 1M NaOH. The molar ratio of the precursors and MSA is 4:1:12 respectively. During the reaction, the color of the solution gradually changed and QDs started to form and aliquots were taken out of the flask for optical measurements to monitor the growth of the QDs. About 50% by volume of the dye solution (Rh-6G) of concentration 10^{-4} is added to it and allowed to mix. A sample is taken in a one mm cuvette for the experiment. For the random laser experiments, the CQD sample was photo-pumped by a frequency-doubled Q-switched Nd:YAG laser yielding 7 ns pump pulses at an excitation wavelength

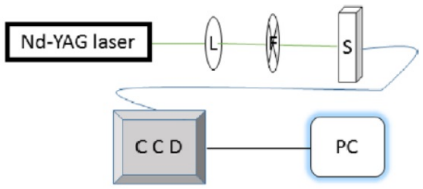

Figure 1. The experimental setup is shown with an Nd–YAG laser, L—cylindrical lens, F—filter, S—sample in cuvette, CCD—charge coupled device.

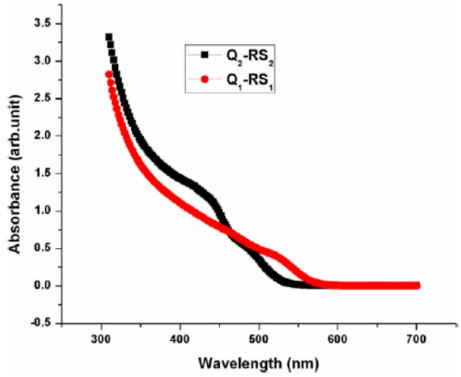

Figure 2. Absorption spectra of the QDs used for samples R-S1 and R-S2 are denoted as Q_1-RS_1 and Q_2-RS_2 respectively.

of 532 nm. A cylindrical lens was aligned to shape the pump beam as a stripe having dimensions of 10 × 3 mm^2. The focused laser pump stripe was horizontal and the pump fluence could be adjusted with the help of a neutral density filter. Emission from the sample could be collected and recorded with an optical fiber connected to a multi-channel grating-CCD spectrometer. The spectral resolution of the spectrometer is 0.03 nm.

The experimental setup is shown in figure 1.

In this letter, the Rh 6G sample alone is referred to as R and the sample with ~ 3 nm average-sized CdSeQDs along with Rh6G is labeled as R-S1 and R-S2 is the sample with a ~ 2.5 nm average size.

The average size of these QDs is measured using the dynamic light-scattering method.

3. Results and discussion

The observed absorption spectra of the QDs selected for samples R-S1 & R-S2 are shown in figure 2 and it is observed that the intensity of the emission gets enhanced by the addition of CdSe CQDs to the Rhodamine 6-G dye solution. Varying the input power also increases the emission intensity and it is given in figures 3(*a*)–(*d*) in respect of sample R-S2 which shows much better intensity.

Figures 4 and 5 show a typical emission spectrum collected at varying excitation intensities for samples of R-S_1 and R-S2 respectively. We observe that at relatively low excitation intensities, the spectrum exhibits a broad spontaneous emission (~ 3 nm). By increasing the pump intensities more and more, intense narrow discrete spikes occur with a line width of ~0.03 nm and once the pump intensity exceeds a certain threshold, a much narrower emission spectrum is obtained which is shown in figure 5. The abrupt increase of the integrated intensity indicates the achievement of random lasing with a threshold of 240 mW in the case of R-S2. The direction in the emission radiation is about 90° from the pump. The physical process behind the increase in the emission intensity with R-S_2 may be due to the presence of a large number of defects in the CdSe nano-particles with this size. Non-radiative recombination of the excited carriers is significant below the lasing threshold in this case. Above the lasing threshold, the fast stimulated emission process makes the radiative recombination of the excited carriers dominate over the non-radiative recombination. This results in a rapid increase in the emission intensity. It may also be due to the suppression of the Auger recombination and the enhanced surface passivation of the transfer of energy to the QDs. It is observed from figure 5 that the emission peak gets shifted to higher energy regions as the pump power increases. We can explain this from the broad absorption cross section of the dye molecule. And at higher pump power, the amplitude-stimulated emission of the dye gets shifted to the blue region due to the emission from higher energy levels. Thus, the QDs which exit with this emission of dye molecule are normally shifted to the blue side.

In order to explain the random lasing action from such a material we could classify it into two categories viz., incoherent random lasing and coherent random lasing, based on the feedback mechanism. In the case of incoherent random lasing, there is only intensity or energy feedback and the spectral shape is attributed to a narrowing peak at the gain maximum with a linewidth of several nanometers, while the feedback for coherent random lasing is provided by the field or amplitude mechanism, where closed optical loops are formed by the interference of multiple scattering and these act as ring cavities. Discrete super-narrow peaks or spikes with a linewidth of usually less than 1 nm will appear in coherent random lasing [9–12]. Based on this, we can attribute the lasing action from our system of colloidal CdSe QDs with Rh-6G to be coherent random lasing. Due to different losses of these random ring cavities, the threshold for the laser action in individual cavities is different. Under higher pumping intensities, more ring cavities can meet the threshold requirements and thus more spikes are developed, which agrees with our results. The feedback for lasing in this system is expected to be due to scattering from CdSe QDs. Many of the clusters with sizes of tens of nanometers are formed during the mixing of colloidal QDs with the dye. These clusters act as scattering centers for the emitted photoluminescent light to form optically closed loops, which is the main factor in the lasing action of such a random medium [13–15]. Here, colloidal CdSe QDs serve as both a gain medium and scattering centers. It is possible to

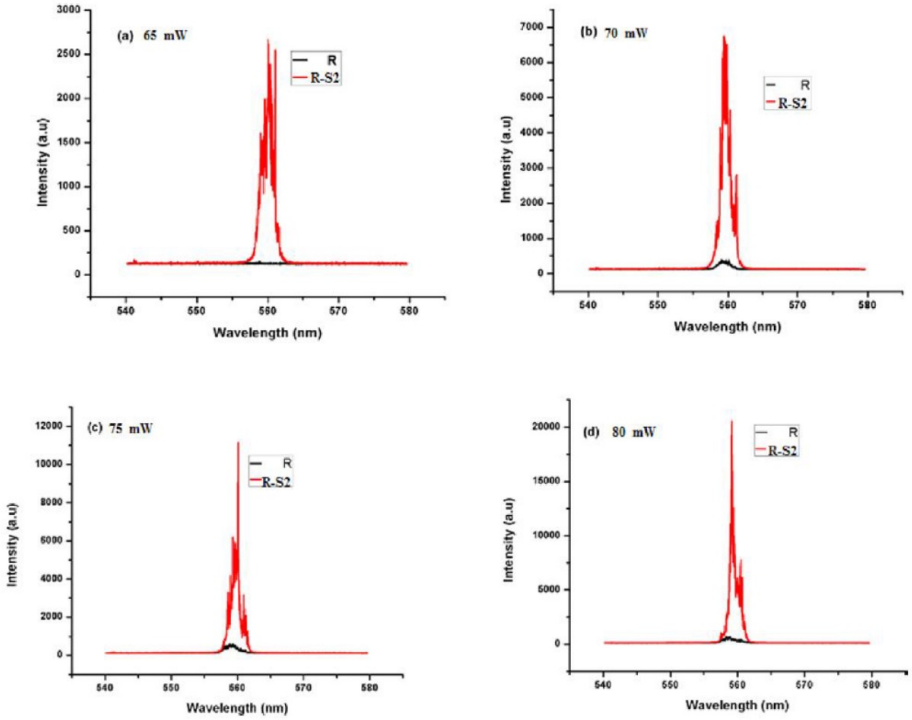

Figure 3. Comparison of emission spectra of the sample (R-S2) and bare Rh-6G at varying power levels.

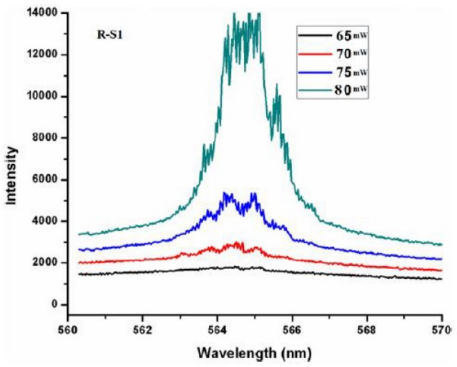

Figure 4. Emission spectrum of R-S_1 with variation of power.

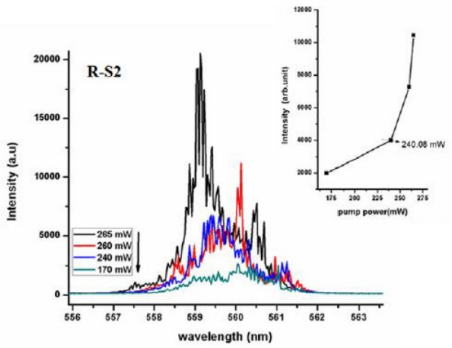

Figure 5. Emission spectrum of R-S_2 with variation of power.

find the path length in terms of the excitation wavelength λ i.e. $\Delta\lambda = \lambda^2/(2nL)$ where n is the refractive index and L is the cavity length and $\Delta\lambda$ is the small change in wavelength obtained. We find the cavity length as 5×10^{-4} while the cavity length of the cuvette used for our sample is 1 mm. Here, we assume that the multiple random resonances are being excited by the non-Lorentzian line shape of the emission peak [12] and are not from the resonating cavity formed by the cuvette. The plot of the peak emission intensity *versus* the pump intensity shown in the inset of figure 5 exhibits a soft threshold curve at 240 mW, which is due to a significant amount of spontaneous emission coupled into the laser mode. The full width

half maximum of the emission peak drops from ~ 3 nm below threshold to 0.3 nm above 240 mW, indicating laser action.

4. Conclusion

In summary, we have demonstrated random laser action in a CQD CdSe–Rhodamine 6G system. The laser is random in the sense that the feedback for the emission generated by the Rhodamine 6 G dye is provided by the random multiple scattering of light from the CdSe QDs. Spectra were recorded to study the process of the laser emission from this system and the results show enhanced emission from the CdSe CQDs compared to that from the bare dye. These lasers could open the door for unconventional sources to be used in a wider range of commercial applications such as document security, remote sensing, ultra-fast displays and diagnostic imaging.

Refrences

[1] Chen Y, Herrnsdorf J, Guilhabert B, Zhang Y, Watson I M, Gu E, Laurand N and Dawson M D 2011 *Opt. Express* **19** 2996–3003

[2] Wu Z, Mi Z, Bhattacharya P, Zhu T and Xu J 2007 *Appl. Phys. Lett.* **90** 171105

[3] Bose R, Yang X D, Chatterjee R, Gao J and Wong C W 2007 *Appl. Phys. Lett.* **90** 111117

[4] Xu J and Xiao M 2005 *Appl. Phys. Lett.* **87** 173117

[5] Yang M, Heo J, Zhu T, Xu J, Topolancik J, Vollmer F, Ilic R and Bhattacharya P 2008 *Appl. Phys. Lett.* **92** 261110

[6] Lawandy N M, Balachandran R M, Gomes A S L and Sauvain E 1994 *Nature* **368** 436–8

[7] Cao H, Zhao Y G, Ho S T, Seelig E W, Wang Q H and Chang R P H 1999 *Phys. Rev. Lett.* **82** 2278–81

[8] Zhao X, Wu Z, Ning S, Liang S, Wang D and Hou X 2011 *Opt. Express* **19** 16126–31

[9] Wang Y, Ta V D, Gao Y, He T C, Chen R, Mutlugun E, Demir H V and Sun H D 2014 *Adv. Mater.* **26** 2954–61

[10] Cerdán L, Enciso E, Martín V, Bañuelos J, López-Arbeloa I, Costela A and Garcia-Moreno I 2012 *Nat. Photon.* **6** 621

[11] Cao H, Zhao Y G, Ho S T, Seelig E W, Wang Q H and Chang R P H 1999 *Phys. Rev. Lett.* **82** 2278

[12] Wiersma D S 2008 *Nat. Phys.* **4** 359–67

[13] Polson R C, Raikh M E and Vardeny Z V 2003 *IEEE J. Sel. Top. Quantum Electron.* **9** 120–3

[14] Boucher Y and Féron P 2009 *Opt. Commun.* **282** 3940–7

[15] Klimov V I, Mikhailovsky A A, McBranch D W, Leatherdale C A and Bawendi M G 2000 *Science* **287** 1011–13

Hindawi Publishing Corporation
Journal of Nanoscience
Volume 2014, Article ID 623742, 7 pages
http://dx.doi.org/10.1155/2014/623742

Research Article

Size Dependent Optical Nonlinearity and Optical Limiting Properties of Water Soluble CdSe Quantum Dots

Anju K. Augustine, S. Mathew, P. Radhakrishnan, V. P. N. Nampoori, and M. Kailasnath

International School of Photonics, Cochin University of Science and Technology, Cochin, Kerala 682022, India

Correspondence should be addressed to Anju K. Augustine; srrosmin2009@gmail.com

Received 4 July 2014; Accepted 4 November 2014; Published 26 November 2014

Academic Editor: Fengqiang Sun

We present third-order optical nonlinear absorption in CdSe quantum dots (QDs) with particle sizes in the range of 4.16–5.25 nm which has been evaluated by the Z-scan technique. At an excitation irradiance of 0.54 GW/cm^2 the CdSe QDs exhibit reverse saturation indicating a clear nonlinear behavior. Nonlinearity increases with particle size in CdSe QDs within the range of our investigations which in turn depends on the optical band gap. The optical limiting threshold of the QDs varies from 0.35 GW/cm^2 to 0.57 GW/cm^2 which makes CdSe QDs a promising candidate for reverse-saturable absorption based devices at high laser intensities such as optical limiters.

1. Introduction

Before the advent of lasers, transparent optical materials were assumed to be essentially passive unaffected by the light travelling through them. The high powers of laser beams made it possible to observe that the effect of light on a medium can indeed change its properties such as refractive index or absorption. These are optical nonlinear phenomena. When this happens, the light itself gets affected by this change in a nonlinear way; for example, the nonlinear response of the material can convert the laser light into new colours, both harmonics of the optical frequency and sum and difference frequencies. With the development of optical communication networks, various nonlinear optical (NLO) devices such as optical switches, optical limiters, optical detectors, and optical sensors have attracted considerable attention because of their widespread usage for scientific and industrial purposes. Among all the NLO properties, optical limiting is one of the most promising practical applications, as it can protect the human eye and photosensitive components from damage caused by intense optical radiation [1, 2]. Optical limiting results from irradiance-dependent NLO responses of materials in which the incoming intense light alters the refractive and absorptive properties, resulting in a greatly reduced transmitted intensity. It is important to select suitable materials as optical limiting media by determining the magnitude of their nonlinearity. Organic materials characterized by large NLO responses are of major interest owing to their large NLO susceptibilities, fast response time, architectural flexibility, low cost, and ease of fabrication [3, 4].

In recent years, interest in the synthesis, characterization, and application of colloidal quantum dot (QD) semiconductor materials has grown markedly. QDs of cadmium selenide (CdSe) are by far the most studied system among all the semiconducting nanocrystals. The bulk CdSe has a direct band gap of 1.74 eV at 300 K and a typical Bohr exciton diameter of around 5.6 nm [5]. Consequently, CdSe QDs show sizable quantum confinement effects with remarkably different optical properties. The size dependent, unusual optical and electronic properties of these QDs have been studied in detail using a wide variety of experimental and theoretical techniques. The linear optical properties of CdSe QDs depend strongly on particle size; for example, the blue shift of excitonic absorption and emission peaks with decreasing particle size is a well-known observation. The unusual properties of the QDs, in the quantum-confined regime, have led to numerous technological applications.

In the past decade, there has been increasing interest in the luminescent and nonlinear optical properties of these nanometer-sized QDs. Large optical nonlinearities in CdSe QDs have been reported using different techniques. These techniques include degenerate four-wave mixing and Z-scan

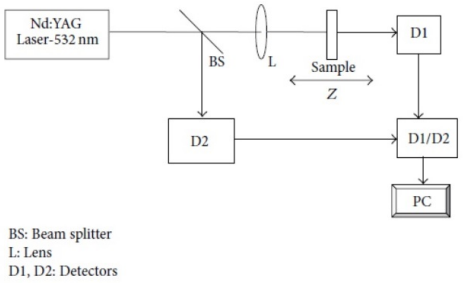

FIGURE 1: Z-scan experimental setup.

techniques with nanosecond and picosecond laser pulses. Z-scan, especially, is an effective technique to investigate nonlinear absorption and nonlinear refraction. An ideal optical limiter, by definition, is a device that exhibits a linear transmittance below a threshold and clamps the output to a constant above it, thus providing safety to sensors and the eyes. A wide range of materials contributing to the optical limiting and nonlinear absorption has been investigated. It is well known that optical limiting devices rely on one or more of the nonlinear optical mechanisms such as excited state absorption, free carrier absorption, two-photon absorption (TPA), thermal defocusing/scattering, photorefraction, nonlinear refraction, and induced scattering with enhancement in limiting performance by coupling two or more of such mechanisms [6–8].

In this paper, we present the study of the effect of size on the nonlinear optical properties of CdSe QDs and estimate the nonlinear absorption coefficient β of CdSe QDs at different particle size at 532 nm. These CdSe QDs exhibit reverse saturable absorption (RSA), in which the excited state absorption cross section is higher than the ground state absorption cross section. The origin of the third-order nonlinearity predicted from Z-scan studies is attributed to resonant two-photon absorption (TPA). We also report the limiting threshold as a function of the particle size of CdSe QDs.

2. Experimental

In the present work, CdSe NPs were prepared by a modified aqueous method using reflux [9, 10]. The precursors used are $CdCl_2 : H_2O$ and Na_2SeO_3. The capping agent used was mercaptosuccinic acid (MSA). The molar ratio of the precursors and MSA is 4 : 1 : 12, respectively. The buffer solution [11] with pH~7 is prepared with sodium borate and citric acid in water. The precursors were added to the buffer with constant stirring. The pH of the corresponding colourless solution is adjusted by adding 1 M NaOH. It was placed in a three-necked flask followed by reflux at 100°C in open-air conditions. Reflux process gives the required thermal energy to the reaction. The colour of the solution turned to bright yellow after a few minutes of reflux. The temperature of the reaction system was maintained at 100°C. During the reflux, the colour of solution gradually changed and NPs started to form and aliquots were taken out of the flask at different times for the optical measurements to monitor the growth of the QDs. The particles tend to form agglomerates due to the strong interaction of the carboxylic groups [11] leading to a possible overestimation of the mean size distribution.

Absorption spectra of the prepared CdSe QDs were recorded using UV-Visible Spectrophotometer (Jasco V-570 UV/VIS/IR). Fluorescence spectra of QDs were obtained on a Cary Eclipse Fluorescence Spectrophotometer (Varian). The excitation wavelength was kept at 390 nm, and the emission spectra were recorded. All absorption and fluorescence spectra were measured without any postpreparative size separation. The structural properties of the samples were investigated by X-ray diffraction (XRD) on a Bruker AXS D8 Advance X-ray diffractometer with Ni-filtered Cu Kα (1.5406 Å) source. The electron micrograph images of CdSe QDs in colloidal form were taken using transmission electron microscope (Philips Tecnai G2 at 120 kV). The FT-IR spectra of the samples were recorded using Thermo *NICOLET 380 FTIR* Spectrometer by means of KBr pellet procedure. Nonlinear absorption coefficient (β) and optical limiting threshold of the samples were calculated using open aperture Z-scan technique employing an Nd-YAG laser (532 nm, 7 ns, 10 Hz). The experimental setup is shown in Figure 1.

3. Results and Discussion

For detailed study, we used samples taken after reflux times of 10 minutes, 1 hour, and 3 hours and they are denoted by C_1, C_2, and C_3, respectively. The variation in absorption peak and the corresponding optical energy band gap (inset) of samples (C_1, C_2, and C_3) are shown in Figures 2(a), 2(b), and 2(c).

Energy band gap of the QDs shows a variation from 2.51 eV to 2.34 eV as the particle size increased during the reflux time from 10 minutes to 3 hours. It is observed that as particle size increases, absorption peak shifts to higher wavelength side and the band gap is enhanced with decrease in particle size. The emission spectra of the C_1, C_2, and C_3 samples are also shown in Figure 3.

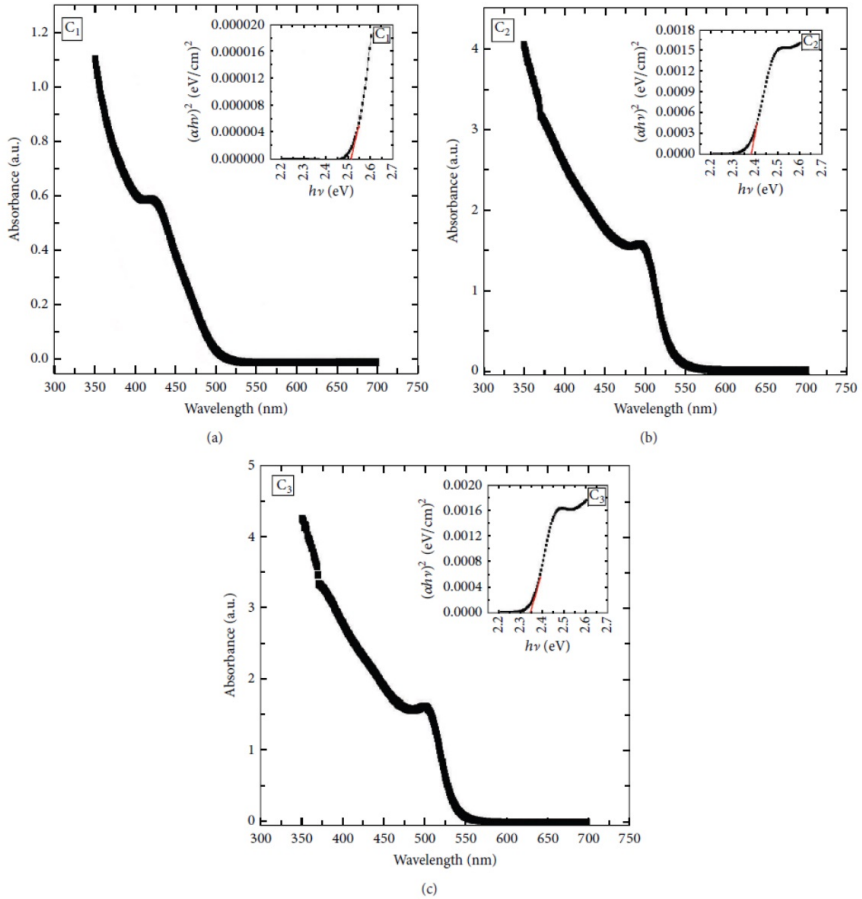

FIGURE 2: ((a), (b), and (c)) The variation in absorption peak and the corresponding optical energy band gap (inset) of samples (C_1, C_2, and C_3).

The particle size is calculated with effective mass approximation [12]. For CdSe, $E_g^{\text{bulk}} = 1.74$ eV, $\epsilon = 10.6$, $m_e^* = 0.13$, $m_h^* = 0.45$:

$$E_g^{\text{nano}} = E_g^{\text{bulk}} + \frac{h^2}{2m_0 d^2}\left(\frac{1}{m_e^*} + \frac{1}{m_h^*}\right) - \frac{36e^2}{4\pi\epsilon\epsilon_0 d}, \quad (1)$$

where d is the particle diameter. The calculated particle size of these QDs is presented in Table 1. A typical XRD spectrum of CdSe QDs is shown in Figure 4 and the average particle size (d) can be measured using Scherrer equation $d = 0.9\lambda/(B\cos\theta)$, where B is the full width at half maximum of the peak.

The calculated average particle size is about 4 nm for the powdered sample. The peak observed at 2θ (hkl) values of 27° (101), 35° (102), 41° (110), 50° (201), and 55° (202) planes shows the existence of CdSe hexagonal phase (JCPDS file no. 01-071-2554).

Figure 5(a) shows histogram and TEM image of C_3 sample with average particle size of 4.09 nm. It shows that the particles formed are in spherical shape and average particle size is calculated to be 4.09 nm. Figure 5(b) represents HRTEM image of C_3 sample which suggests that the prepared

Table 1: Data showing particle size, energy band gap, nonlinear absorption coefficient (β), optical limiting threshold, and imaginary part of susceptibility (Im $\chi^{(3)}$) of the samples (C_1, C_2, and C_3).

Sample	Particle size (nm)	Energy B.G (eV)	β (m/W)	Optical limiting threshold (GW/cm^2)	Im $\chi^{(3)} \times 10^{-11}$ (e.s.u)
C_1	4.17	2.52	0.27×10^{-10}	0.57	0.16
C_2	4.96	2.38	0.69×10^{-10}	0.48	0.41
C_3	5.25	2.34	2.47×10^{-10}	0.35	1.45

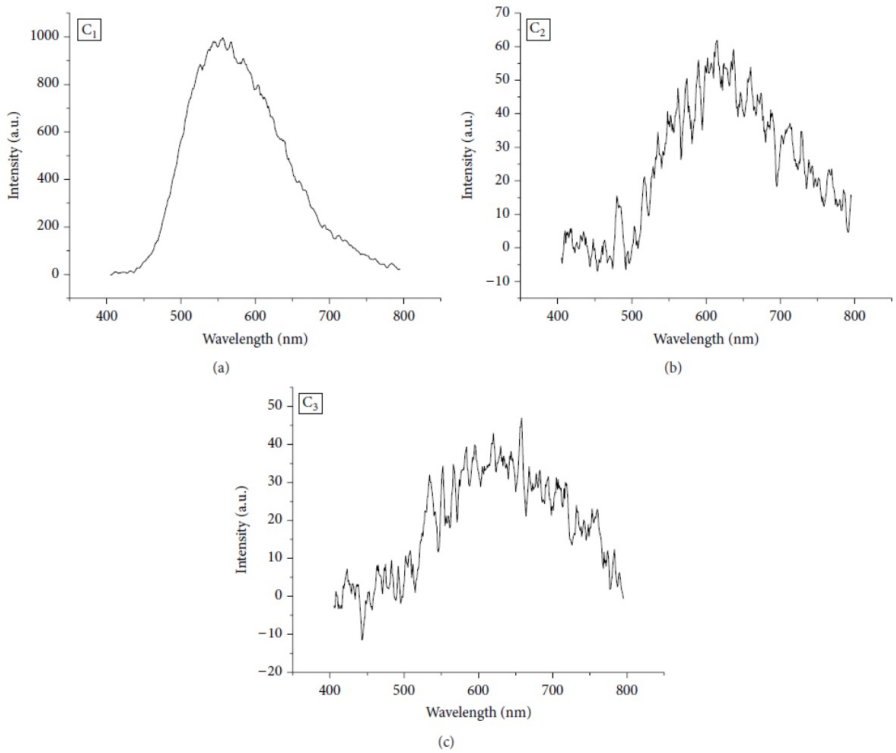

Figure 3: The emission spectra of C_1, C_2, and C_3 samples under the excitation wavelength of 390 nm.

CdSe QDs have good crystallinity and this may enable them to possess high-quality optical property.

FTIR spectrum of the C_3 sample is shown in Figure 6. A broad peak at 3430 cm^{-1} is assigned to –OH stretching. The Cd–Se band stretching can be observed at ~843 cm^{-1}. The double peaks of the carboxylate vibration at 1587 cm^{-1} (in the range 1540–1650 cm^{-1}, asymmetric) and 1403 cm^{-1} (in the range 1360–1450 cm^{-1}, symmetric) in the spectra of CdSe particles show that the organics exist as carboxyl salts on the particle surface. The peak position of this doublet is similar to that observed for other mercaptocarboxylic salts.

The nonlinear optical characterization of the samples was carried out using the Z-scan technique at 532 nm [13, 14]. The samples to be investigated were translated through the focal point of a lens of focal length of 20 cm. The beam waist radius ω_0 was estimated to be 35.4 μm. The Rayleigh length $Z_0 = \pi\omega_0^2/\lambda$ was calculated to be 7.4 mm. The samples were taken in a 1 mm cuvette which is much less than Z_0 which is an essential prerequisite for Z-scan experiment. The normalized transmittance for TPA in the open aperture condition is given by [15]

$$T(Z, s = 1) = \frac{1}{\sqrt{\pi} q_0(Z, 0)} \int_{-\infty}^{+\infty} \ln\left[1 + q_0(Z, 0)\, e^{-\tau^2}\right] d\tau, \quad (2)$$

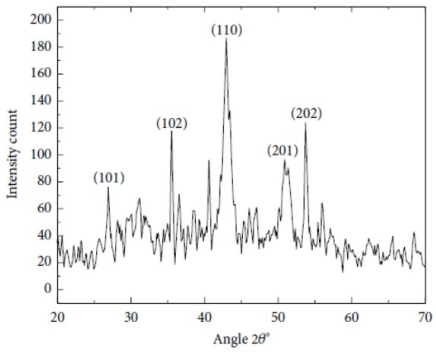

FIGURE 4: XRD spectra of C_3 sample with the average radius of the particle being 4 nm.

where

$$q_0(Z,0) = \frac{\beta I_0 L_{\text{eff}}}{\left(1 + Z^2/Z_0^2\right)}. \tag{3}$$

The parameter q_0 is the depth of the open aperture Z-scan curve obtained from the theoretical fit and it is the measure of the intensity dependent absorption. Here, I_0 is the laser intensity in the focal plane, β is the nonlinear optical absorption coefficient, and L_{eff} is the effective thickness with linear absorption coefficient α.

L_{eff} is given by

$$L_{\text{eff}} = \frac{\left(1 - e^{-\alpha l}\right)}{\alpha}. \tag{4}$$

The open-aperture curve exhibits a normalized transmittance valley at the focal point, indicating the presence of reverse saturable absorption (RSA) in the nanocolloidal solutions. The open aperture Z-scan plot for samples having different particle size is depicted in Figure 7. The fits of (2) to experimental data are shown as solid curves.

The data can be fitted well by assuming two-photon absorption (TPA) in the nonlinear optical absorption process. From this fit, we can confirm that the basic mechanism involved in the nonlinear absorption of nanocolloidal solutions of CdSe QDs is TPA process because the photon energy of the 532 nm laser is within the range $E_g < 2h\nu < 2E_g$, where $h\nu = 2.33$ eV [15]. The nonlinear absorption coefficient (β) calculated from the above fits shows a dependence on the particle size of the QDs. The experimental data show that β value increases with increasing particle size. With a small decrease in the band gap, a significant increase in the nonlinear absorption is observed. In order to explain the optical nonlinearity, we mainly consider the band gap variation of CdSe QDs samples (C_1, C_2, and C_3).

C_1 and C_2 samples have band gap very near to 2.4 (2.39 ± 0.02) and 2.5 (2.52 ± 0.02), respectively, which is more than one-photon energy corresponding to 532 nm. The data fitting shows that the nonlinear optical absorption is through two-photon absorption process in these samples. Our studies show that sample C_3has large optical nonlinearity (2.47×10^{-10} m/W) enhancement, compared to other samples as seen in Figure 7.

Band gap corresponding to this sample is 2.33 eV to 2.33 ± 0.02 eV which is very near to the one-photon energy corresponding to 532 nm (2.33 eV). The fact that optical nonlinearity in this case is also due to the two-photon absorption reveals that two-photon excitation cross section is enhanced due to resonant one-photon absorption level. A small mismatch between band gap of sample C_3 and one by photon energy will be compensated by phonon-assisted excitation. The enhancement also arises due to increased optical nonlinear interaction between the radiations and the particles. This can be explained by the fact that, with increase in particle size, there is an increase in the multiple scattering from the QDs. This increase in multiple scattering leads to large effective interaction length which in turn results in an enhancement in nonlinear absorption [14].

The open Z-scan scheme was also used to measure $\text{Im}\,\chi^{(3)}$. The imaginary part of third-order susceptibility, $\text{Im}\,\chi^{(3)}$, is related to β through the following equation:

$$\text{Im}\,\chi^{(3)} = \frac{n_0^2 C^2 \beta}{240\pi^2 \omega}, \tag{5}$$

where $n_0 = 2.34$ is the linear refractive index of CdSe, C is the velocity of light in vacuum, and ω is the angular frequency of the radiation used. The measured values of optical band gap for different particle size and nonlinear absorption coefficient at a wavelength of 532 nm for input laser power density of 0.54 GW/cm^2 are given in Table 1.

To study the optical limiting property of the sample, the nonlinear transmission of the sample is measured as a function of input fluence. Optical power limiting is effected through the nonlinear optical processes of the sample. An important term in the optical limiting study is the optical limiting threshold. Optical limiters are essentially those systems which transmit light at low input fluence or intensities but become opaque at high inputs. The optical limiting property is mainly found to be absorptive nonlinearity, which corresponds to the imaginary part of third-order susceptibility [16]. From the values of fluence at focus, the fluence values at other positions could be calculated using the standard equations for Gaussian beam waist. Such plots give a better comparison of the nonlinear absorption or transmission in the sample and are generated from Z-scan trace. Figure 8 illustrates the optical limiting response of the samples (C_1, C_2, and C_3).

The line in Figure 8 indicates the approximate fluence at which the normalized transmission begins to deviate from linearity. The fluence value corresponding to the onset of optical limiting (optical limiting threshold) is found to vary from 0.35 GW/cm^2 to 0.572 GW/cm^2 for the samples with input fluence of 0.54 GW/cm^2. Our work shows that the semiconductor nanomaterial which has got a one-photon resonant absorption can be employed for third-order optical nonlinear material in which two-photon absorption will get

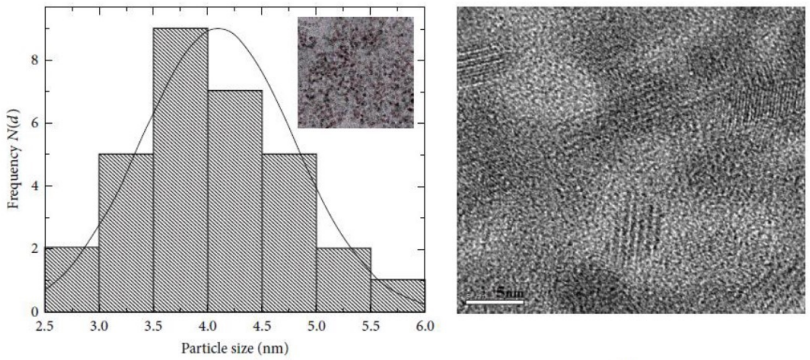

FIGURE 5: (a): Histogram and TEM image of C_3 sample with average particle size of 4.09 nm. (b) HRTEM image of C_3 sample.

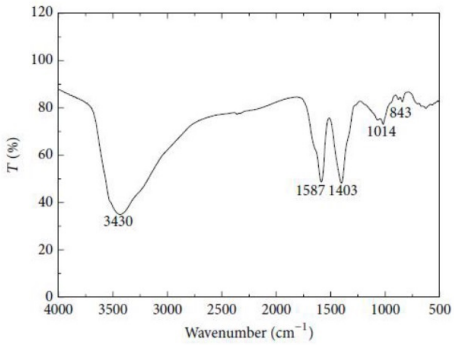

FIGURE 6: FTIR spectrum of the C_3 sample.

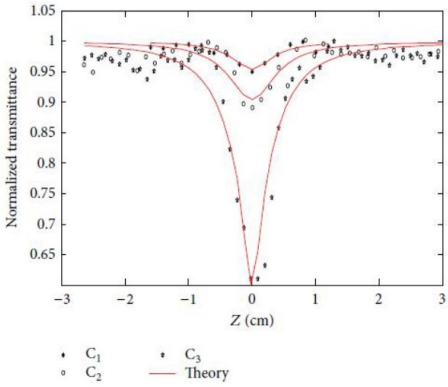

FIGURE 7: The open aperture Z-scan plot for different particle sizes of CdSe QDs (C_1, C_2, and C_3).

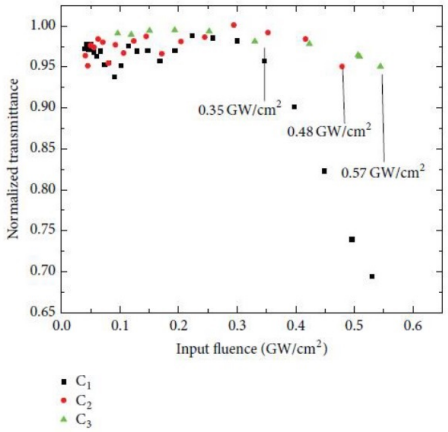

FIGURE 8: Optical limiting response of the samples (C_1, C_2, and C_3).

enhanced by the one-photon resonance energy level (Table 1). Such materials are useful as optical limiters with low threshold energy. Thus, it is clear from Figure 8 that the CdSe quantum dots with large particle size can be used for optical power limiting at high laser fluences. Thus, size of QDs has a significant effect on limiting performance.

4. Conclusion

To conclude, a simple synthetic route described in this paper permits the synthesis of high-quality CdSe QDs of different particle size in aqueous solution. The MSA-capped CdSe QDs possess a tuning effect in particle size and in band gap. Linear and nonlinear optical properties were studied using optical

absorption, fluorescence spectroscopy, and open aperture Z-scan technique. The nonlinear absorption in the nanocolloidal solution can be attributed to the phenomenon of two-photon absorption. The measured β values were found to enhance with decrease in optical energy gap. Our work shows that the semiconductor nanomaterial which has got a one-photon resonant absorption can be employed for third-order optical nonlinear material in which two-photon absorption will get enhanced by the one-photon resonance energy level.

Conflict of Interests

The authors declare that there is no conflict of interests regarding the publication of this paper.

Acknowledgments

The authors acknowledge DST for financial assistance and SAIF-STIC for XRD analysis.

References

[1] H. Fan, X. Wang, Q. Ren et al., "Investigation of the nonlinear absorption and optical limiting properties of two $[Q]_2[Cu(C_3S_5)_2]$ compounds," *Optics and Laser Technology*, vol. 42, no. 5, pp. 732–736, 2010.

[2] I. Gerdova and A. Hache, "Third-order non-linear spectroscopy of CdSe and CdSe/ZnS core shell quantum dots," *Optics Communications*, vol. 246, no. 1–3, pp. 205–212, 2005.

[3] D. Maikhuri, S. P. Purohit, and K. C. Mathur, "Linear and nonlinear intraband optical properties of ZnO quantum dots embedded in SiO_2 matrix," *AIP Advances*, vol. 2, no. 1, Article ID 012160, 2012.

[4] N. Venkatram, R. S. S. Kumar, and D. Narayana Rao, "Nonlinear absorption and scattering properties of cadmium sulphide nanocrystals with its application as a potential optical limiter," *Journal of Applied Physics*, vol. 100, no. 7, Article ID 074309, 2006.

[5] R. W. Meulenberg, J. R. I. Lee, A. Wolcott, J. Z. Zhang, L. J. Terminello, and T. van Buuren, "Determination of the exciton binding energy in CdSe quantum dots," *ACS Nano*, vol. 3, no. 2, pp. 325–330, 2009.

[6] A. Patra, N. Venkatram, D. Narayana Rao, and T. P. Radhakrishnan, "Optical limiting in organic molecular nano/microcrystals: nonlinear optical effects dependent on size distribution," *Journal of Physical Chemistry C*, vol. 112, no. 42, pp. 16269–16274, 2008.

[7] W. Sun, C. M. Lawson, G. M. Gray, C. Zhan, and D. Wang, "Degenerate four-wave mixing and Z-scan measurements of stilbazolium derivatives," *Applied Physics Letters*, vol. 78, no. 13, pp. 1817–1819, 2001.

[8] S. Mathew, A. D. Saran, B. Singh Bhardwaj et al., "Size dependent optical properties of the CdSe-CdS core-shell quantum dots in the strong confinement regime," *Journal of Applied Physics*, vol. 111, no. 7, Article ID 074312, 2012.

[9] X. Chen, J. L. Hutchison, P. J. Dobson, and G. Wakefield, "Highly luminescent monodisperse CdSe nanoparticles synthesized in aqueous solution," *Journal of Materials Science*, vol. 44, no. 1, pp. 285–292, 2009.

[10] B. Su, D. J. Fermin, J. P. Abid, N. Eugster, and H. H. Girault, "Adsorption and photoreactivity of CdSe nanoparticles at liquid—liquid interfaces," *Journal of Electroanalytical Chemistry*, vol. 583, no. 2, pp. 241–247, 2005.

[11] A. L. Rogach, A. Kornowski, M. Gao, A. Eychmüller, and H. Weller, "Synthesis and characterization of a size series of extremely small thiol-stabilized CdSe nanocrystals," *The Journal of Physical Chemistry B*, vol. 103, no. 16, pp. 3065–3069, 1999.

[12] L. Brus, "Zero-dimensional "excitons" in semiconductor clusters," *IEEE Journal of Quantum Electronics*, vol. 22, no. 9, pp. 1909–1914, 1986.

[13] A. Thankappan, S. Thomas, and V. P. N. Nampoori, "Effect of betanin natural dye extracted from red beet root on the non linear optical properties ZnO nanoplates embedded in polymeric matrices," *Journal of Applied Physics*, vol. 112, no. 12, Article ID 123104, 2012.

[14] I. Sebastian, S. Divya, V. P. N. Nampoori, P. Radhakrishnan, and S. Thomas, "Impact of intermediate localized states on nonlinear optical absorption of Ga-Ge-Se nanocolloidal solutions," *Applied Physics Letters*, vol. 102, no. 3, Article ID 031115, 2013.

[15] M. Sheik-Bahae, A. A. Said, T.-H. Wei, D. J. Hagan, and E. W. Van Stryland, "Sensitive measurement of optical nonlinearities using a single beam," *IEEE Journal of Quantum Electronics*, vol. 26, no. 4, pp. 760–769, 1990.

[16] F. M. Qureshi, S. J. Martin, X. Long et al., "Optical limiting properties of a zinc porphyrin polymer and its dimer and monomer model compounds," *Chemical Physics*, vol. 231, no. 1, pp. 87–94, 1998.

Thermo-optic and nonlinear-optical methods as well as linear optical spectroscopy have been utilized to characterize CdSe based nanofluids. The influence of metal nanoparticles on CdSe QDs is discussed using these methods. Applications of such materials in the field of solar cells, random lasers and optical limiters are also investigated.